PLANT SAFETY EVALUATION

FOR

BEAVER VALLEY POWER STATION UNIT 2

VANTAGE 5H

FUEL UPGRADE

August 1991

Edited by:

W. H Slagle

Approved: _____

E. H. Novendstern, Manager
T/H Design and Fuel Licensing
Commercial Nuclear Fuel Division

Westinghouse Electric Corporation
Commercial Nuclear Fuel Division
P. O. Box 355
Pittsburgh, PA 15230

ACKNOWLEDGEMENTS

The editor would like to acknowledge the efforts of the contributors to the design Sections and Appendices to this Plant Safety Evaluation. Major contributors included:

Mechanical Design	- Y. C. Lee
Fuel Performance Technology	- R. L. Oelrich
Nuclear Design	- J. A. Penkrot, R. A Warsaw
Thermal and Hydraulic Design	- T. C. Stoddard
Non-LOCA Analysis	- U. Bachrach, J. Stacknouse
LOCA Analysis	- J. Petzold, J. M. Tanz
Reactor Plant Vessel System Analysis	- D. R. Bhandari
Containment Design and BWR Technology	- L. C. Smith
Technical Specifications	- A. J. Baker
Operating Plant Licensing	- P. J. Cortazzo

In addition, acknowledgement is given to B. D. McKenzie and P. J. Cortazzo for their assistance in providing the necessary interfaces between CNFD, NATD and the Duquesne Light Company.

PLANT SAFETY EVALUATION

BEAVER VALLEY POWER STATION UNIT 2

VANTAGE 5H FUEL UPGRADE

TABLE OF CONTENTS

PLANT SAFETY EVALUATION

BEAVER VALLEY POWER STATION UNIT 2

VANTAGE 5H FUEL UPGRADE

TABLE OF CONTENTS (Cont.)

PLANT SAFETY EVALUATION

BEAVER VALLEY POWER STATION UNIT 2

VANTAGE 5H FUEL UPGRADE

LIST OF TABLES

PLANT SAFETY EVALUATION

BEAVER VALLEY POWER STATION UNIT 2

VANTAGE 5H FUEL UPGRADE

LIST OF FIGURES

LIST OF FIGURES (Cont.)

1.0 Introduction and Summary

1.0 INTRODUCTION AND SUMMARY

1.1 Introduction

The Beaver Valley Power Station Unit 2 plans to refuel and operate with upgraded Westinghouse fuel features. This report summarizes the safety evaluations that were performed to confirm the acceptable use of these features for three loop operation. Sections 2.0 through 5.0 of the Plant Safety Evaluation (PSE) provide the results of the Mechanical, Nuclear, Thermal and Hydraulic, and Accident Evaluations, respectively. Appendix A gives a summary of the Technical Specification changes required and the corresponding change pages. Recommended changes to the Beaver Valley Unit 2 UFSAR[1] are included in Appendix B.

The Beaver Valley Unit 2 Plant Safety Evaluation is to serve as a reference safety evaluation/analysis report for the region-by-region reload transition from the present Beaver Valley Unit 2 core (Cycle 3) to a core containing the upgraded features described below. Thus, the PSE will be used as a basic reference document in support of future Beaver Valley Unit 2 Reload Safety Evaluations (RSEs) for upgraded fuel reloads.

Parameters are chosen to maximize the applicability of the PSE evaluations for future cycles which will utilize the Westinghouse standard reload methodology[2]. The objective of subsequent cycle specific RSE will be to verify that applicable safety limits are not exceeded based on the reference analyses currently in the UFSAR[1] or established in the safety evaluation.

1.2 Upgraded Fuel Features (VANTAGE 5 Hybrid)

Beaver Valley Unit 2 Cycle 4 and subsequent core loadings will have fuel assemblies that incorporate a low pressure drop Zircaloy grid. This upgraded fuel feature is known as VANTAGE 5 Hybrid (VANTAGE 5H) and has been submitted to the NRC as an Addendum[3] to the "VANTAGE 5 Reference Core Report," WCAP-10444-P-A[4]. VANTAGE 5H has received generic NRC approval[5].

In addition to the VANTAGE 5H design feature, Beaver Valley Unit 2 reloads will also contain several VANTAGE 5 design features[4] and other upgraded fuel design features. Beaver Valley Unit 2 Cycle 3 has already incorporated the Reconstitutable Top Nozzle (RTN)[4][5], Debris Filter Bottom Nozzles (DFBNs), snag resistant grids, standardized fuel pellets, Integral Fuel Burnable Absorbers (IFBAs)[4][5] and Axial Blanket design features of VANTAGE 5. A brief summary of the upgraded fuel features is presented in Section 2 of this report.

1.3 Thimble Plug Assembly Removal

Thimble Plug assemblies have been used to limit the core bypass flow in guide thimble tubes that are not in RCCA positions or containing other core components. Evaluations have been performed by Westinghouse assuming the complete removal of thimble plug assemblies from the Beaver Valley Power Station Unit 2 core. Removal of thimble plug assemblies will result in an increased core bypass flow and a reduction to the fuel assembly hydraulic loss coefficient. There is also a reduction in the hydraulic lift force on the fuel assembly due to a reduced fuel assembly loss coefficient. Thus, the thimble plug assembly removal is acceptable from a fuel assembly lift force standpoint. The effect of the thimble plug assembly removal on the distribution of outlet loss coefficients has been evaluated, and it was demonstrated that the variations in outlet loss coefficient are within the bounds of the sensitivity studies that have been performed by Westinghouse. Safety evaluations for thimble plug assembly removal have been performed to show that the licensing analyses referenced here will bound plant operations whether or not thimble plugs are removed from the core.

1.4 Conclusions

The results of evaluation/analysis described herein lead to the following conclusions:

1. The Westinghouse fuel assemblies containing VANTAGE 5H and the additional upgraded fuel features for Beaver Valley Unit 2 are mechanically compatible with the current fuel assemblies, control rods, and reactor internals interfaces. The current design bases for Beaver Valley Unit 2 have been changed as described in this report to accommodate the VANTAGE 5H design.

2. Changes in the nuclear characteristics due to the transition to upgraded fuel will be within the range normally seen from cycle to cycle due to fuel management.

3. The reload upgraded fuel assemblies are hydraulically compatible with the fuel assemblies from previous reload cores.

4. The core design and safety results documented in this report show the core's capability for operating safely at the rated Beaver Valley Unit 2 design thermal power.

5. This report establishes a reference upon which to base Westinghouse reload safety evaluations for future reloads with the upgraded fuel features and thimble plug removal.

2.0 Design Features

2.0 DESIGN FEATURES

2.1 Introduction

The mechanical design of the upgraded fuel assemblies for Beaver Valley Unit 2 is the same as previous reload fuel assemblies except that the upgraded fuel assemblies will incorporate a few fuel design improvements. An improvement is the VANTAGE 5H Zircaloy grid. Previous VANTAGE 5 features that were incorporated are Reconstitutable Top Nozzles (RTNs), Debris Filter Bottom Nozzles (DFBNs), Snag Resistant Grids, Standardized Fuel Pellets, Enriched Integral Fuel Burnable Absorbers (IFBAs) and Axial Blankets. The previous and new design changes are described in more detail in the following sections.

2.2 VANTAGE 5H Fuel Assembly

The VANTAGE 5H fuel assembly design evolved from the current VANTAGE 5, Optimized Fuel Assembly (OFA) and Standard (STD) fuel assembly designs. It is based on substantial design and operating experience. Design features from each of these previous designs are incorporated into the VANTAGE 5H fuel assembly design. The VANTAGE 5H design is characterized by the use of Zircaloy grids with 0.374 inch OD standard fuel rods. To accommodate the Zircaloy grids, the VANTAGE 5H thimble tube diameter was modified to be the same as the 17x17 OFA or VANTAGE 5 fuel. A comparison of the STD and VANTAGE 5H fuel assembly design parameters is given in Table 2.1. Figure 2.1 demonstrates the similarity of the two designs and shows a comparison of overall dimensions.

Comparative fuel assembly flow testing results indicate that the VANTAGE 5H and the STD 17x17 fuel assembly are hydraulically equivalent. Full assembly testing has confirmed that the VANTAGE 5H fuel assembly has hydraulic stability and that the fuel rod contact wear with the spacer grids is within the allowable design limits.

The major components that determine the structural integrity of the fuel assembly are the grids. Mechanical testing and analysis of the VANTAGE 5H Zircaloy grid and fuel assembly have demonstrated that the VANTAGE 5H structural integrity under seismic/LOCA loads will provide

margins comparable to the STD 17x17 fuel assembly design and will meet all design bases.

The VANTAGE 5H Zircaloy grid is based on the OFA Zircaloy grid design and operating experience. The grid strap thickness, type of strap welding, basic mixing vane design and pattern, method of thimble tube attachment, type of fuel rod support (6 point), material and envelope are identical to the OFA Zircaloy grid. This evaluation of the VANTAGE 5H grid performance is based on the extensive design and irradiation experience with previous grid designs and full grid testing completed with the VANTAGE 5H grid design.

In order to demonstrate early performance of the Zircaloy grid design, fuel assembly demonstration programs were conducted inserting OFA fuel assemblies containing Zircaloy grids into 14x14, 15x15 and 17x17 cores. Subsequent to the satisfactory performances observed in these programs, the OFA with Zircaloy grids were loaded and have operated successfully since the early 1980's in many Westinghouse cores[6].

2.3 Fuel Features and Other Upgrades

Beaver Valley Unit 2 Cycle 4 and subsequent reloads will contain fuel assemblies that incorporate Reconstitutable Top Nozzles, Debris Filter Bottom Nozzle, Snag Resistant Grids, Standardized Fuel Pellets, Integral Fuel Burnable Absorbers and Axial Blankets as well as the VANTAGE 5H Zircaloy grids described in the previous section. These design features and other changes, described below, are currently part of the licensing basis in other plants and meet all fuel assembly and fuel rod design criteria.

Debris Filter Bottom Nozzle (DFBN) - The bottom nozzle is designed to inhibit debris from entering the active fuel region of the core and thereby improves fuel performance by minimizing debris related fuel failures. The DFBN is a low profile bottom nozzle design made of stainless steel, with reduced end plate thickness and leg height. The DFBN is structurally and hydraulically equivalent to the existing bottom nozzle.

Reconstitutable Top Nozzle (RTN) - The RTN differs from the current design in two ways: a groove is provided in each thimble thru-hole in the nozzle plate to facilitate attachment and removal; and

the nozzle plate thickness was reduced to provide additional space for fuel rod growth. In conjunction with the RTN, a long tapered fuel rod bottom end plug is used to facilitate removal and reinsertion of the fuel rods.

Standardized Fuel Pellets - The standardized pellet is a refinement to the current pellet design with the objective of improving manufacturability while maintaining or improving performance. This design incorporates a reduced pellet length, modification to the previous dish size and the addition of a chamfer.

Snag-Resistant Grids - The snag-resistant grids contain outer grid straps which are modified to help prevent assembly hangup from grid strap interference during fuel assembly removal. This was accomplished by changing the grid strap corner geometry and the addition of guide tabs on the outer grid strap.

Integral Fuel Burnable Absorbers - The IFBA coated fuel pellets are identical to the enriched uranium dioxide pellets except for the addition of a thin zirconium diboride or enriched zirconium diboride coating (less than one mil) on the pellet cylindrical surface along the central portion of the fuel stack length. The enriched IFBA properties are the same mechanically and chemically (except for the small reduction in density) as the natural boron material. A safety evaluation for the application of enriched boron in the current IFBA design was performed by Westinghouse and concluded that the enriched boron did not adversely affect core safety considerations[7]. IFBAs provide power peaking and moderator temperature coefficient control.[4]

Axial Blankets - The axial blanket consists of natural uranium dioxide pellets at each end of the fuel stack to reduce neutron leakage and to improve uranium utilization. The axial blanket pellets are of the same design as the enriched and IFBA pellet designs except for an increase in length. The length difference in the axial blanket pellets will help prevent accidental mixing with the enriched and IFBA pellets.

2.4 Fuel Rod Performance

The 0.374 inch OD fuel rod used in the VANTAGE 5H fuel assembly is the same as that used in the Beaver Valley Unit 2 17x17 STD fuel assemblies. The design bases, methodology, and models are the same as those described previously[4]. No changes in fuel rod design criteria, methods, or models are necessary because of the transition to VANTAGE 5H fuel. The STD and VANTAGE 5H fuel are designed according to the Westinghouse fuel performance models[8][9]. All fuel rod design criteria are satisfied for the planned irradiation life.

FIGURE 2.1

COMPARISON OF THE 17x17 VANTAGE 5H FUEL ASSEMBLY

AND THE 17x17 STD FUEL ASSEMBLY

17x17 VANTAGE 5H Fuel Assembly

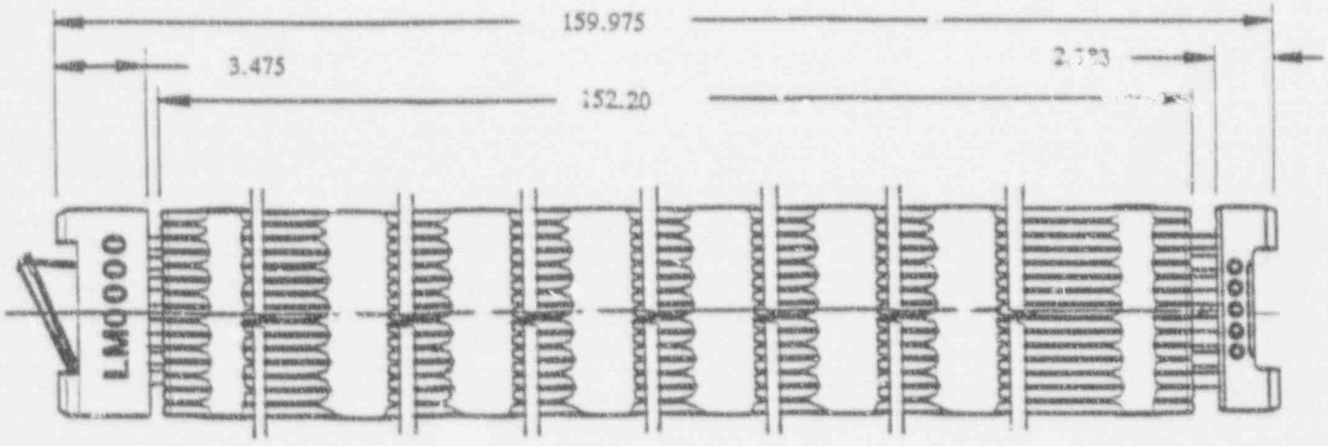

17x17 Reconstitutable STD Fuel Assembly

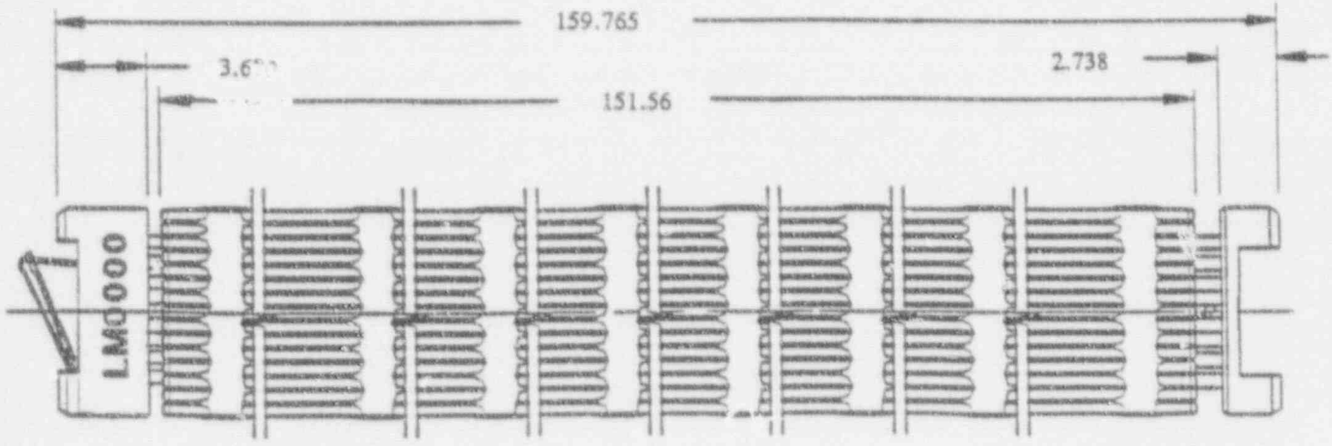

Table 2.1

COMPARISON OF 17X17 STANDARD, OPTIMIZED, VANTAGE 5
AND VANTAGE 5 HYBRID FUEL ASSEMBLY MECHANICAL DESIGN PARAMETERS

	Standard	OFA	VANTAGE 5	VANTAGE 5H
Fuel Assembly Overall Length, inch	159.8	159.8	160.0	160.0
Fuel Rod Overall Length, inch	151.6	151.6	152.3	152.2
Assembly Envelope, inches	8.426	8.426	8.426	8.426
Fuel Rod Pitch, inch	0.496	0.496	0.496	0.496
Number of Fuel Rods/Assembly	264	264	264	264
Number of Guide Thimbles/Assembly Assembly	24	24	24	24
Number of Instrumentation Tube/Assembly	1	1	1	1
Fuel Tube Material	Zirc-4	Zirc-4	Zirc-4	Zirc-4
Fuel Tube Clad OD, inch	0.374	0.360	0.360	0.374
Fuel Rod Clad Thickness, inch	0.0225	0.0225	0.0225	0.0225
Fuel Clad Gap, mil	6.5	6.2	6.2 (uncoated pellets)	6.5 (uncoated pellets)
Fuel Pellet diameter, inch	0.3225	0.3088	0.3088 (uncoated pellets)	0.3225 (uncoated pellets)

COMPARISON OF 17X17 STANDARD, OPTIMIZED, VANTAGE 5
AND VANTAGE 5 HYBRID FUEL ASSEMBLY MECHANICAL DESIGN PARAMETERS

	Standard	OFA	VANTAGE 5	VANTAGE 5H
Fuel Rod End Plugs	Standard	Standard	Tapered and Radiused	Tapered and Radiused
Relative Clad Thickness/ Diameter Ratio	1.0	1.04	1.04	1.0
Relative Moderator/Fuel Ratio for Assembly	1.0	1.2	1.2	1.0
Relative UO_2/Rod	1.0	0.92	0.92	1.0
Guide Thimble Material	Zirc-4	Zirc-4	Zirc-4	Zirc-4
Guide Thimble OD, inch	0.482	0.474	0.474	0.474
Guide Thimble Wall Thickness, inch	0.016	0.016	0.016	0.016
Grid Material, Inner Mid Grid (6)	Inconel	Zirc-4	Zirc-4	Zirc-4
Edges Modified	No	No	No	Yes
Grid Material, End Grids (2)	Inconel	Inconel	Inconel	Inconel

COMPARISON OF 17X17 STANDARD, OPTIMIZED, VANTAGE 5
AND VANTAGE 5 HYBRID FUEL ASSEMBLY MECHANICAL DESIGN PARAMETERS

	Standard	OFA	VANTAGE 5	VANTAGE 5H
Material, Intermediate Flow Mixer (3)	None	None	Zirc-4	Zirc-4*
Grid Types Utilized				
Inconel Mid grids	Yes	No	No	No
Zircaloy Mid grids	No	Yes	Yes	Yes
Flow Mixers	No	No	Yes	Yes (Optional)
Inconel Top & Bottom Grids	Yes	Yes	Yes	Yes
Inner Spring (Mid Grids)	Vertical	Vertical	Vertical	Non-Vertical
Grid Fabrication Inconel Grids	Brazed joining of interlocking stamped straps	Brazed joining of interlocking stamped straps	Brazed joining of interlocking stamped straps	Brazed joining of interlocking stamped straps
Zircaloy Mid Grid & Flow Mixers	None	Laser weld joining of interlocking stamped straps	Laser weld joining of interlocking stamped straps	Laser weld joining of interlocking stamped straps
Grid/Guide Thimble Attach. Inconel Grids	Thimbles bulged together with sleeve prebrazed	Thimbles bulged together with sleeve prebrazed	Thimbles bulged together with sleeve prebrazed	Thimbles bulged together with sleeve prebrazed
Zircaloy Mid Grids and Flow Mixers	None	Thimbles bulged together with sleeves laser prewelded to grid straps	Thimbles bulged together with sleeves laser prewelded to grid straps	Thimbles bulged together with sleeves laser prewelded to grid straps

* Not incorporated into Beaver Valley Power Station - 2 Design

COMPARISON OF 17X17 STANDARD, OPTIMIZED, VANTAGE 5
AND VANTAGE 5 HYBRID FUEL ASSEMBLY MECHANICAL DESIGN PARAMETERS

	Standard	OFA	VANTAGE 5	VANTAGE 5H
Top Nozzle	Welded stainless steel Standard	Welded Stainless steel Standard	Reconstitutable stainless steel reduced height removable design	Reconstitutable stainless steel reduced height removable design
Compatible with Fuel Handling Equipment	Yes	Yes	Yes	Yes

3.0 Nuclear Design

3.0 NUCLEAR DESIGN

3.1 Introduction and Summary

The effects of using upgraded Westinghouse fuel features on the nuclear design bases and methodologies for Beaver Valley Power Station Unit 2 are evaluated in this section.

The grid material and grid volume of the VANTAGE 5H fuel are different than that of 17x17 standard fuel assemblies. The effects of these changes on core physics characteristics are small and are explicitly modeled in the neutronics code system. The specific values of core safety parameters, e.g., power distributions, peaking factors, rod worths, are primarily loading pattern dependent. The variations in the loading pattern dependent safety parameters are expected to be typical of the normal cycle to cycle variations for the standard fuel reloads. In addition, the present Beaver Valley spent fuel pool criticality analysis is applicable to the upgraded Westinghouse fuel features, including the use of VANTAGE 5H fuel.

Thimble Plugs have been removed from the Beaver Valley Power Station Unit 2 core. The removal of thimble plugs is analyzed by changing the flow input to the nuclear design code system. There is significant experience in modeling fuel with thimble plugs removed.

In summary, the changes from the current standard fuel core to a core containing the upgraded fuel product will not cause changes to the current Beaver Valley Unit 2 UFSAR[1] nuclear design bases. Nuclear design methodology is not affected by the use of upgraded fuel features.

3.2 Methodology

No changes to the nuclear design philosophy or methods are necessary because of the upgraded fuel product. The reload design philosophy includes the evaluation of the reload core key safety parameters which comprise the nuclear design dependent input to the UFSAR[1] safety evaluation for each reload cycle[2]. These key safety parameters will be evaluated for each Beaver Valley Unit 2 reload cycle. If one or more of the parameters fall outside the bounds assumed in the safety analysis, the affected transients will be re-evaluated and the results documented in the RSE for that cycle.

The 0.374 inch diameter fuel rod has had extensive nuclear design and operating experience with the current Beaver Valley Unit 2 17x17 STD fuel assembly design. The Zircaloy grid material has also had extensive nuclear design and operating experience with the current 17x17 VANTAGE 5 and 17x17 OFA fuel assembly designs. These changes have a negligible effect on the use of standard nuclear design analytical models and methods to accurately describe the neutronic behavior of the VANTAGE 5H fuel.

4.0 Thermal and Hydraulic Design

4.0 THERMAL AND HYDRAULIC DESIGN

4.1 Introduction and Summary

This section describes the calculational methods used for the thermal-hydraulic analysis, the DNB performance, and the hydraulic compatibility during the transition from a Standard through mixed-fuel cores to an all VANTAGE 5H core. Based on minimal hardware design differences and prototype hydraulic testing of the fuel assemblies, it is concluded[3] that the STD and VANTAGE 5H fuel assembly designs are hydraulically compatible. Table 4-1 summarized the thermal-hydraulic design parameters for Beaver Valley Unit 2 that were used in this analysis. The thermal-hydraulic design criteria and methods remain the same as those presented in the Beaver Valley Unit 2 UFSAR[1] with the exceptions noted in the following sections. All of the current UFSAR[1] thermal-hydraulic design criteria are satisfied.

4.2 Methodology

The existing thermal-hydraulic analysis of the 17x17 STD fuel used in the Beaver Valley Unit 2 plant is based on the standard thermal and hydraulic methods and the W-3 (R-Grid) DNB correlation as described in the Beaver Valley Unit 2 UFSAR. The DNB analysis of the core containing both 17x17 STD and VANTAGE 5H fuel assemblies has been modified to incorporate the WRB-1 DNB correlation[10] and a conservative application of the Revised Thermal Design Procedure (RTDP)[11] which is called MINI-RTDP[12].

The WRB-1 DNB correlation is based entirely on rod bundle data and takes credit for the significant improvement in the accuracy of the critical heat flux predictions over previous DNB correlations. The approval by the NRC that a 95/95 limit DNBR of 1.17 is appropriate for the 17x17 STD fuel assemblies has been documented[13].

The WRB-1 DNB correlation is applicable to VANTAGE 5H fuel since, from a DNB perspective, the Zircaloy mixing vane grids of the VANTAGE 5H assembly are virtually identical in performance to the 17x17 Inconel R-Grid design. For regions outside the mixing vane grids, the W-3 correlation is used. As documented in the VANTAGE 5H Fuel Assembly Report[3], the use of the WRB-1 DNB correlation with a 95/95 limit DNBR of 1.17 is applicable to the VANTAGE 5H fuel assembly.

With MINI-RTDP methodology, peaking factor uncertainties are combined statistically with the DNB correlation uncertainties to obtain the overall DNBR uncertainty factor which is used to define the design limit DNBR that satisfies the DNB design criterion. This criterion is that the probability that DNB will not occur on the most limiting fuel rod is at least 95% (at 95% confidence level) for any Condition I or II event.

The uncertainties included in the combined peaking factor uncertainty are the nuclear enthalpy rise hot channel factor, ($F^N_{\Delta H}$); the enthalpy rise engineering hot channel factor, ($F^E_{\Delta H}$); and uncertainties in the THINC-IV and transient codes. The increase in DNB margin is realized when nominal values of the peaking and hot channel factors are used in the DNB safety analyses.

With MINI-RTDP, uncertainties in the plant primary system parameters (reactor power, flow, temperature and pressure) are excluded from the statistical combination process and, therefore, no additional surveillance of these parameters is required. Initial condition assumptions for the DNB safety analyses will use the same conservative values for these plant system parameters that are used in the standard thermal design methods.

For this application, the design limit DNBR for typical and thimble cells is 1.21 which applies for both 17x17 STD and VANTAGE 5H fuel assemblies. For use in the DNB safety analyses, the limit DNBR is conservatively increased to provide DNB margin to offset the effect of rod bow and any other DNB penalties that may occur, and to provide flexibility in design and operation of the plant. The safety analysis limit DNBR providing for 9% margin is calculated as follows:

$$\text{Safety Analysis Limit DNBR} = \frac{\text{Design Limit DNBR}}{1.0 - \text{Margin}} = \frac{1.21}{1.0 - 0.09} = 1.33$$

Table 4-2 summarizes the available DNBR margin for Beaver Valley Power Station Unit 2.

4.3 Hydraulic Compatibility

The STD fuel assembly and VANTAGE 5H designs have been shown to be hydraulically compatible in the VANTAGE 5H Fuel Assembly Report[3].

4.4 Effects of Fuel Rod Bow on DNBR

The phenomenon of fuel rod bowing must be accounted for in the DNBR safety analysis of Condition I and Condition II events. Currently, the maximum rod bow penalty is 1.3% DNBR at an assembly average burnup of 24,000 MWD/MTU. For burnups greater than 24,000 MWD/MTU, credit is taken for the effect of $F^N_{\Delta H}$ burndown, due to the decrease in fissionable isotopes and the buildup of fission product inventory. Therefore, no additional rod bow penalty is required at burnups greater than 24,000 MWD/MTU. Based on the similarities between 17x17 STD and VANTAGE 5H fuel assemblies, (i.e. fuel rod diameter, fuel rod pitch and grid spacing), this penalty is also applicable to VANTAGE 5H fuel assemblies.

For this application, the rod bow penalty will be offset with DNB margin retained between the safety analysis and design DNBR limits (Table 4-2).

4.5 Fuel Temperature Analysis

There is no difference in the fuel temperatures used in the safety analysis calculations between the VANTAGE 5H fuel and the STD fuel. The fuel temperatures for the standardized pellets are the same as those for unchamfered pellets and slightly less than those for the current chamfered pellet design.

4.6 Transition Core Effect

The VANTAGE 5H hydraulic test program showed identical results for the VANTAGE 5H grid and the STD fuel Inconel mixing vane grid, therefore, no transition core DNBR penalty is necessary[3].

4.7 Conclusion

The thermal hydraulic evaluation of the fuel upgrade for Beaver Valley Unit 2 has shown that 17x17 STD and VANTAGE 5H fuel assemblies are hydraulically compatible and that the DNB margin gained through use of the MINI-RTDP methodology and the WRB-1 DNB correlation is sufficient

for future changes. The core limit curves (Technical Specifications Figure 2.1-1 for three loops in operation) remain valid for both STD and VANTAGE 5H fuel assemblies with or without thimble plug assemblies. More than sufficient DNBR margin in the safety limit DNBR exists to cover any rod bow penalties. The upgraded fuel features described in Section 2 do not affect the core flow rate, core flow distribution, or any other safety related parameters. All current thermal-hydraulic design criteria are satisfied.

TABLE 4-1
BEAVER VALLEY UNIT 2 THERMAL AND HYDRAULIC DESIGN PARAMETERS

Thermal and Hydraulic Design Parameters		Design Parameters
Reactor Core Heat Output, MWt		2,652
Reactor Core Heat Output, 10^6, BTU/Hr		9,051
Heat Generated in Fuel, %		97.4
Core Pressure, Nominal, psia		2250
Radial Power Distribution*		1.62[1+0.3(1-P)]
Limit DNBR for Design Transients**		1.33
DNB Correlation**		WRB-1
HFP Nominal Coolant Conditions		
Vessel Thermal Design Flow Rate (including Bypass), 10^6 lb_m/hr		100.8
GPM		265,500
Core Flow Rate*** (excluding Bypass, based on TDF) 10^6 lb_m/hr		94.25
GPM		248,242
Core Flow Area, ft^2	(STD)	41.5
	(V5H)	41.7
Core Inlet Mass Velocity, 10^6 $lb_m/hr\text{-}ft^2$ (Based on TDF)	(STD)	2.27
	(V5H)	2.26

* Includes 4% measurement uncertainty - Analysis assumed value bounds licensed value of 1.55 peak.

** Applies to STD and VANTAGE 5H fuel.

*** Based on design bypass flow of 6.5% without thimble plugs.

TABLE 4-1
BEAVER VALLEY UNIT 2 THERMAL AND HYDRAULIC DESIGN PARAMETERS
(continued)

ıermal and Hydraulic Design Parameters		Design Parameters
Nominal Vessel/Core Inlet Temperature, °F		542.5
Vessel Average Temperature, °F		576.2
Core Average Temperature, °F		580.2
Vessel Outlet Temperature, °F		609.9
Average Temperature Rise in Vessel, °F		67.4
Average Temperature Rise in Core, °F		71.6
Heat Transfer		
Active Heat Transfer Surface Area, ft^2	(STD)	48,600
	(V5H)	48,600
Average Heat Flux, BTU/hr-ft^2	(STD)	181,405
	(V5H)	181,405
Average Linear Power, kw/ft		5.20
Peak Linear Power for Normal Operation,* kw/ft		12.48
Temperature at Peak Linear Power for Prevention of Centerline Melt, °F		4700

* Based on maximum F_Q of 2.40 - Analysis assumed value bounds licensed value of 2.32 peak.

TABLE 4-2
DNBR MARGIN SUMMARY

	17x17 STD and VANTAGE 5H Fuel
DNB Correlation	WRB-1
Correlation Limit	1.17
Design Limit	1.21
Safety Limit	1.33
DNBR Margin*	9%
Rod Bow DNBR Penalty	1.3%
Available DNBR Margin	7.7%

* DNBR margin between the safety limit and the desig limit DNBRs.

5.0 Accident Analysis

5.0 ACCIDENT ANALYSIS

The primary effect of the proposed modifications on the LOCA and non-LOCA design basis calculations is due to the introduction of the VANTAGE 5H Zircaloy grid and the thimble plug removal. The safety analysis justification for these design modifications is summarized for the non-LOCA and LOCA design basis calculations in Sections 5.1 and 5.2, respectively. The balance of the fuel upgrade features described in Section 1.2 of this report have been introduced and acceptably evaluated for previous reload designs.

5.1 Non-LOCA Accidents

This section summarizes the non-LOCA reanalyses and evaluations performed for the Beaver Valley Unit 2 upgrade to VANTAGE 5H fuel and the deletion of thimble plugs. This evaluation bounds the case where some or all of the thimble plugs are present. In addition, this evaluation continues to support steam generator tube plugging, up to a level of 20%, provided that the per loop licensed Thermal Design Flow is maintained.

The major effect of changing from STD 17x17 fuel to VANTAGE 5H fuel on the non-LOCA transients is the increased design Rod Control Cluster Assembly (RCCA) drop time. The VANTAGE 5H fuel assembly has a thimble tube I.D. of 0.442 inches. STD fuel has a thimble tube I.D. of 0.450 inches. The smaller VANTAGE 5H thimble tube will increase the design RCCA drop time from a current maximum of 2.2 seconds to 2.7 seconds. This slower drop time will affect the results of the fast non-LOCA limiting transients such as Loss of Forced Reactor Coolant Flow, Locked Rotor, RCCA Bank Withdrawal from Subcritical and Rod Ejection. The balance of the non-LOCA accidents are evaluated for this fuel upgrade.

Non-LOCA events that are not mentioned above did not require reanalysis for one or more of the following reasons:

1) Transient results are insensitive to the rod insertion rate.
2) Reactor trip was not assumed or explicitly modeled in the analysis.
3) Reactor trip has no effect on the minimum or maximum value of the critical parameter of interest.

The main impact of removing the thimble plugs on non-LOCA transients is an increase in the core bypass flow from 4.5% to 6.5%. This increase in bypass flow results in an equivalent decrease in the flow through the core active fuel region.

The DNB limited events have either been re-analyzed incorporating the core active flow decrease, or have been evaluated for the core active flow decrease such that the results of previous analyses remain valid. In addition, the reactor core thermal limit curves have not changed such that the current Technical Specification Overtemperature ΔT and Overpower ΔT setpoints remain valid.

For events that are not DNB related, or for which prevention of DNB is not the only safety criterion, the effects of decreased core flow have been evaluated with respect to the applicable acceptance criteria. Reduced core active region flow results in an increase in the nominal core coolant exit temperature. However, the total RCS flow is not decreased. Also, for the small increase in core bypass flow, the additional bypass flow is mixed with the core coolant at the core exit such that the vessel average and the vessel outlet coolant temperatures remain unchanged. Thus the overall transient system response in terms of parameters such as RCS pressure or RCS volumetric expansion is unaffected. Only core related results such as peak clad temperature are potentially affected.

A summary of the non-LOCA design basis calculations that were performed or evaluated for these modifications follows.

5.1.1 Overtemperature and Overpower ΔT Protection (UFSAR 15.0)

As noted in Section 4.7, the current Beaver Valley Unit 2 Technical Specification core thermal limits (Figure 2.1-1 for 3 loops in operation) are valid for VANTAGE 5H and STD fuel assemblies with or without thimble plugs. As discussed in the following paragraphs, the system transient responses for the UFSAR events that rely on Overtemperature and Overpower ΔT (OTDT/OPDT) for protection are not affected by the increased rod drop time. Therefore, the revised[14] N-loop Technical Specification OTDT/OPDT setpoint equation constants continue to protect the core safety limits as shown in the revised Figure 15.0-1 in Reference 15.

5.1.2 Increase in Heat Removal by the Secondary System

Feedwater System Malfunctions Causing a Reduction in Feedwater Temperature (UFSAR[1] 15.1.1)

The decrease in feedwater temperature transient, as discussed in the UFSAR[1], is bounded by the Increase in Secondary Steam Flow event.

Feedwater System Malfunctions Causing an Increase in Feedwater Flow (UFSAR[1] 15.1.2)

This ANS Condition II event is analyzed to show that the DNB design basis is met. Cases are analyzed for both full power and zero power conditions. The zero power case, as discussed in the UFSAR[1], is bounded by the Uncontrolled RCCA Bank Withdrawal from Subcritical event. For the full power case, the transient is effectively terminated by a turbine trip and feedwater isolation on high-high steam generator level. A conservative evaluation of the effects of the 0.5 second increase in control rod insertion time was performed by extrapolating the transient DNBR results assuming that reactor trip was delayed by 0.5 second. The extrapolation showed that ample margin to the DNB limit still exists with a 0.5 second delay. Therefore, the UFSAR[1] conclusions remain valid.

Excessive Increase in Secondary Steam Flow (UFSAR[1] 15.1.3)

This ANS Condition II event is analyzed to show that the DNB design basis is met following a step load increase from rated power. Cases are analyzed at BOL and EOL conditions with and without automatic rod control. In all cases analyzed, the reactor stabilized without a reactor trip. Therefore, the increased control rod insertion time will have no effect on this event. Therefore, the conclusions of the UFSAR[1] remain valid.

Inadvertent Opening of a Steam Generator Relief or Safety Valve Causing a Depressurization of the Main Steam System (UFSAR[1] 15.1.4) and Steam System Piping Failure (UFSAR[1] 15.1.5)

The inadvertent opening of a steam generator relief or safety valve is an ANS Condition II event which is analyzed to show that the DNB design basis is met. The steam system piping failure is an ANS Condition IV transient analyzed to show that the core remains intact and in place and that the

radiation doses do not exceed the guidelines of 10CFR100. This is demonstrated by showing that the DNB design basis is met, even though DNB and possible clad perforation are not necessarily unacceptable for a Condition IV event.

The analyses are performed assuming zero power initial conditions and peaking factors consistent with the most reactive RCCA stuck out of the core. The transient is started assuming the reactor is tripped and the core is at the minimum design shutdown margin. Therefore, the 0.5 second increase in rod insertion time will have no effect on the results of this analysis. The safety analysis DNBR limits are met. The conclusions of the UFSAR[1] remain valid.

5.1.3 Decrease in Heat Removal by the Secondary System

Steam Pressure Regulator Malfunction or Failure That Results in Decreased Steam Flow (UFSAR[1] 15.2.1)

Any steam flow decrease caused by a malfunction or failure of any steam pressure regulator is conservatively bounded by the turbine trip event.

Loss of External Load (UFSAR[1] 15.2.2)

The Loss of External Load Transient, as discussed in the UFSAR[1], is bounded by the Turbine Trip event.

Turbine Trip (UFSAR[1] 15.2.3)

This ANS Condition II event is analyzed to show that the DNB design basis is met and that primary and secondary side system pressures do not exceed 110% of design values. Four cases are analyzed:

Beginning of Cycle (BOC) with pressurizer pressure control
BOC without pressurizer pressure control
End of Cycle (EOC) with pressurizer pressure control
EOC without pressurizer pressure control.

The increased rod insertion time to the dashpot will not result in system pressures exceeding 110% of design values. Pressure transients from the current analysis of record were evaluated by extrapolation assuming the reactor trip was delayed 0.5 seconds. In all cases there was ample margin to account for the slight expected pressure rise due to the increased design rod drop times. As previously noted, the RCS pressure transient is not affected by the elimination of the thimble plugs, since the total RCS flow and vessel outlet temperature remain the same. The increased rod drop time to the dashpot will not result in DNBR below the design limit.

DNBR for the BOC case without pressure control and both EOC cases rises continuously throughout the transients. Therefore, the increased insertion time will have no effect on the minimum DNBR for these cases. DNBR during the BOC with pressure control case initially rises and then decreased to a minimum value well above the safety analysis limit at the time of reactor trip. The margin to the design DNB limit is very large at the time of reactor trip for this case and the increased rod drop time will not result in a DNBR below the design basis. Therefore, the UFSAR[1] conclusions remain valid for the introduction of VANTAGE 5H fuel.

Loss of Nonemergency AC Power to the Station Auxiliaries (Loss of Offsite Power) (UFSAR[1] 15.2.6)

This ANS Condition II event is analyzed to show that adequate heat removal capability exists via natural circulation flow as aided by the Auxiliary Feedwater System to remove core decay heat and stored energy following reactor trip. This is demonstrated by ensuring that the RCS heatup is turned around prior to the time when coolant expansion causes the pressurizer to become filled with water. The calculated RCS volumetric expansion is not affected by the VANTAGE 5H fuel. As previously noted, the RCS volumetric expansion is not affected by the elimination of the thimble plugs, since the total RCS flow and vessel outlet temperature remain the same. This transient is an slow long-term heatup event and is not sensitive to the rate at which the rods are inserted during a reactor trip. With respect to the DNB criterion, this event is bounded by the Complete Loss of Forced Reactor Coolant Flow analysis which was reanalyzed and shown to be acceptable. The results of the current analysis of record and the conclusions of the UFSAR[1] remain valid.

Loss of Normal Feedwater Flow (UFSAR[1] 15.2.7)

This ANS Condition II event is analyzed to show that adequate heat removal capability exists via the Auxiliary Feedwater System to remove core decay heat, stored energy and RCS pump heat following reactor trip. This is demonstrated by ensuring that the RCS heatup is turned around prior to the time when coolant expansion causes the pressurizer to become filled with water. As previously noted, the RCS pressure and temperature transients are not affected by the elimination of the thimble plugs, since the total RCS flow and vessel outlet temperature remain the same. The Loss of Feedwater transient is a slow long-term heatup event and is not sensitive to the rate at which control rods are inserted following a reactor trip. The results of the current analysis of record and conclusions of the UFSAR[1] remain valid.

Feedwater System Pipe Break (UFSAR[1] 15.2.8)

This ANS Condition IV event is analyzed to show that adequate heat removal capability exists using the Auxiliary Feedwater System to remove core decay heat, stored energy and RCS pump heat following reactor trip. This is demonstrated by ensuring that the RCS heatup is turned around prior to the time at which the hotlegs would become saturated.

The Feedline Break accident is a long-term heatup event and is not sensitive to the rate at which the control rods are inserted following a reactor trip. The heat up transient continues for many minutes following the reactor trip. The 0.5 second increase in control rod insertion time will result in an insignificant increase in the integrated heat produced by the core during the transient. No significant increase in hotleg temperature or system pressures would occur due to the increase in control rod insertion time. As an ANS Condition IV event, the minimum DNBR limit acceptance criterion is not applied. As previously noted, the overall transient system response is not affected by the core flow redistribution caused by the elimination of the thimble plugs. The results of the current analysis of record and the conclusions of the UFSAR[1] therefore remain valid.

5.1.4 Decrease in RCS Flow Rate

Partial and Complete Loss of Forced Reactor Coolant Flow (UFSAR[1] 15.3.1 & 15.3.2)

The Partial Loss of Flow accident is an ANS Condition II event. The Complete Loss of Flow accident is an ANS Condition III event. Both of these transients have been reanalyzed in support of N-loop operation. The Partial Loss of Flow transient assumes the coastdown of one RCP during 3-loop, full power operation while the Complete Loss of Flow transient assumes the coastdown of 3 RCPs. The analyses have incorporated the VANTAGE 5H design RCCA drop time of 2.7 seconds in the determination of the thermal-hydraulic conditions existing at the time of minimum DNBR.

The results of these two transients are shown in Figures 5.1-1 through 5.1-4 and 5.1-5 through 5.1-8, respectively. The coastdown transients are shown in Figure 5.1-1 and 5.1-5. Transient calculations were performed to provide a basis for comparison of the analytical pump coastdown characteristics to the plant startup test data. On the basis of this comparison, the analysis calculations are verified to be conservative with respect to actual plant behavior. For both transients, the FACTRAN code[16] is used to calculate the heat flux transient based upon nuclear power and flow from LOFTRAN[17]. The partial loss of flow transient is terminated by a low RCS loop flow reactor trip; the Complete Loss of Flow transient is terminated by reactor trip on reactor coolant pump undervoltage. In both cases, the DNBR safety analysis limit is not violated for the VANTAGE 5H and STD fuel assemblies. Therefore, the safety analysis DNBR limits are met and the conclusions of the UFSAR[1] remain valid.

Forced reactor coolant pump frequency decay in all three RCPs was also reanalyzed for the VANTAGE 5H fuel. The transient assumptions for this case are identical to the Complete Loss of Flow case except for the flow coastdown. The Underfrequency analysis assumed a constant frequency decay rate of 5 Hz/second. No credit is taken for RCP trip on underfrequency. The transient is terminated by reactor trip on RCP underfrequency. The transient results indicate that the safety analysis DNBR limit is not violated for the VANTAGE 5H and STD fuel assemblies. Therefore, the safety analysis acceptance criteria are met for this loss of flow event. It is determined that the underfrequency event is the limiting loss of flow case for these analyzed conditions.

The recommended UFSAR[1] markups for the Partial and Complete Loss of Forced Reactor Coolant Flow accidents are included in Appendix B.

Reactor Coolant Pump Shaft Seizure (UFSAR[1] 15.3.3)

Reactor Coolant Pump Locked Rotor is an ANS Condition IV event analyzed for determination of peak RCS pressure and peak fuel clad temperature assuming DNB to occur in the core. The accident is postulated as an instantaneous seizure of one reactor coolant pump rotor at full power conditions with N loops in operation. Flow through the faulted reactor coolant pump is rapidly reduced leading to an initiation of a reactor trip on a low flow signal. If the reactor is not tripped promptly, clad temperature may exceed the limit value of 2700°F and RCS pressure may increase above that which would cause stresses to exceed the faulted condition stress limits. Therefore, the Locked Rotor transient can be sensitive to an increase in RCCA drop time.

The Locked Rotor transient was reanalyzed to incorporate a 2.7 second RCCA drop time and assuming thimble plug deletion. The FACTRAN code[16] is used to calculate the core hot spot heat flux transient based upon nuclear power and flow from LOFTRAN[17]. The results of the analysis are shown in Figures 5.1-9 through 5.1-12 and Table 5.1-1. Cases with and without offsite power were examined. The case without offsite power assumes coastdown of the unaffected RCPs to be initiated at the beginning of the transient. For both cases analyzed, the peak RCS pressure reached during the transient is less than that which would cause stresses to exceed the faulted condition stress limits. Additionally, the peak clad temperature calculated for the hot spot remains less than 2700°F and the amount of zirconium-water reaction is small. Therefore, it is concluded that the integrity of the primary coolant system is not endangered and the core will remain intact with no consequential loss of core cooling capability.

An analysis was performed to determine the percent of fuel rods in DNB for the Locked Rotor accident. The coolant conditions were calculated with the THINC-IV computer code as specified in the Beaver Valley Unit 2 UFSAR[1]. The MINI-RTDP DNB methodology described in Section 4.2 was used to evaluate the DNB criterion.

It was found that 18% of the fuel rods would be predicted to have minimum DNBRs less than the safety analysis DNBR limit. This calculation is based on a fuel rod power census which is conservative for Cycle 4 operation and is expected to bound all future cycles.

The recommended UFSAR[1] markups for the Single Reactor Coolant Pump Locked Rotor accident are included in Appendix B.

5.1.5 Reactivity and Power Distribution Anomalies

Uncontrolled Rod Cluster Control Assembly (RCCA) Bank Withdrawal from a Subcritical or Low Power Start-Up Condition (UFSAR[1] 15.4.1)

The UFSAR[1] RCCA Withdrawal from Subcritical accident was reanalyzed for the Cycle 2 reload to allow a Beginning-of-Life Least Negative Doppler Power Defect of -0.9% $\Delta\rho$. The analysis performed conservatively assumed a rod drop time of 2.7 seconds, consistent with the design rod drop time for VANTAGE 5H fuel. It was determined that the safety analysis DNBR limits are met. The UFSAR[1] has already been updated to reflect that analysis.

Uncontrolled RCCA Bank Withdrawal at Power (UFSAR[1] 15.4.2)

This ANS Condition II event is analyzed to show that the DNB . ρ basis is met. Various power levels and reactivity insertion rates for both minimum and maximum . activity feedback are analyzed. The transients are terminated by an Overtemperature ΔT or High Neutron Flux reactor trip. As previously noted, the Overtemperature ΔT setpoints are not changed for the transition to VANTAGE 5H, so that the time the reactor trip setpoint is reached would remain the same. The core thermal limits remain unchanged; therefore, only the increase in rod drop time remains to be evaluated. A conservative evaluation of the effects of the 0.5 second increase in control rod drop time was performed by extrapolating the transient DNBR results assuming that the reactor trip was delayed by 0.5 second. The extrapolations showed that ample margin to the DNBR limit still exists with a 0.5 second delay. The conclusions of the UFSAR[1] remain valid.

Control Rod Misalignment (Dropped Full Length Assembly or Statically Misaligned Full Length Assembly) (UFSAR[1] 15.4.3)

RCCA Misoperation is categorized into four types of events. Three of these are classified as ANS Condition II events: dropped RCCA, dropped RCCA bank, and statically misaligned RCCA. The fourth, single RCCA withdrawal, is classified as an ANS Condition III event. The current calculation of the thermal-hydraulic conditions at the time of minimum DNBR for the Condition II events is based on an RCCA insertion time which is greater than the VANTAGE 5H design insertion time of 2.7 seconds. The calculation of percent rods in DNB for the Condition III event conservatively does not credit rod insertion due to reactor trip. In all cases, the conclusions in the UFSAR[1] are

verified for each reload. Specifically, the DNB acceptance criteria is met for the Condition II events and the calculated number of fuel rods experiencing DNB is confirmed to be within the current safety analysis limit of 5% for the Condition III event.

Startup of an Inactive Reactor Coolant Loop (UFSAR[1] 15.4.4)

The Startup of an Inactive Loop transient is an ANS Condition II event analyzed to demonstrate that the DNB design basis is met. The transient was previously reanalyzed incorporating the VANTAGE 5H increased rod drop time of 2.7 seconds. It was determined that the safety analysis DNBR limits are met. The UFSAR[1] has already been updated to reflect that analysis.

Chemical and Volume Control System Malfunction that Results in a Decrease in the Boron Concentration in the Reactor Coolant (UFSAR[1] 15.4.6)

This ANS Condition II event is analyzed to show that adequate time exists for operator action to terminate an inadvertent dilution prior to the loss of shutdown margin. The transient is analyzed for Mode 1 in automatic and manual rod control and in Modes 2 and 3. The Mode 1 case for manual rod control assumes reactor trip on Overtemperature ΔT. The impact of a 0.5 second increase in rod drop time on an operator action time of approximately 15 minutes is imperceptible. The Mode 1 automatic rod control case does not assume reactor trip. The Mode 2 calculation of available operator action time starts at the time of reactor trip. The core flow and the mechanics of the trip are not explicitly modeled in the analysis. In mode 3, all rods are inserted. Thus the analysis results for all three modes are unaffected by the thimble plug elimination and all the UFSAR[1] cases are unaffected by the increase in rod drop time. The UFSAR[1] Boron Dilution accident reactivity insertion transients are bounded by those examined for the Rod Withdrawal at Power accident. Therefore, the Boron Dilution transient calculation does not include an explicit evaluation for the Condition II DNB acceptance criterion. Therefore, the UFSAR[1] conclusions remain valid for these modifications.

Inadvertent Loading and Operation of a Fuel Assembly in an Improper Condition (UFSAR[1] 15.4.7)

This ANS Condition III event addresses the possibility and consequences of one or more fuel pellets having the wrong enrichment or the loading of a fuel assembly without the prescribed amount of burnable poisons. The UFSAR[1] concludes that any significant perturbation from the intended core inventory would be detectable due to the resulting effects on power distribution. VANTAGE 5H

fuel does not affect the ability of core instrumentation to detect unexpected power shapes. Therefore, the UFSAR[1] conclusions remain valid.

Spectrum of Rod Cluster Control Assembly Ejection Accidents (UFSAR[1] 15.4.8)

The RCCA ejection accident is an ANS Condition IV event that is characterized by a rapid power burst. Due to the speed at which the power increases this transient can be sensitive to the RCCA drop time. The limiting criteria for this event are:

1) Average fuel pellet enthalpy at the hot spot below 225 cal/gm for unirradiated fuel and 200 cal/gm for irradiated fuel.
2) Average clad temperature 2700°F.
3) Fuel melting limited to less than the innermost 10 percent of the pellet at the hot spot. (Melting is assumed to occur at 4900°F for BOL conditions and 4800°F for EOL conditions).

The UFSAR[1] RCCA ejection transient beginning and end-of-life cases at hot full power and hot zero power were reanalyzed for the Cycle 2 reload to allow a beginning-of-life least negative doppler power defect of -0.9% $\Delta\rho$. The analysis performed conservatively assumed a rod drop time of 2.7 seconds, consistent with the design rod drop time for VANTAGE 5H fuel. The effects of the thimble plug deletion have been evaluated for these cases. It was determined that in all cases the applicable safety analysis acceptance criteria are met. The UFSAR[1] has already been updated to reflect that analysis.

5.1.6 Increase in Reactor Coolant Inventory

Inadvertent Operation of Emergency Core Cooling System During Power Operation (UFSAR[1] 15.5.1)

The Spurious Operation of the Safety Injection System is an ANS Condition II event. The transient produces a negative reactivity transient causing a reduction in core power. The power reduction causes a decrease in reactor coolant average temperature and consequent coolant shrinkage. Pressurizer pressure and level decrease until the reactor is tripped on the low pressurizer pressure signal. During the transient the DNB ratio never decreases below the initial value, therefore the 0.5

second increase in control rod insertion time will have no effect on the minimum DNBR. Therefore, the conclusions of the UFSAR[1] remain valid.

5.1.7 Decrease in Reactor Coolant Inventory

Inadvertent Opening of a Pressurizer Relief Valve (UFSAR[1] 15.6.1)

This ANS Condition II event is analyzed to show that the DNB design basis is met. This transient is terminated by a reactor trip on Overtemperature ΔT. Minimum DNBR occurs immediately following reactor trip. A conservative evaluation of the effect of the 0.5 second increase in control rod drop time was performed by extrapolating the transient DNBR results assuming that the reactor trip was delayed by 0.5 second. The extrapolations showed that abundant margin to the DNB limit still exists with a 0.5 second increase in rod insertion time. Therefore, the conclusions of the UFSAR[1] remain valid.

5.1.8 Steamline Break Mass and Energy Releases for Postulated Ruptures Inside Containment and Equipment Environmental Qualification Outside Containment

The limiting Steamline Break transient for core response is found in UFSAR[1] Section 15.1.5. The Steamline Break transients analyzed for containment response and equipment qualification, alternatively, are designed to maximize break mass and energy releases. The calculation results are insensitive to the rate at which control rods are inserted. The calculations are not affected by the small decrease in core active flow caused by the deletion of the thimble plugs. Therefore, the mass and energy releases used in containment response calculations and the mass and energy release calculated for equipment qualification outside containment[18] remain valid.

TABLE 5.1-1

Single Reactor Coolant Pump Locked Rotor Accident Results

	3 Loops Operating (with Offsite Power)	3 Loops Operating (without Offsite Power)
Maximum Reactor Coolant System Pressure (psia)	2597	2642
Maximum Clad Temperature (°F) Core Hot Spot	1795	1870
Amount of Zr-H_2O at Core Hot Spot (% by Weight)	0.269	0.415

Figure 5.1-1
Flow Transients for Partial Loss of Flow
Three Loops in Operation,
One Pump Coasting Down

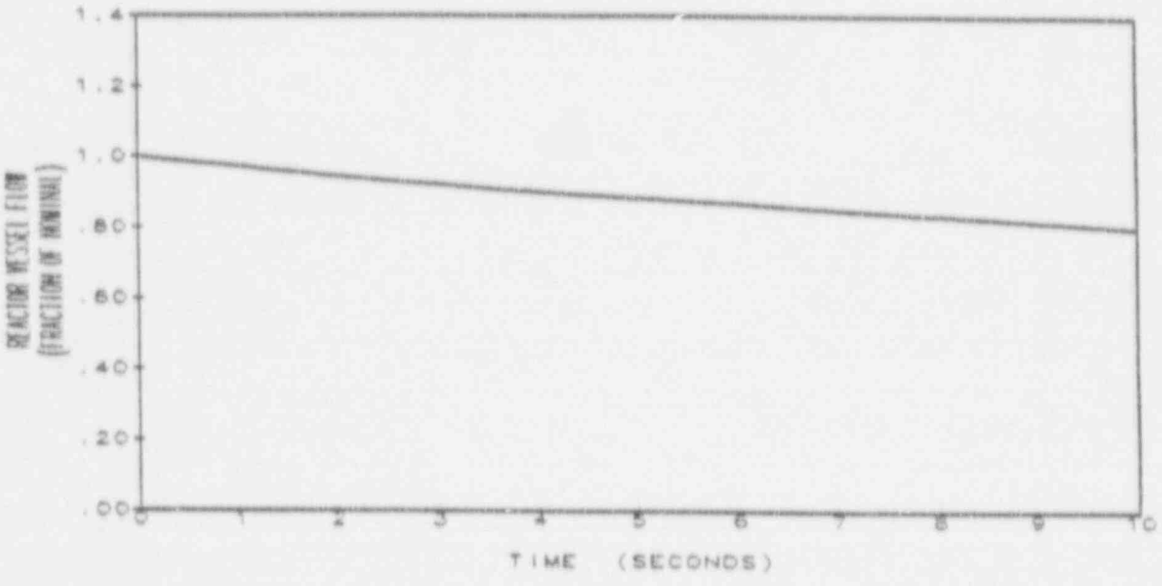

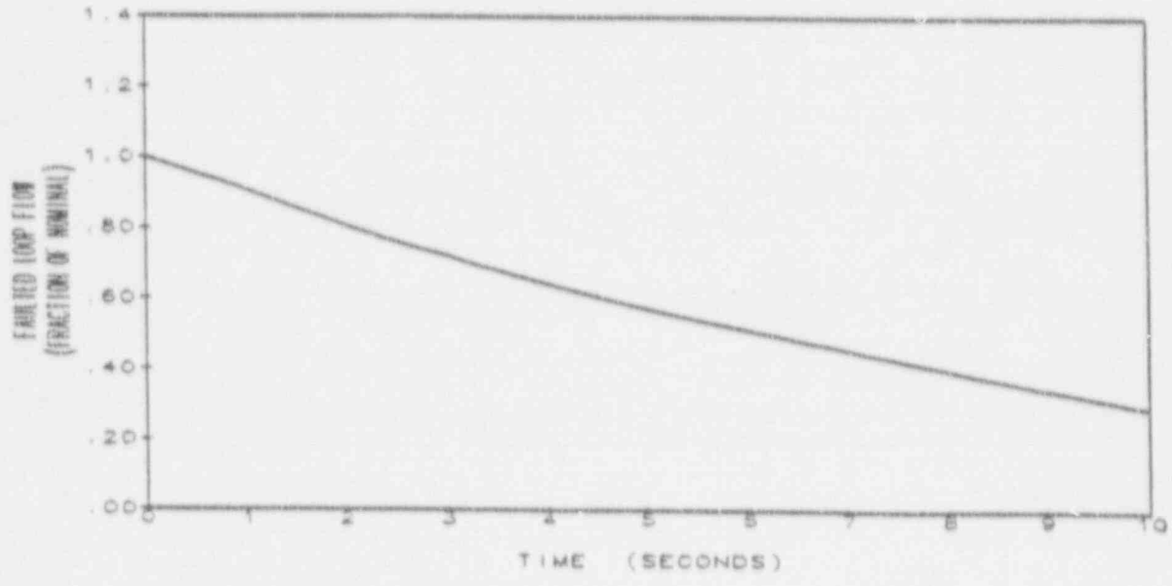

Figure 5.1-2

Nuclear Power and RCS Pressure for Partial Loss of Flow

Three Loops of Operation.

One Pump Coasting Down

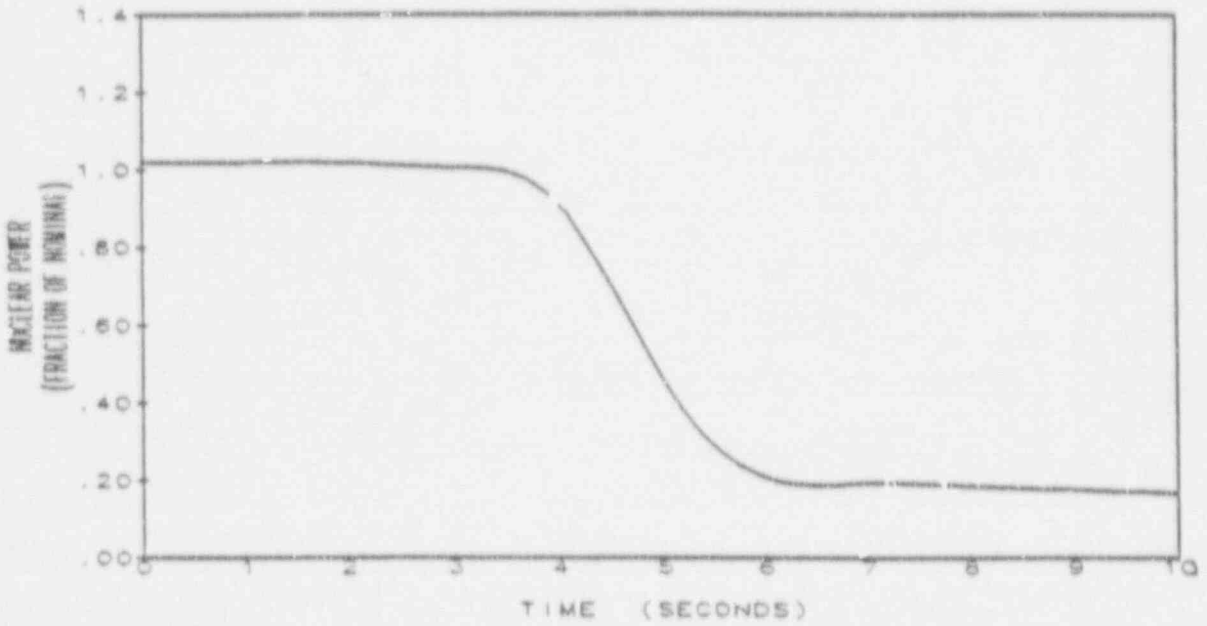

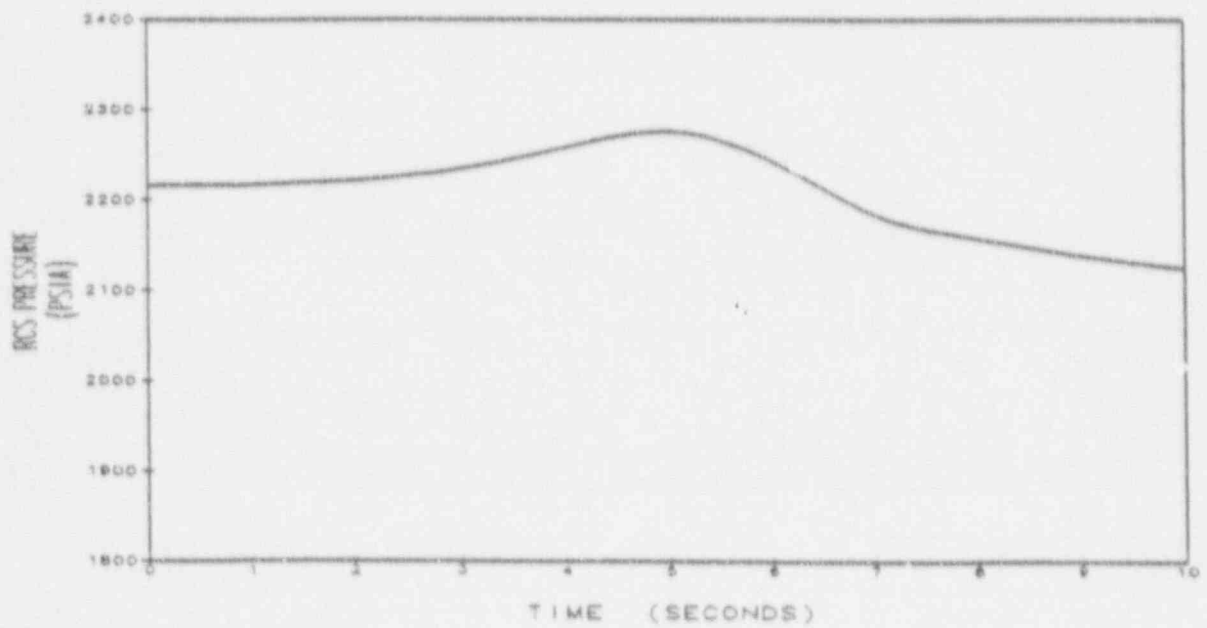

Figure 5.1-3

Average and Hot Channel Heat Flux Transient for Partial Loss of Flow

Three Loops of Operation,

One Pump Coasting Down

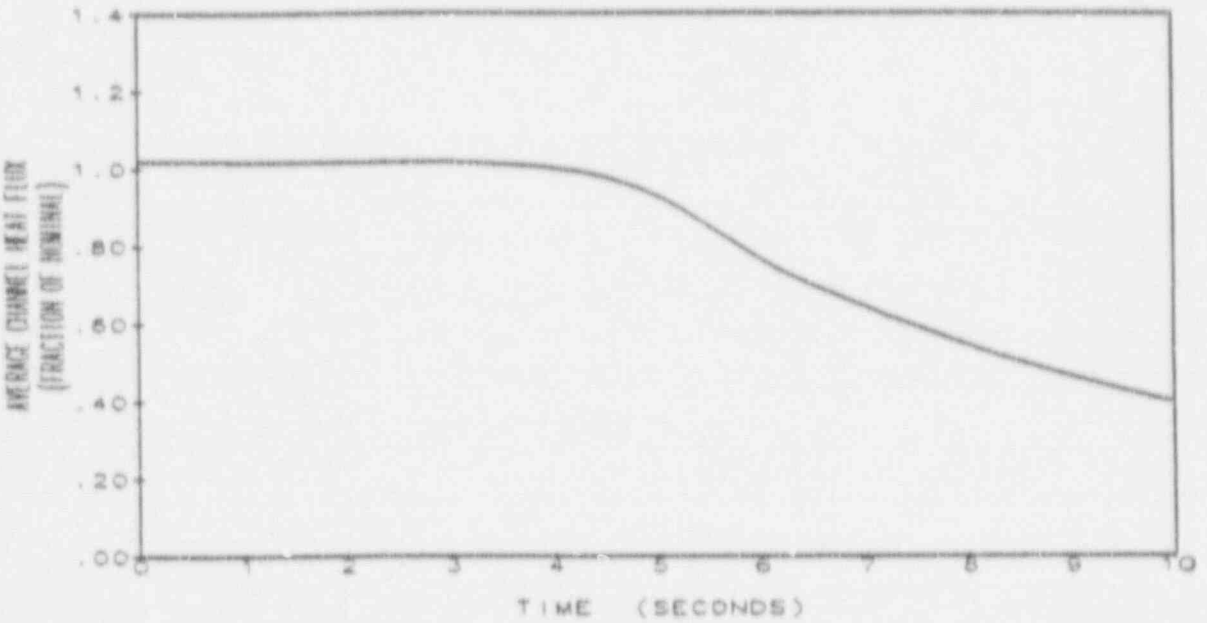

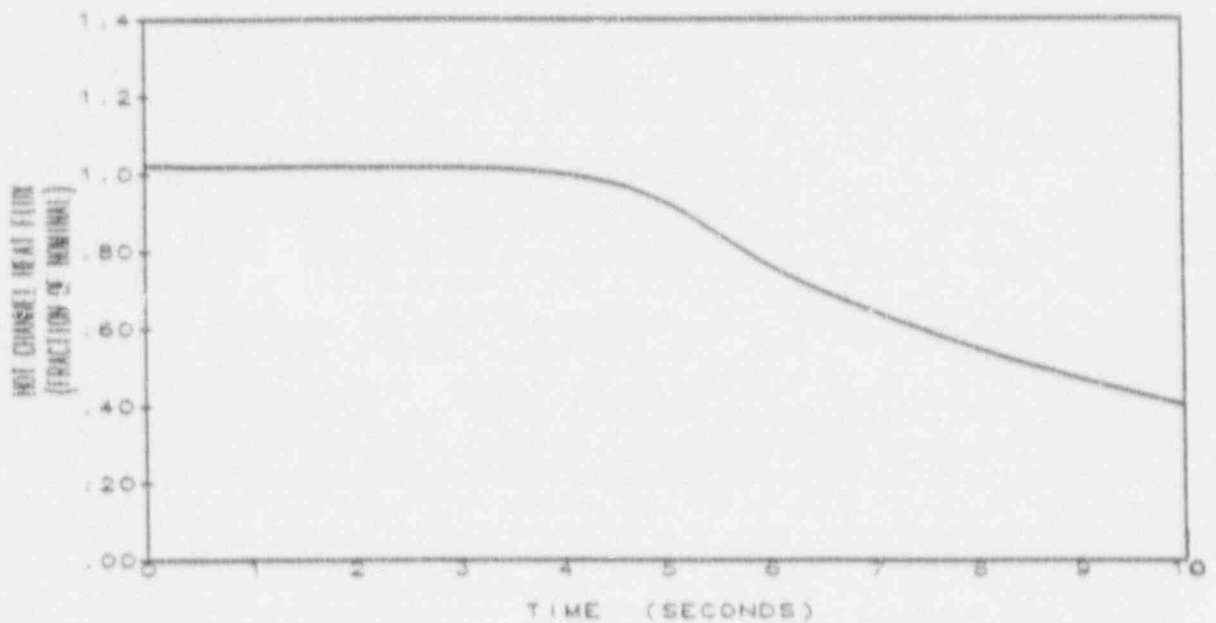

Figure 5.1-4

DNBR versus Time for Partial Loss of Flow

Three Loops in Operation,

One Pump Coasting Down

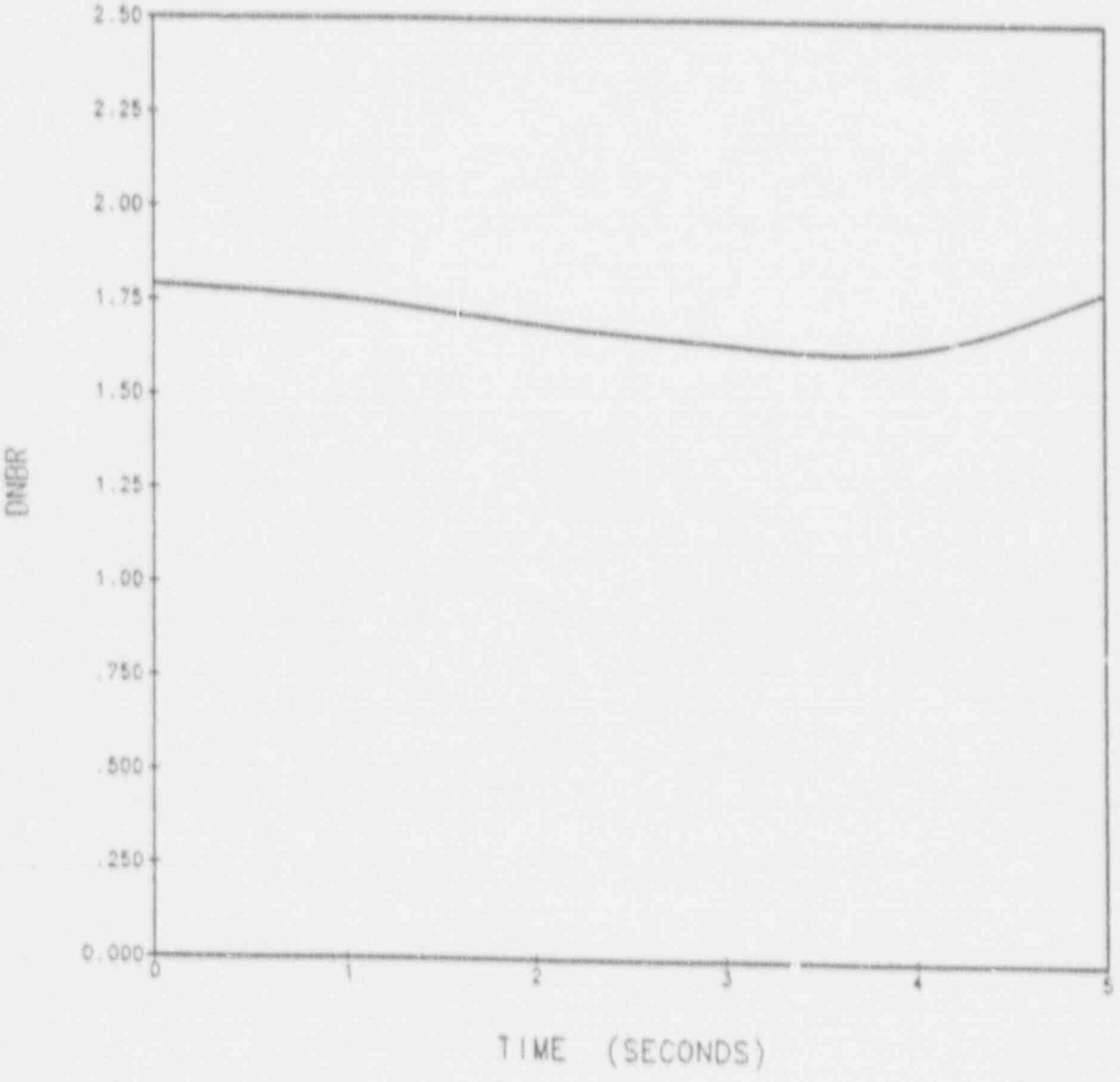

Figure 5.1-5

Core Flow Coastdown versus Time for Three Loops in Operation,

Three Pumps Coasting Down,

Complete Loss of Flow

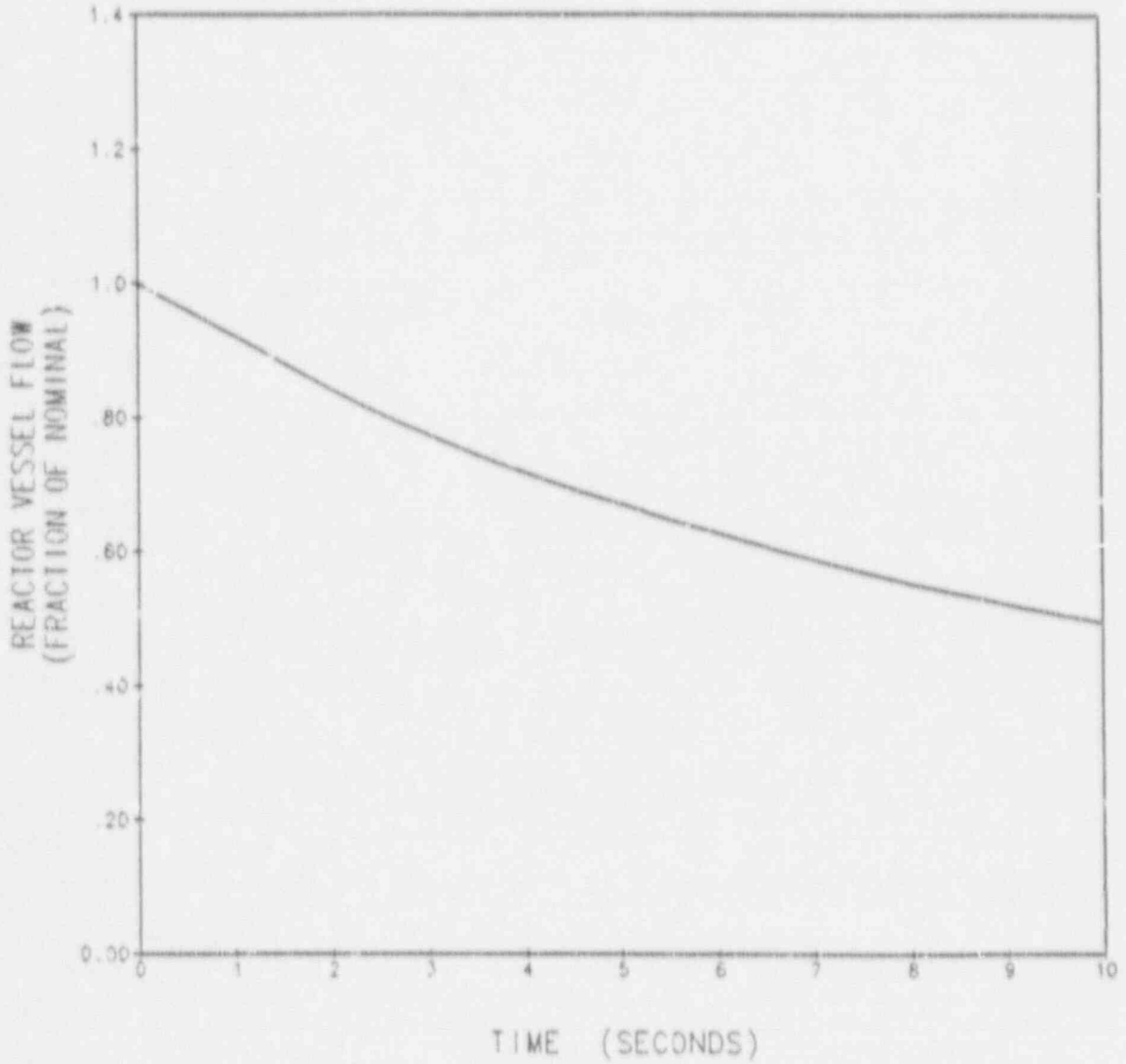

Figure 5.1-6

Nuclear Power Transient and Pressurizer Pressure Transient

For Three Loops in Operation,

Three Loops Coasting Down, Complete Loss of Flow

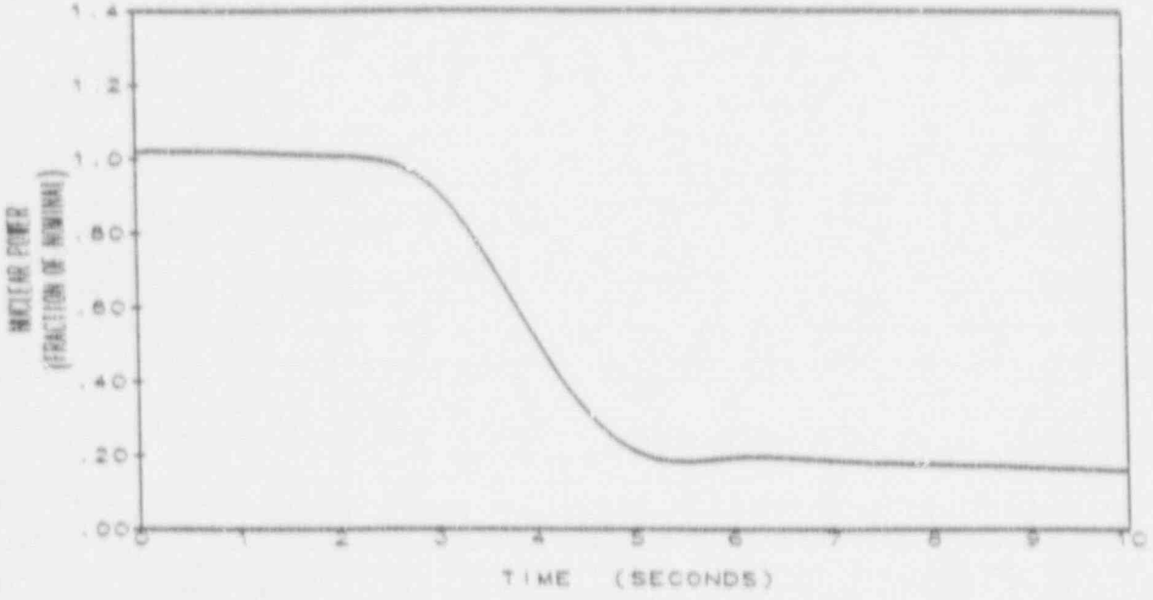

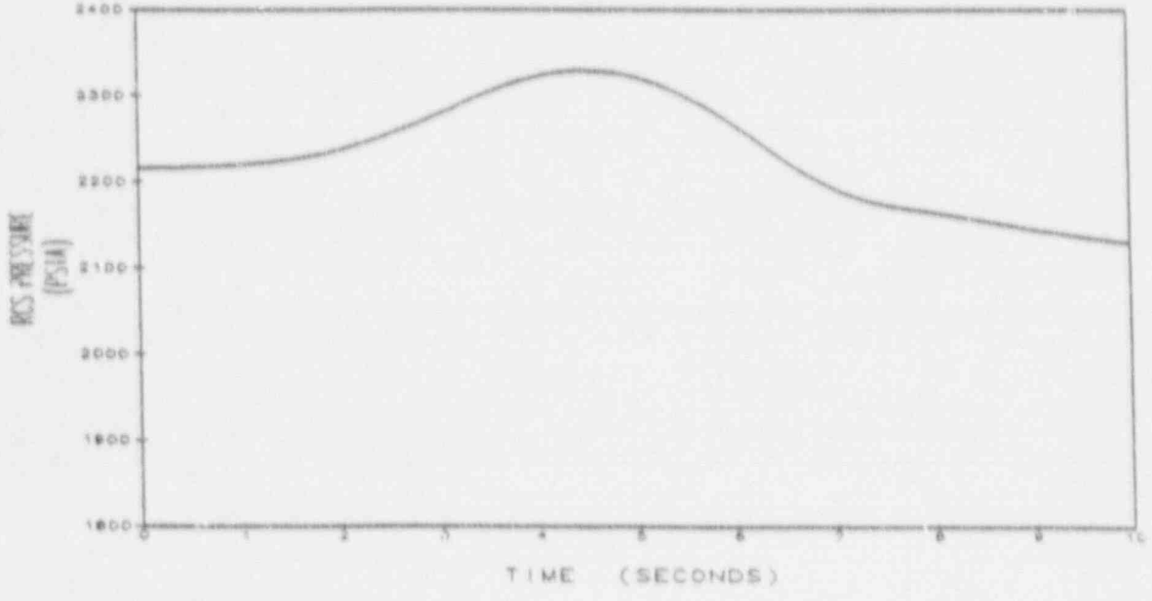

Figure 5.1-7

Average and Hot Channel Heat Flux Transients

For Three Loops in Operation,

Three Loops Coasting Down, Complete Loss of Flow

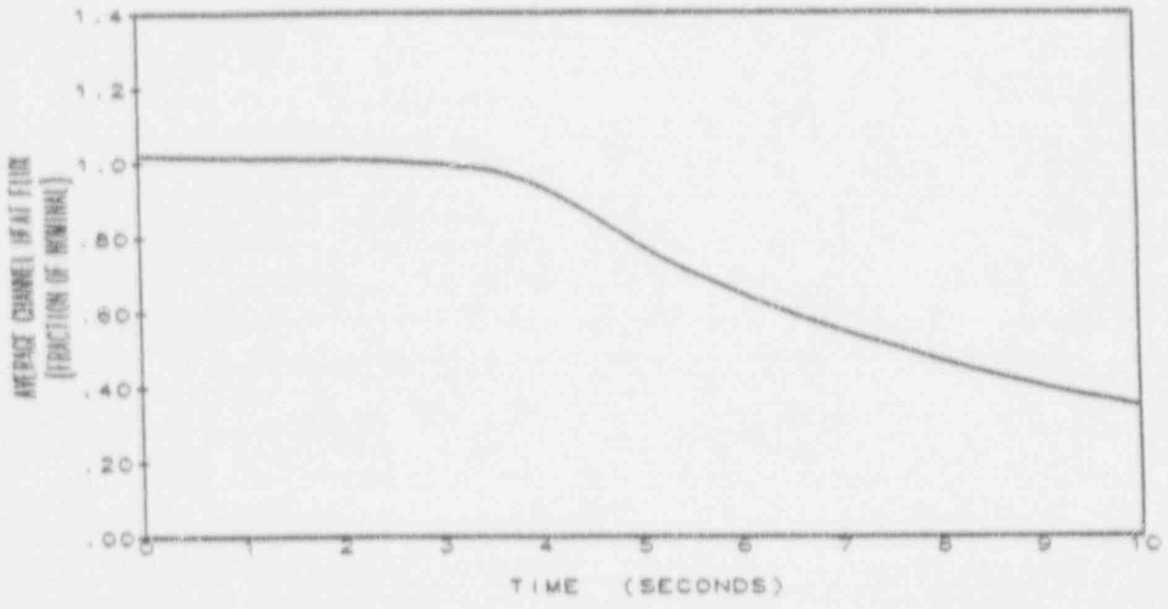

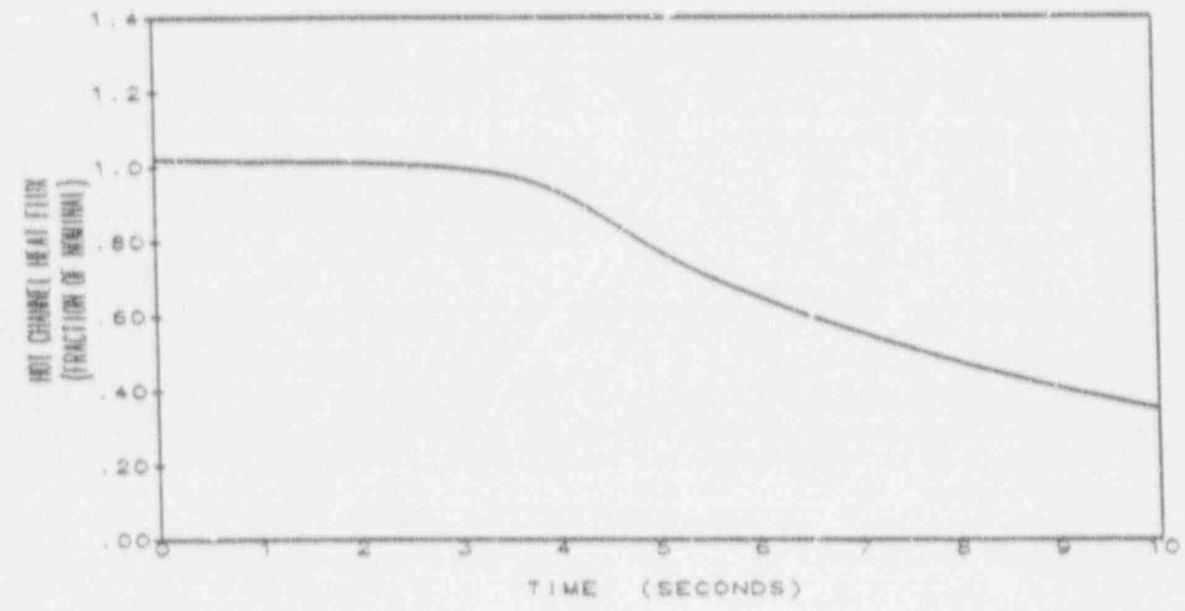

Figure 5.1-8

DNBR vs Time for Three Loops in Operation,

Three Loops Coasting Down,

Complete Loss of Flow

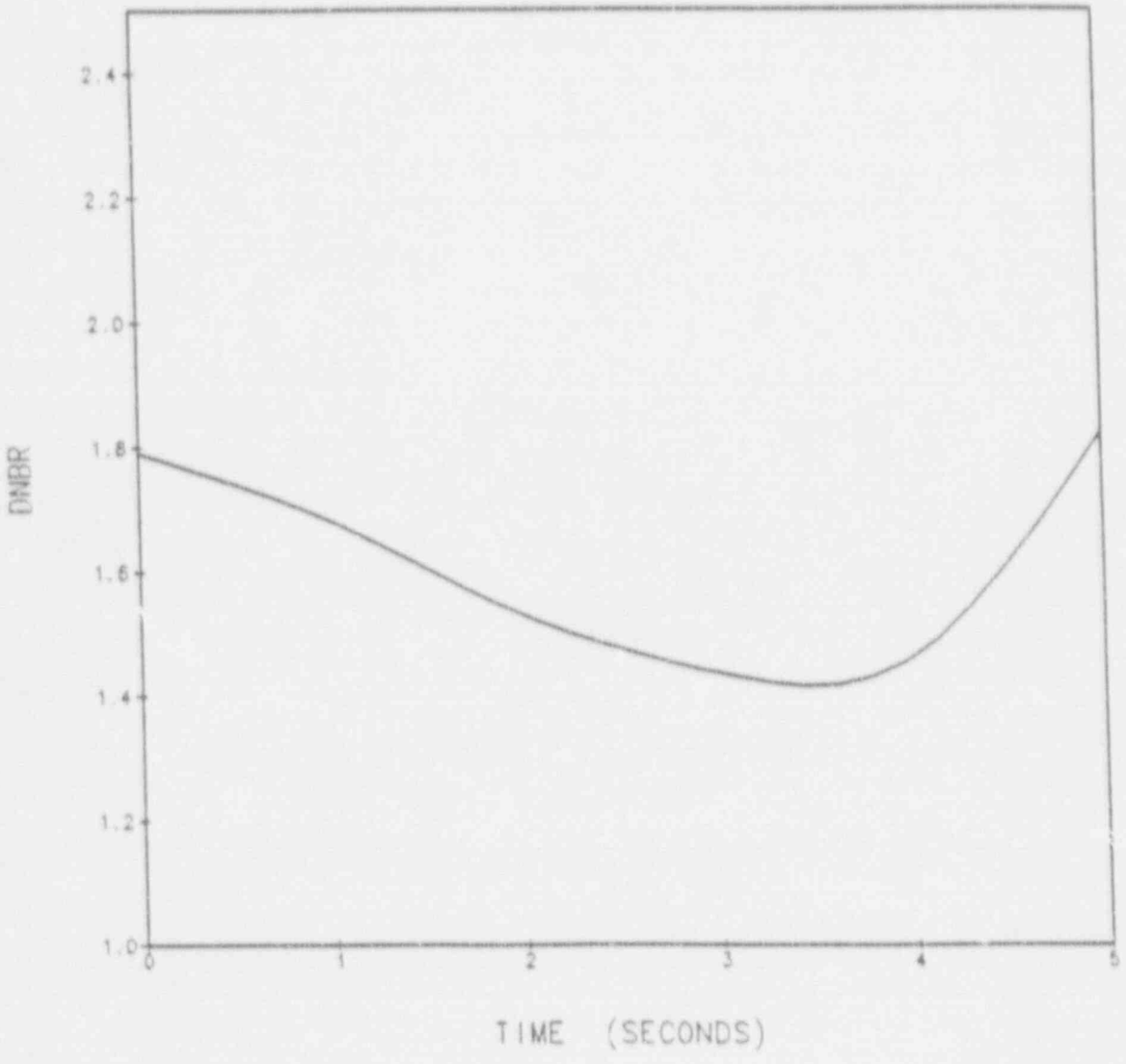

Figure 5.1-9

Flow Transients for Three Loops in Operation, One Locked Rotor

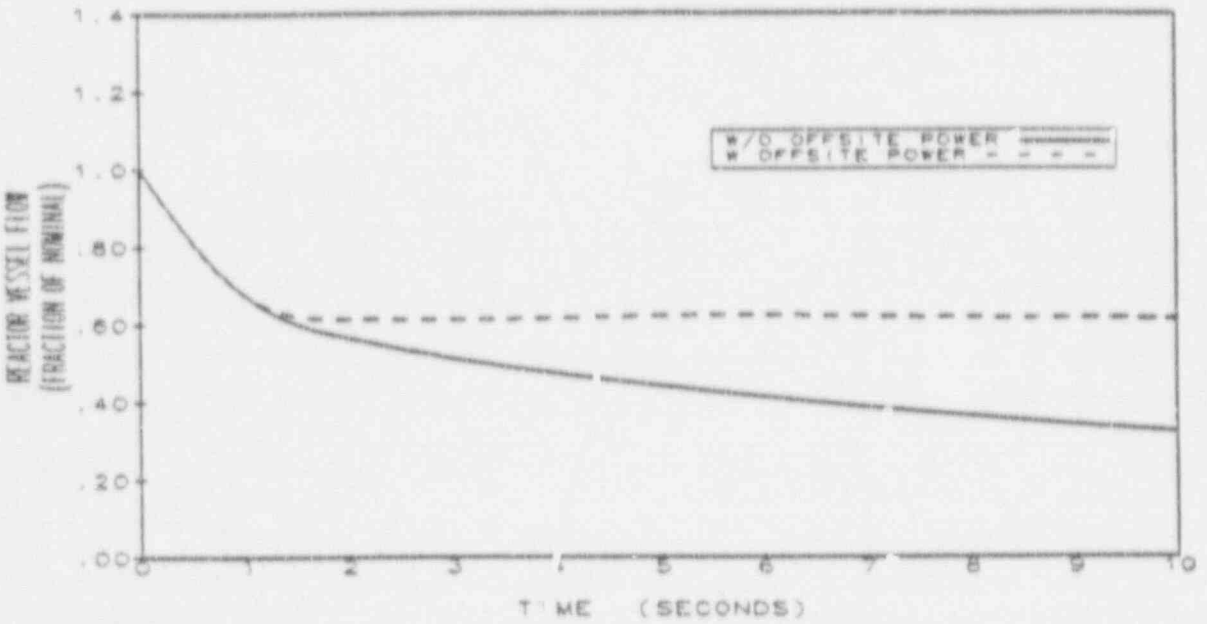

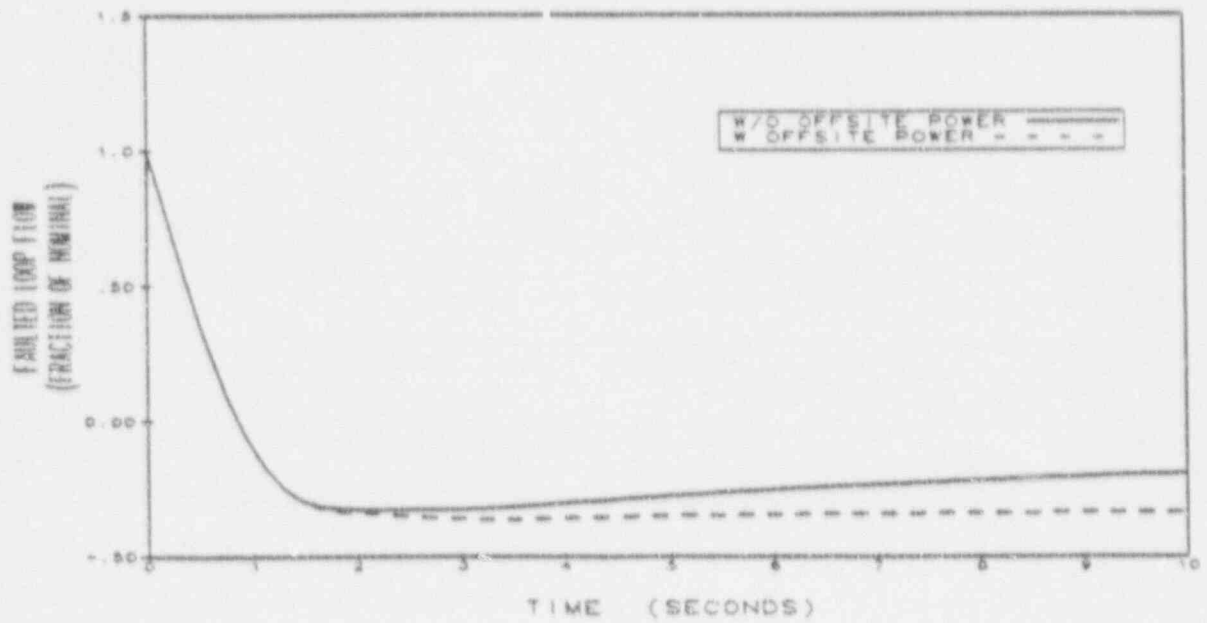

Figure 5.1-10

Reactor Coolant System Pressure Transient

for Three Loops in Operation

One Locked Rotor

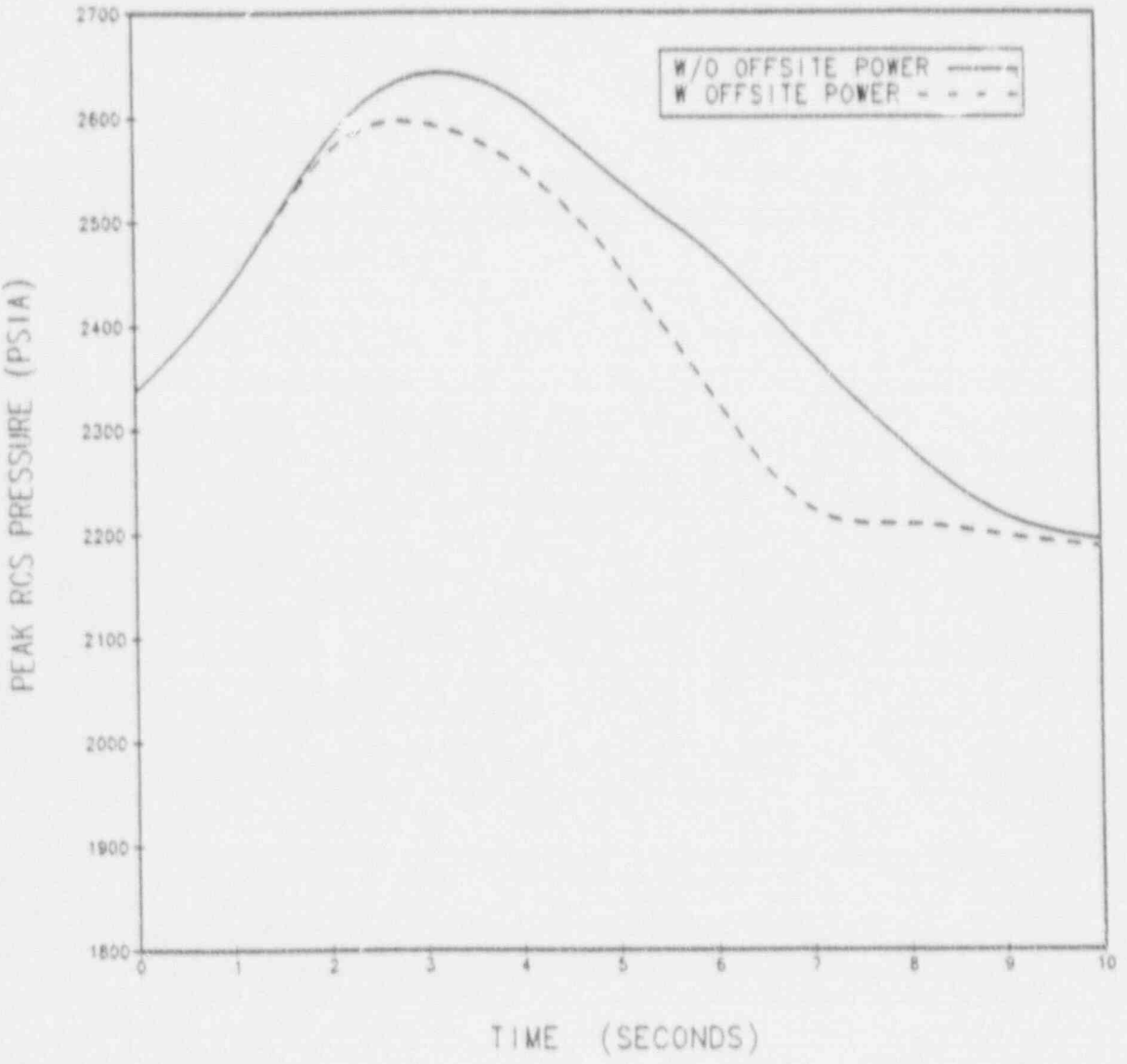

Figure 5.1-11

Nuclear Power Transient, Average and Hot Channel Heat Flux Transients for Three Loops in Operation, One Locked Rotor

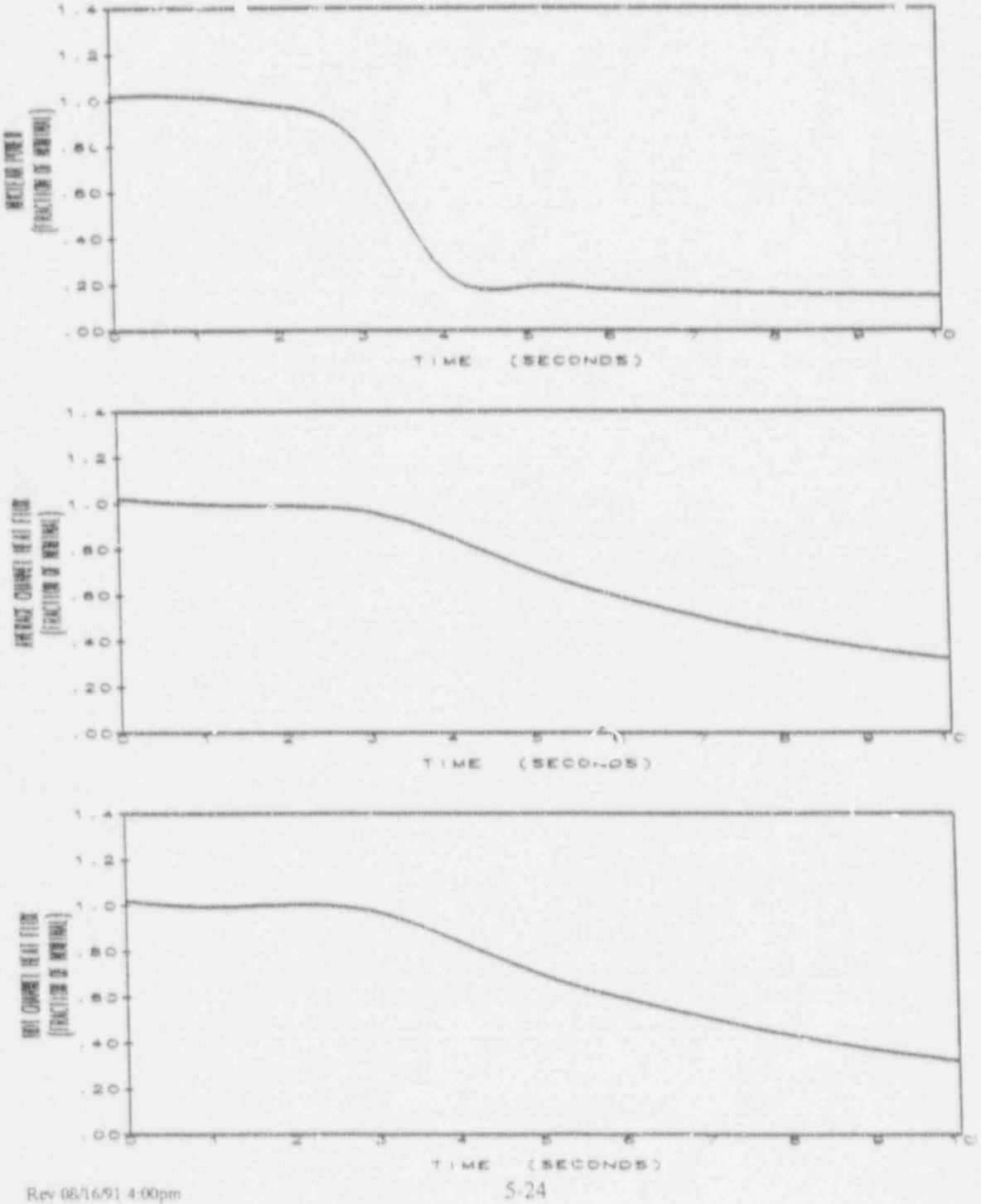

Figure 5.1-12
Maximum Clad and Fuel Centerline Temperatures
at Hot Spot for Three Loops in Operation
One Locked Rotor

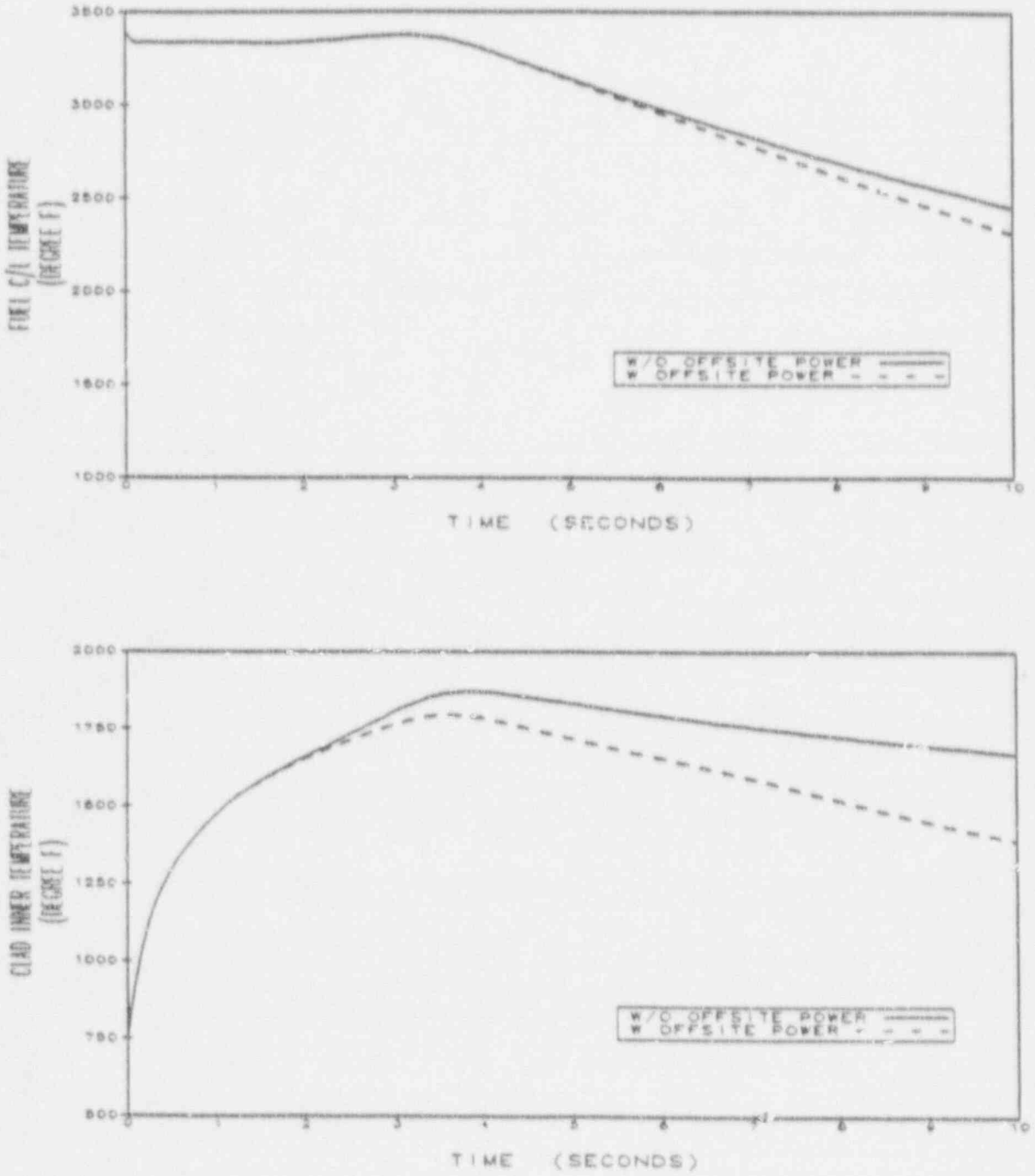

5.2 LOCA Accidents

This section summarizes the evaluations performed to assess the effects of the thimble plug removal and the VANTAGE 5H low pressure drop Zircaloy grid fuel feature on the Beaver Valley Unit 2 LOCA analyses.

Large Break LOCA (LBLOCA)(UFSAR[1] Section 15.6.5)

The Beaver Valley Unit 2 LBLOCA analysis of record, which is presented in the UFSAR[1], is a BART Evaluation Model (EM) analysis with a PCT of 2120°F. PCT penalties to the analysis have been assigned as most recently documented in Reference 19, which indicated a cumulative PCT of 2176°F.

As noted in the VANTAGE 5H Fuel Assembly Report[3], the low pressure drop Zircaloy grids have no adverse effect on the LOCA analyses due to the mechanical and hydraulic similarity to 17x17 STD fuel. The Zircaloy grids provide a Peak Clad Temperature (PCT) benefit due to increased rewetting when compared with the 17x17 STD grid. Additional differences introduced by the VANTAGE 5H assembly, such as slight flow area changes attributed to thimble tube diameter, have been evaluated as having negligible impact on the LBLOCA analysis.

An evaluation has been performed, based upon the BART EM, to consider any other effects on the analysis due to the VANTAGE 5H fuel. The LBLOCA evaluation model does not take credit for the negative reactivity introduced by the control rods. Instead, the reactor is brought to a subcritical condition by the presence of voids in the core caused by the rapid depressurization of the RCS. Since credit is not taken for the negative reactivity introduced by the control rods, the increase in design rod drop time will have no effect on the results.

As noted in the VANTAGE 5H Fuel Assembly Report[3], LOCA reanalysis is not needed in transitioning from 17x17 STD to 17x17 VANTAGE 5H without Intermediate Flow Mixers (IFMs) if there is available margin to the 10CFR50.46 limits to accommodate any LOCA transition core penalty. The transition from 17x17 STD fuel to 17x17 VANTAGE 5H fuel without IFMs results in no transition core peak cladding temperature penalty[3][5].

Thimble plug removal results in a decrease in the core pressure drop. Core pressure drop is modeled primarily in the SATAN blowdown portion of the LBLOCA transient. Sensitivity studies have shown that a lower core pressure drop results in a more benign transient. Therefore, for LBLOCA, thimble plug removal is an unquantified benefit.

A temporary allocation of 16°F of PCT margin has been assessed for an issue under investigation associated with Beginning-of-Life (BOL) Rod Internal Pressure Uncertainty.

Based on the discussion given above, the use of VANTAGE 5H zircaloy grids and thimble plug removal will not result in an increase in the peak clad temperature for Beaver Valley Unit 2 LBLOCA. Therefore, these changes are [redacted]able and the resulting cumulative LBLOCA PCT (2176°F + 16°F = 2192°F) remains within the regulatory limit.

Small Break LOCA (SBLOCA)(UFSAR[1] Section 15.6.5)

The Beaver Valley Unit 2 SBLOCA analysis of record, which is presented in the UFSAR[1], is a NOTRUMP EM analysis with a PCT of 1399°F. PCT penalties to the analysis have been assigned as most recently documented in Reference 19, which indicated a cumulative PCT of 2121°F.

The only VANTAGE 5H Zircaloy grid feature which significantly affects the SBLOCA analysis is the increase in design rod drop time. The Westinghouse Small Break model assumes the reactor core is brought to a subcritical condition by the negative reactivity of the control rods. The increase in the design rod drop time to a maximum value of 2.7 seconds exceeds the 2.4 second value in the existing SBLOCA analysis.

An evaluation was performed which determined that a 3°F PCT penalty applied for the increase in rod drop time of 0.3 seconds. The decrease in core pressure drop associated with thimble plug removal has an inconsequential effect on the SBLOCA analysis. However, the SBLOCA analysis did not model the effect of the guide thimble interior area and volume on the transient response. Studies have shown that the fluid in this volume will interact with the remaining core fluid. An assessment of this interaction based on previous sensitivities indicated that a 17°F PCT penalty applies.

A temporary allocation of 20°F of PCT margin has been assessed for an issue under investigation associated with Beginning-of-Life (BOL) Rod Internal Pressure Uncertainty.

The revised cumulative SBLOCA PCT after considering the VANTAGE 5H Zircaloy grid, and thimble plug removal, is 2161°F (2121°F + 3°F + 17°F + 20°F). Therefore, these changes are acceptable and the resulting cumulative PCT remains within the regulatory limit.

Steam Generator Tube Failure (UFSAR[1] Section 15.6.3)

For the Steam Generator Tube Rupture (SGTR) event, the Beaver Valley Unit 2 UFSAR[1] SGTR analysis was performed using the LOFTRAN computer code. Reference 15 documents the evaluation of steam generator tube plugging levels up to 20% (with thermal design flow maintained on a per loop basis) to determine the impact on the UFSAR[1] SGTR analysis. The referenced evaluation also integrated the effects of the incorporation of VANTAGE 5H fuel and thimble plug deletion. The results of this evaluation indicated that the offsite doses reported in the Beaver Valley Unit 2 UFSAR[1] for an SGTR remain bounding, therefore, no changes are recommended for the transition to VANTAGE 5H fuel.

Presently a change in the steam generator tube rupture methodology for Beaver Valley Unit 2 is being reviewed by the Nuclear Regulatory Commission. This change incorporates the LOFTTR2 analysis for steam generator overfill and offsite radiation doses as documented in Reference 20. This "updated" SGTR analysis was expressly performed to be applicable for Beaver Valley Unit 2 operation with either Standard or VANTAGE 5H fuel, and incorporated the thimble plug deletion.

Blowdown Reactor Vessel and Loop Forces (UFSAR[1] Section 3.9N)

An evaluation has been prepared that considered the effects of VANTAGE 5 Hybrid fuel implementation and Thimble Plug deletion on the LOCA hydraulic forces and structural analyses. The LOCA hydraulic forces are unaffected by the proposed changes because the significant input parameters to the codes used to calculate the LOCA hydraulic forces, MULTIFLEX, LATFORC, and FORCE2[21], were essentially unchanged. Additionally, differences in fuel type have traditionally had a small effect on the magnitude of the hydraulic forces. The evaluation of the structural integrity

showed that, since the magnitude of the LOCA hydraulic forces do not change appreciably, the conclusions of WCAP-8784-P-A Addendum 1 remain unchanged by the proposed modifications. Thus, the conclusions of WCAP-11523-NP-A[22] remain unchanged as well.

Post LOCA Long-Term Cooling, Subcriticality Evaluation (related to UFSAR[1] Section 15.6.5)

The Westinghouse licensing position for satisfying the requirements of 10CFR Part 50 Section 46 Paragraph (b) Item (5) "Long-Term Cooling" is defined in WCAP-8339-NP-A[23], WCAP-8472-NP-A[24], and Technical Bulletin NSID-TB-86-08[25]. The Westinghouse commitment is that the reactor will remain shutdown by borated ECCS water alone after a LOCA. Since credit for the control rods is not taken for a LBLOCA, the borated ECCS water provided by the accumulators and the RWST must have a concentration that, when mixed with other sources of borated and non-borated water, will result in the reactor core remaining sub ritical assuming all control rods out.

Since the use of VANTAGE 5H Zircaloy grids (including the associated increase in design rod drop time) and thimble plug removal will have a negligible affect on the sources of borated and non-borated water assumed in the long term cooling calculation, it is concluded that there would be no change to the long term cooling capability of the ECCS system. Further, this licensing commitment is checked by Westinghouse on a cycle by cycle basis, ensuring compliance with this requirement independent of this safety evaluation.

Hot Leg Switchover to Prevent Potential Boron Precipitation/Long Term SI Verification (UFSAR[1] 6.3.2.5/Table 6.3-7)

Post-LOCA hot leg recirculation time is determined for inclusion in emergency procedures to ensure no boron precipitation in the reactor vessel following boiling in the core. This recirculation time is dependent on power level, and the RCS, RWST, and accumulator water volumes and boron concentrations. The VANTAGE 5H Zircaloy grids (including the associated increase in design rod drop time) and thimble plug removal will have a negligible effect on the assumptions for the RCS, RWST, and the accumulators in the hot leg switchover calculation. Thus, there is no effect on the post-LOCA hot leg switchover time.

Westinghouse recently performed the Long Term ECCS Safety Injection (SI) Verification (Cold Leg and Hot Leg Recirculation) for Unit 2 as part of the Recirc Spray Modification Safety Evaluation[26]. Since the HLSO time was not affected, and the VANTAGE 5H and thimble plug removal upgrades do not effect SI performance, the Cold Leg and Hot Leg Recirculation Long Term Cooling SI Verifications contained therein remain appropriate.

LOCA Containment Integrity (UFSAR[1] 15.3.4)

There is no impact on the short term mass and energy and subcompartment pressure analysis since fuel design changes and upgrades, including the increase in design rod drop time and peaking factor increases, have a negligible affect on the transient. For the short term subcompartment analyses, approximately only the first 3 seconds of the blowdown are negligibly affected.

The long term mass and energy and containment peak pressure analysis is not adversely affected by the fuel upgrade, including the associated increase in design rod drop time, or increased peaking factors since the plant T_{avg} remains the same. Additionally, the VANTAGE 5H fuel rod is the same as that used in the STD 17x17 fuel assembly. Since the fuel rod designs are the same, there is no difference in initial core stored energy, and hence no additional energy would be available for release to containment.

In summary, there is no impact on the UFSAR[1] LOCA containment integrity analyses due to the increase in peaking factors and the use of upgraded Westinghouse fuel features, including the VANTAGE 5H fuel design, for Beaver Valley Unit 2.

5.3 Accident Analysis Conclusion

Sections 5.0, 5.1 and 5.2 have summarized the impact on the LOCA and non-LOCA design basis calculations of the introduction of the VANTAGE 5H low pressure Zircaloy grids and thimble plug removal that will be in Cycle 4 of Beaver Valley, Unit 2.

In most cases it was found that all the intended Cycle 4 modifications are supported by the existing licensing basis safety analyses. In these cases it was concluded that specific safety analyses are

insensitive to the fuel and thimble plug removal upgrades or have otherwise incorporated bounding analyses assumptions, such as the LBLOCA analysis. A total of 20°F of permanent SBLOCA PCT margin, 20°F of temporary SBLOCA PCT margin and 16°F of temporary LBLOCA PCT margin were assessed. Explicit reanalyses were required for non-LOCA transients sensitive to the increased design RCCA drop time associated with the VANTAGE 5 Hybrid fuel. The WRB-1 correlation and the MINI-RTDP methodology have been introduced to evaluate transient DNBRs for both the Standard and VANTAGE 5 Hybrid fuel.

All transient reanalyses and evaluations demonstrate that all applicable safety analysis acceptance criteria continue to be met for the intended fuel and design upgrades that will be introduced in Cycle 4 of Beaver Valley Unit 2.

6.0 References

6.0 REFERENCES

1. Updated Final Safety Analysis Report, Beaver Valley Power Station, Unit 2, Revision 2B/3, 1991.

2. Davidson, S. L. (Ed.), et. al., "Westinghouse Reload Safety Evaluation Methodology," WCAP-9273-NP-A, July 1985.

3. Davidson, S. L. (Ed.), et. al., "VANTAGE 5H Fuel Assembly," WCAP-10444-P-A, Addendum 2, April 1988 and Letter from W. J. Johnson (Westinghouse) to M. W. Hodges (NRC), NS-NRC-88-3363, dated July 29, 1988, "Supplemental Information for WCAP-10444-P-A Addendum 2, 'VANTAGE 5H Fuel Assembly'".

4. Davidson, S. L. (Ed.), et. al., "VANTAGE 5 Fuel Assembly Reference Core Report," WCAP-10444-P-A, September 1985.

5. Letters from A. C. Thadani (NRC) to R. A. Wiesemann (Westinghouse): "Acceptance for Referencing of Topical Report WCAP-10444-P-A, Addendum 2, 'VANTAGE 5H Fuel Assembly'," November 1, 1988 and Clarifications on the Safety Evaluation of the Topical Report WCAP-10444-P-A Addendum 2, January 5, 1989.

6. Skaritka, J. (Ed.), "Operational Experience with Westinghouse Cores," (through December 31, 1989) WCAP-8183, Revision 18, December 1990.

7. Letter from W. J. Johnson (Westinghouse) to M. W. Hodges (NRC), "Application of Enriched Boron in the Westinghouse Integral Fuel Burnable Absorber Design," NS-NRC-89-3454, September 6, 1989.

8. Miller, J. V. (Ed.), "Improved Analytical Model used in Westinghouse Fuel Rod Design Computations," WCAP-8785, October 1976.

9. Weiner, R. A., et. al., "Improved Fuel Performance Models for Westinghouse Fuel Rod Design and Safety Evaluations," WCAP-10851-P-A, August 1988.

10. F. E. Motley, K. W. Hill, F. F. Cadek, and J. Shefchek, "New Westinghouse Correlation WRB-1 for Predicting Critical Heat Flux in Rod Bundles with Mixing Vane Grids," WCAP-8762-P-A, July 1984.

11. Friedland, A. J., and Ray, S., "Revised Thermal Design Procedure," WCAP-11397, February 1987. [Also Letter from A. C. Thadani (NRC) to W. J. Johnson (Westinghouse), "Acceptance for Referencing of Licensing Topical Report WCAP-11397, 'Revised Thermal Design Procedure'," January 17, 1989.]

12. Ray, S., "MINI Revised Thermal Design Procedure (MINI RTDP)," WCAP-12178-P, March 1989.

13. Letter from D. F. Ross, Jr. (NRC) to D. B. Vassala (NRC), "Topical Report Evaluation for WCAP-8762," April 10, 1978.

14. Letter from Steinmetz (Westinghouse) to Halliday (DLCo), "Beaver Valley Power Station Unit 2 Justification for Continued Operation with current Overtemperature and Overpressure ΔT Setpoints," DLW-91-147, June 3, 1991.

15. Letter from Steinmetz (Westinghouse) to Halliday (DLCo), "SGTP Analysis Program Engineering and Licensing Report," DLW-91-155, June 5, 1991.

16. Gunin, C., "FACTRAN, A FORTRAN IV Code for Thermal Transients in a UO_2 Fuel Rod," WCAP-7908, June 1972.

17. Burnett, T. W., McIntyre, C. J., Baker, J. C., and Rose, R. P., "LOFTRAN Code Description," WCAP-7907, June 1972.

18. Butler, J. C., Love, D. S., et. al., "Steam Line Break Mass/Energy Releases for Equipment Environmental Qualification Outside Containment - Report to Westinghouse Owner's Group," WCAP-10961-P, Revision 1, October 1985.

19. Letter from Steinmetz (Westinghouse) to Noonan (DLCo), "ECCS Evaluation Model Reporting," DLW-91-159, June 20, 1991.

20. Schrader, K. J., Holderbaum, D. F., Lewis, R. N., Marmo, C. A., and Rubin, K., "LOFTTR2 Analysis for a Steam Generator Tube Rupture for Beaver Valley Power Station Unit 2," WCAP-12737, October 1990.

21. Takeuchi, K., et. al., "A FORTRAN-IV Computer Program for Analyzing Thermal-Hydraulic Structure System Dynamics," WCAP-8709-NP-A, February 1976.

22. Garner, D. C., et. al., "Response to NRC Questions on the LOCA Hydraulic Forces Analysis of Beaver Valley Power Station Unit 2," WCAP-11523-NP-A, July 1987.

23. Bordelon, F. M., Massie, H. W., and Zordan, T. A., "Westinghouse ECCS Evaluation Model Summary," WCAP-8339-NP-A, July 1974.

24. Bordelon, F. M., et. al., "Westinghouse ECCS Evaluation Model: Supplementary Information," WCAP-8472-NP-A, April 1975.

25. Letter from J. A. Triggiani (Westinghouse) to W. S. Lacey (DLCo), "DLCo BV Unit 1 Technical Bulletin NSID-TB-86-08 Post-LOCA Long-Term Cooling: Boron Requirements," DLW-86-670, December 1, 1986.

26. Letter from Steinmetz (Westinghouse) to Halliday (DLCo), "Beaver Valley Power Station Unit 2 Recirculation Spray System Modification Safety Evaluation," DLW-91-182, July 3, 1991.

REFERENCE CROSS-REFERENCE LISTING

Reference Number	Page Number
1.	1-1, 3-1, 4-1, 5-3, 5-4, 5-5, 5-6, 5-7, 5-8, 5-9, 5-10, 5-11, 5-12, 5-26, 5-27, 5-28, 5-29, 5-30
2.	1-1, 3-1
3.	1-1, 4-1, 4-2, 4-3, 5-25
4.	1-1, 1-2, 2-3, 2-4
5.	1-1, 1-2, 5-26
6.	2-2
7.	2-3
8.	2-4
9.	2-4
10.	4-1
11.	4-1
12.	4-1
13.	4-1
14.	5-2
15.	5-2, 5-28
16.	5-7, 5-8
17.	5-7, 5-8
18.	5-12
19.	5-26, 5-27
20.	5-28
21.	5-28
22.	5-29
23.	5-29
24.	5-29
25.	5-29
26.	5-30

Appendix A
Technical Specifications Revisions

Technical Specification Markup

SUMMARY OF TECHNICAL SPECIFICATION CHANGES
FOR FUEL UPGRADE FOR
BEAVER VALLEY POWER STATION UNIT 2

Page	Section	Description	Justification
B 2-1 B 2-3 B 3/4 2-1 B 3/4 2-4 B 3/4 2-5 B 3/4 4-1	2.1.1 2.2.1 Basis 3/4.2 Basis 3/4.2.2 Basis 3/4.2.3 Basis 3/4.4.1 Basis	Changed W-3 (R-Grid) correlation to WRB-1 correlation and added design DNBR limits.	This change reflects the LNB correlation used for Standard and VANTAGE 5H fuel.
3/4 1-23	3.1.3.4	Revised rod drop time to less than or equal to 2.7 seconds.	This change is a result of changes in the fuel due to the VANTAGE 5H fuel design. The effect of this increase on safety analysis has been considered.
B 3/4 2-4	3/4.2.3	Revised DNBR margin for meeting rod bow penalty.	This change reflects change in DNB correlation and methods.

BASES

2.1.1 REACTOR CORE

The restrictions of this safety limit prevent overheating of the fuel and possible cladding perforation which would result in the release of fission products to the reactor coolant. Overheating of the fuel cladding is prevented by restricting fuel operation to within the nucleate boiling regime where the heat transfer coefficient is large and the cladding surface temperature is slightly above the coolant saturation temperature.

Operation above the upper boundary of the nucleate boiling regime could result in excessive cladding temperatures because of the onset of departure from nucleate boiling (DNB) and the resultant sharp reduction in heat transfer coefficient. DNB is not a directly measurable parameter during operation and therefore THERMAL POWER and Reactor Coolant Temperature and Pressure have been related to DNB through the [redacted] correlation. The [redacted] DNB correlation has been developed to predict the DNB flux and the location of DNB for axially uniform and non-uniform heat flux distributions. The local DNB heat flux ratio, DNBR, defined as the ratio of the heat flux that would cause DNB at a particular core location to the local heat flux, is indicative of the margin to DNB.

WRB-1

WRB-1

INSERT 1

The minimum value of the DNBR during steady state operation, normal operational transients, and anticipated transients is limited to 1.30. This value corresponds to a 95 percent probability at a 95 percent confidence level that DNB will not occur and is chosen as an appropriate margin to DNB for all operating conditions.

The curve of Figure 2.1-1 shows the loci of points of THERMAL POWER, Reactor Coolant System pressure and average temperature for which the minimum DNBR is no less than [redacted], or the average enthalpy at the vessel exit is equal to the enthalpy of saturated liquid.

conservatively the safety analysis DNBR limit,

The curves are based on an enthalpy hot channel factor, $F^N_{\Delta H}$, of ~~1.55~~ 1.62* (see specification 3/4.2.3) and a reference cosine with a peak of 1.55 for axial power shape. An allowance is included for an increase in $F^N_{\Delta H}$ at reduced power based on the expression:

actual plant operation which is restricted to an $F^N_{\Delta H}$ limit of 1.55 These will soon provided in the CORE OPERATING LIMITS REPORT (COLR).

~~$F^N_{\Delta H} = 1.55 [1 + 0.3 (1-P)]$~~

~~where P is the fraction of RATED THERMAL POWER~~

These limiting heat flux conditions are higher than those calculated for the range of all control rods fully withdrawn to the maximum allowable control rod insertion assuming the axial power imbalance is within the limits of the f(ΔI) function of the Overtemperature ΔT trip. When the axial power imbalance is not within the tolerance, the axial power imbalance effect on the Overtemperature ΔT trip will reduce the setpoint to provide protection consistent with core safety limits.

INSERT 2

BASES 2.1.1 REACTOR CORE

INSERT 1

The DNB design basis is as follows: there must be at least a 95 percent probability that the minimum DNBR of the limiting fuel rod during Condition I and II events is greater than or equal to the DNBR limit of the DNB correlation being used (the WRB-1 correlation in this application). The correlation DNBR limit is based on the entire applicable experimental data set such that there is a 95 percent probability with 95 percent confidence that DNB will not occur when the minimum DNBR is at the DNBR limit (1.17 for the WRB-1 correlation).

Incorporating the peaking factor uncertainties in the correlation limit results in a DNBR design limit value of 1.21. This DNBR value must be met in plant safety analyses using nominal values of the input parameters that were included in the DNBR uncertainty evaluation. In addition, margin has been maintained in the design by meeting a safety analysis DNBR limit of 1.33 in performing safety analyses.

INSERT 2

* The Thermal-Hydraulic and non-LOCA analyses that were conducted for Unit 1 bounds the Unit 2 analyses [i.e., $F(N\Delta H)$ of 1.62]. The LOCA and Core Design licensing basis is 1.55.

specified in Table 2.2-1, in percent span, from the analysis assumptions. Use of Equation 2.2-1 allows for a sensor drift factor, an increased rack drift factor, and provides a threshold value for REPORTABLE EVENTS.

The methodology to derive the trip setpoints is based upon combining all of the uncertainties in the channels. Inherent to the determination of the trip setpoints are the magnitudes of these channel uncertainties. Sensors and other instrumentation utilized in these channels are expected to be capable of operating within the allowances of these uncertainty magnitudes. Rack drift in excess of the Allowable Value exhibits the behavior that the rack has not met its allowance. Being that there is a small statistical chance that this will happen, an infrequent excessive drift is expected. Rack or sensor drift, in excess of the allowance that is more than occasional, may be indicative of more serious problems and should warrant further investigation.

Manual Reactor Trip

The Manual Reactor Trip is a redundant channel to the automatic protective instrumentation channels and provides manual reactor trip capability.

Power Range, Neutron Flux

The Power Range, Neutron Flux channel high setpoint provides reactor core protection against reactivity excursions which are too rapid to be protected by temperature and pressure protective circuitry. The low setpoint provides redundant protection in the power range for a power excursion beginning from low power. The trip associated with the low setpoint may be manually bypassed when P-10 is active (two of the four power range channels indicate a power level of above approximately 10 percent of RATED THERMAL POWER) and is automatically reinstated when P-10 becomes inactive (three of the four channels indicate a power level below approximately 10 percent of RATED THERMAL POWER).

Power Range, Neutron Flux, High Rates

The Power Range Positive Rate trip provides protection against rapid flux increases which are characteristic of rod ejection events from any power level. Specifically, this trip complements the Power Range Neutron Flux High and Low trips to ensure that the criteria are met for rod ejection from partial power.

The Power Range Negative Rate trip provides protection to ensure that the minimum DNBR is maintained above the design DNBR limit for control rod drop accidents. At high power a multiple rod drop accident could cause local flux peaking which, when in conjunction with nuclear power being maintained equivalent to turbine power by action of the automatic rod control system, could cause an unconservative local DNBR to exist. The Power Range Negative Rate trip will prevent this from occurring by tripping the reactor. No credit is taken for operation of the Power Range Negative Rate trip for those control rod drop accidents for which DNBRs will be greater than the design DNBR limit.

ROD DROP TIME

2.7

LIMITING CONDITION FOR OPERATION

3.1.3.4 The individual full length (shutdown and control) rod drop time from the fully withdrawn position shall be ≤ [2.2] seconds from beginning of decay of stationary gripper coil voltage to dashpot entry with:

a. $T_{avg} \geq 541°F$, and

b. All reactor coolant pumps operating.

APPLICABILITY: MODE 3.

ACTION:

a. With the drop time of any full length rod determined to exceed the above limit, restore the rod drop time to within the above limit prior to proceeding to MODE 1 or 2.

SURVEILLANCE REQUIREMENTS

4.1.3.4 The rod drop time of full length rods shall be demonstrated through measurement prior to reactor criticality:

a. For all rods following each removal of the reactor vessel head.

b. For specifically affected individual rods following any maintenance on or modification to the control rod drive system which could affect the drop time of those specific rods, and

c. At least once per 18 months.

the design DNBR limit

BASES

The specifications of this section provide assurance of fuel integrity during Condition I (Normal Operation) and II (Incidents of Moderate Frequency) events by: (a) maintaining the minimum DNBR in the core ≥ 1.30 during normal operation and in short term transients, and (b) limiting the fission gas release, fuel pellet temperature and cladding mechanical properties to within assumed design criteria. In addition, limiting the peak linear power density during Condition I events provides assurance that the initial conditions assumed for the LOCA analyses are met and the ECCS acceptance criteria limit of 2200°F is not exceeded.

The definitions of hot channel factors as used in these specifications are as follows:

$F_Q(Z)$ Heat Flux Hot Channel Factor, is defined as the maximum local heat flux on the surface of a fuel rod at core elevation Z divided by the average fuel rod heat flux, allowing for manufacturing tolerances on fuel pellets and rods.

$F^N_{\Delta H}$ Nuclear Enthalpy Rise Hot Channel Factor, is defined as the ratio of the integral of linear power along the rod with the highest integrated power to the average rod power.

3/4.2.1 AXIAL FLUX DIFFERENCE (AFD)

The limits on AXIAL FLUX DIFFERENCE assure that the $F_Q(Z)$ upper bound envelope times the normalized axial peaking factor is not exceeded during either normal operation or in the event of xenon redistribution following power changes.

Target flux difference is determined at equilibrium xenon conditions. The full length rods may be positioned within the core in accordance with their respective insertion limits and should be inserted near their normal position for steady state operation at high power levels. The value of the target flux difference obtained under these conditions divided by the fraction of RATED THERMAL POWER is the target flux difference at RATED THERMAL POWER for the associated core burnup conditions. Target flux differences for other THERMAL POWER levels are obtained by multiplying the RATED THERMAL POWER value by the appropriate fractional THERMAL POWER level. The periodic updating of the target flux difference value is necessary to reflect core burnup considerations.

Although it is intended that the plant will be operated with the AXIAL FLUX DIFFERENCE within the target band about the target flux difference, during rapid plant THERMAL POWER reductions, control rod motion will cause the AFD to deviate outside of the target band at reduced THERMAL POWER levels. This deviation will not affect the xenon redistribution sufficiently to change the envelope of peaking factors which may be reached on a subsequent return to RATED THERMAL POWER (with the AFD within the target band) provided the time

BASES

3/4.2.2 and 3/4 2.3 HEAT FLUX AND NUCLEAR ENTHALPY HOT CHANNEL FACTORS $F_Q(Z)$ AND $F^N_{\Delta H}$ (Continued)

c. The control rod insertion limits of Specifications 3.1.3.5 and 3.1.3.6 are maintained.

d. The axial power distribution, expressed in terms of AXIAL FLUX DIFFERENCE is maintained within the limits.

The relaxation in $F^N_{\Delta H}$ as a function of THERMAL POWER allows changes in the radial power shape for all permissible rod insertion limits. $F^N_{\Delta H}$ will be maintained within its limits provided conditions a thru d above, are maintained.

When an F_Q measurement is taken, both experimental error and manufacturing tolerance must be allowed for. 5% is the appropriate experimental error allowance for a full core map taken with the incore detector flux mapping system and 3% is the appropriate allowance for manufacturing tolerance.

The specified limit of $F^N_{\Delta H}$ contains an 8% allowance for uncertainties which means that normal, full power, three loop operation will result in $F^N_{\Delta H}$ less than or equal to the design limit specified in the CORE OPERATING LIMITS REPORT.

INSERT 2

Fuel rod bowing reduces the value of the DNB ratio. Credit is available to offset this reduction in the generic margin. The generic design margins, totaling 8.1% DNBR, and completely offsets any rod bow penalties (< 1.2% for the worst case which occurs at a burnup of 24,000 MWD/MTU).

This margin includes the following:

1. Design Limit DNBR of 1.30 vs. 1.28
2. Grid Spacing (K_s) of 0.046 vs. 0.059
3. Thermal Diffusion Coefficient of 0.038 vs. 0.059
4. DNBR Multiplier of 0.865 vs. 0.88
5. Pitch reduction

The radial peaking factor $F_{xy}(Z)$ is measured periodically to provide assurance that the hot channel factor, $F_Q(Z)$, remains within its limit. The F_{xy} limit for Rated Thermal Power (F^{RTP}_{xy}) provided in the CORE OPERATING LIMITS REPORT was determined from expected power control maneuvers over the full range of burnup conditions in the core.

3/4.2.4 QUADRANT POWER TILT RATIO

The Quadrant Power Tilt Ratio limit assures that the radial power distribution satisfies the design values used in the power capability analysis.

BASES 3/4.2.1 AXIAL FLUX DIFFERENCE

Insert 2.

Fuel rod bowing reduces the value of DNB ratio. Margin has been maintained between the DNBR value used in the safety analyses ~~(1.33)~~ and the design limit (1.21) to offset the rod bow penalty and other penalties which may apply.

BASES

3/4.2.4 QUADRANT POWER TILT RATIO (Continued)

Radial power distribution measurements are made during startup testing and periodically during power operation.

The limit of 1.02 at which corrective action is required provides DNB and linear heat generation rate protection with x-y plane power tilts.

The two-hour time allowance for operation with a tilt condition greater than 1.02 but less than 1.09 is provided to allow identification and correction of a dropped or misaligned rod. In the event such action does not correct the tilt, the margin for uncertainly on F_Q is reinstated by reducing the maximum allowed power by 3 percent for each percent of tilt in excess of 1.0.

3/4.2.5 DNB PARAMETERS

The limits on the DNB related parameters assure that each of the parameters are maintained within the normal steady state envelope of operation assumed in the transient and accident analyses. The limits are consistent with the initial FSAR assumptions and have been analytically demonstrated adequate to maintain a minimum DNBR ~~of 1.30~~ greater than or equal to the design DNBR limit throughout each analyzed transient.

The 12 hour periodic surveillance of these parameters through instrument readout is sufficient to ensure that the parameters are restored within their limits following load changes and other expected transient operation. The 18 month periodic measurement of the RCS total flow rate is adequate to detect flow degradation and ensure correlation of the flow indication channels with measured flow such that the indicated percent flow will provide sufficient verification of flow rate on a 12 hour basis.

BASES

3/4.4.1 REACTOR COOLANT LOOPS AND COOLANT CIRCULATION

The plant is designed to operate with all reactor coolant loops in operation and maintain DNBR above [redacted] during all normal operations and anticipated transients. In MODES 1 and 2, with one reactor coolant loop not in operation, this specification requires that the plant be in at least HOT STANDBY within 6 hours. — the design DNBR limit

In MODE 3, a single reactor coolant loop provides sufficient heat removal capability for removing decay heat; however, due to the initial conditions assumed in the analysis for the control rod bank withdrawal from a subcritical condition, two operating coolant loops are required to meet the DNB design basis for this Condition II event when the rod control system is capable of control bank rod withdrawal.

In MODES 4 and 5, a single reactor coolant loop or RHR subsystem provides sufficient heat removal capability for removing decay heat; but single failure considerations require that at least two loops be OPERABLE. Thus, if the reactor coolant loops are not OPERABLE, this specification requires two RHR loops to be OPERABLE.

The operation of one Reactor Coolant Pump or one RHR pump provides adequate flow to ensure mixing, prevent stratification and produce gradual reactivity changes during boron concentration reductions in the Reactor Coolant System. The reactivity change rate associated with boron reduction will, therefore, be within the capability of operator recognition and control.

The restrictions on starting a Reactor Coolant Pump with one or more RCS cold legs less than or equal to 350°F are provided to prevent RCS pressure transients, caused by energy additions from the secondary system, which could exceed the limits of Appendix G to 10 CFR Part 50. The RCS will be protected against overpressure transients and will not exceed the limits of Appendix G by restricting starting of the RCPs to when the secondary water temperature of each steam generator is less than 50°F above each of the RCS cold leg temperatures.

Appendix B
FSAR Revisions

FSAR Chapter 4 Markup

Section 4.1

CHAPTER 4

REACTOR

4.1 SUMMARY DESCRIPTION

4.1.1 General

This chapter describes: 1) the mechanical components of the reactor core including the fuel rods, fuel assemblies, and control rods; 2) the nuclear design; and 3) the thermal-hydraulic design.

17x17 STANDARD (STD) and VANTAGE 5H (V5H)

The reactor core is composed of an array of fuel assemblies. ~~which are identical in mechanical design, but different in fuel enrichment. Within each fuel assembly, all rods are of the same enrichment. The reference design described herein employs three enrichments in a three-region core, whereas more enrichments may be employed for a particular refueling scheme.~~

Insert A

The core is cooled and moderated by light water at a normal operating pressure of 2,250 psia in the reactor coolant system (RCS). The reactor coolant contains boron as a neutron absorber. The concentration of boron in the reactor coolant is varied as required to control relatively slow reactivity changes including the effects of fuel burnup. Additional boron, in the form of burnable absorber rods, is employed ~~in the first core~~ to establish the desired initial reactivity.

Two hundred and sixty-four fuel rods are mechanically joined in a square 17 by 17 array to form a fuel assembly. The fuel rods are supported in intervals along their length by grid assemblies which maintain the lateral spacing between the rods throughout the design life of the assembly. The grid assembly consists of an "egg-crate" arrangement of interlocked straps. The straps contain spring fingers and dimples for fuel rod support as well as reactor coolant mixing vanes. The fuel rods consist of slightly enriched uranium dioxide ceramic cylindrical pellets contained in ~~slightly cold worked~~ Zircaloy-4 tubing which is plugged and seal welded at the ends to encapsulate the fuel. All fuel rods are pressurized with helium during fabrication to reduce stresses and strains in order to increase fatigue life.

The center array position in each assembly is reserved for the incore instrumentation, 24 additional positions in the array are equipped with guide thimbles joined to the grids and the top and bottom nozzles. Depending upon the position of the assembly in the core, the guide thimbles are used as core locations for rod cluster control assemblies (RCCAs), neutron source assemblies, and burnable absorber rods. ~~Otherwise, the guide thimbles are fitted with plugging devices to limit bypass flow.~~

INSERT A

The significant new mechanical design features of the VANTAGE 5H fuel assembly design are described in References 1 and 2. These features include the following:

- Integral Fuel Burnable Absorbers (IFBAs)
- Axial Blankets (six inches of natural uranium dioxide at both ends of the fuel stack)
- Replacement of six intermediate Inconel grids with Zircaloy grids
- Slightly longer fuel rods and thinner top and bottom nozzle end plates to accommodate extended burnup
- Reconstitutable Top Nozzles (RTNs)
- Redesigned fuel rod bottom end plug to facilitate reconstitution capability
- Reduction in guide thimble and instrumentation tube diameter

4.1.2 Reference for Section 4.1

Hellman, J. M. (Ed.) 1975. Fuel Densification Experimental Results and Model and Reactor Application. WCAP-8218-P-1 (Proprietary) and WCAP-8219-A (Non-Proprietary).

Davidson, S. L. (Ed.), et. al., "VANTAGE 5H Fuel Assembly," WCAP-10444-P-A, Addendum 2-A, February 1989.

Davidson, S. L. (Ed.), et. al., "VANTAGE 5 Fuel Assembly Reference Core Report," WCAP-10444, September 1985.

TABLE 4.1-1

REACTOR DESIGN COMPARISON TABLE

Thermal and Hydraulic Design Parameters	BVPS-2	Virgil C. Summer Nuclear Station
Reactor core heat output (Mwt)	2,652	2,775
Reactor core heat output (10^6 Btu/hr)	9,051	9,471
Heat generated in fuel (percent)	97.4	97.4
System pressure, nominal (psia)	2,250	2,250
System pressure, minimum steady-state (psia)	2,220	2,220
Minimum departure from nucleate boiling ratio for design transients	>1.30	>1.30
Coolant Flow		
Total thermal flow rate (10^6 lb_m/hr)	100.8	109.6
Effective flow rate for heat transfer (10^6 lb/hr)	96.3	102.6
Effective flow area for heat transfer (ft^2)	41.6 (STD) 41.7 (VSH)	41.6
Average velocity along fuel rods (ft/sec)	14.4	15.6
Average mass velocity (10^6 lb_m/hr-ft^2)	2.32	2.47
Coolant Temperature (°F)		
Nominal inlet	542.5	556.0
Average rise in vessel	67.5	62.8
Average rise in core	70.3	66.6

TABLE 4.1-1 (Cont)

Thermal and Hydraulic Design Parameters	BVPS-2	Virgil C. Summer Nuclear Station
Average in core	579.3	591.2
Average in vessel	576.2	589.0
Heat Transfer		
Active heat transfer, surface area (ft^2)	48,600	48,600
Average heat flux (Btu/hr-ft^2)	181,400	189,800
Maximum heat flux for normal operation (Btu/hr-ft^2)	420,900	440,400
Average thermal output (kW/ft)	5.20	5.44
Maximum thermal output for normal operation (kW/ft)	12.1	12.6
Peak linear power resulting from overpower transients, operator errors, assuming a maximum overpower of 118 percent kW/ft	18.0*	18.0*
Heat flux hot channel factor (F_Q)	2.32**	2.32**
Peak fuel central temperature at 100 percent power (°F)	2,960	3,250
Peak fuel central temperature at maximum thermal output for maximum overpower trip point (°F)	<4,700	<4,700
Core Mechanical Design Parameters		
Fuel Assemblies		
Design	RCC canless	RCC canless
Number of fuel assemblies	157	157
UO^2 rods per assembly	264	264

TABLE 4.1-1 (Cont)

Core Mechanical Design Parameters	BVPS-2	Virgil C. Summer Nuclear Station
Number of absorber rods per cluster	24	24
Core Structure		
Core barrel, I.D./O.D. (in)	133.85/137.875	133.85/137.875
Core barrel design	Neutron pad design	Neutron pad design
Structure Characteristics		
Core equivalent diameter (in)	119.7	119.7
Core active fuel height (in)	144	144
Reflector Thickness and Composition		
Top - water plus steel (in)	~10	10
Bottom - water plus steel (in)	~10	10
Side - water plus steel (in)	~15	15
H_2O/U molecular ratio core, lattice (cold)	2.42	2.42
First Core Fuel enrichment, weight percent		
Region 1	2.10	2.10
Region 2	2.60	2.60
Region 3	3.10	3.10

NOTES:

*Refer to Section 4.3.2.2.6.
**This is the value of F_Q for normal operation.

TABLE 4.1-2

ANALYTIC TECHNIQUES IN CORE DESIGN

Analysis	Technique	Computer Code	Section Reference
Fuel rod design			
1. Fuel performance characteristics (temperature, internal pressure clad stess, etc)	Semi-empirical thermal model of fuel rod consideration of fuel density changes, heat transfer, fission gas release, etc.	Westinghouse fuel rod design model	4.2.1.3.1 4.3.3.1 4.4.2.2
Nuclear design			
1. Cross sections and group constants	Microscopic data; Macroscopic constants for homogenized core regions	Modified ENDF/B library LEOPARD/CINDER type and PHOENIX-P	4.3.3.2 4.3.3.2
	Group constants for control rods with self-shielding	HAMMER-AIM	4.3.3.2
2. X-Y Power distributions, fuel depletion, critical boron concentrations, X-Y xenon distributions, reactivity coefficients	2-D 2-group diffusion theory	TURTLE and ANC	4.3.3.3
4 3. Axial power distributions, control rod worths, and axial xenon distribution	1-D, 2-group diffusion theory	PANDA	4.3.3.3
5 4. Fuel rod power	Integral transport theory	LASER	4.3.3.1
Effective resonance temperature	Monte Carlo weighting function	REPAD	
3. X-Y-Z Power Distributions, Fuel Depletion, Critical Boron Concentrations, X-Y-Z Xenon Distributions, Reactivity Coefficients and Control Rod Worths	3D, 2 Group Diffusion Theory	3D ANC	4.3.3.3

Section 4.2

flow so that the heat transfer performance requirements can be met for all modes of operation.

The following section provides the fuel sytem design bases and design limits. This information, augmented by the clarifying information submitted to the USNRC during their review of Westinghouse Topical Report, ~~WCAP 9500, "Reference Core Report - 17 x 17 Optimized Fuel Assembly" (T. M. Anderson (Westinghouse) to J.R. Miller (NRC), Letter No. NS-TMA-2366, dated January 12, 1981. T.M. Anderson (Westinghouse) to J.R. Miller (NRC), Letter No. NS-TMA-2436, dated April 21, 1981.)~~ provide information consistent with the acceptance criteria of the Standard Review Plan (SRP) 4.2.

Insert A

4.2.1 Design Bases

The fuel rod and fuel assembly design bases are established to satisfy the general performance and safety criteria presented in Section 4.2.

~~The fuel rods are designed for a peak pellet burnup of approximately 53,000 megawatt days per metric ton of uranium (MWD/MTU) in the fuel cycle equilibrium condition.~~

The detailed fuel rod design established such parameters as pellet size and density, clad/pellet diametral gap, gas plenum size, and helium pressurization level. The design also considers effects such as fuel density changes, fission gas release, clad creep, and other physical properties which vary with burnup. The integrity of the fuel rods is ensured by designing to prevent excessive fuel temperatures, excessive internal rod gas pressures due to fission gas releases, and excessive cladding stresses and strains. This is achieved by designing the fuel rods so that the conservative design bases in the following subsections are satisfied during ANS Condition I and ANS Condition II events over the fuel lifetime. For each design basis, the performance of the limiting fuel rod must not exceed the limits specified by the design basis.

Integrity of the fuel assembly structure is ensured by setting limits on stresses and deformations due to various loads and by preventing the assembly structure from interfering with the function of other components. Three types of loads are considered.

1. Nonoperational loads such as those due to shipping and handling.

2. Normal and abnormal loads which are defined for ANS Conditions I and II.

Insert A p.4.2-2

WCAP-10444-A, Addendum 2-A, "VANTAGE 5H Fuel Assembly" (W. J. Johnson (Westinghouse) to M. W. Hodges (NRC), Letter No. NS-NRC-88-3319, dated April 15, 1988. W. J. Johnson (Westinghouse) to M. W. Hodges (NRC), Letter No. NS-NRC-88-3363, dated July 29, 1988.)

3. Abnormal loads which are defined for ANS Conditions III and IV.

The design bases for the incore control components are described in Section 4.2.1.6.

4.2.1.1 Cladding

1. Zircaloy-4 combines neutron economy (low absorption cross-section); high corrosion resistance to reactor coolant, fuel, and fission products; and high strength and ductility at operating temperature (Skaritka 1985)[5]... (continued on next page)

. . . . documents the operating experience with Zircaloy-4 as a clad material. Information on the materials, chemical, and mechanical properties of the cladding is given by Beaumont (et al 1978).

2. Stress Limits

   a. Clad stress - The clad stresses under ANS Conditions I and II are less than the Zircaloy 0.2 percent offset yield stress, with due consideration of temperature and irradiation effects. While the clad has some capability for accommodating plastic strain, the yield stress has been accepted as a conservative design basis.

   b. Clad tensile strain - The total tensile creep strain is less than one percent from the unirradiated condition. The elastic tensile strain during a transient is less than one percent from the pretransient value. This limit is consistent with proven practice (Beaumont et al 1978).

3. Vibration and Fatigue

   a. Strain fatigue - The cumulative strain fatigue cycles are less than the design strain fatigue life. This basis is consistent with proven practice (Section 4.2.3.3)(Christensen; Allio; and Biancheria 1965).

   b. Vibration - Potential fretting wear due to vibration is limited, ensuring that the stress limits are not exceeded during design life. Fretting of the clad surface can occur due to flow-induced vibration between the fuel rods and fuel assembly grid springs. Vibration and fretting forces vary during the fuel life due to clad diameter creepdown combined with grid spring relaxation.

4. Chemical properties of the cladding are discussed by Beaumont (et al 1978).

4.2.1.2 Fuel Material

1. Thermal-physical properties - fuel pellet temperature. The center temperature of the hottest pellet is to be below the melting temperature of the unirradiated UO_2 melting point of 5,080°F (Christensen, Allio, and Biancheria 1965) and decreasing by 58°F per 10,000 MWD/MTU). While a limited amount of center melting can be tolerated, the design conservatively precludes center melting. A calculated fuel centerline temperature of 4,700°F has been selected as an overpower limit to assure no fuel melting. This provides

sufficient margin for uncertainties as described in Section 4.4.2.9.

The normal design density of the fuel is 95 percent of theoretical. Additional information on fuel properties is given by Beaumont (et al 1978).

2. Fuel densification and fission product swelling - The design bases and models used for fuel densification and swelling are provided by Hellman (1975) and Miller (1976).

3. Chemical properties - Beaumont (et al 1978) provides the basis for justifying that no adverse chemical interactions occur between the fuel and its adjacent material.

4.2.1.3 Fuel Rod Performance

1. Fuel rod models - The basis fuel rod models and the ability to predict operating characteristics are given by Miller (1976), Davidson (1985), and Weiner (1988) (Section 4.2.3).

2. Mechanical design limits - Cladding collapse shall be precluded during the fuel rod design lifetime. The models described by George (et al 1974), and Weiner (1988) are used for this evaluation.

The rod internal gas pressure remains below the value which causes the fuel/clad diametral gap to increase due to outward cladding creep during steady state operation. Rod pressure is also limited such that extensive departure from nucleate boiling (DNB) propagation shall not occur during normal operation and any accident event. Risher (et al 1977) show that the DNB propagation criteria is satisfied.

4.2.1.4 Spacer Grids

1. Mechanical limits and materials properties - The grid component strength criteria are based on experimental tests. The grid strength was based on the 95 percent confidence level on the true mean as taken from the distribution of measurements. This limit is sufficient to assure that under worst-case combined seismic and blowdown loads from an ANS Condition IV, loss-of-coolant accident (LOCA), the core will maintain a geometry amenable to cooling. As an integral part of the fuel assembly structure, the grids must satisfy the applicable fuel assembly design bases and limits defined in Section 4.2.1.5.

The grid material and chemical properties are given by Beaumont (et al 1978).

4.2.1.5 Fuel Assembly

Structural design - As discussed in Section 4.2.1, the structural intergrity of the fuel assembly is ensured by setting design limits on stresses and deformations due to various nonoperational, operational, and

to the required fuel height. The spring is then inserted into the top end of the fuel tube and the end plugs pressed into the ends of the tube and welded. All fuel rods are internally pressurized with helium during the welding process in order to minimize compressive clad stresses and prevent clad flattening due to reactor coolant operating pressures.

The fuel rods are prepressurized and designed so that: 1) the internal gas pressure mechanical design limit discussed in Section 4.2.1.3 is not exceeded, 2) the cladding stress-strain limits (Section 4.2.1.1) are not exceeded for ANS Condition I and II events, and 3) clad flattening will not occur during the fuel core life.

4.2.2.2 Fuel Assembly Structure

The fuel assembly structure consists of a bottom nozzle, top nozzle, guide thimbles, and grids, as shown on Figure 4.2-2.

4.2.2.2.1 Bottom Nozzle

The bottom nozzle serves as bottom structural element of the fuel assembly and directs the reactor coolant flow distribution to the assembly. The ~~square~~ nozzle is fabricated from Type 304 stainless steel and consists of a perforated plate, and four angle legs with bearing plates as shown on Figure 4.2-2. The legs form a plenum for the inlet coolant flow to the fuel assembly. The plate also prevents accidental downward ejection of the fuel rods from the fuel assembly. The bottom nozzle is fastened to the fuel assembly guide tubes by screws which penetrate through the nozzle and mate with a threaded plug in each guide tube. The screw is prevented from loosening by a stainless steel ~~lock pin which is welded to the bottom nozzle.~~ thimble screw with integral locking cap.

Insert A →

Reactor coolant flows from the plenum in the bottom nozzle upward through the penetration in the plate to the channels between the fuel rods. The penetrations in the plate are positioned between the rows of fuel rods.

Axial loads (holddown) imposed on the fuel assembly and the weight of the fuel assembly are transmitted through the bottom nozzle to the lower core plate. Indexing and positioning of the fuel assembly are provided by alignment holes in two diagonally opposite bearing plates which mate with locating pins in the lower core plate. Lateral loads on the fuel assembly are transmitted to the lower core plate through the locating pins.

4.2.2.2.2 Top Nozzle

reconstitutable

The top nozzle assembly functions as the upper structural element of the fuel assembly in addition to providing a partial protective housing for the RCCA or other components, which are installed in the guide thimble tubes. It ~~The top nozzle assembly~~ consists of an adapter plate, enclosure, top plate, and pads. ~~Holddown springs are mounted on the assembly~~ as shown on Figure 4.2-2. The springs and ~~bolts~~ are made of Inconel-718, whereas other components are made of Type 304 stainless steel.

Insert B

spring screws

and -600, respectively

Insert A p. 4.2-11

The design will include use of the Debris Filter Bottom Nozzle (DFBN) to reduce the possibility of fuel rod damage due to debris-induced fretting. The relatively large flow holes in a conventional nozzle are replaced with a new pattern of smaller flow holes. The holes are sized to minimize passage of debris particles large enough to cause damage while providing sufficient flow area, comparable pressure drop, and continued structural integrity of the nozzle.

Insert B p. 4.2-11

The top nozzle assembly comprises holddown springs, screws and clamps mounted on the top plate.

Insert A.

The ~~square~~ adapter plate is provided with round penetrations and semicircular ended slots to permit the flow of coolant upward through the top nozzle. Other round holes are provided to accept ~~sleeves which are welded to the adapter plate and mechanically attached to the thimble tubes.~~ The ligaments in the plate cover the tops of the fuel rods and prevent their upward ejection from the fuel assembly. The enclosure is a box-like structure which sets the distance between the adapter plate and the top plate. The top plate has a large square hole in the center to permit access for the control rods and the control rod spiders. Holddown springs are mounted on the top plate and are ~~fastened in place by bolts~~ and clamps located at two diagonally opposite corners. On the other two corners, integral pads are positioned which contain alignment holes for locating the upper end of the fuel assembly.

retained by spring screws

4.2.2.2.3 Guide Thimbles and Instrument ~~Thimbles~~ Tubes

Insert B

The guide thimbles are structural members which also provide channels for the neutron absorber rods, burnable absorber rods, neutron source, or thimble plug assemblies. Each thimble is fabricated from Zircaloy-4 tubing having two different diameters. The tube diameter at the top section provides the annular area necessary to permit rapid control rod insertion during a reactor trip. The lower portion of the guide thimble is swaged to a smaller diameter to reduce diametral clearances and produce a dashpot action near the end of the control rod travel during normal trip operation. Holes are provided in the thimble tube above the dashpot to reduce the rod drop time. The dashpot is closed at the bottom by means of an end plug which is provided with a small flow port to avoid fluid stagnation in the dashpot volume during normal operation. The top end of the guide thimble is fastened to ~~a tubular sleeve~~ by three expansion swages. The ~~sleeve~~ fits into and is ~~welded to~~ the top nozzle adapter plate. The lower end of the guide thimble is fitted with an end plug which is then fastened into the bottom nozzle by a integral locking cup thimble screw. ~~A stainless steel lock pin is welded to the bottom nozzle to prevent the screw from loosening.~~

an insert locked into ... insert ... using a lock tube

Fuel rod support grids are fastened to the guide thimble assemblies to create an integrated structure. ~~Since welding of~~ the Inconel grids ~~and~~ are attached to the Zircaloy thimble ~~is not possible, a~~ mechanical fastening technique, depicted on Figures 4.2-4 and 4.2-5 ~~is used~~ for ~~all but~~ the ~~top and~~ bottom grids, ~~in a fuel assembly.~~

using the ... and zircaloy ... , except ... Insert C

An ~~expanding~~ tool is inserted into the inner diameter of the Zircaloy thimble tube at the elevation of ~~stainless steel~~ sleeves which have been ~~brazed into~~ the ~~Inconel~~ grid assembly. The four lobed tool forces the thimble and sleeve outward to a predetermined diameter, thus joining the two components.

the grid ... previously attached to ...

Insert D. →

~~The top grid to thimble attachment is shown on Figure 4.2-6. The stainless steel sleeves are brazed into the Inconel grid assembly. The Zircaloy guide thimbles are fastened to the long sleeves by expanding the two members as shown on Figures 4.2-4 and 4.2-5. Finally, the top ends of the sleeves are welded to the top nozzle adapter plate as shown on Figure 4.2-6.~~

Insert A p. 4.2-12

inserts which are locked into internal grooves in the adapter plate at their upper ends using a lock tube and mechanically attached to the thimble tubes at the lower end.

insert B p. 4.2-12

With the exception of a reduction in the guide thimble diameter above the dashpot, the VANTAGE 5H (V5H) guide thimbles are identical to those in the LOPAR design. A 0.008 inch reduction to the guide thimble OD and ID is required due to the thicker zircaloy grid straps. The V5H guide thimble tube ID provides an adequate nominal diametral clearance of 0.061 inch for the control rods. The reduced V5H thimble tube ID also provides sufficient diametral clearance for burnable absorber rods, source rods, and any dually compatible thimble plugs.

Insert C p. 4.2-12

which is retained by clamping between the thimble end plug and the bottom nozzle.

Insert D p. 4.2-12

The top inconel grid sleeve, top nozzle insert, and thimble tube are joined together using three joint mechanical attachments as shown in Figure 4.2-6. This bulge joint connection was mechanically tested and found to meet all applicable design criteria.

The mixing vane zircaloy grids employ a single bulge connection to the sleeve and thimble as compared to a three bulge connection used in the top inconel grid (Figure 4.2-5). Mechanical testing of this bulge joint connection was also found to be acceptable.

The bottom grid assembly is joined to the assembly as shown on Figure 4.2-7. The stainless steel insert is spot welded to the bottom grid and later captured between the guide thimble and plug and the bottom nozzle by means of a stainless steel integral locking cup thimble screw.

These methods of grid fastening are standard and have, with the exception of the integral locking cup thimble screw, been used successfully since the introduction of Zircaloy guide thimble in 1969.

The central instrumentation tube ~~thimble~~ of each fuel assembly is constrained by seating in counterbores in the bottom nozzle at its lower end and ~~each nozzle~~. This tube is of constant diameter and guides the incore neutron detectors. ~~This thimble~~ is expanded at the top and mid grids in the same manner as the previously discussed expansion of the guide thimbles to the grids.

Insert A →

4.2.2.2.4 Grid Assemblies

The fuel rods, as shown on Figure 4.2-2, are supported at intervals along their length by grid assemblies which maintain the lateral spacing between the rods. Each fuel rod is supported within each grid by the combination of support dimples and springs. The grid assembly consists of individual slotted straps assembled and interlocked ~~and brazed in~~ an "egg-crate" arrangement ~~to join~~ with the straps permanently joined at their points of intersection. ~~The straps contain spring fingers, support dimples, and mixing vanes.~~

Insert B →

~~The grid material is Inconel-718, chosen because of its corrosion resistance and high strength.~~ The magnitude of the grid restraining force on the fuel rod is set high enough to minimize possible fretting, without overstressing the cladding at the points of contact between the grids and fuel rods. The grid assemblies also allow axial thermal expansion of the fuel rods without imposing restraint sufficient to develop buckling or distortion of the fuel rods.

~~Two types of grid assemblies are used in each fuel assembly. Six grids, with mixing vanes projecting from the edges of the straps into the RCS, are used in the high heat flux region of the fuel assemblies to promote mixing of the reactor coolant. Two grids, one at each end of the assembly, do not contain mixing vanes on the internal straps. The outside straps on all grids contain mixing vanes which, in addition to their mixing function, aid in guiding the grids and fuel assemblies past projecting surfaces during handling or during loading and unloading of the core.~~

4.2.2.3 Core Components

Reactivity control is provided by neutron absorbing rods and a soluble chemical neutron absorber (boric acid). The boric acid concentration is varied to control long term reactivity changes such as:

1. Fuel depletion and fission product buildup.

2. Cold to hot, zero power reactivity change.

Insert A p. 4.2-13

The V5H instrumentation tube also has an 0.008 inch diametral decrease compared to the LOPAR assembly instrumentation tube. This decrease still allows sufficient diametral clearance for the incore neutron detector to traverse the tube without binding.

Insert B p. 4.2-13

The top and bottom Inconel (non-mixing vane) grids of the LOPAR and V5H assemblies are nearly identical in design. The only differences are: 1) V5H interactions during core loading/unloading, 2) V5H top and bottom grids have dimples which are rotated 90 degrees to minimize fuel rod fretting and dimple cocking, 3) V5H top and bottom grid heights have been increased to 1.522 inches, 4) the V5H top grid spring force has been reduced to minimize rod bow, and 5) the V5H top grid uses 304L stainless steel sleeves.

The six intermediate (mixing vane) grids are made of zircaloy material rather than Inconel which is currently used in the LOPAR design. These V5H grids (known as the VANTAGE 5H zircaloy grid) are designed to give the same pressure drop as the Inconel grid. Relative to the Inconel grid, the V5H zircaloy grid strap thickness and strap height are increased for structural performance. In addition to the snag-resistant design noted above, the upstream strap edges of the V5H zircaloy grid are chamfered and a diagonal grid spring is employed to reduce pressure drop. The V5H zircaloy grids incorporate the same grid cell support configuration as the Inconel grids (six support locations per cell: four dimples and two springs). The zircaloy grid interlocking strap joints and grid/sleeve joints are fabricated by laser welding whereas the Inconel grid joints are brazed.

The V5H zircaloy grid has superior dynamic structural performance relative to the inconel grid. Structural testing was performed and analyses have shown the V5H zircaloy grid seismic/LOCA load margin is superior to that of the Inconel grid.

3. Reactivity change produced by intermediate term fission products such as xenon and samarium.

4. Burnable absorber depletion.

The Chemical and Volume Control System (CVCS) is discussed in Section 9.3.4.

The RCCAs provide reactivity control for:

1. Shutdown,

2. Reactivity changes due to reactor coolant temperature changes in the power range,

3. Reactivity changes associated with the power coefficient of reactivity, and

4. Reactivity changes resulting from void formation.

It is desirable to have a negative moderator temperature coefficient throughout the entire cycle in order to reduce possible deleterious effects caused by a positive coefficient during LOCA, loss-of-flow, or steam line break (SLB) accidents. A combination of burnable absorber assemblies with soluble boron is used to ensure a negative moderator temperature coefficient during all portions of the fuel operating cycle.

The RCCAs and their CRDMs are the only moving parts in the reactor. Figure 4.2-8 illustrates the rod cluster control (RCC) and CRDMs assembly, in addition to the arrangement of these components in the reactor, relative to the interfacing fuel assembly and guide tubes. In the following paragraphs, each reactivity control component is described in detail. The CRDM assembly is described in Section 3.9N.4.

The neutron source assemblies provide a neutron source for monitoring the core during periods of low neutron flux level. The thimble plug assemblies limit bypass flow through those fuel assembly thimbles which do not contain control rods, burnable absorber rods, or neutron source rods.

4.2.2.3.1 Rod Cluster Control Assembly

The RCCAs are divided into two categories: control and shutdown. The control groups compensate for reactivity changes associated with variations in operating conditions of the reactor, that is, power and temperature variations. Two nuclear design criteria have been employed for selection of the control group. First, the total reactivity worth must be adequate to meet the nuclear requirements of the reactor. Second, in view of the fact the these rods may be partially inserted at power operation, the total power peaking factor should be low enough to ensure that the power capability is met. The control and shutdown groups provide adequate shutdown margin.

The RCCA is comprised of 24 neutron absorber rods fastened at the top end to common spider assembly, as illustrated on Figure 4.2-9.

of neutrons. The primary source assemblies are normally removed after the first cycle of operation.

Four source assemblies are installed in the initial reactor core: two primary source assemblies and two secondary source assemblies. Each primary source assembly contains one primary source rod and a number of burnable absorber rods and thimble plugs. Each secondary source assembly contains a symmetrical grouping of four secondary source rods and thimble plugs in the remaining locations. The source assemblies are shown on Figure 4.2-11.

Neutron source assemblies are employed at opposite sides of the core (Figure 4.3-5). The assemblies are inserted in the guide thimbles of fuel assemblies at selected unrodded locations.

As shown on Figure 4.2-11, the source assemblies contain a holddown assembly identical to that of the burnable absorber assembly.

The primary and secondary source rods both utilize the same cladding material as the absorber rods. The secondary source rods contain Sb-Be pellets stacked to a height of approximately 88 inches. The primary source rods contain capsules of Californium source material and an alumina spacer to position the source material within the cladding. The rods in each assembly are permanently fastened at the top end to a holddown assembly.

The other structural members are constructed of Type 304 stainless steel except for the springs. The springs exposed to the reactor coolant are Inconel-718.

4.2.2.3.4 Thimble Plug Assembly

Thimble plug assemblies limit bypass flow through the guide thimbles in fuel assemblies which do not contain either control rods, source rods, or burnable absorber rods.

The thimble plug assemblies consist of a hold down assembly with short rods suspended from the base plate and a spring pack assembly, as shown on Figure 4.2-11. The 24 thimble plugs, project into the upper ends of the guide thimbles to reduce the bypass flow. Each thimble plug is permanently attached to the base plate by a nut which is ~~lock-welded~~ crimped to the threaded end of the plug. Similar thimble plugs are also used on the source assemblies and burnable absorber assemblies to plug the ends of all vacant fuel assembly guide thimbles. When in the core, the thimble plug assemblies interface with both the upper core plate and with the fuel assembly top nozzles by resting on the adapter plate. The spring pack is compressed by the upper core plate when the upper internals assembly is lowered into place.

All components in the thimble plug assembly, except for the springs, are constructed from Type 304 stainless steel. The springs are Inconel-718.

fuel assembly based on out-of-pile flow tests (DeMario, 1974), performance of similarly designed fuel in operating reactors (Skaritka 1985), and design analyses.

2. Fuel rod internal pressure and cladding stresses - The Burnup dependent fission gas release model (Miller 1976 and Weiner 1988 are used in determining the internal gas pressures as a function of irradiation time. The plenum height of the fuel rod has been designed to ensure that the maximum internal pressure of the fuel rod will not exceed the value which would cause, 1) the fuel/clad diametral gap to increase during steady state operation and, 2) extensive DNB propagation to occur.

The clad stresses at a constant local fuel rod power are low. Compressive stresses are created by the pressure differential between the reactor coolant pressure and the rod internal gas pressure. Because of the prepressurization with helium, the volume average effective stresses are always less than approximately ~~10,000~~ 13,600 psi at the pressurization level used in this fuel rod design. Stresses due to the temperature gradient are not included in this average effective stress because thermal stresses are, in general, negative at the clad inside diameter and positive at the clad outside diameter and their contributions to the clad volume average stress is small. Furthermore, the thermal stress decreases with time during steady state operation due to stress relaxation. The stress due to pressure differential is highest in the minimum power rod at the beginning-of-life due to low internal gas pressure and the thermal stress is highest in the maximum power rod due to the steep temperature gradient.

The internal gas pressure at beginning-of-life ranges from approximately ~~1,400~~ 100 to 1,000 psia for a typical lead power fuel rod. The total tangential stress at the clad inside diameter at beginning-of-life is approximately ~~14,400~~ 19,300 psi compressive (~~13,000~~ psi due to ΔP and ~~1,400~~ 1,200 due to ΔT) for an average power rod operating at 5.5 kW/ft and approximately ~~12,000~~ 20,500 psi compressive (~~8,500~~ psi due to ΔP and ~~3,500~~ 3,300 psi due to ΔT) for a high power rod operating at 13.1 kw/ft. 15 However, the volume average effective stress at beginning-of-life is between approximately 8,000 psi (high power rod) and approximately ~~10,000~~ 13,600 psi (low power rod). These stresses are substantially below even the unirradiated clad strength (55,500 psi) at a typical clad mean operating temperature of 700°F.

Tensile stresses could be created once the clad has come in contact with the pellet. These stresses would be irduced by the fuel pellet swelling during irradiation. Fuel swelling can result in small clad strains (<1 percent) for expected discharge burnups, but the associated clad stresses are very low because of clad creep (thermal and irradiation-induced). The one percent strain criterion is extremely conservative for fuel-swelling driven clad strain because the strain rate associated with solid fission products swelling is very slow. A detailed discussion on fuel rod performance is given in Section 4.2.3.3.

than the manufactured values. Fuel densification and subsequent settling of the fuel pellets can result in local and distributed gaps in the fuel rods. Fuel densification has been minimized by improvements in the fuel manufacturing process and by specifying a nominal 95 percent initial fuel density.

The evaluation of fuel densification effects and their considerations in fuel design are described by Hellman (1975) and Miller (1976), and Weiner (1988). The treatment of fuel swelling and fission gas release is described by Miller (1976) and Weiner (1988).

The effects of waterlogging on fuel behavior are discussed in Section 4.2.3.3.

4.2.3.3 Fuel Rod Performance

In the calculation of the steady state performance of a nuclear fuel rod, the following interacting factors must be considered:

1. Clad creep and elastic deflection.

2. Pellet density changes, thermal expansion, gas release, and thermal properties as a function of temperature and fuel burnup.

3. Internal pressure as a function of fission gas release, rod geometry, and temperature distribution.

These effects are evaluated using fuel rod design models ~~(Miller 1976). The model modifications for time dependent fuel densification are given by Hellman (1975) and Miller (1976). With the previous~~ (Miller 1976 and Weiner 1988) which include appropriate models for time-dependent fuel densification. With the above ....

Replace

interacting factors considered, the model determines the fuel rod performance characteristics fo a given rod geometry, power history, and axial power shape. In particular, internal gas pressure, fuel and clad temperatures, and clad deflections are calculated. The fuel rod is divided into several axial sections and radially into a number of annular zones. Fuel density changes are calculated separately for each segment. The effects are integrated to obtain the internal rod pressure.

The initial rod internal pressure is selected to delay fuel/clad mechanical interaction and to avoid the potential for flattened rod formation. It is limited, however, by the design criteria for the rod internal pressure (Section 4.2.1.3).

The gap conductance between the pellet surface and the clad inner diameter is calculated as a function of the composition, temperature, and pressure of the gas mixture, and the gap size of contact pressure between clad and pellet. After computing the fuel temperature for each pellet annular zone, the fractional fission gas release is assessed using an empirical model derived from experimental data (Miller 1976). The total amount of gas released is based on the average fractional release within each axial and radial zone and the gas generation rate which in turn is a function of burnup. Finally, the gas released is summed over all zones and the pressure is calculated. and Weiner 1988

The model shows good agreement in fit for a variety of published and proprietary data of fission gas release, fuel temperatures, and clad deflections (Miller 1976). These data include variations in power, time, fuel density, and, geometry. and Weiner 1988

Fuel/cladding mechanical interaction - One factor in fuel element duty is potential mechanical interaction of fuel and clad. This fuel/clad interaction produces cyclic stresses and strains in the clad, and these in turn consume clad fatigue life. The reduction of fuel/clad interaction is therefore a goal of design. The technology of using prepressurized fuel rods has been developed to further this objective.

The gap between the fuel and clad is initially sufficient to prevent hard contact between the two. However, during power operation, a gradual compressive creep of the clad onto the fuel pellet occurs due to the external pressure exerted on the rod by the reactor coolant. Clad compressive creep eventually results in the fuel/clad contact. Once fuel/clad contact occurs, changes in power level result in changes in clad stresses and strains. By using prepressurized fuel rods to partially offset the effect of the reactor coolant external pressure, the rate of clad creep toward the surface of the fuel is reduced. Fuel rod prepressurization delays the time at which fuel/clad interaction and contact occurs, and significantly reduces the number and extent of cyclic stresses and strains experienced by the clad both before and after fuel/clad contact. These factors result in an increase in the fatigue life margin of the clad and lead to greater clad reliability. If gas should form in the fuel stacks,

2. A biaxial fatigue experiment in gas autoclave on unirradiated Zircaloy-4 cladding both hydrided and nonhydrided.

3. A fatigue test program on irradiated cladding from the Carolina-Virginia Tube Reactor and Yankee Core V conducted at Battelle Memorial Institute.

The results of these test programs provided information on different cladding conditions including the effect of irradiation, hydrogen level, and temperature.

The design equations followed the concept for the fatigue design criterion according to the ASME Code, Section III. Namely,

1. The calculated pseudo-stress amplitude (S_a) has to be multiplied by a factor of 2 in order to obtain the allowable number of cycles (N_f).

2. The allowable cycles for a given S_a is 5 percent of N_f, or a safety factor of 20 on cycles.

The lesser of the two allowable number of cycles is selected. The cumulative fatigue life fraction is then computed as:

$$\sum_{k}^{k} \frac{n_k}{N_{fk}} \leq 1 \qquad (4.2\text{-}2)$$

where:

n_k = number of daily cycles of mode k,

N_{fk} = number of allowable cycles.

It is recognized that a possible limitation to the satisfactory behavior of the fuel rods in a reactor which is subjected to daily load follow is the failure of the clad by low-cycle strain fatigue. During their normal residence time in the reactor, the fuel rod may be subjected to ~~approximately~~ 1,000 cycles or more with typical changes in power level from 50 to 100 percent of their steady state values.

The assessment of the fatigue life of the fuel rod clad is subject to a considerable uncertainty due to the difficulty of evaluating the strain range which results from the cyclic interaction of the fuel pellets and clad. This difficulty arises, for example, from such highly unpredictable phenomena as pellet cracking, fragmentation, and relocation. Nevertheless, since early 1968, this particular phenomenon has been investigated analytically and experimentally (O'Donnell et al 1964). Strain fatigue tests on irradiated and nonirradiated hydrided Zircaloy-4 claddings were performed which

7. Provisions for detection of fuel rod failure include high- and low-range off-line liquid monitors in the reactor coolant letdown line as discussed in Section 11.5.2.5.10.

4.2.3.4 Spacer Grids

The reactor coolant flow channels are established and maintained by the structure composed of grids and guide thimbles. The lateral spacing between fuel rods is provided and controlled by the support dimples of adjacent grid cells. Contact of the fuel rods on the dimples is maintained through the clamping force of the grid springs. Lateral motion of the fuel rods is opposed by the spring force and the internal moments generated between the spring and the support dimples.

Time history numerical integration techniques are used to analyze the fuel assembly responses resulting from the lateral safe shutdown earthquake, SSE, and the most limiting main coolant pipe break accident, LOCA. The reactor vessel motions resulting from the transient loading are asymmetric with respect to the geometrical center of the reactor core. The complete fuel assembly core finite element model is employed to determine the fuel assembly deflections and grid impact forces.

A comparison of the seismic (SSE) response spectrum at the reactor vessel supports versus the response spectrum of the time history indicates that the time history spectrum conservatively bounds the design acceleration spectrum curves for BVPS-2. The seismic analyses performed for a number of plants indicate that the maximum impact response is, in general, influenced by the acceleration level of the input forcing function at the fuel assembly fundamental mode. Thus, the data in seismic time histories corresponding to the design envelope are conservatively used for the fuel evaluation.

The reactor core finite element model consisting of the maximum number of fuel assemblies across the core diameter was used. The BVPS-2 plant has fifteen 17x17 8-grid ~~(Inconel)~~ fuel assemblies arranged in a planar array. Gapped elements simulate the clearances between the peripheral fuel assemblies and the baffle plates.

The fuel assembly finite element model preserves essential dynamic properties, such as the fuel assembly vibration frequencies, mode shapes, and mass distribution. The time history motions for the upper and lower core plates and the motions for the core barrel at the upper core plate elevations are simultaneously introduced into the simulated core model. The analytical procedures, the fuel assembly and core modeling, and the methodology are detailed in Gensinski and Chiang (1973) and Davidson (et al 1981). The time history inputs representing the SSE motions and the coolant pipe rupture transients were obtained from the time history analyses of the reactor vessel internals.

GRID ANALYSIS

~~With respect to the guidelines of Appendix A of SRP Section 4.2, Westinghouse has demonstrated that a simultaneous SSE and LOCA event is~~

highly unlikely. The fatigue cycles, crack initiation and crack growth due to normal operating and seismic events will not realistically lead to a pipe rupture (Witt et al 1978). The factor applied to the LOCA grid impact load due to flashing has been demonstrated by Westinghouse to be unrealistic for Westinghouse fuel in Westinghouse plants. Therefore, this factor was not applied to the BVPS-2 analysis results.

The maximum grid impact forces for both the seismic and asymmetric LOCA accidents occur at the peripheral fuel assembly locations adjacent to the baffle wall. The maximum grid impact force for the enveloped SSE analysis was 97 percent of the allowable grid strength. The corresponding value for the nozzle inlet break was 37 percent. In order To comply with the requirements in SRP Section 4.2 the maximum grid impact responses obtained from the two transient analyses are combined. The square-root-of-sum-of-squares (SRSS) method is used to calculate the results. The maximum combined impact force for the BVPS-2 fuel assemblies was 99 percent of the allowable grid strength. The grid strength was established experimentally. It was based on the 95 percent confidence level on the true mean as taken from the distribution of measurements.

below

NON-GRIL COMPONENT ANALYSES

The stresses induced in the various fuel assembly non-grid components are calculated. The calculations are based on the maximum responses obtained from the most limiting seismic and LOCA accident conditions. The fuel assembly axial forces resulting from the LOCA accident are the primary sources of stresses in the thimble guide tube and the fuel assembly nozzles. The induced stresses in the fuel rods result from the relative deflections during the hypothetical seismic and LOCA accidents. The stresses are generally small. The combined seismic and LOCA induced stresses of the various fuel assembly components presented in Table 4.2-1 are expressed as a percentage of the allowable limit. Consequently, the fuel assembly components are structurally acceptable under the postulated accident design conditions for BVPS-2.

below

4.2.3.5 Fuel Assembly

4.2.3.5.1 Stresses and Deflections

The fuel assembly component stress levels are limited by the design. For example, stresses in the fuel rod due to thermal expansion and Zircaloy irradiation growth are limited by the relative motion of the rod as it slips over the grid spring and dimple surfaces. Clearances between the fuel rod ends and nozzles are provided so that Zircaloy irradiation growth does not result in the rod end interferences. Stresses in the fuel assembly caused by tripping of the RCCA have little influence on fatigue because of the small number of events during the life of an assembly. Assembly components and prototype fuel assemblies made from production parts have been subjected to structural tests to verify that the design bases requirements are met.

The fuel assembly design loads for shipping have been established at 6g lateral and 4g axial. Accelerometers are permanently placed into the

results of the surveillance and operating experience with Westinghouse fuel and incore control components.

4.2.4.6 Onsite Inspection

Detailed written procedures are used for receipt inspection of new fuel assemblies and associated components, such as control rods, plugs, and inserts. Loaded fuel containers, are visually inspected upon receipt for possible evidence of damage or improper handling. Shock indicators attached to the interior of the container are inspected to verify that excessive forces caused by movement have not been applied to the fuel assemblies. The fuel assemblies and associated components are subjected to inspections which verify sufficient attributes to assure that damage or deterioration during shipping was avoided.

Post-irradiation fuel inspections are routinely conducted during refueling. These inspections include a qualitative visual examination of some discharged fuel assemblies from each refueling. Gross problems of structural integrity, fuel rod failure, rod bowing and crud deposition are identified. Additional surveillance is provided if the visual examination identifies unusual behavior or if the plant instrumentation indicates gross fuel failures.

4.2.4.7 On-line Fuel System Monitoring

Reactor coolant letdown radiation monitors which can detect conditions which indicate fuel rod failure are discussed in Section 11.5.2.2.

4.2.5 References for Section 4.2

Beaumont, M. D. et al 1978. Properties of Fuel and Core Component Materials. WCAP-9179, Revision 1 (Proprietary) and WCAP-9224 (Non-Proprietary), and Appendix B (Al_2O_3-B_4C) 1980.

Burian, R. J.; Frowui, E. O.; and Gatas, J. E. 1963. Effect of High Burnups on B_4C and ZrB_2 Dispersions in the Al_2O_3 and Zircaloy. BMI 1627.

Christensen, J. A.; Allio, R. J.; and Biancheria, A. 1965. Melting Point of Irradiated UO_2 WCAP-6065.

Cohen, J. 1959. Development and Properties of Silver Base Alloys as Control Rod Materials for Pressurized Water Reactors; WAPD-214.

Davidson, S. L. et al 1981. Verification Testing and Analysis of the 17 x 17 Optimized Fuel Assembly, WCAP-9401-P-A (Proprietary) and WCAP-9402-A (Non-Proprietary).

Insert A →

DeMario, E. E. 1974. Hydraulic Flow Test of the 17 x 17 Fuel Assembly. WCAP-8278 (Proprietary) and WCAP-8279 (Non-Proprietary).

Eggleston, F. T. 1978. Safety-Related Research and Development for Westinghouse Pressurized Water Reactors, Program Summaries - Winter 1977 - Summer 1978. WCAP-8768, Revision 2.

Insert A p. 4.2-34

Davidson, S. L. (Ed.), et. al., "Reference Core Report VANTAGE 5 Fuel Assembly," WCAP-10444-P-A, September 1985.

Insert B p. 4.2-35

Davidson, S. L., et. al., "Extended Burnup Evaluation of Westinghouse Fuel," WCAP-10125-P-A and WCAP-10126-NP-A, December 1985.

Weiner, R. A., et. al., "Improved Fuel Performance Models for Westinghouse Fuel Rod Design and Safety Evaluations," WCAP-10851-P-A and WCAP-11873-A, August 1988.

George, R. A.; Lee, Y. C.; and Eng, G. H. 1974. Revised Clad Flattening Model. WCAP-8377 (Proprietary) and WCAP-8381 (Non-Proprietary).

Cesinski, L. and Chiang, D. 1973. Safety Analysis of the 17 x 17 Fuel Assembly for Combined Seismic and Loss-of-Coolant Accident. WCAP-8236 (Proprietary) and WCAP-8288 (Non-Proprietary).

Hellman, J. M. (Ed.) 1975. Fuel Densification Experimental Results and Model for Reactor Application. WCAP-8218-P-A (Proprietary) and WCAP-8219-A (Non-Proprietary).

Miller, J. V. (Ed.) 1976. Improved Analytical Models Used in Westinghouse Fuel Rod Design Computations. WCAP-8720 (Proprietary) and WCAP-8785 (Non-Proprietary).

O'Donnell, W. J. and Langer, B. F. 1964. Fatigue Design Basis for Zircaloy Components. Nuclear Science and Engineering, 20, 1-12.

Risher, D. et al 1977. Safety Analysis for the Revised Fuel Rod Internal Pressure Design Basis. WCAP-8963 (Proprietary) and WCAP-8964 (Non-Proprietary).

Skaritka, J. (Ed.) 1979. Fuel Rod Bow Evaluation. WCAP-8691, Revision 1 (Proprietary) and WCAP-8692, Revision 1 (Non-Proprietary).

Skaritka, J. et al 1983. Westinghouse Wet Annular Burnable Absorber Evaluation Report. WCAP-10021-P-A, Revision 1 (Proprietary).

Skaritka, J. July 1985. Operational Experience with Westinghouse Cores (up to December 31, 1984). WCAP-8183, Revision 14.

Stephan, L. A. 1970. The Effects of Cladding Material and Heat Treatment on the Response of Waterlogged UO_2 Fuel Rods to Power Bursts. IN-ITR-111.

Western New York Nuclear Research Center 1971. Correspondence with the USAEC on February 11 and August 27, 1971, Docket 50-57.

Westinghouse Electric Corporation 1979. Nuclear Fuel Division Quality Assurance Program Plan. WCAP-7800, Revision 5A.

~~Witt, F. J. et al 1978. Integrity of the Primary Piping Systems of Westinghouse Nuclear Plants During Postulated Seismic Events. WCAP-9253 (Non-Proprietary).~~

Insert B →

TABLE 4.2-1

FUEL ASSEMBLY COMPONENT STRESSES
(PERCENT OF ALLOWABLE)

Component	Uniform Stresses (Direct/Membrane)	Combined Stresses (Membrane + Bending)
Thimble	78.6	64.2
Fuel Rod*	32.8	26.6
Top Nozzle Plate	**	6.0
Bottom Nozzle Plate	**	47.5
Bottom Nozzle Leg	7.7	8.9

NOTES:

*Including primary operating stresses
**A negligible value

Delete this Page

Replace this page with the following

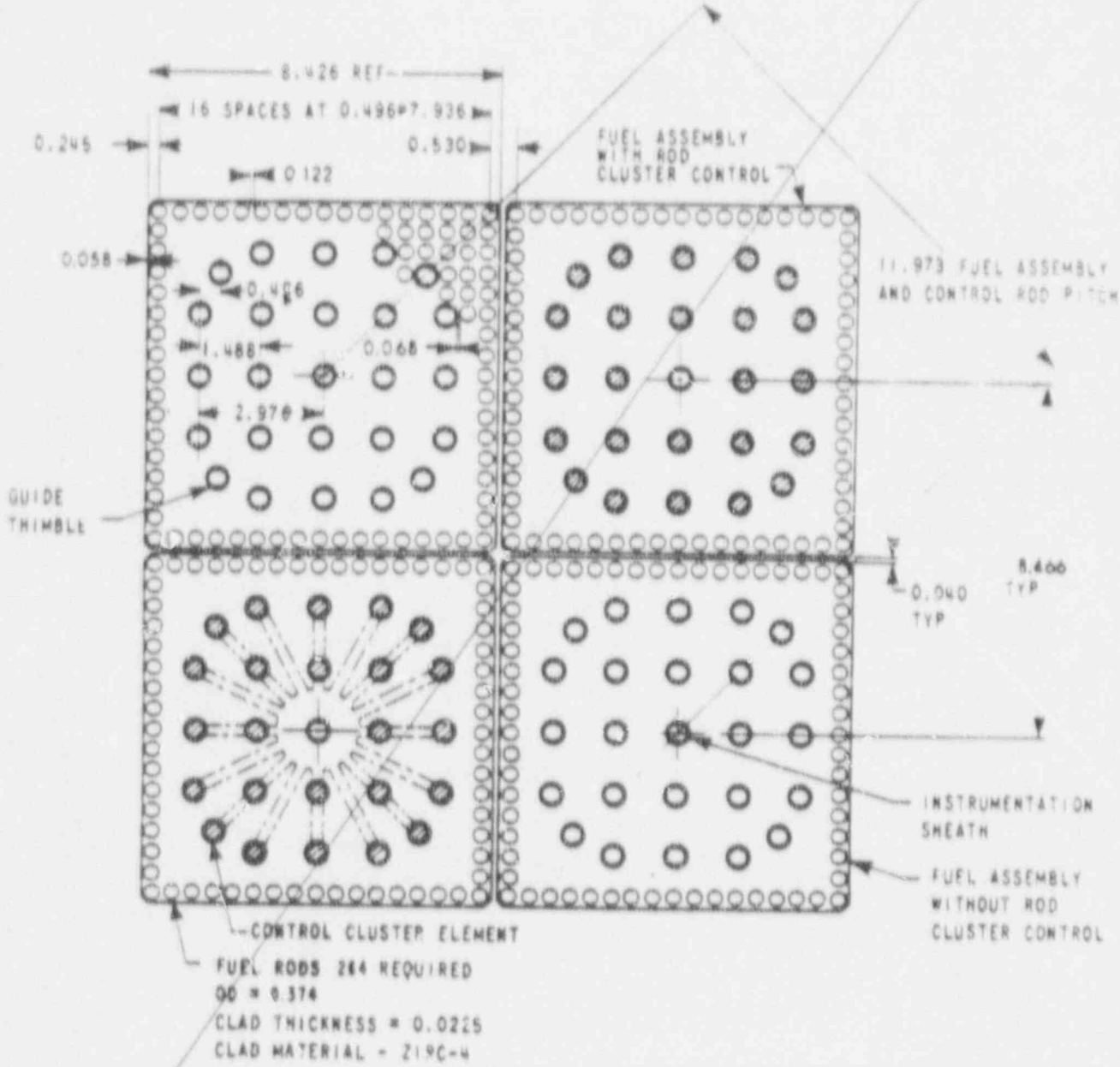

FIGURE 4.2-1
FUEL ASSEMBLY CROSS SECTION
17 x 17
BEAVER VALLEY POWER STATION - UNIT 2
FINAL SAFETY ANALYSIS REPORT

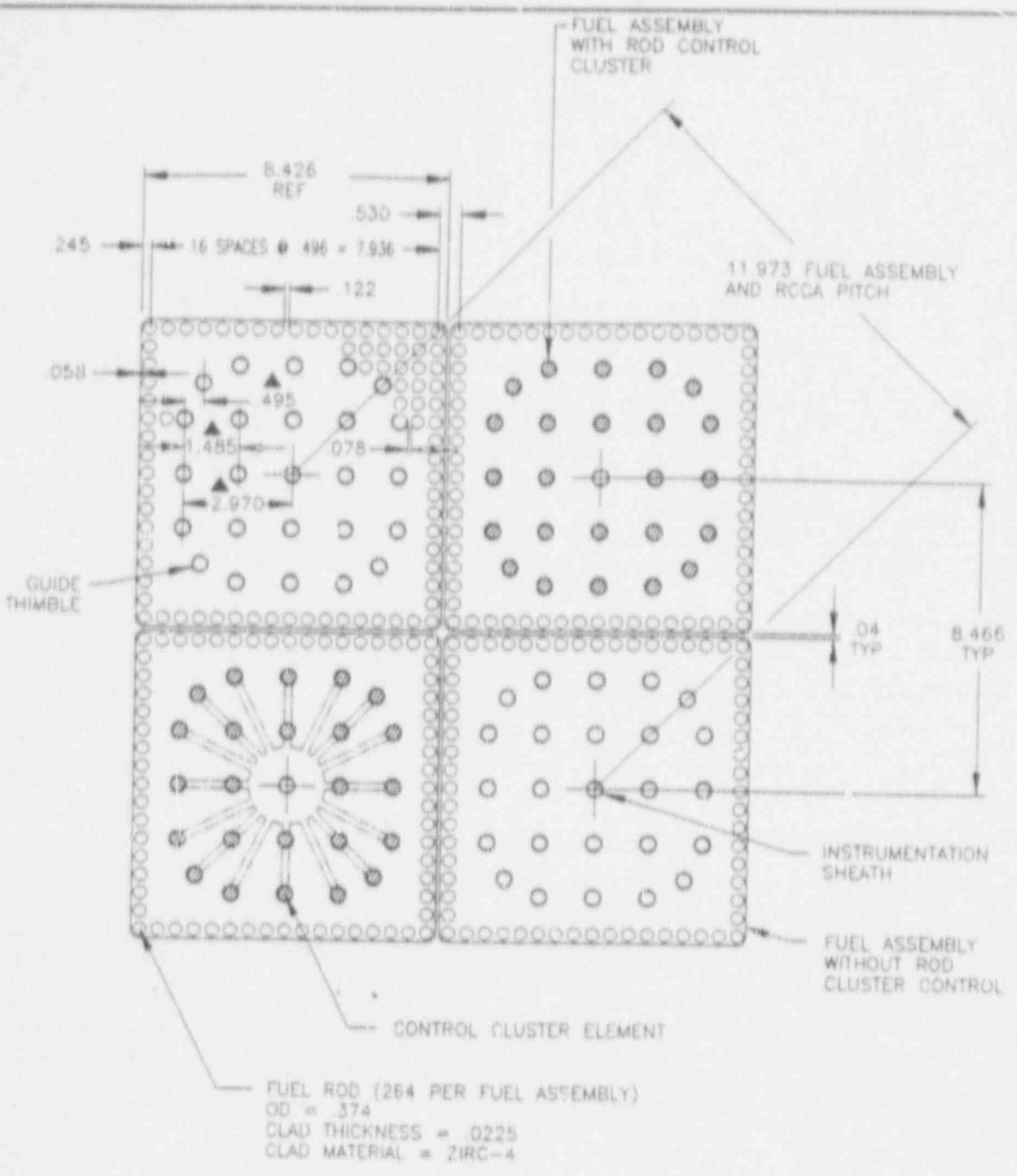

▲ GUIDE THIMBLE DIMENSIONS
AT TOP NOZZLE ADAPTOR PLATE

DIMENSIONS ARE IN INCHES (NOMINAL)

BEAVER VALLEY POWER STATION - UNIT 2
FIGURE 4.2-1

FUEL ASSEMBLY CROSS SECTION
17x17 VANTAGE 5H

Replace this figure with the following

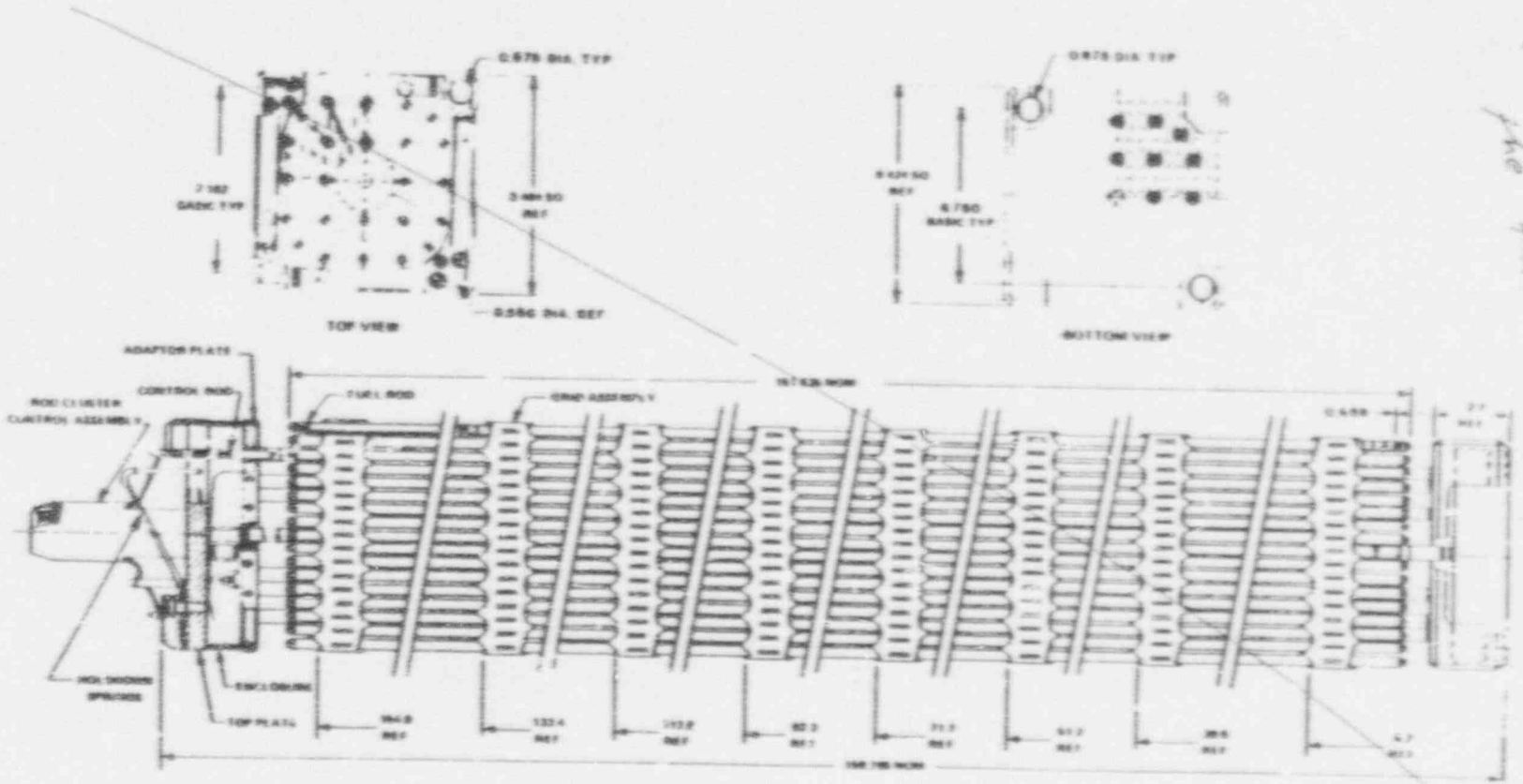

FIGURE 4.2-2
FUEL ASSEMBLY OUTLINE 17 x 17
BEAVER VALLEY POWER STATION - UNIT 2
FINAL SAFETY ANALYSIS REPORT

BEAVER VALLEY POWER STATION - UNIT 2

FIGURE 4.2-2

FUEL ASSEMBLY OUTLINE

17x17 VANTAGE 5H

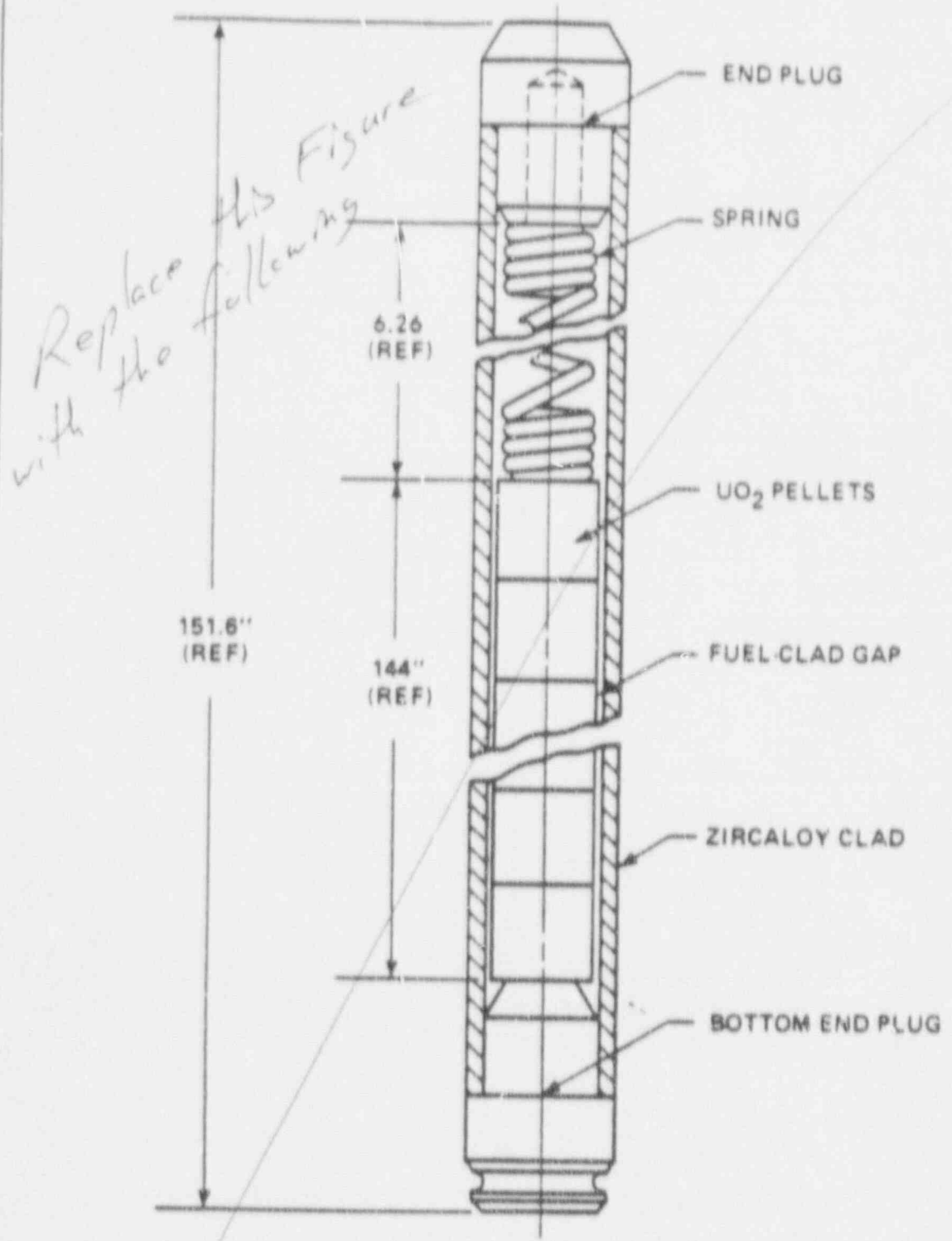

SPECIFIC DIMENSIONS DEPEND ON DESIGN VARIABLES SUCH AS PRE-PRESSURIZATION, POWER HISTORY, AND DISCHARGE BURNUP

FIGURE 4.2-3
FUEL ROD SCHEMATIC
BEAVER VALLEY POWER STATION - UNIT 2
FINAL SAFETY ANALYSIS REPORT

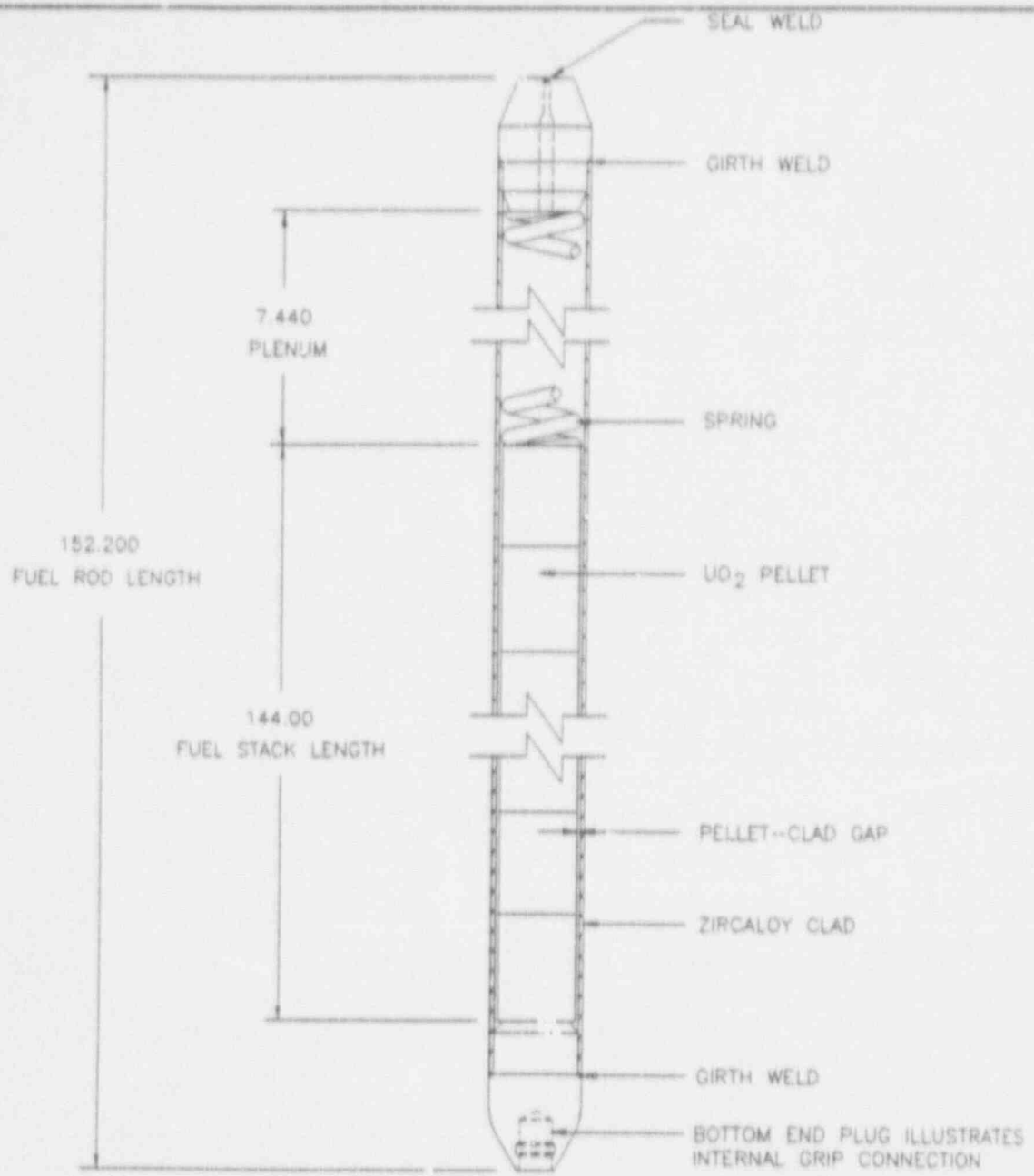

SPECIFIC DIMENSIONS DEPEND ON DESIGN VARIABLES SUCH AS PREPRESSURIZATION, POWER HISTORY, AND DISCHARGE BURNUP

BEAVER VALLEY POWER STATION - UNIT 2
FIGURE 4.2-3

FUEL ROD SCHEMATIC

Replace this Figure with the following

MID GRID EXPANSION JOINT DESIGN

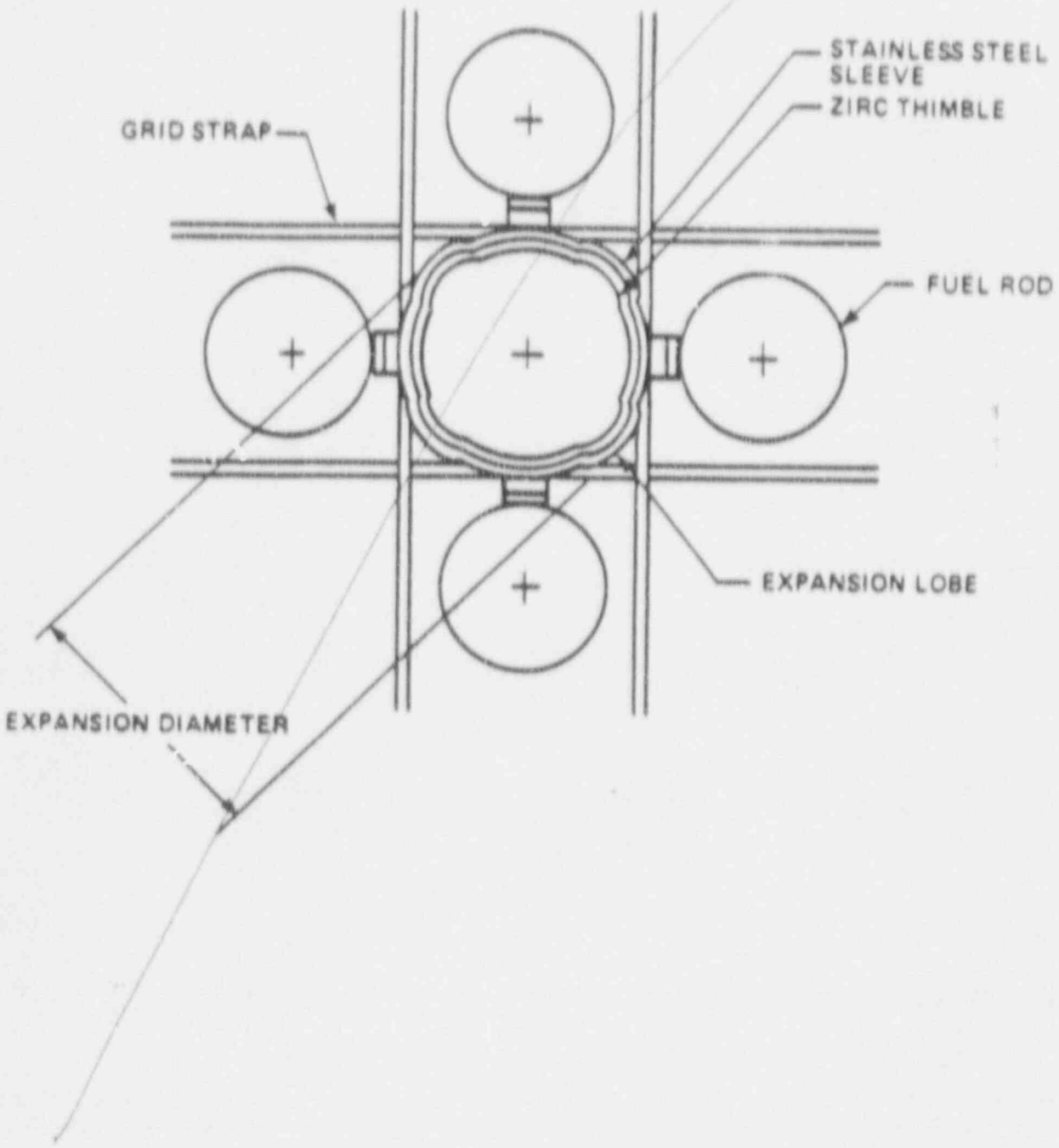

FIGURE 4.2-4
PLAN VIEW MID GRID EXPANSION JOINT DESIGN
BEAVER VALLEY POWER STATION - UNIT 2
FINAL SAFETY ANALYSIS REPORT

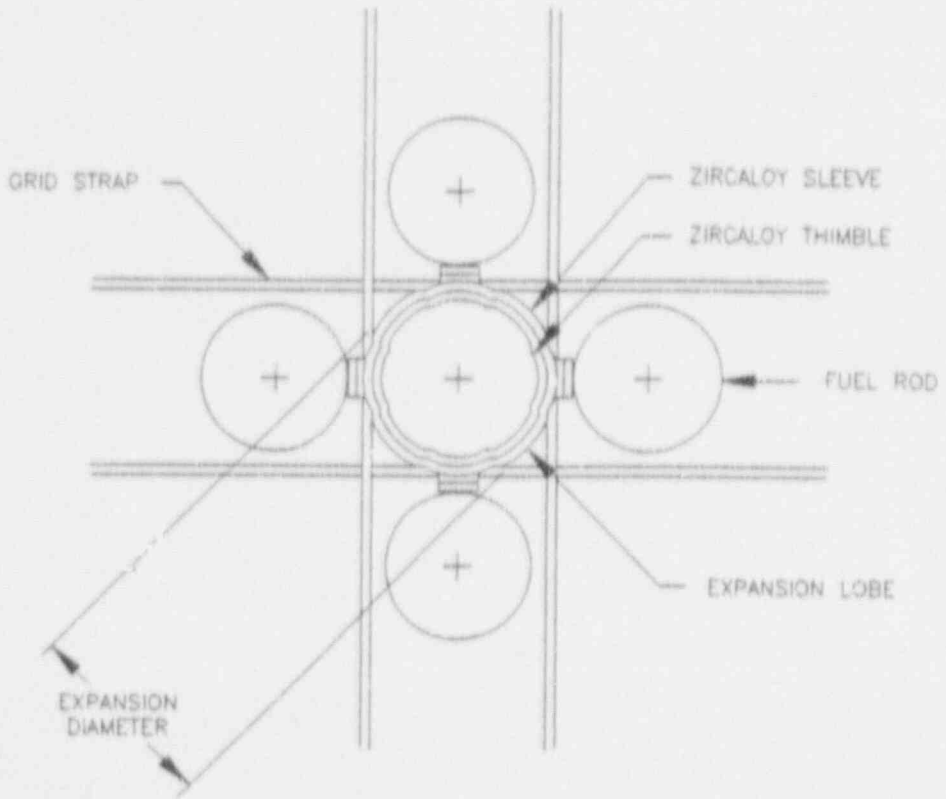

MID GRID EXPANSION JOINT DESIGN

BEAVER VALLEY POWER STATION - UNIT 2 FIGURE 4.2-4
MID GRID EXPANSION JOINT PLAN VIEW

Replace this figure with the following

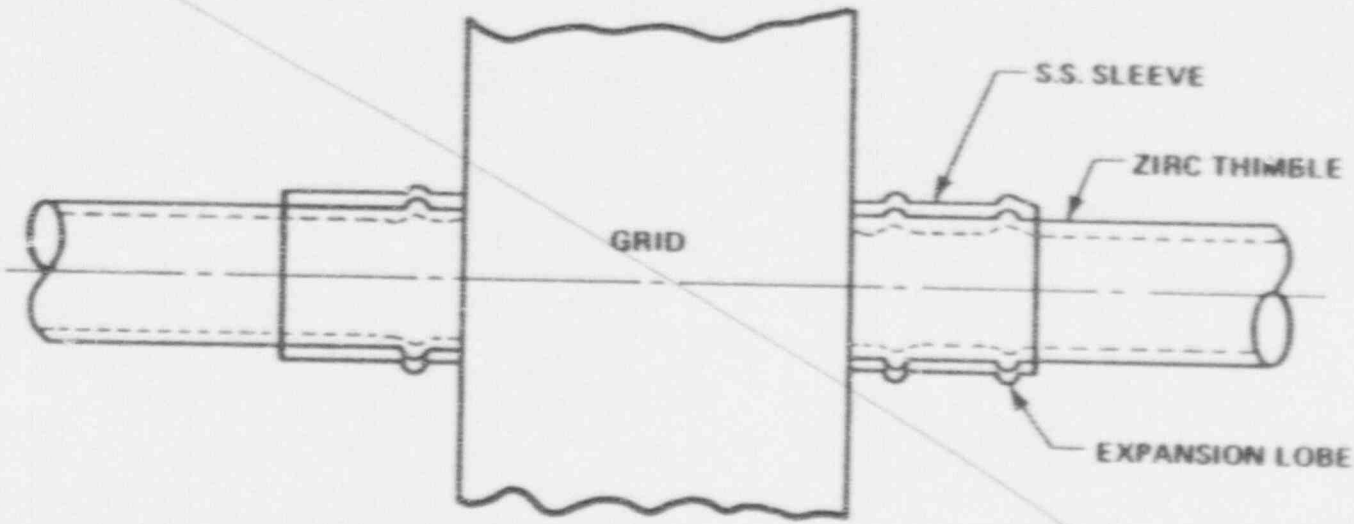

FIGURE 4.2-5
ELEVATION VIEW GRID TO THIMBLE ATTACHMENT
BEAVER VALLEY POWER STATION - UNIT 2
FINAL SAFETY ANALYSIS REPORT

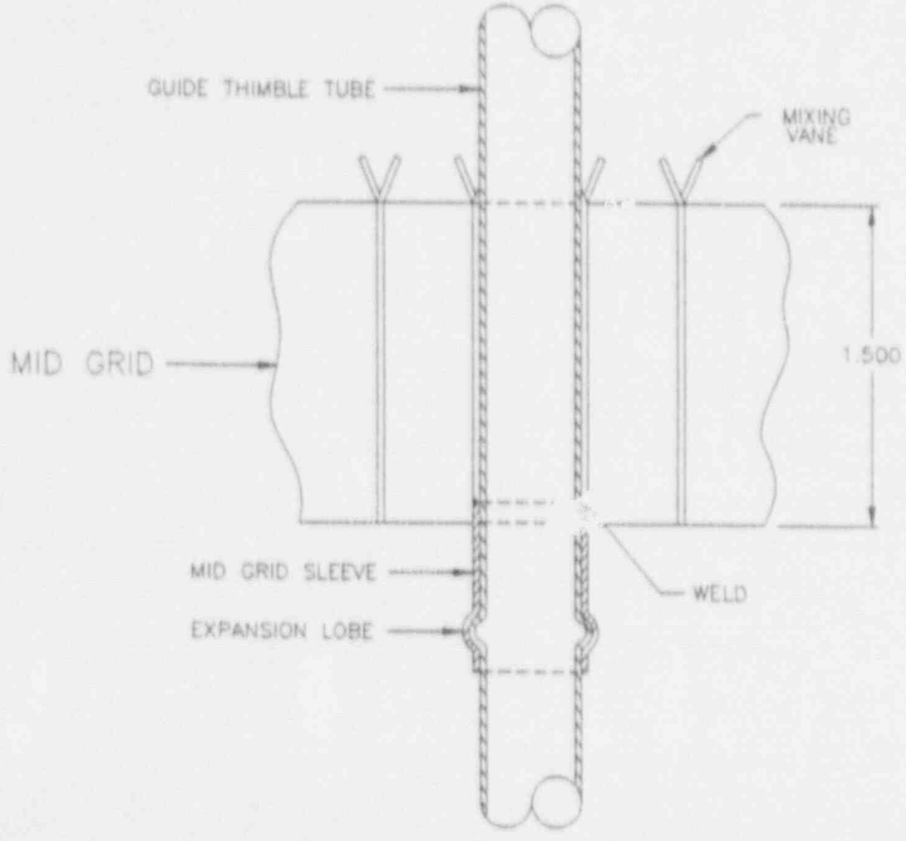

BEAVER VALLEY POWER STATION - UNIT 2

FIGURE 4.2-5

MID GRID EXPANSION JOINT

ELEVATION VIEW

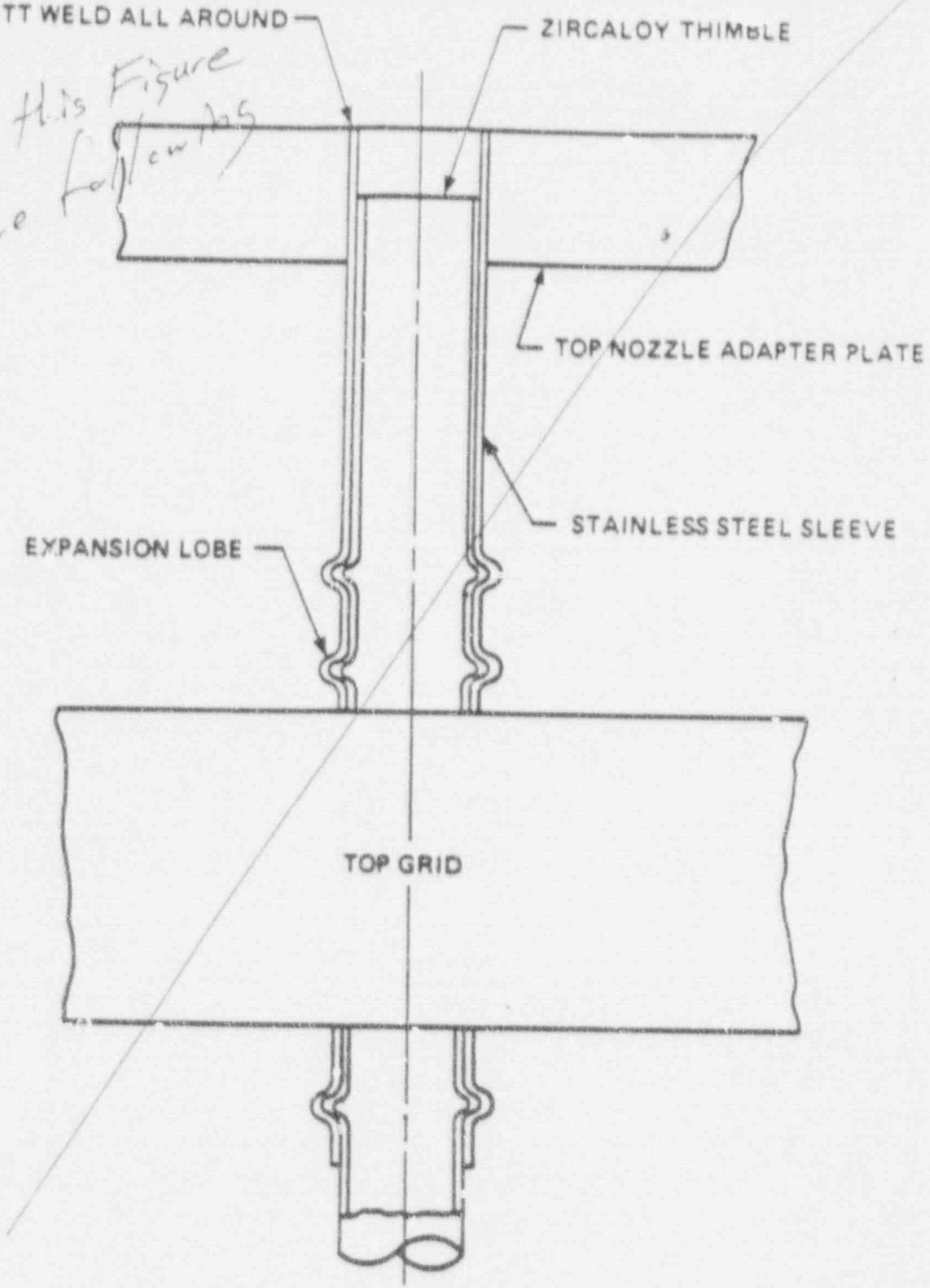

Replace this Figure with the following

FIGURE 4.2-6
TOP GRID TO NOZZLE ATTACHMENT
BEAVER VALLEY POWER STATION-UNIT 2
FINAL SAFETY ANALYSIS REPORT

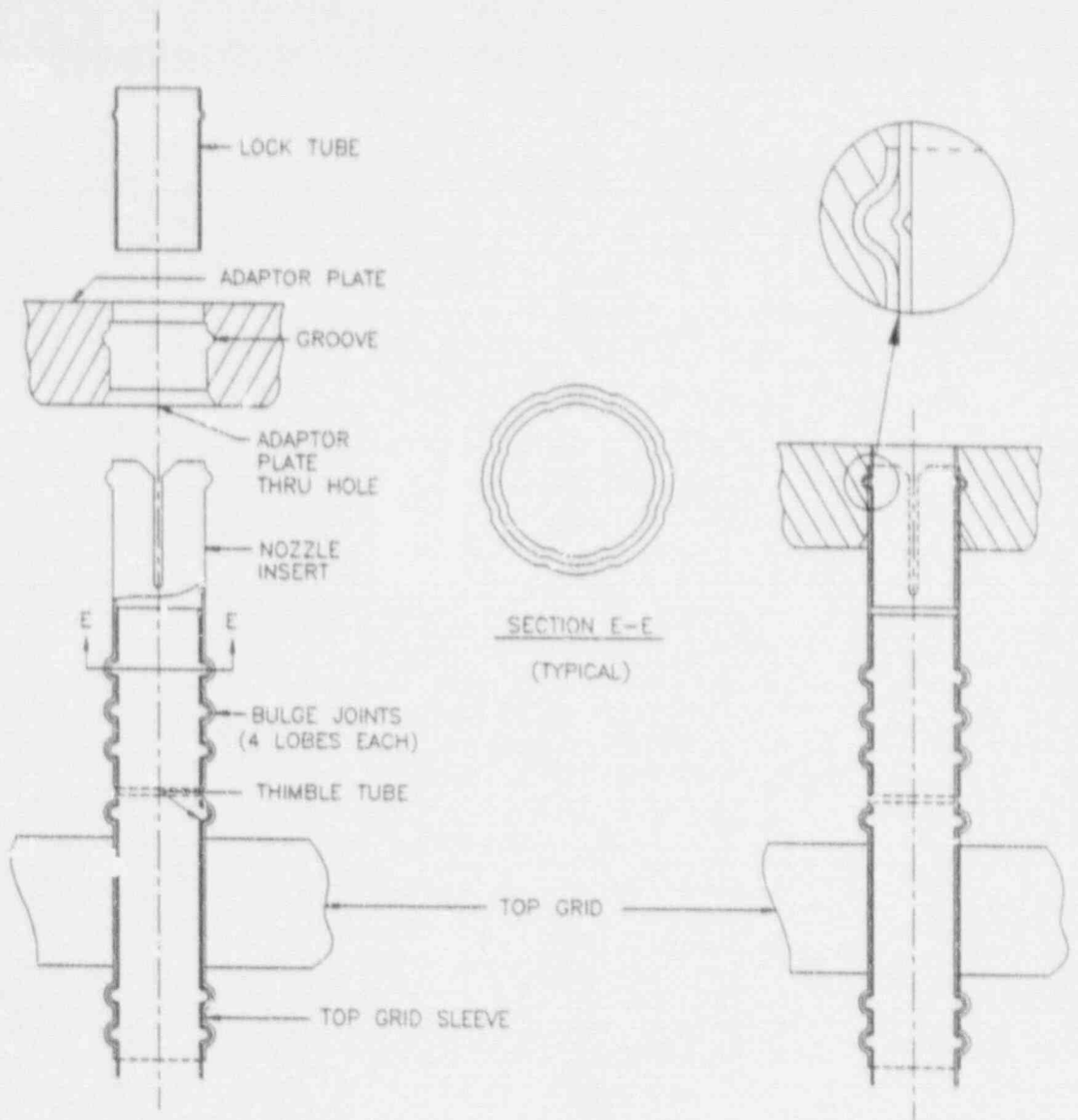

BEAVER VALLEY POWER STATION - UNIT 2
FIGURE 4.2-6

THIMBLE / INSERT / TOP GRID SLEEVE
BULGE JOINT GEOMETRY

Replace this Figure with the followings.

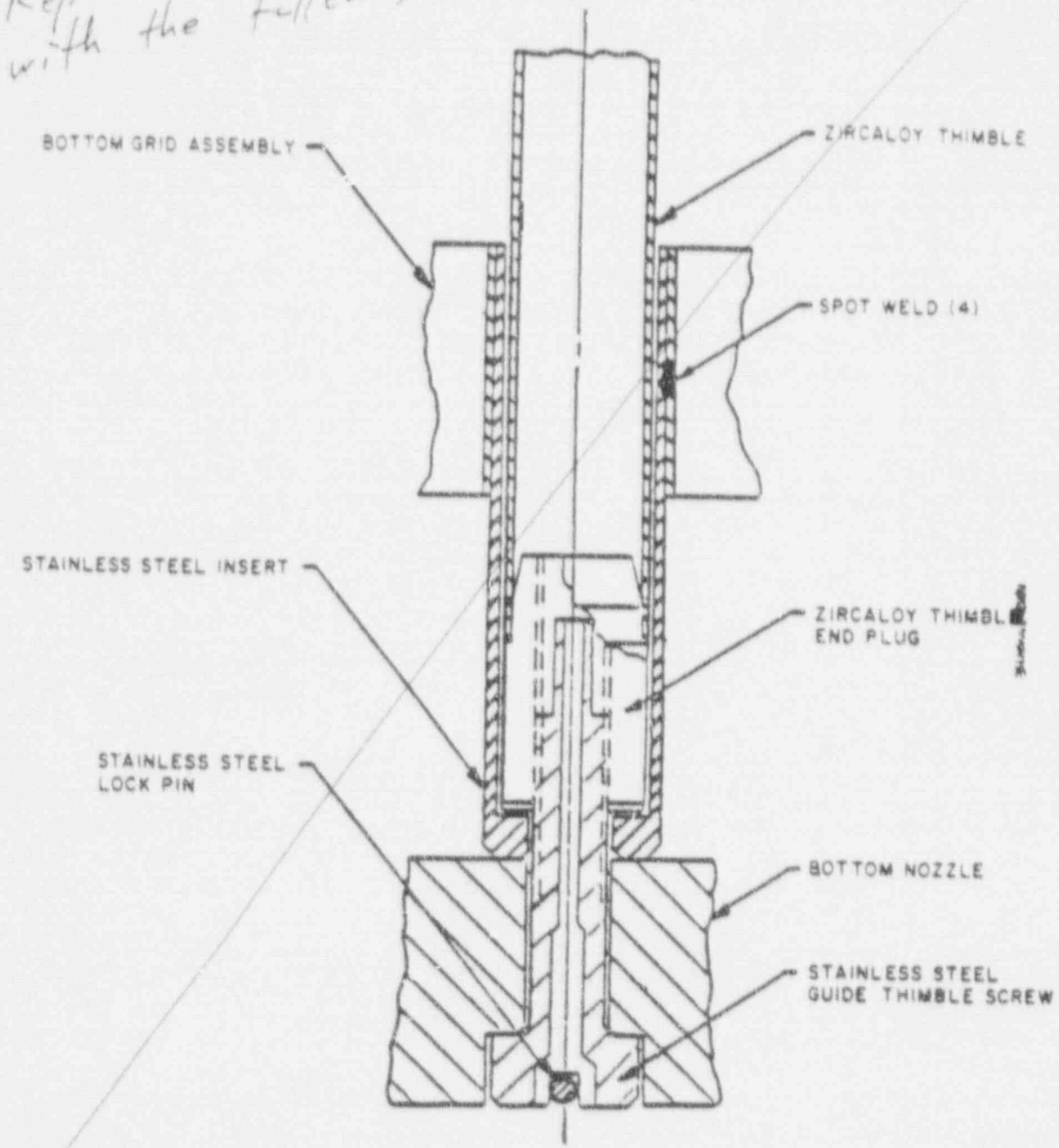

FIGURE 4.2-7
GUIDE THIMBLE TO BOTTOM NOZZLE JOINT
BEAVER VALLEY POWER STATION-UNIT 2
FINAL SAFETY ANALYSIS REPORT

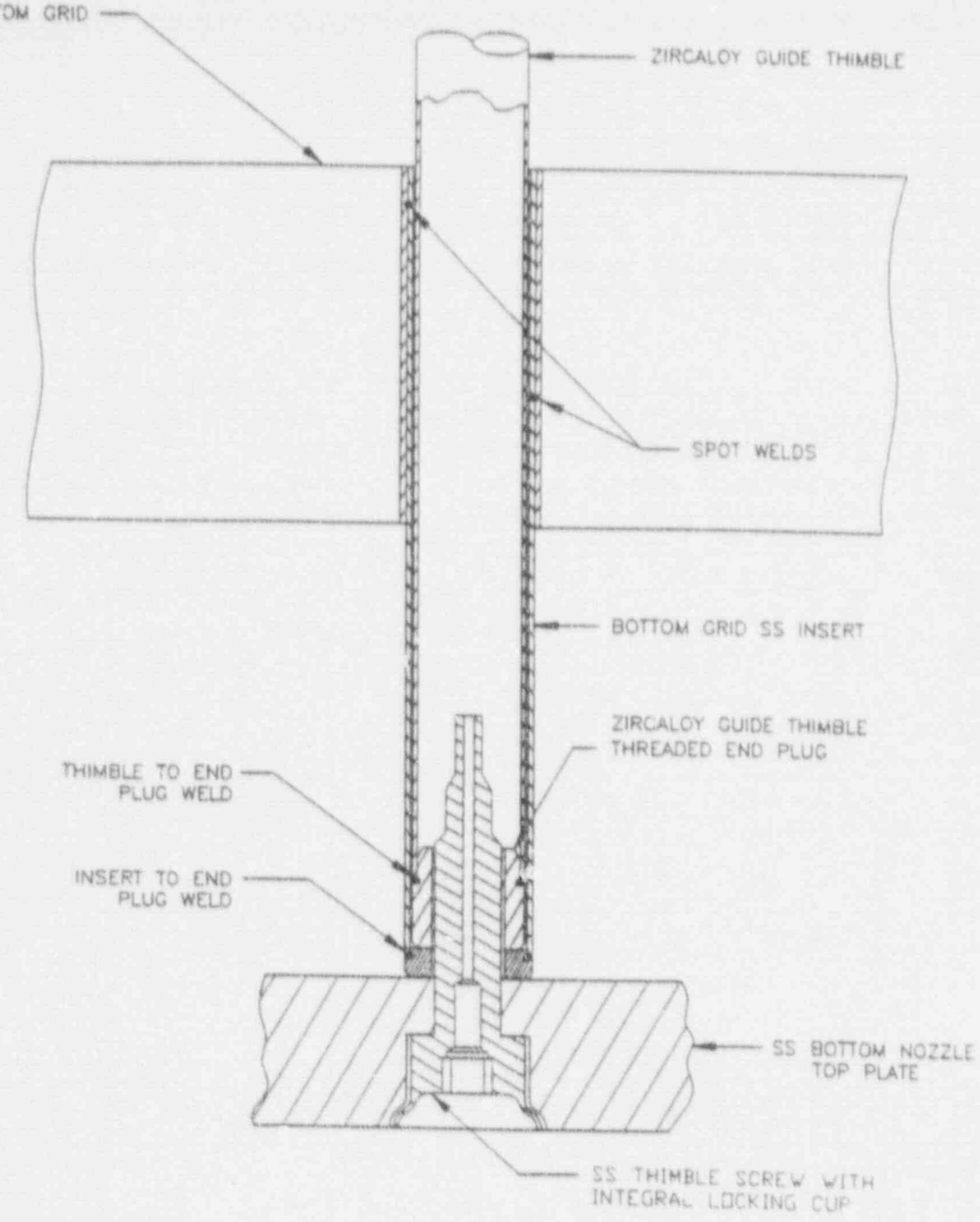

BEAVER VALLEY POWER STATION - UNIT 2
FIGURE 4.2-7

GUIDE THIMBLE TO BOTTOM NOZZLE JOINT

Section 4.3

against. ANS Condition IV faults shall not cause a release of radioactive material that results in an undue risk to public health and safety.

The core design power distribution limits related to fuel integrity are met for ANS Condition I occurrences through conservative design and maintained by the action of the control system. The requirements for ANS Condition II occurrences are met by providing an adequate protection system which monitors reactor parameters. The control and protection systems are described in Chapter 7, and the consequences of ANS Condition II, III, and IV occurrences are given in Chapter 15.

4.3.1.1 Fuel Burnup

Basis

The fuel rod design basis is described in Section 4.2. The nuclear design basis is to install sufficient reactivity in the fuel to attain a region discharge burnup of 32,000 MWD/MTU. The above, along with the design basis in Section 4.3.1.3, satisfies GDC-10.

Discussion

Fuel burnup is a measure of fuel depletion which represents the integrated energy output of the fuel (MWD/MTU) and is a convenient means for quantifying fuel exposure criteria.

The core design lifetime or design discharge burnup is achieved by installing sufficient initial excess reactivity in each fuel region and by following a fuel replacement program (such as that described in Section 4.3.2.1) that meets all safety-related criteria in each cycle of operation.

Initial excess reactivity installed in the fuel, although not a design basis, must be sufficient to maintain core criticality at full power operating conditions throughout cycle life with equilibrium xenon, samarium, and other fission products present. The end of design cycle life is defined to occur when the chemical shim concentration is essentially zero with control rods present to the degree necessary for operational requirements (e.g., the controlling bank at the "bite" position). In terms of chemical shim boron concentration, this represents approximately 10 ppm with no control rod insertion.

A limitation on initial installed excess reactivity is not required other than as is quantified in terms of other design bases, such as core negative reactivity feedback and shutdown margin, discussed below.

Discussion

ANSI Standard N18.2 specifies a k_{eff} not to exceed 0.95 in spent fuel storage racks and transfer equipment flooded with pure water and a k_{eff} not to exceed 0.98 in normally dry new fuel storage racks, assuming optimum moderation. No criterion is given for the refueling operation. However, a 5-percent margin, which is consistent with spent fuel storage and transfer and the new fuel storage, is adequate for the controlled and continuously monitored operations involved.

The boron concentration required to meet the refueling shutdown criteria is specified in the Technical Specifications. Verification that this shutdown criteria is met, including uncertainties, is achieved using standard Westinghouse design methods, such as the ~~LEOPARD~~ PHOENIX-P/ANC codes (~~Barry 1963~~ Nguyen 1988). ~~TURTLE (Barry and Altomare 1975), a diffusion theory code, and PALADON (Camden et al 1978), a nodal analysis code~~. The subcriticality of the core is continuously monitored as described in the Technical Specifications.

4.3.1.6 Stability

Basis

The core will be inherently stable to power oscillations at the fundamental mode. This satisfies GDC-12.

Spatial power oscillations within the core with a constant core power output, should they occur, can be reliably and readily detected and suppressed.

Discussion

Oscillations of the total power output of the core, from whatever cause, are readily detected by the reactor coolant loop temperature sensors and by the nuclear instrumentation. The core is protected by these systems, and a reactor trip would occur if power increased unacceptably, preserving the design margins to fuel design limits. The stability of the turbine/steam generator/core systems and the reactor control system is such that total core power oscillations are not normally possible. The redundancy of the protection circuits ensures an extremely low probability of exceeding design power levels.

The core is designed so that diametral and azimuthal oscillations due to spatial xenon effects are self-damping, and no operator action or control action is required to suppress them. The stability to diametral oscillations is so great that this excitation is highly improbable. Convergent azimuthal oscillations can be excited by prohibited motion of individual control rods. Such oscillations are readily observable and alarmed, using the excore power range ion chambers. Indications are also continuously available from incore thermocouples and loop temperature measurements. Movable incore

detectors can be activated to provide more detailed information. In all proposed cores, these horizontal plane oscillations are self-damping by virture of reactivity feedback effects designed into the core.

Axial xenon spatial power oscillations may occur late in core life. The control bank and excore detectors are provided for control and monitoring of axial power distributions. Assurance that fuel design limits are not exceeded is provided by reactor overpower ΔT and overtemperature ΔT trip functions which use the measured axial power imbalance as an input.

4.3.1.7 Anticipated Transients Without Trip

The effects of anticipated transients with failure to trip are not considered in the design bases of the plant. Analysis has shown that the likelihood of such a hypothetical event is negligibly small. Furthermore, analysis of the consequences of a hypothetical failure to trip following anticipated transients has shown that no significant core damage would result, system peak pressures would be limited to acceptable values, and no failure of the reactor coolant system would result (Westinghouse 1974).

4.3.2 Description

4.3.2.1 Nuclear Design Description

The reactor core consists of a specified number of fuel rods which are held in bundles by spacer grids and top and bottom nozzles. The fuel rods are constructed of cylindrical Zircaloy tubes containing UO_2 fuel pellets. The bundles, known as fuel assemblies, are arranged in a pattern which approximates a right circular cylinder.

Each fuel assembly contains a 17 x 17 rod array composed of 264 fuel rods, 24 rod cluster control thimbles, and an incore instrumentation thimble. Figure 4.2-1 shows a cross-sectional view of a 17 x 17 fuel assembly and the related rod cluster control locations. Further details of the fuel assembly are given in Section 4.2.

Insert A The fuel rods within a given assembly have the same uranium enrichment ~~in both the radial and axial planes~~. Fuel assemblies of several → ~~three~~ different enrichments are used in the ~~initial~~ core loading to establish a favorable radial power distribution. ~~Figure 4.3-1 shows the fuel loading pattern to be used in the first core. Two regions consisting of the two lower enrichments are interspersed so as to form a checkerboard pattern in the central portion of the core. The third region is arranged around the periphery of the core and contains the highest enrichment. The enrichments for the first core are shown in Table 4.3-1.~~

The reference reloading pattern is typically similar to Figure 4.3-1 with depleted fuel interspersed checkerboard style in the center and

Insert A p. 4.3-7

in the radial plane. However, the uranium enrichment may change with fuel height (e.g., the fuel assemblies may use unenriched uranium fuel in the top and bottom six inches of the fuel rods. The middle 120 inches of each assembly would then contain the enriched uranium fuel.).

~~new~~ burned fuel on the periphery. The core will normally operate approximately ~~one year~~ eighteen months between refueling, accumulating approximately 16 13,000 MWD/MTU per ~~year~~ cycle. The exact reloading pattern, initial and final positions of assemblies, and the number of fresh assemblies and their placement are dependent on the energy requirement for the next cycle and burnup and power histories of the previous cycles.

The core average enrichment is determined by the amount of fissionable material required to provide the desired core lifetime and energy requirements, namely a region average discharge burnup of 33,000 MWD/MTU. The physics of the burnout process is such that operation of the reactor depletes the amount of fuel available due to the absorption of neutrons by the U-235 atoms and their subsequent fission. The rate of U-235 depletion is directly proportional to the power level at which the reactor is operated. In addition, the fission process results in the formation of fission products, some of which readily absorb neutrons. These effects, depletion, and the buildup of fission products, are partially offset by the buildup of plutonium, as shown on Figure 4.3-2 for a typical 17 x 17 fuel assembly, which occurs due to the nonfission absorption of neutrons in U-238. Therefore, at the beginning of any cycle, a reactivity reserve equal to the depletion of the fissionable fuel and the buildup of fission product poisons over the specified cycle life must be "built" into the reactor. This excess reactivity is controlled by removable neutron absorbing material in the form of boron dissolved in the primary coolant and burnable ~~poison rods~~ absorber.

The concentration of boric acid in the reactor coolant is varied to provide control and to compensate for long-term reactivity requirements. The concentration of the soluble neutron absorber is varied to compensate for reactivity changes due to fuel burnup; fission product poisoning, including xenon and samarium; burnable poison depletion; and the cold-to-operating moderator temperature change. Using its normal makeup path, the chemical and volume control system (CVCS) is capable of inserting negative reactivity at a rate of approximately 30 pcm/min when the reactor coolant boron concentration is 1,000 ppm and approximately 35 pcm/min when reactor coolant boron concentration is 100 ppm. If the emergency boration path is used, the CVCS is capable of inserting negative reactivity at a rate of approximately 65 pcm/min when the reactor coolant concentration is 1,000 ppm and approximately 75 pcm/min when the reactor coolant boron concentration is 100 ppm. The peak burnout rate for xenon is 25 pcm/min (Section 9.3.4 discusses the capability of the CVCS to counteract xenon decay). Rapid transient reactivity requirements and safety shutdown requirements are met with control rods.

As the boron concentration is increased, the moderator temperature coefficient becomes less negative. The use of a soluble absorber alone would result in a positive moderator coefficient at beginning-of-life, ~~for the first cycle~~. Therefore, burnable absorbers ~~rods~~ are used ~~in the first core~~ to sufficiently reduce the soluble boron concentration to

ensure that the moderator temperature coefficient is negative for power operating conditions. The use of control rods may be required early in the cycle at low power to ensure a negative moderator temperature coefficient is achieved. During operation, the poison content in the burnable absorber ~~rods~~ is depleted, thus adding positive reactivity to offset some of the negative reactivity from fuel depletion and fission product buildup. The depletion rate of the burnable absorber ~~rods~~ is not critical since chemical shim is always available and flexible enough to cover any possible deviations in the expected burnable absorber depletion rate. Figure 4.3-3 shows plots of typical core depletion with and without burnable absorber, ~~rods. Note that even at end-of-life conditions, presence of the burnable absorber rods results in a net decrease in the first cycle lifetime. Upon completion of the first cycle, all the burnable absorber rods are normally removed because the moderator temperature coefficient in reload cores is sufficiently negative.~~

In addition to reactivity control, the burnable absorber rods are strategically located to provide a favorable radial power distribution. Figures 4.3-4 and 4.3-4 a through h shows the burnable absorber distributions within a fuel assembly for the several burnable absorber patterns used in a 17 x 17 array. A typical ~~initial~~ reload core burnable absorber loading pattern is shown in Figure 4.3-5. Integral or Integral Fuel Burnable Absorbers (IFBA)

Table 4.3-1 through 4.3-3 contain summaries of the reactor core design parameters for the first fuel cycle, including reactivity coefficients, delayed neutron fraction, and neutron lifetimes. Sufficient information is included to permit an independent calculation of the nuclear performance characteristics of the core.

4.3.2.2 Power Distributions

The accuracy of power distribution calculations has been confirmed through approximately 1,000 flux maps during some 20 years of operation under conditions very similar to those expected. Details of this confirmation are given in Langford and Nath (1971) and in Section 4.3.3.2.7.

4.3.2.2.1 Definitions

Power distributions are quantified in terms of hot channel factors. These factors are a measure of the peak pellet power within the reactor core and the total energy produced in a coolant channel, relative to the total reactor power output, and are expressed in terms of quantities related to the nuclear or thermal design, namely:

1. Power density - the thermal power produced per unit volume of the core (kW/liter).

2. Linear power density - the thermal power produced per unit length of active fuel (kW/ft). Because fuel assembly geometry is standardized, this is the unit of power density

Including densification allowance:

$$F_Q = \max \left[F^N_{XY} (Z) \times P (Z) \times S (Z) \right] \times F^N_U \times F^E_Q$$

4.3.2.2.2 Radial Power Distributions

The power shape in horizontal sections of the core at full power is a function of the fuel and burnable absorber loading patterns, and the presence or absence ~~for~~ of a single bank of control rods. Thus, at any time in the cycle, a horizontal section of the core can be characterized as unrodded or with group D control rods. These two situations, combined with burnup effects, determine the radial power shapes which can exist in the core at full power. The effect on radial power shapes of power level, xenon, samarium, and moderator density effects are also considered but these are quite small. The effect of nonuniform flow distribution is negligible. While radial power distributions in various planes of the core are often illustrated, the core radial enthalpy rise distribution, as determined by the integral of power up each channel, is of greater interest. Figures 4.3-6 through 4.3-10 show typical radial power distributions for 1/8th of the core for representative operating conditions. These conditions are: 1) hot full power (HFP) at beginning-of-life (BOL), no xenon, 2) HFP at BOL, unrodded, equilibrium xenon, 3) HFP near BOL, bank D in, equilibrium xenon, 4) HFP near middle-of-life (MOL), unrodded, equilibrium xenon, and 5) HFP near end-of-life (EOL), unrodded, equilibrium xenon.

partially

Because the position of the hot channel varies from time to time, a single reference radial design power distribution is selected for DNB calculations. This reference power distribution is conservatively chosen to concentrate power in one area of the core, minimizing the benefits of flow redistribution. Assembly powers are normalized to core average power. The radial power distribution within a fuel rod and its variation with burnup as utilized in thermal calculations and fuel rod design is discussed in Section 4.4.

4.3.2.2.3 Assembly Power Distributions

For the purpose of illustration, typical assembly power distributions for the BOL and EOL conditions, corresponding to Figures 4.3-7 and 4.3-10, respectively, are given for the same assembly in Figures 4.3-11 and 4.3-12, respectively.

Because the detailed power distribution surrounding the hot channel varies from time to time, a conservatively flat assembly power distribution is assumed in the DNB analysis, described in Section 4.4, with the rod of maximum $F^N_{\Delta H}$ integrated power artificially raised to the design value of $F_{\Delta H}$. Care is taken in the nuclear design of all fuel cycles and all operating conditions to ensure that

1. Control rods in a single bank move together with no individual rod insertion differing by more than 13 steps (indicated) from the bank demand position.

2. Control banks are sequenced with overlapping banks.

3. The control rod bank insertion limits are not violated.

4. Axial power distribution control procedures, which are given in terms of flux difference control and control bank position, are observed.

The axial power distribution procedures referred to above are part of the required operating procedures which are followed in normal operation. Briefly, they require control of the axial offset (flux difference divided by fractional power) at all power levels within a permissible operating band of a target value corresponding to the equilibrium full power value. In ~~the first~~ cycle, the target value changes ~~linearly~~ from about ~~minus 10 to 0~~ percent through the life of the cycle. This minimizes xenon transient effects on the axial power distribution, because the procedures essentially keep the xenon distribution in phase with the power distribution.

Calculations are performed for normal operation of the reactor, including load following maneuvers. Beginning, middle, and end-of-cycle conditions are included in the calculations. Different histories of operation are assumed prior to calculating the effect of load follow transients on the axial power distribution. These different histories assume base loaded operation and extensive load following. For a given plant and fuel cycle, a finite number of maneuvers are studied to determine the general behavior of the local power density as a function of core elevation.

These cases represent many possible reactor states in the life of one fuel cycle, and they have been chosen as sufficiently definitive of the cycle by comparison with much more exhaustive studies performed on some 20 or 30 different, but typical, plant and fuel cycle combinations. The cases are described in detail in Morita et al (1974), and they are considered to be necessary and sufficient to generate a local power density limit which, when increased by 5 percent for conservatism, will not be exceeded with a 95-percent confidence level. Many of the points do not approach the limiting envelope. However, they are part of the time histories which lead to the hundreds of shapes which do define the envelope. They also serve as a check that the reactor studied is typical of those more exhaustively studied.

Thus, it is not possible to single out any transient or steady-state condition which defines the most limiting case. It is not even possible to separate out a small number which form an adequate analysis. The process of generating a myriad of shapes is essential to the philosophy that leads to the required level of confidence. A

maneuver which provides a limiting case for one reactor fuel cycle (defined as approaching the line of Figure 4.3-20) is not necessarily a limiting case of another reactor or fuel cycle with different control bank worths, enrichments, burnup, coefficient, etc. Each shape depends on the detailed history of operation up to that time and on the manner in which the operator conditioned xenon in the days immediately prior to the time at which the power distribution is calculated.

The calculated points are synthesized from axial calculations combined with radial factors appropriate for rodded and unrodded planes, ~~in the first cycle.~~ In these calculations, the effects on the unrodded radial peak of xenon redistribution that occurs following the withdrawal of a control bank (or banks) from a rodded region is obtained from two-dimensional X-Y calculations. A 1.03 factor to be applied on the unrodded radial peak was obtained from calculations in which xenon distribution was preconditioned by the presence of control rods and then allowed to redistribute for several hours. A detailed discussion of this effect may be found in Morita et al (1974). The calculated values have been increased by a factor of 1.05 for conservatism and a factor of 1.03 for the engineering factor F_Q^E.

The envelope drawn over the calculated points (max F_Q x power) in Figure 4.3-20 represents an upper bound envelope on local power density versus elevation in the core. It should be emphasized that this envelope is a conservative representation of the bounding values of local power density. Expected values are considerably smaller, and, in fact, less conservative bounding values may be justified with additional analysis or surveillance requirements. For example, Figure 4.3-20 bounds both BOL and EOL conditions but without consideration of radial power distribution flattening with burnup, i.e., both BOL and EOL points presume the same radial peaking factor. Inclusion of the burnup flattening effect would reduce the local power densities corresponding to EOL conditions which may be limiting at the higher core elevations.

Finally, as previously discussed, this upper bound envelope is based on procedures of load follow which require operation within an allowed deviation from a target equilibrium value of axial flux difference. These procedures are detailed in the Technical Specifications and are followed by relying only upon excore surveillance supplemented by the normal monthly full core map requirement and by computer-based alarms on deviation and time of deviation from the allowed flux difference band.

Accident analyses are presented in Chapter 15. The results of these analyses determined a limiting value of total peaking factor, F_Q, of 2.32 under normal operation, including load following maneuvers. This value is derived from the conditions necessary to satisfy the limiting conditions specified in the LOCA analyses of Section 15.6.5. As noted previously in this section, an upper bound envelope of

Chapter 15. The reactivity coefficients are calculated on a corewise basis by radial and axial diffusion theory methods and with nodal analysis methods. The effect of radial and axial power distribution on core average reactivity coefficients is implicit in those calculations and is not significant under normal operating conditions. For example, a skewed xenon distribution which results in changing axial offset by 5 percent, changes the moderator and Doppler temperature coefficients by less than 0.01 pcm/°F and 0.03 pcm/°F, respectively. An artificially skewed xenon distribution which results in changing the radial $F^N_{\Delta H}$ by 3 percent, changes the moderator and Doppler temperature coefficients by less than 0.03 pcm/°F and 0.001 pcm/°F, respectively. The spatial effects are accentuated in some transient conditions; for example, in the postulated rupture of the main steam line and rupture of a rod cluster control assembly mechanism housing described in Sections 15.1.5 and 15.4.8, and are included in these analyses.

The analytical methods and calculational models used in calculating the reactivity coefficients are given in Section 4.3.3. These models have been confirmed through extensive testing of more than 30 cores similar to the plant described herein; results of these tests are discussed in Section 4.3.3.

Quantitative information for calculated reactivity coefficients, including fuel-Doppler coefficient, moderator coefficients (density, temperature, pressure, and void), and power coefficient is given in the following sections.

4.3.2.3.1 Fuel Temperature (Doppler) Coefficient

The fuel temperature (Doppler) coefficient is defined as the change in reactivity per degree change in effective fuel temperature and is primarily a measure of the Doppler broadening of U-238 and Pu-240 resonance absorption peaks. Doppler broadening of other isotopes, such as U-236 and Np-237, is also considered but their contribution to the Doppler effect is small. An increase in fuel temperature increases the effective resonance absorption cross-section of the fuel and produces a corresponding reduction in reactivity.

Insert A ~~The fuel temperature coefficient is calculated by performing two-group X-Y calculations, using an updated version of the TURTLE Code (Barry and Altomare 1975).~~ Moderator temperature is held constant, and the power level is varied. Spatial variation of fuel temperature is taken into account by calculating the effective fuel temperature as a function of power density, as discussed in Section 4.3.3.1.

A typical Doppler temperature coefficient is shown in Figure 4.3-26 as a function of the effective fuel temperature (at BOL and EOL conditions). The effective fuel temperature is lower than the volume averaged fuel temperature, since the neutron flux distribution is non-uniform through the pellet and gives preferential weight to the surface temperature. A typical Doppler-only contribution to the

Insert A p. 4.3-23

The fuel temperature coefficient is calculated by performing two-group X-Y calculations using: a) an updated version of the TURTLE code (Barry and Altomare 1975), or b) the Advanced Nodal Code (ANC) (Liu, et.al., 1986)

With burnup, the moderator coefficient becomes more negative, primarily as a result of boric acid dilution, but also to a significant extent from the effects of the buildup of plutonium and fission products.

The moderator coefficient is calculated for the various plant conditions by performing two-group ~~X-Y~~ dimensional calculations, varying the moderator temperature (and density) by about ±5°F about each of the mean temperatures. The moderator coefficient is shown as a function of core temperature and boron concantration for a typical unrodded and rodded core in Figures 4.3-29 through 4.3-31. The temperature range covered is from cold (68°F) to about 600°F. The contribution due to Doppler coefficient (because of change in moderator temperature) has been subtracted from these results. Figure 4.3-32 shows the hot, full power moderator temperature coefficient for a typical core plotted as a function of ~~burnup~~ cycle lifetime for the just critical boron concentration condition based on the design boron concentration reduction as a function of burnup (Figure 4.3-3.).

The moderator coefficients presented here are calculated on a corewide basis, since they are used to describe the core behavior in normal and accident situations when the moderator temperature changes can be considered to affect the entire core.

Moderator Pressure Coefficient

The moderator pressure coefficient relates the change in moderator density, resulting from a reactor coolant pressure change, to the corresponding effect on neutron production. This coefficient is of much less significance in comparison with the moderator temperature coefficient.

A change of 50 psi in pressure has approximately the same effect on reactivity as a 1/2 degree change in moderator temperature. This coefficient can be determined from the moderator temperature coefficient by relating change in pressure to the corresponding change in density. The moderator pressure coefficient may be negative over a portion of the moderator temperature range at BOL (-0.004 pcm/psi, BOL) but is always positive at operating conditions and becomes more positive during life (+0.3 pcm/psi, EOL).

Moderator Void Coefficient

The moderator void coefficant relates the change in neutron multiplication to the presence of voids in the moderator. In a pressurized water reactor, this coefficient is not very significant because of the low void content in the coolant. The core void content is less than 1/2 of 1 percent and is due to local or statistical boiling. The void coefficient varies from 50 pcm/percent void at BOL and at low temperatures to -250 pcm/percent void at EOL and at operating temperatures. The negative void coefficient at operating temperature becomes more negative with fuel burnup.

transient analysis even though the extreme coefficients assumed may not simultaneously occur at the conditions of lifetime, power level, temperature and boron concentration assumed in the analysis. The need for a reevaluation of any accident in a subsequent cycle is contingent upon whether or not the coefficients for that cycle fall within the identified range used in the analysis presented in Chapter 15 with due allowance for the calculational uncertainties given in Section 4.3.3.3. Control rod requirements are given in Table 4.3-3 for ~~the core described and for a hypothetical equilibrium cycle, since these are markedly different. Those latter numbers are provided for information only and their validity in a particular cycle would be an unexpected coincidence~~ both a first cycle and a typical reload

4.3.2.4 Control Requirements

To ensure the shutdown margin stated in the Technical Specifications under conditions where a cooldown to ambient temperature is required, concentrated soluble boron is added to the reactor coolant. Boron concentrations for several core conditions are listed in Table 4.3-2. For all core conditions including refueling, the boron concentration is well below the solubility limit. The rod cluster control assemblies are employed to bring the reactor to the hot standby condition. The minimum required shutdown margin is given in the Technical Specifications.

The ability to accomplish the shutdown for hot conditions is demonstrated in Table 4.3-3 by comparing the difference between the rod cluster control assembly reactivity available with an allowance for the worst struck rod with that required for control and protection purposes. The shutdown margin includes an allowance of 10 percent for analytical uncertainties (see Section 4.3.2.4.9). The largest reactivity control requirement appears at the EOL when the moderator temperature coefficient reaches its peak negative value as reflected in the larger power defect.

The control rods are required to provide sufficient reactivity to account for the power defect from full power to zero power and to provide the required shutdown margin. The reactivity addition resulting from power reduction consists of contributions from Doppler, variable average moderator temperature, flux redistribution, and reduction in void content, as discussed below.

4.3.2.4.1 Doppler

The Doppler effect arises from the broadening of U-238 and Pu-240 resonance cross-section peaks with an increase in effective pellet temperature. This effect is most noticeable over the range of zero power to full power due to the large pellet temperature increase with power generation.

4.3.2.4.11 Chemical Poison

Boron in solution as boric acid is used to control relatively slow reactivity changes associated with:

1. The moderator temperature defect in going from cold shutdown at ambient temperature to a constant moderator temperature at equilibrium no load value.

2. The transient xenon and samarium poisoning, such as that following power changes or changes in rod cluster control position.

3. The excess reactivity required to compensate for the effects of fissile inventory depletion and buildup of long-life fission products.

4. The ~~burnable~~ absorber poison depletion.

The boron concentrations for various core conditions are presented in Table 4.3-2.

4.3.2.4.12 Rod Cluster Control Assemblies

The number of rod cluster control assemblies is shown in Table 4.3-1. The rod cluster control assemblies are used for shutdown and control purposes to offset fast reactivity changes associated with:

1. The required shutdown margin in the hot zero power, stuck rods condition.

2. The reactivity compensation as a result of an increase in power above hot zero power (power defect, including Doppler, and moderator reactivity changes).

3. Unprogrammed fluctuations in boron concentration, reactor coolant temperature, or xenon concentration (with rods not exceeding the allowable rod insertion limits).

4. Reactivity ramp rates resulting from load changes.

The allowed control bank reactivity insertion is limited at full power to maintain shutdown capability. As the power level is reduced, control rod reactivity requirements are also reduced, and more rod insertion is allowed. The control bank position is monitored, and the operator is notified by an alarm if the limit is approached. The determination of the insertion limit uses convervative xenon distributions and axial power shapes. In addition, the rod cluster control assembly withdrawal pattern determined from these analyses is used in determining power distribution factors and in determining the maximum worth of an inserted rod cluster control assembly ejection accident. For further

discussion, refer to the Technical Specifications on rod insertion limits.

Power distribution, rod ejection, and rod misalignment analyses are based on the arrangement of the shutdown and control groups of the rod cluster control assemblies shown in Figure 4.3-35. All shutdown rod cluster control assemblies are withdrawn before withdrawal of the control banks is initiated. In going from zero to 100-percent power, control banks A, B, C, and D are sequentially withdrawn. The limits of rod positions and further discussion on the basis for rod insertion limits are provided in the Technical Specifications.

4.3.2.4.13 Burnable Absorbers ~~Rods~~

~~The~~ Burnable absorbers ~~rods~~ provide partial control of the excess reactivity available ~~during the first fuel cycle~~. In doing so, ~~these rods~~ prevent the moderator temperature coefficient from being positive at normal operating conditions. ~~They~~ perform this function by reducing the requirement for soluble poison in the moderator at the beginning of the ~~first fuel~~ cycle, as previously described. For purposes of illustration, a typical burnable absorber ~~rod~~ pattern in the core, ~~together with the number of rods per assembly~~, ~~are~~ shown in Figure 4.3-5, while the arrangement within an assembly ~~are~~ displayed in Figure 4.3-4. The reactivity worth of ~~these rods~~ is shown in Table 4.3-1. The boron in the ~~rods~~ is depleted with burnup, but at a sufficiently slow rate so that the resulting critical concentration of soluble boron is such that the moderator temperature coefficient remains negative at all times for power operating conditions.

4.3.2.4.14 Peak Xenon Startup

Compensation for the peak xenon buildup is accomplished using a chemical shim control system. Startup from the peak xenon condition is accomplished with a combination of rod motion and boron dilution. The boron dilution may be made at any time, including during the shutdown period, provided the shutdown margin is maintained.

4.3.2.4.15 Load Follow Control and Xenon Control

During load follow maneuvers, power changes are accomplished using control rod motion and dilution or boration by the chemical shim control system as required. Control rod motion is limited by the control rod insertion limits on the control rods, as provided in the Technical Specifications and discussed in Section 4.3.2.4.12. The power distribution is maintained within acceptable limits through location of the control rod bank. Reactivity changes due to the changing xenon concentration can be controlled by rod motion and/or changes in the soluble boron concentration.

Rapid power increases (5 percent/min) from part power during load follow operation are accomplished with a combination of rod motion and boron dilution. Compensation for the rapid power increase is

It was observed in the second X-Y xenon test that the pressurized water reactor core with 157 fuel assemblies had become more stable due to an increased fuel depletion, and the stability index was not determined.

4.3.2.7.5 Comparison of Calculations with Measurements

The analysis of the axial xenon transient tests was performed in an axial slab geometry, using a flux synthesis technique. The direct simulation of the axial offset data was carried out using the PANDA Code (Barry et al 1975). The analysis of the X-Y xenon transient tests was performed in an X-Y geometry, using a modified TURTLE Code (Barry and Altomare 1975). Both the PANDA and TURTLE Codes solve the two-group time-dependent neutron diffusion equation with time-dependent xenon and iodine concentrations. The fuel temperature and moderator density feedback is limited to a steady-state model. All the X-Y calculations were performed in an average enthalpy plane. ← Insert A.

The basic nuclear cross-sections used in this study were generated from a unit cell depletion program which has evolved from the codes LEOPARD (Barry 1963) and CINDER (England 1962). The detailed experimental data during the tests, including the reactor power level, enthalpy rise, and the impulse motion of the control rod assembly, as well as the plant follow burnup data, were closely simulated in the study. ← Insert B

The results of the stability calculation for the axial tests are compared with the experimental data in Table 4.3-5. The calculations show conservative results for both of the axial tests with a margin of approximately -0.01 hr^{-1} in the stability index.

An analytical simulation of the first X-Y xenon oscillation test shows a calculated stability index of -0.081 hr^{-1}, in good agreement with the measured value of -0.076 hr^{-1}. As indicated earlier, the second X-Y xenon test showed that the core had become more stable compared to the first test, and no evaluation of the stability index was attempted. This increase in the core stability in the X-Y plane due to increased fuel burnup is due mainly to the increased magnitude of the negative moderator temperature coefficient.

Previous studies of the physics of xenon oscillations, including three-dimensional analysis, are reported in the series of topical reports: Poncelet and Christie (1968); Skogen and McFarlane (1969a); and Skogen and McFarlane (1969b). A more detailed description of the experimental results and analysis of the axial and X-Y xenon transient tests is presented in Lee et al (1971) and Section 1 of Eggleston (1977).

4.3.2.7.6 Stability Control and Protection

The excore detector system is utilized to provide indications of xenon-induced spatial oscillations. The readings from the excore

Insert A p. 4.3-39

Current designs use ANC, a two group time dependent neutron diffusion equation solution. Iodine, Xenon, and feedback modeling has been preserved from prior methods.

Insert B p. 4.3-39

Current designs use PHOENIX-P. This code has been extensively benchmarked against prior methods and actual data.

provide a sensitive measure of the Doppler coefficient near full power (see Section 4.3.2.7). It can be seen that Doppler defect data is typically within 0.2 percent Δρ of prediction.

4.3.3.2 Macroscopic Group Constants

Insert A

Westinghouse

Macroscopic few-group constants and consistent microscopic cross-sections (needed for feedback and microscopic depletion calculations) can be ~~are~~ generated for fuel cells by a ~~recent~~ version of the LEOPARD (Barry 1963) and CINDER (England 1962) codes, which are internally linked and provide burnup-dependent cross-sections. Normally, a simplified approximation of the main fuel chains is used. However, where needed, a complete solution for all the significant isotopes in the fuel chains, from Th-232 to Cm-244, is available (Nodvik et al 1969). Fast and thermal cross-section library tapes contain microscopic cross-sections taken for the most part from the ENDF/B (Drake 1970) library, with a few exceptions where other data provided better agreement with critical experiments, isotopic measurements, and plant critical boron values. The effect on the unit fuel cell of nonlattice components in the fuel assembly is obtained by supplying an appropriate volume fraction of these materials in an extra region which is homogenized with the unit cell in the fast (MUFT) and thermal (SOFOCATE) flux calculations. In the thermal calculation, the fuel rod, clad, and moderator are homogenized by energy-dependent disadvantage factors derived from an analytical fit to integral transport theory results.

Group constants for guide thimbles, instrument thimbles, and interassembly gaps are generated in a manner analogous to the fuel cell calculations. Reflector group constants are taken from infinite medium LEOPARD calculations. Baffle group constants are calculated from an average of core and radial reflector microscopic group constants for stainless steel.

Group constants for control rods and burnable absorbers are calculated in a linked version of the HAMMER (Suich and Honeck 1967) and AIM (Flatt and Buller 1960) codes. The Doppler broadened cross sections of the control rod and burnable absorber materials are represented as smooth cross sections in the 54-group LEOPARD fast group structure and in 30 thermal groups. The four-group constants in the rod cell and appropriate extra region are generated in the coupled space-energy transport HAMMER calculation. A corresponding AIM calculation of the homogenized rod cell with extra region is used to adjust the absorption cross-sections of the rod cell to match the reaction rates in HAMMER. These transport-equivalent group constants are reduced to two-group constants for use in space-dependant diffusion calculations. In discrete X-Y calculations, only one mesh interval per cell is used, and the rod group constants are further adjusted for use in this standard mesh by reaction rate matching the standard mesh unit assembly to a fine mesh unit assembly calculation.

Insert A p. 4.3-43

There are two lattice codes used for the generation of macroscopic group constants for use in the spatial few group diffusion codes. The first code is a linked version of LEOPARD (Barry 1963) and CINDER (England 1962) and the second code is PHOENIX-P (Nguyen, et. al., 1988). A description of each code follows.

Nodal group constants are obtained by a flux-volume homogenization of the fuel cells, burnable absorber cells, guide thimbles, instrumentation thimbles, interassembly gaps, and control rod cells from one mesh interval per cell X-Y unit fuel assembly diffusion calculations.

Validation of the cross-section method is based on analysis of critical experiments, as shown in Table 4.3-4, isotopic data, as shown in Table 4.3-8, plant critical boron (C_B) values at HZP, BOL, as shown in Table 4.3-9, and at HFP as a function of burnup, as shown in Figures 4.3-42 through 4.3-44. Control rod worth measurements are shown in Table 4.3-10.

Confirmatory critical experiments on burnable absorbers are described in Moore (1971a).

Insert A →

4.3.3.3 Spatial Few-Group Diffusion Calculations

Spatial few-group diffusion calculations primarily consist of two-group X-Y calculations using an updated version of the TURTLE Code two-group X-Y nodal calulations using PALADON(Camden et al 1978), and two-group axial calculations using an updated version of the PANDA Code.

Discrete X-Y calculations (1 mesh per cell) are carried out to determine critical boron concentrations and power distributions in the X-Y plane. An axial average in the X-Y plane is obtained by synthesis from unrodded and rodded planes. Axial effects in unrodded depletion calculations are accounted for by the axial buckling, which varies with burnup and is determined by radial depletion calculations which are matched in reactivity to the analogous R-Z depletion calculation. The moderator coefficient is evaluated by varying the inlet temperature in the same X-Y calculations used for power distribution and reactivity predictions.

Delete and replace with Insert B

Validation of TURTLE reactivity calculations is associated with the validation of the group constants themselves, as discussed in Section 4.3.3.2. Validation of the Doppler calculations is associated with the fuel temperature validation discussed in Section 4.3.3.1. Validation of the moderator coefficient calculations is obtained by comparison with plant measurements at hot zero power conditions, as shown in Table 4.3-11.

PALADON is used in two-dimensional and three-dimensional calculations. PALADON may be used in safety analysis calculations in the calculation of critical boron concentrations, control rod worths, reactivity coefficients, etc.

Insert C →

Axial calculations are used to determine differential control rod worth curves (reactivity versus rod insertion) and axial power shapes during steady-state and transient xenon conditions (flyspeck curve). Group constants and the radial buckling used in the axial calculation

Insert "A" (to page 4.3-4)

The PHOENIX-P computer code is a two-dimensional, multigroup, transport based lattice code and capable of providing all necessary data for PWR analysis. Being a dimensional lattice code, PHOENIX-P does not rely on pre-determined spatial/spectral interaction assumptions for a heterogeneous fuel lattic., henc .ll provide a more accurate multi-group flux solution than versions of LE ARD/CINDER. The PHOENIX-P computer code is approved by the USNRC as the lattice code for generating macroscopic and microscopic few group cross sections for PWR analysis (Nguyen 1988)

The solution for the detailed spatial flux and energy distribution is divided into two major steps in PHOENIX-P . In the first step, a two-dimensional fine energy group nodal solution is obtained which couples individual subcell regions (pellet clad and moderator) as well as surrounding pins. PHOENIX-P uses a method based on the Carlvik's collision probability approach and heterogeneous response fluxes which preserves the heterogeneity of the pin cells and their surroundings. The nodal solution provides accurate and detailed local flux distribution which is then used to spatially homogenize the pin cells to fewer groups.

The second step in the solution process solves for the angular flux distribution using a standard S4 discrete ordinates calculation. This step is based on the group-collapsed and homogenized cross sections obtained from the first step of the solution. The S4 fluxes are then used to normalize the detailed spatial and energy nodal fluxes. The normalized nodal fluxes are used to compute reaction rates, power distribution and to deplete the fuel and burnable absorbers. A standard B1 calculation is employed to evaluate the fundamental mode critical spectrum and to provide an improved fast diffusion coefficient for the core spatial codes.

The PHOENIX-P code employs a 42 energy group library which has been derived mainly from ENDF/B-V files. The PHOENIX-P cross sections library was designed to properly capture integral properties of the multi-group data during group collapse, and enabling proper modeling of important resonance parameters. The library contains all neutronic data necessary for modeling fuel, fission products, cladding and structural, coolant, and control/burnable absorber materials present in Light Water Reactor cores.

Group constants for burnable absorber cells, guide thimbles, instrument thimbles, control rod cells and other non-fuel cells can be obtained directly from PHOENIX-P without any adjustments such as those required in the cell or 1D lattice codes.

(Nguyen 1988 and Mildrum 1985)

B

Insert "B" (to page 4.3-4)

Spatial few-group diffusion calculations have primarily consisted of two-group X-Y calculations using an updated version of the TURTLE code, and two-group axial calculations using an updated version of the PANDA code. However, with the advent of VANTAGE 5 fuel and, hence, axial features such as axial blankets and part length burnable absorbers, there will be a greater reliance on three dimensional nodal codes such as 3D ANC (Advanced Nodal Code) (~~Reference 25~~ 38). The three dimensional nature of the nodal codes provides both the radial and axial power distributions.

Nodal three dimensional calculations are carried out to determine the critical boron concentrations and power distributions. The moderator coefficient is evaluated by varying the inlet temperature in the same calculations used for power distribution and reactivity predictions.

(Lin, 1986)

C 4 4d

Insert "C" (to page 4.3-4d)

ANC is used in two-dimensional and three-dimensional calculations. ANC can be used for safety analyses and to calculate critical boron concentrations, control rod worths, reactivity coefficients, etc.

are obtained from the three dimensional ~~TURTLE~~ ANC calculation from which constants are homogenized by flux-volume weighting.

Validation of the spatial codes for calculating power distributions involves the use of incore and excore detectors and is discussed in Section 4.3.2.2.7.

Based on comparison with measured data, it is estimated that the accuracy of current analytical methods is:

±0.1 percent $\Delta\rho$ for Doppler defect

±2 x 10^{-5}/°F for moderator coefficient

±50 ppm for critical boron concentration with depletion

±3 percent for power distributions

±0.2 percent $\Delta\rho$ for rod bank worth

±4 pcm/step for differential rod worth

±0.5 pcm/ppm for boron worth

±0.1 percent $\Delta\rho$ for moderator defect

4.3.4 Revisions

The design methods for the criticality of fuel assemblies outside the reactor now use the AMPX/KENO system of codes as described in Section 4.3.2.6.

~~The design methods for the nuclear analysis of the core now use both TURTLE (Barry and Altomare 1975) and PALADON (Camden et al 1978) for multi-dimensional analyses.~~

4.3.5 References for Section 4.3

Insert A →

Barry, R.F. 1963. LEOPARD - A Spectrum Dependent Non-Spatial Depletion Code for the IBM-7094. WCAP-3269-26.

Barry, R.F. et al 1975. The PANDA Code. WCAP-7048-P-A (Proprietary) and WCAP-7757-A (Nonproprietary).

Barry, R.F. and Altomare, S. 1975. The TURTLE 24.0 Diffusion Depletion Code. WCAP-7213-P-A (Proprietary) and WCAP-7758-A (Nonproprietary).

Insert A
References for Section 4.3

Strawbridge, L.E., and Barry, R. F., "Criticality Calculation for Uniform Water-Moderated Lattices," Nuclear Science and Eng. 23, 58 (1965).

Nodvik, R.J., "Saxton Core II Fuel Performance Evaluation," WCAP-3385-56 Part II, "Evaluation of Mass Spectrometric and Radiochemical Analyses of Irradiated Saxton Plutonium Fuel," July, 1970.

Leamer, R.D., et.al., "PUO2-UO2 Fueled Critical Experiments," WCAP-3726-1, July, 1967.

Liu, Y. S., et.al., "ANC: A Westinghouse Advanced Nodal Computer Code," WCAP-10965-P-A, September, 1986.

Nguyen, T.Q., et.al., "Qualification of the PHOENIX-P/ANC Nuclear Design System for Pressurized Water Reactor Cores," WCAP-11596-P-A, June, 1988.

Mildrum, C.M., Mayhue, L.T., et.al., "Qualification of the PHOENIX/POLCA Nuclear Design and Analysis Program for Boiling Water Reactors," WCAP-10841 (Proprietary) and WCAP-10842 (Non-proprietary), June, 1985.

Baldwin M.N.; Critical Experiments Supporting Close Proximity Water Storage of Power Reactor Fuel, BAW-1484-7, July 1979.

~~Camden, T.M. et al 1978. PALADON - Westinghouse Nodal Computer Code. WCAP-9485A (Proprietary) and WCAP-9486A (Nonproprietary).~~

Cermak, J.O. et al 1968. Pressurized Water Reactor pH - Reactivity Effect Final Report. WCAP-3696-8 (EURAEC-2074).

Drake, M.K. (Ed) 1970. Data Formats and Procedure for the ENDF/B Neutron Cross Section Library BNL-50274, ENDF-102 Vol. 1.

Eggleston, F.T. 1977. Safety-Related Research and Development for Westinghouse Pressurized Water Reactors Program Summaries - Winter 1976, WCAP-8768, Revision 1.

England, T.R. 1962. CINDER - A One-Point Depletion and Fission Product Program. WAPD-TM-334.

Flatt, H.P. and Buller, D.C. 1960. AIM-5, A Multigroup, One Dimensional Diffusion Equation Code. NAA-SR-4694.

Ford, W.E., III, CSRL-V: Processed ENDF/B-V 227-Neutron-Group and Pointwise Cross-Section Libraries for Criticality Safety, Reaction and Shielding Studies, ORNL/CSD/TM-160, June 1982.

Greene, N.M. et al 1976. AMPX: A Modular Code System for Generating Coupled Multigroup Neutron-Gamma Libraries from ENDF/B. ORNL/TM-06.

Hellman, J.M. and Yang, J.W. 1974. Effects of Fuel Densification Power Spikes on Clad Thermal Transients. WCAP-8359.

Hellman, J.M. (Ed) 1975. Fuel Densification Experimental Results and Model for Reactor Application. WCAP-8218-P-A (Proprietary) and WCAP-8219-A (Nonproprietary).

Langford, F.L. and Nath, R.J. 1971. Evaluation of Nuclear Hot Channel Factor Uncertainties. WCAP-7308-L (Proprietary) and WCAP-7810 (Nonproprietary).

Leamer, R.D. et al 1967. PUO2-UO2 Fueled Critical Experiments.

WCAP-3726-1.

Lee, J.C. et al 1971. Axial Xenon Transient Tests at the Rochester Gas and Electric Reactor. WCAP-7964.

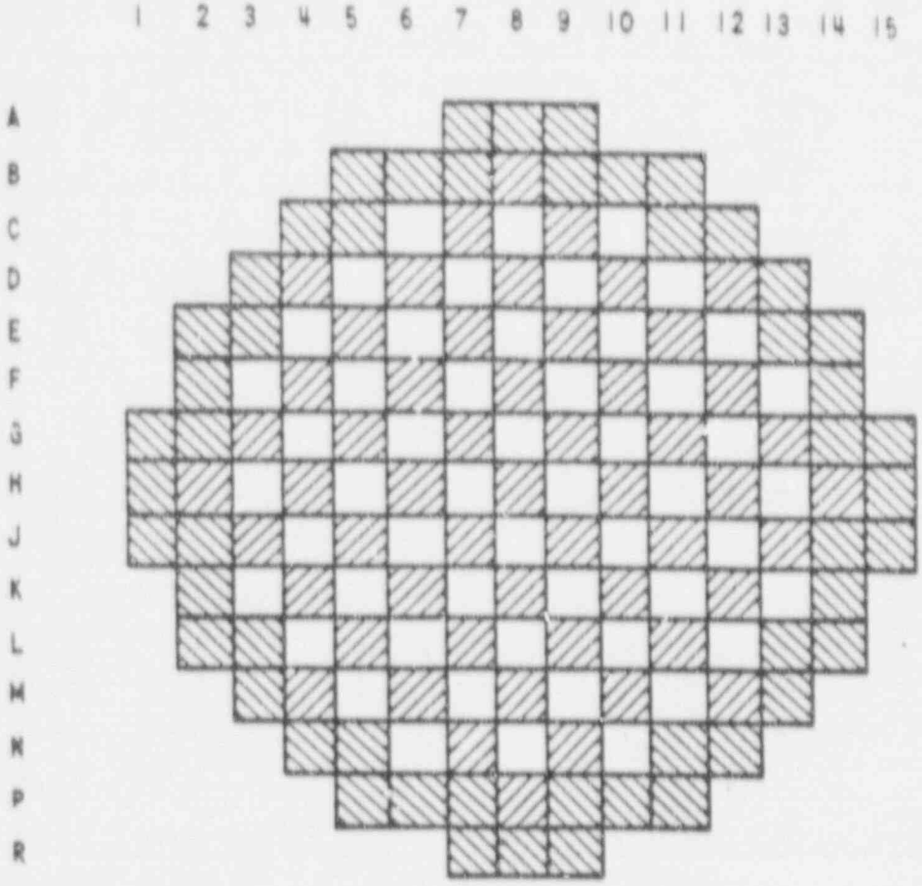

FIRST CORE — RELOAD CORE

REGION 1 — ONCE OR TWICE BURNED FUEL

REGION 2 — ~~ONCE OR TWICE~~ FRESH ~~BURNED~~ FUEL

REGION 3 — ONCE OR TWICE BURNED ~~FRESH~~ FUEL

FIGURE 4.3-1
FUEL LOADING ARRANGEMENT
BEAVER VALLEY POWER STATION-UNIT 2
FINAL SAFETY ANALYSIS REPORT

Figure ~~2.6-60~~ 4.3-4a
Configuration for 16 IFBA Rod Assembly (17x17)

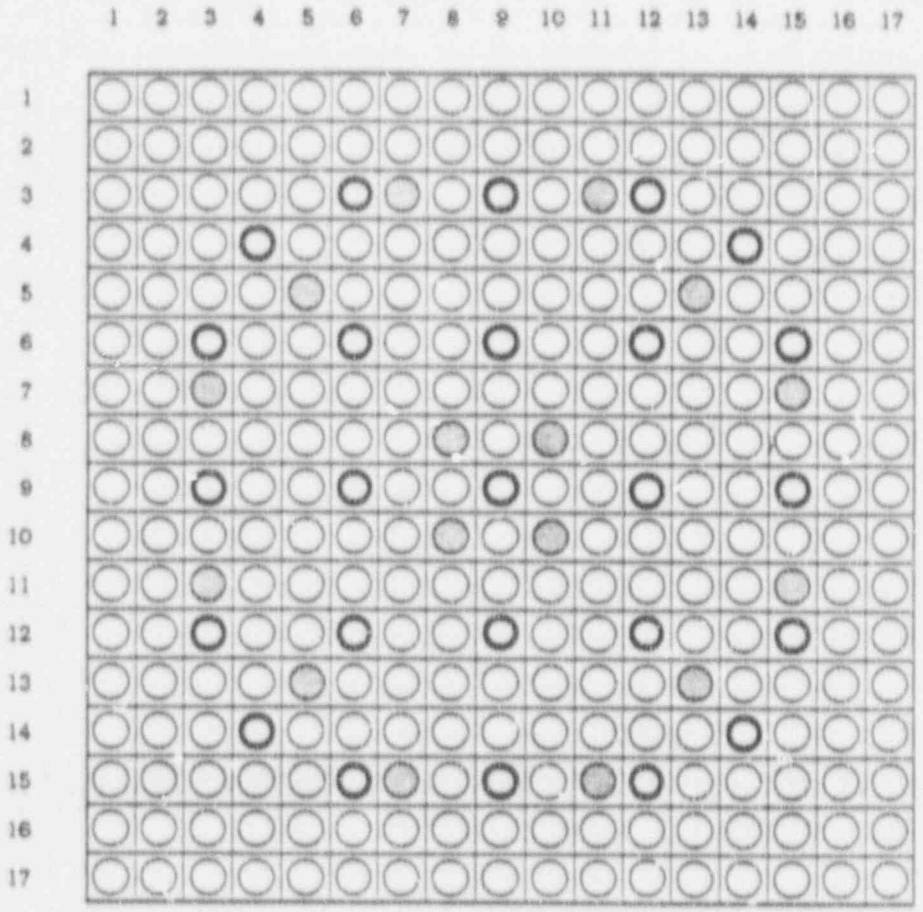

○ Fuel Rod

◎ Fuel Rod with IFBA

● Guide Tube / Inst. Tube

~~Figure 2.5-29~~ 4.3-46
Configuration for 32 IFBA Rod Assembly (17x17)

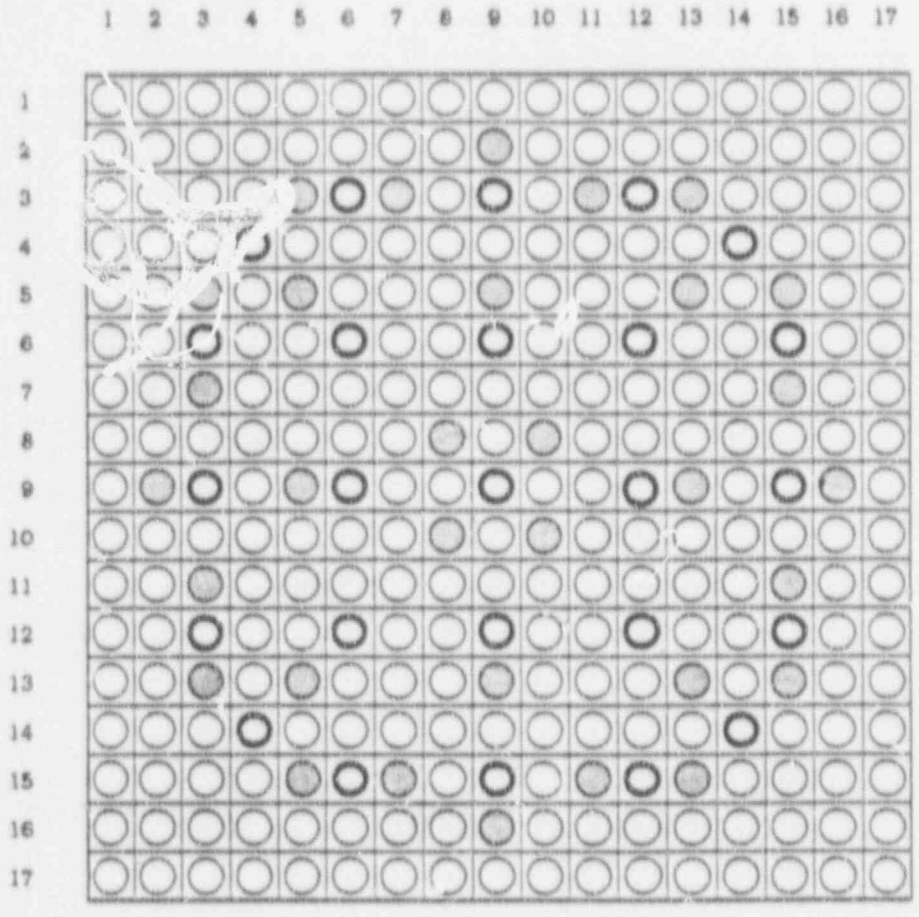

○ Fuel Rod

◎ Fuel Rod with IFBA

◎ Guide Tube / Inst. Tube

Figure ~~2.5-30~~ 4.3-4c
Configuration for 48 IFBA Rod Assembly (17x17)

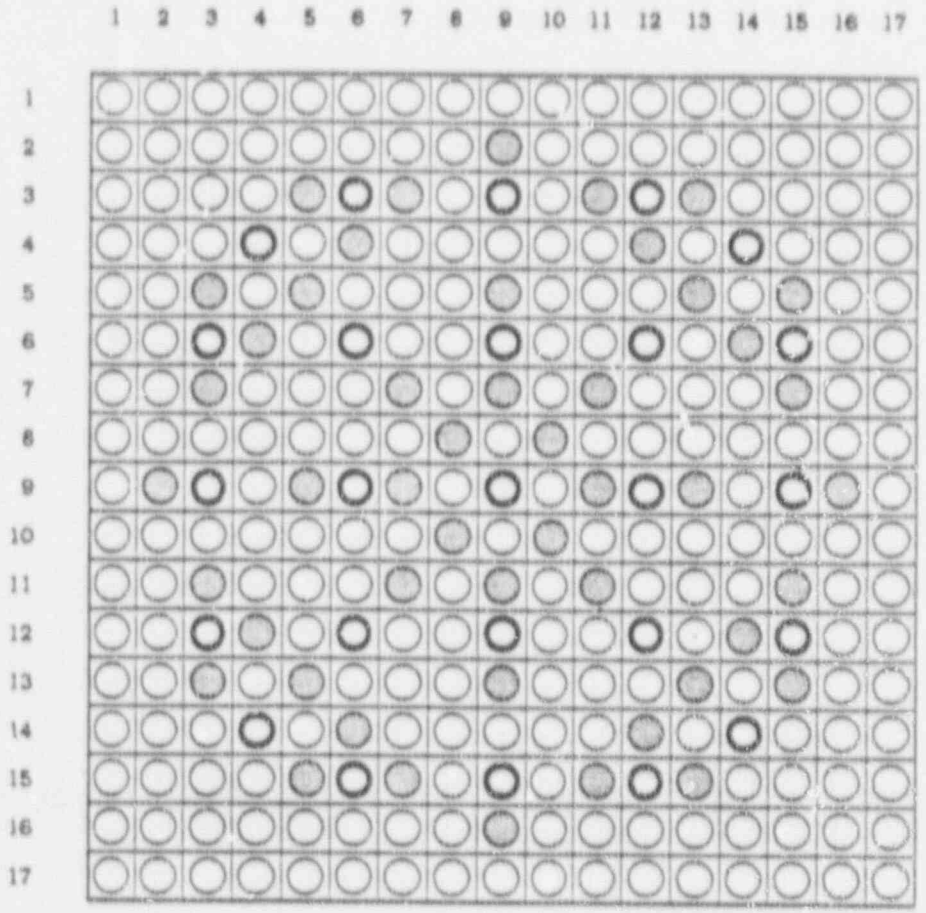

○ Fuel Rod

◎ Fuel Rod with IFBA

◎ Guide Tube / Inst. Tube

Figure ~~2.5-31~~ Y.3-Y2
Configuration for 64 IFBA Rod Assembly (17x17)

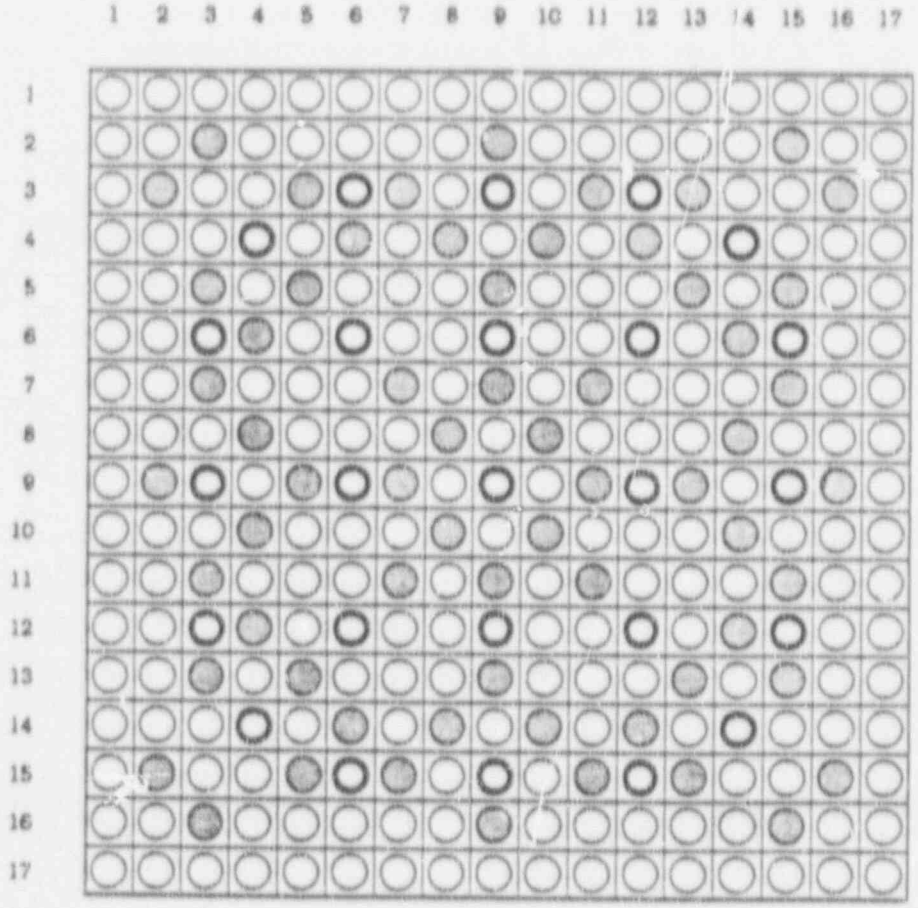

○ Fuel Rod

◎ Fuel Rod with IFBA

◎ Guide Tube / Inst. Tube

Figure ~~2.5-32~~ 4.3-4a
Configuration for 80 IFBA Rod Assembly (17x17)

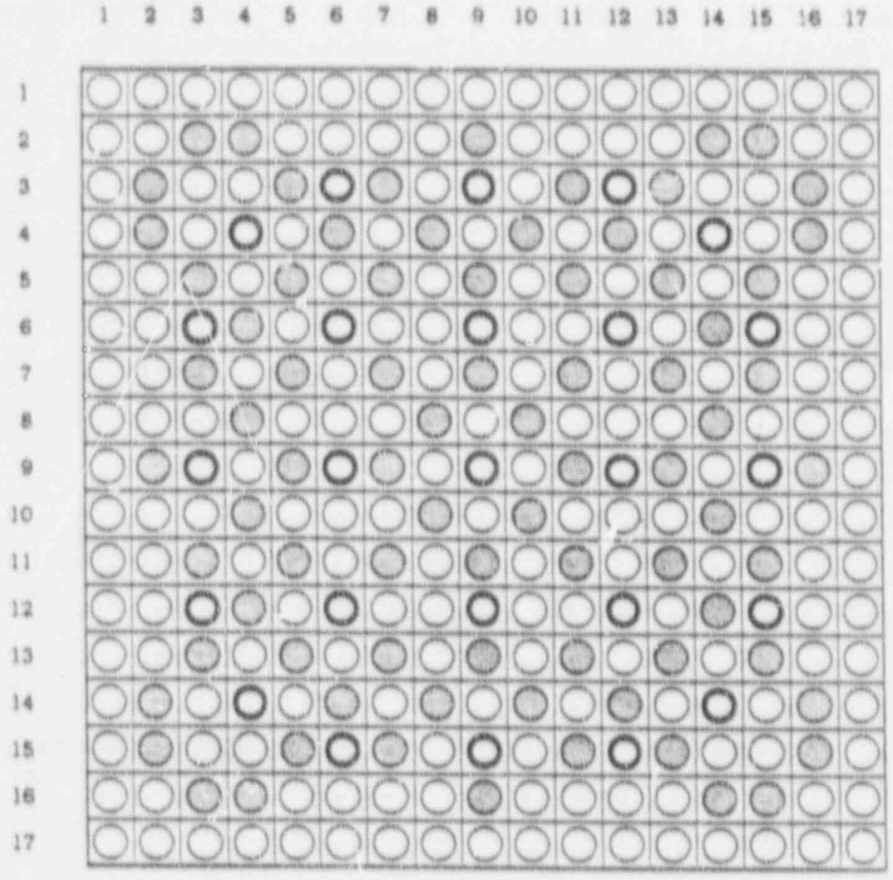

○ Fuel Rod

◎ Fuel Rod with IFBA

◎ Guide Tube / Inst. Tube

Figure ~~2.5-65~~ 4.3-4 5
Configuration for 104 IFBA Rod Assembly (17x17)

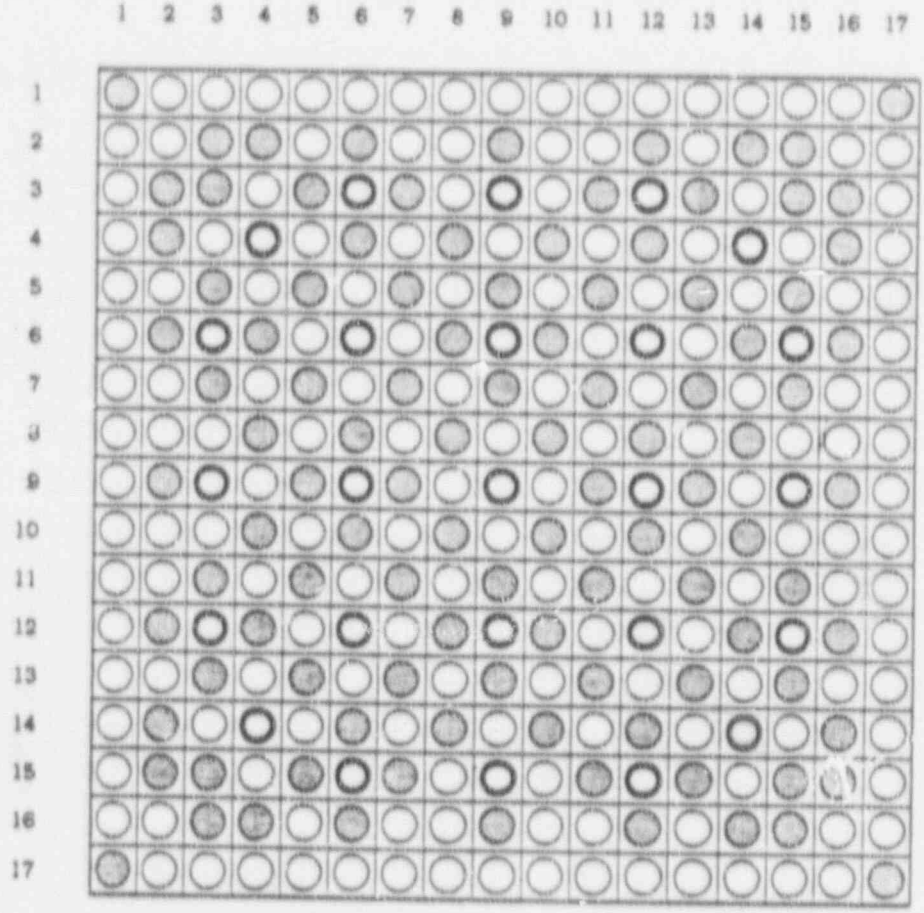

○ Fuel Rod

◎ Fuel Rod with IFBA

◎ Guide Tube / Inst. Tube

Figure ~~2.5-34~~ 4.3-4 9
Configuration for 128 IFBA Rod Assembly (17x17)

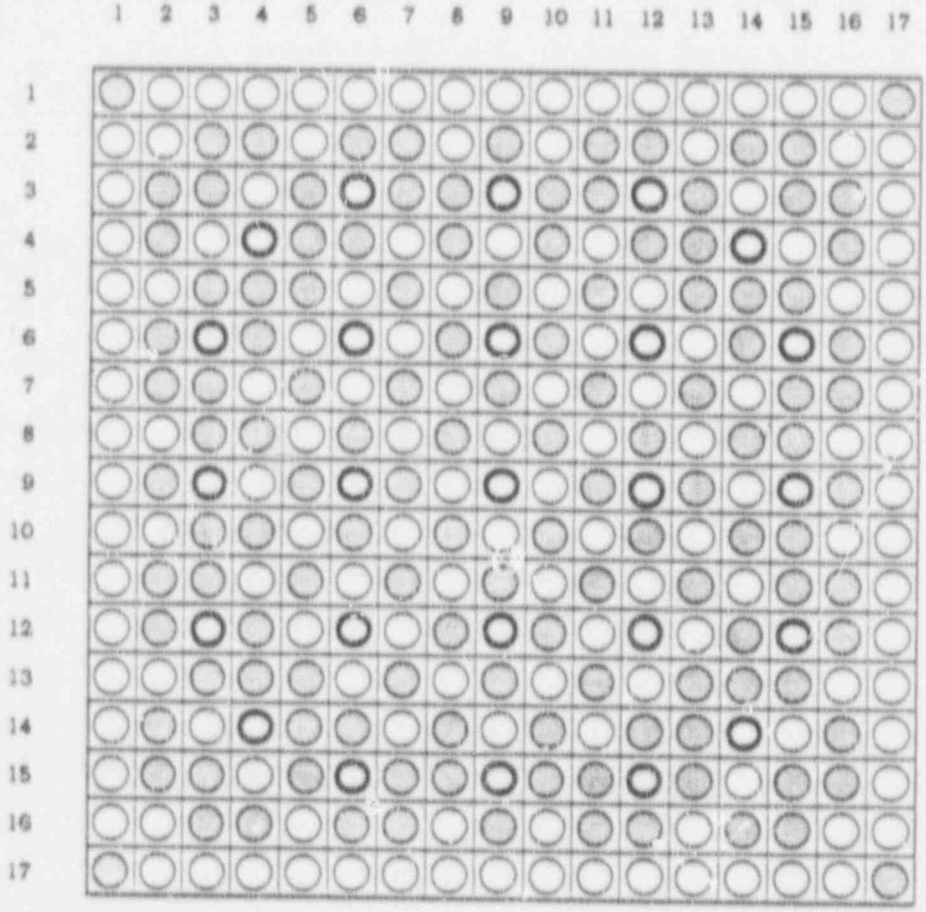

○ Fuel Rod

○ Fuel Rod with IFBA

○ Guide Tube / Inst. Tube

Figure ~~2.5-35~~ 4.3-4h
Configuration for 156 IFBA Rod Assembly (17x17)

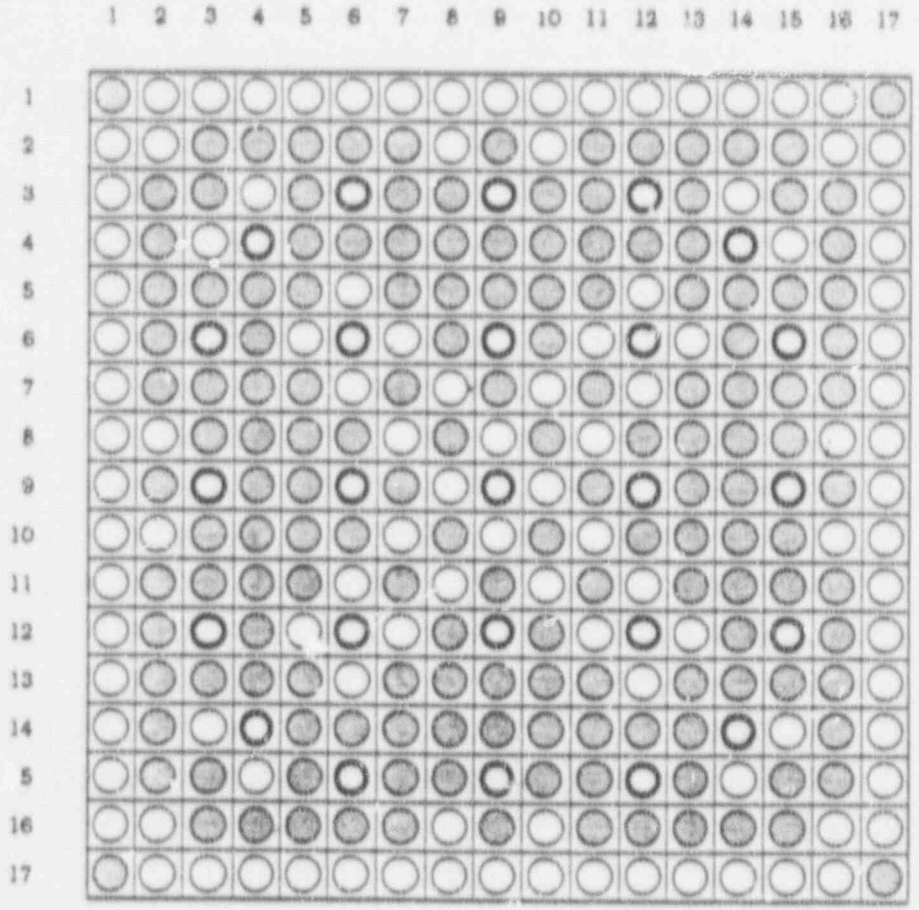

○ Fuel Rod

○ Fuel Rod with IFBA

○ Guide Tube / Inst. Tube

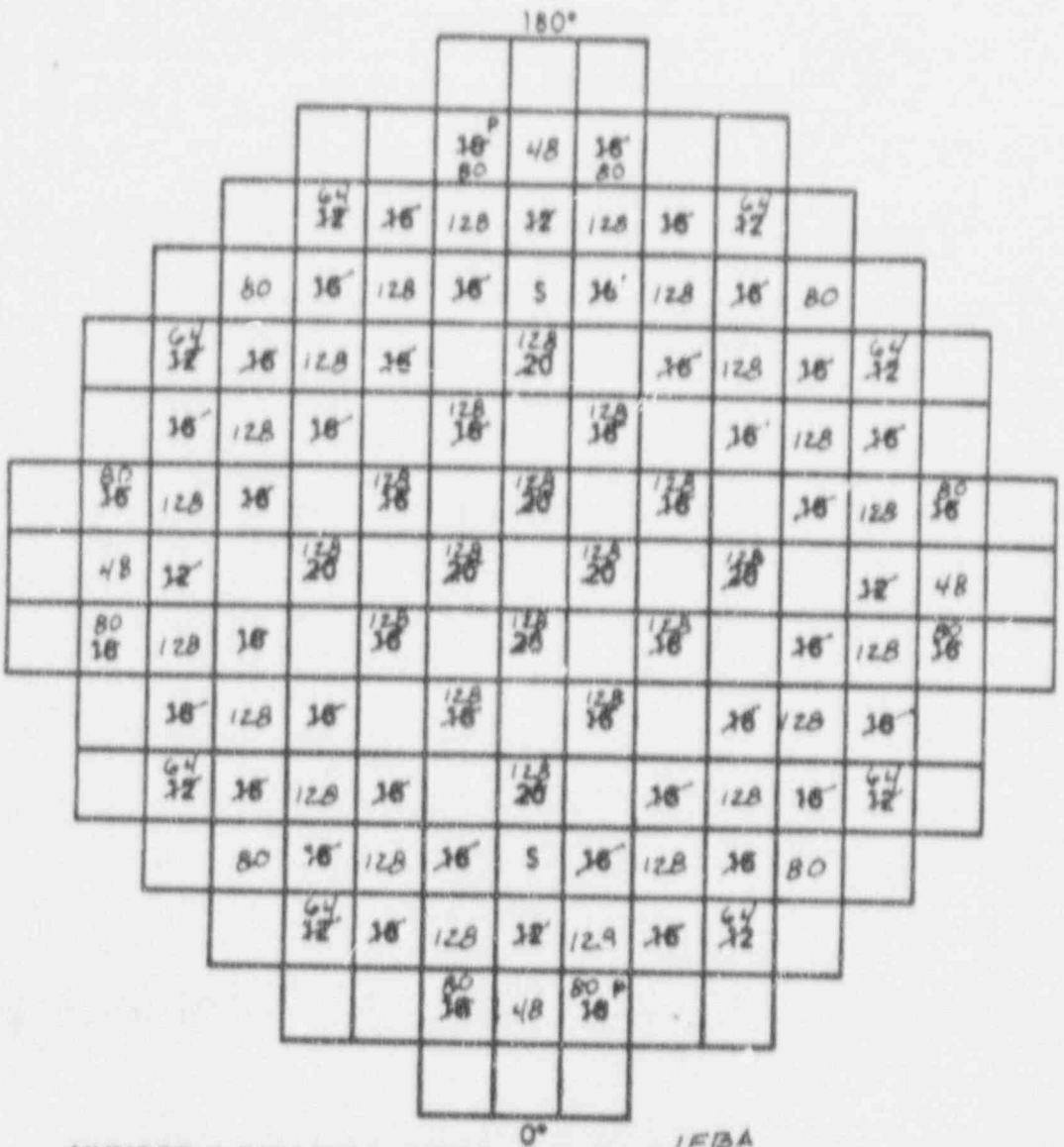

NUMBER INDICATES NUMBER OF ~~BURNABLE ABSORBER~~ IFBA RODS
S INDICATES SECONDARY SOURCE RODS
P INDICATES PRIMARY RODS

Integral Fuel

FIGURE 4.3-5
BURNABLE ABSORBER LOADING PATTERN
BEAVER VALLEY POWER STATION-UNIT 2
FINAL SAFETY ANALYSIS REPORT

Section 4.4

4.4 THERMAL AND HYDRAULIC DESIGN

4.4.1 Design Bases

The overall objective of the thermal and hydraulic design of the reactor core is to provide adequate heat transfer which is compatible with the heat generation distribution in the core such that heat removal by the reactor coolant system (RCS) or the emergency core cooling system (ECCS) (when applicable) assures that the following performances and safety criteria requirements are met:

1. Fuel damage (defined as penetration of the fission product barrier, that is, the fuel rod clad) is not expected during normal operation and operational transients (ANS Condition I) or any transient conditions arising from faults of moderate frequency (ANS Condition II). It is not possible, however, to preclude a very small number of rod failures resulting in the release of fission products. The chemical and volume control system is designed to remove the fission products from the reactor coolant, keeping the reactor coolant activity within plant design bases limits.

2. The reactor can be brought to a safe state following a Condition III event with only a small fraction of the fuel rods damaged, as defined previously, although sufficient fuel damage might occur to preclude resumption of operation without considerable outage time.

3. The reactor can be brought to a safe state and the core can be kept subcritical with acceptable heat transfer geometry following transients arising from Condition IV events.

In order to satisfy these requirements, the following design bases have been established for the thermal and hydraulic design of the reactor core.

4.4.1.1 Departure from Nucleate Boiling Design Basis

Basis

There will be at least a 95 percent probability that departure from nucleate boiling (DNB) will not occur on the limiting fuel rods during normal operation, operational transients, or during transient conditions arising from faults of moderate frequency (ANS Condition I and II events), at a 95 percent confidence level. ~~Historically this has been conservatively met by adhering to the following thermal design basis: there must be at least a 95 percent probability that the minimum departure from nucleate boiling ratio (DNBR) of the limiting power rod during ANS Condition I and II events is greater than or equal to the DNBR limit of the DNB correlation being used. The DNBR limit for the~~ ← Insert A.

INSERT A PAGE 4.4-1

For this application, this criterion is met by limiting the minimum departure from nucleate boiling ratio (DNBR) to a design value of 1.21. Plant specific margin to accomodate rod bow and other DNB penalties and allow for flexibility in the design, operation and analysis of the plant is provided by performing the safety analyses to a DNBR limit value of 1.33.

INSERT B PAGE 4.4-2

Historically, the DNBR limit has been 1.30 for Westinghouse applications. In this application, the WRB-1 correlation Motley 1984) is used. With the significant improvement in the accuracy of the critical heat flux prediction by using this correlation instead of the previous correlation, a DNBR correlation limit of 1.17 can be used with at least a 95 % probability with a 95 % confidence level.

The design method used to meet the DNB design basis is the MINI-Revised Thermal Design Procedure (Ray 1989) which is a conservative application of the Revised Thermal Design Procedure (Friedland, Ray 1987). In the MINI-RTDP method, uncertainties in the nuclear peaking factors and fuel fabrication parameters are combined statistically with the DNB correlation uncertainties to define the DNBR design limit such that there is at least a 95 percent probability (with 95 percent confidence) that DNB will not occur when the calculated minimum DNBR is equal to or greater than the design limit. The uncertainties included in the MINI-RTDP method are for the nuclear enthalpy hot-channel factor, ($F_{N\Delta H}$); the enthalpy rise hot-channel factor, $F(E,\Delta H)$; and the THINC-IV and transient codes. Incorporating the peaking factor uncertainties in the correlation limit results in a DNBR design limit value of 1.21.

In addition to the considerations above, a specific plant allowance has been considered in the present analysis. In particular, a DNBR limit value of 1.33 has been used in the safety analyses for the plant. The difference between the DNBR value used in the safety analyses and the design DNBR value (1.33 versus 1.21) provides plant specific DNB margin to offset the rod bow penalty and other DNB penalties that may occur. This DNB margin may also be used for flexibility in the design, operation or analysis of the plant.

For conditions outside the range of parameters for the WRB-1 correlation (refer to Section 4.4.2.2.1), the W-3 correlation is used with a DNBR correlation limit of 1.30 for pressure equal to or greater than 1000 psia. For low pressure applications (500-1000 psia), the W-3 DNBR correlation limit is 1.45 (Thadani, USNRC, 1989).

~~correlation is established based on the variance of the correlation such that there is a 95 percent probability with 95 percent confidence that DNB will not occur when the calculated DNBR is at the DNBR limit. For Beaver Valley Power Station - Unit 2 (BVPS-2), a minimum DNBR of 1.30 was used.~~

Discussion

By preventing DNB, adequate heat transfer is assured between the fuel clad and the reactor coolant, thereby preventing clad damage as a result of inadequate cooling. Maximum fuel rod surface temperature is not a design basis as it will be within a few degrees of the coolant temperature during operation in the nucleate boiling region. Limits provided by the RCS and the reactor protection system are such that this design basis will be met for transients associated with ANS Condition II events, including overpower transients. There is an additional large DNBR margin at rated power operation and during normal operating transients.

Insert B. →

4.4.1.2 Fuel Temperature Design Basis

Basis

During modes of operation associated with ANS Condition I and ANS Condition II events, there is at least a 95 percent probability at the 95 percent confidence level that the peak kW/ft fuel rods will not exceed the UO_2 melting temperature. The melting temperature of unirradiated UO_2 is taken as 5,080°F (Christensen et al 1965), and decreasing 58°F per 10,000 MWD/MTU. By precluding UO_2 melting, the fuel geometry is preserved and possible adverse effects of molten UO_2 on the cladding are eliminated. To preclude center melting and as a basis for overpower protection system set points, a calculated centerline fuel temperature of 4,700°F has been selected as the overpower limit. This provides sufficient margin for uncertainties in the thermal evaluations as described in Section 4.4.2.9.1.

Discussion

Fuel rod thermal evaluations are performed at rated power, maximum overpower and during transients at various burnups. These analyses assure that this design basis as well as the fuel integrity design bases given in Section 4.2 are met. They also provide input for the evaluation of ANS Condition III and IV events given in Chapter 15.

4.4.1.3 Core Flow Design Basis

Basis

A minimum of ~~95.5~~ 93.5 percent of the thermal flow rate passes through the fuel rod region of the core and is effective for fuel rod cooling. Coolant flow through the thimble tubes as well as the

leakage from the core barrel-baffle region into the core are not considered effective for heat removal.

Discussion

Core cooling evaluations are based on the thermal flow rate (minimum flow) entering the reactor vessel. A maximum of ~~4.5~~ 6.5 percent of this value is allotted as bypass flow. This includes rod cluster control (RCC) guide thimble cooling flow, head cooling flow, baffle leakage, and leakage to the vessel outlet nozzle.

4.4.1.4 Hydrodynamic Stability Design Basis

Basis

Modes of operation associated with ANS Condition I and II events shall not lead to hydrodynamic instability.

4.4.1.5 Other Considerations

The above design bases together with the fuel clad and fuel assembly design bases given in Section 4.2.1 are sufficiently comprehensive that no additional limits are required.

Fuel rod diametral gap characteristics, moderator-coolant flow velocity and distribution, and moderator void are not inherently limiting. Each of these parameters is incorporated into the thermal and hydraulic models used to ensure that the design criteria mentioned previously are met. For instance, the fuel rod diametral gap characteristics change with time (Section 4.2.3.3) and the fuel rod integrity is evaluated on that basis. The effect of the moderator flow velocity and distribution (Section 4.4.2.2) and moderator void distribution (Section 4.4.2.4) are included in the core thermal (THINC) evaluation and thus affect the design bases.

Meeting the fuel clad integrity criteria covers possible effects of clad temperature limitations. As noted in Section 4.2.3.3, the fuel rod conditions change with time. A single clad temperature limit for ANS Condition I or II events is not appropriate because it would be overly conservative. A clad temperature limit is applied to the loss-of-coolant accident (LOCA), control rod ejection accident, and locked rotor accident.

4.4.2 Description

4.4.2.1 Summary Comparison

The design of BVPS-2 described in this final safety analysis report has similar thermal-hydraulic parameters ~~similar to~~ as those for the Virgil C. Summer Nuclear Power Station.

Values of pertinent parameters, along with critical heat flux ratios, fuel temperatures, and linear heat generation rates, are

meet the DNB design criterion of Section 4.4.

presented in Table 4.4-1 for all reactor coolant loops in service. It is also noted that in this power capability evaluation, there is no change in the design criteria. The reactor is still designed to ~~a minimum DNBR = 1.30~~ as well as no fuel centerline melting during normal operation, operational transients, and faults of moderate frequency.

These using the W-3 correlation

All DNB analyses performed for the BVPS-2 have included a DNBR multiplier of 0.865. The results of 17 by 17 geometry DNB tests, (Motley et al 1975a) discussed in Section 4.4.2.2.1 and indicating a DNBR multiplier of 0.88, is required for the "R" grid DNB correlation. Thus, the multiplier used results in conservative DNB evaluations.

Fuel densification has been considered in the DNB and fuel temperature evaluations utilizing the methods and models described by Hellman (1975).

4.4.2.2 Critical Heat Flux Ratio and ~~or~~ Departure from Nucleate Boiling Ratio and Mixing Technology

The minimum DNBRs for the rated power, design overpower, and anticipated transient conditions are given in Table 4.4-1. The minimum DNBR in the limiting flow channel is downstream of the peak heat flux location (hot spot) due to the increased downstream enthalpy rise. Insert C

Departure from nucleate boiling ratios are calculated by using the correlation and definitions described in Sections 4.4.2.2.1 and 4.4.2.2.2. The THINC-IV computer code (Section 4.4.4.5.1) is used to determine the flow distribution in the core and the local conditions in the hot channel for use in the DNB correlation. The use of hot channel factors is discussed in Section 4.4.4.3.1 (nuclear hot channel factor) and in Section 4.4.2.2.4 (engineering hot channel factors).

4.4.2.2.1 Departure from Nucleate Boiling Technology

~~The W-3 correlation, and several modifications of it, have been used in Westinghouse critical heat flux calculations. The W-3 was originally developed from single tube data (Tong 1972), but was subsequently modified to apply to the 0.422 inch outside diameter rod "R" grid (Tong 1972) and "L" grid (Motley and Cadek 1972), as well as the 0.374 inch outside diameter (Motley et al 1975a and Hill et al 1975) rod bundle data. These modifications to the W-3 correlation have been demonstrated to be adequate for reactor rod bundle design.~~

~~A description of the 17 by 17 fuel assembly test program and a summary of the results are described by Motley (et al 1975c). A correction factor was developed to adapt the W-3 correlation to 17 by 17 assemblies with top split mixing vane grids referred to as R grid. This correction factor, termed the "modified spacer factor," was developed as a multiplier on the W-3 correlation.~~

Delete. Replace with Insert D.

Insert C p. 4.4-4

The core average DNPR is not a safety related item as it is not directly related to the minimum DNBR in the core, which occurs at some elevation in the limiting flow channel. Similarly, the DNBR at the hot spot is not directly safety related.

Insert D p. 4.4-4 to 4.4-5

Early experimental studies of DNB were conducted with fluid flowing inside single heated tubes or channels and with single annulus configurations with one or both walls heated. The results of the experiments were analyzed using many different physical models for describing the DNB phenomenon, but all resultant correlations are highly empirical in nature. The evolution of these correlations is given by Tong 1965, 1972 including the W-3 correlation which is in wide use in the pressurized water reactor industry.

As testing methods progressed to the use of rod bundles, instead of single channels, it became apparent that the bundles average flow conditions cannot be used in DNB correlations. As outlined by Tong 1969, test results showed that correlations based on average conditions were not accurate predictors of DNB heat flux. This indicated that a knowledge of the local subchannel conditions within the bundle is necessary.

In order to determine the local subchannel conditions, the THINC computer code was developed (Chelemer, Weisman and Tong 1969). In the THINC code, a rod bundle is considered to be an array of subchannels each of which includes the flow area formed by four adjacent rods. The subchannels are also divided into axial steps such that each may be treated as a control volume. By solving simultaneously the mass, energy, and momentum equations, the local fluid conditions in each control volume are calculated. The W-3 correlation, developed from single channel data, can be applied to rod bundles by using the subchannel local fluid conditions calculated by the THINC code.

It was shown by Tong 1969, that the above approach yielded conservative predictions particularly in rod bundles with mixing vane grid spacers.

The WRB-1 DNB correlation (Motley, Hill, Cadek, and Shefchek 1984) was developed based exclusively on the large bank of mixing vane grid rod bundle CHF data (over 1100 points) that Westinghouse has collected. The WRB-1 correlation, based on local fluid conditions, represents the rod bundle data with better accuracy over a wide range of variables than the previous correlation used in design. This correlation accounts directly for both typical and thimble cold wall cell effects, uniform and non-uniform heat flux profiles and variations in rod heated length and grid spacing. The WRB-1 correlation is applicable to the 17x17 STD and VANTAGE 5H fuel.

The applicable range of variables is:

Pressure	: $1440 \leq P \leq 2490$ psia
Local Mass Velocity	: $0.9 \leq G_{loc}/10^6 \leq 3.7$ lb/ft^2-hr
Local Quality	: $-0.2 \leq X_{loc} \leq 0.3$
Heated length, Inlet to CHF Location	: $L_h \leq 14$ feet
Grid Spacing	: $13 \leq g_{sp} \leq 32$ inches
Equivalent Hydraulic Diameter	: $0.37 \leq d_e \leq 0.60$ inches
Equivalent Heated Hydraulic Diameter	: $0.46 \leq d_h \leq 0.68$ inches

Insert D p. 4.4-4 to 4.4-5 (cont.)

Figure 4.4-1 shows the measured critical heat flux plotted against predicted critical heat flux using the WRB-1 correlation.

In order to meet the design criterion that DNB will not occur at a 95 percent probability with a 95 percent confidence level, a limiting value of DNBR is determined by the method of Owen 1963. Owen has prepared tables which give values of K such that "at least a proportion P of the population [illegible] greater than M/P - K_ps with confidence γ," where M/P and s are the sample mean and standard [illegible]. When this method was carried out using the data on Figure 4.4-1, the results indicated [illegible] for core with these fuel geometries may operate with a minimum DNBR of 1.17 and satisfy [illegible] criterion.

[illegible] Fuel Densification on DNB/Effect of Heat Flux Spikes

As discussed in Section 4.3.2.2.5 and Hellman 1973, a gap or combination of gaps results in a heat flux spike on the individual or adjacent fuel rods. Recent Westinghouse high pressure DNB Water Tests (Hill, Motley, and Cadek 1973) on a 14 foot axially non-uniformly heated 4x4 rod bundle were carried out to measure the effect of heat flux spikes. The rod bundle incorporated mixing vane grids on a 26 inch spacing. A 20 % heat flux spike was placed on three adjacent rods at the axial location where DNB is most likely to occur. This test series was run at the same conditions as those of two earlier test series which had unspiked rods so that a comparison of spiked and unspiked data could be made and the spike effects isolated. Figure 4.4-1A shows the relative positions of the three spiked rods. Figure 4.4-2 shows the heat flux profile of the spiked rods.

The test facilities consisted of a high pressure loop capable of supplying water at pressures up to 2400 psia with flow rates up to 400 GPM and inlet temperatures in excess of 600° F. The power supply was capable of delivering up to 4.5 MW.

Using these test facilities, a 14 foot, 16 rod test section can be operated over a wide range of test parameters. For the present tests, these ranges were:

1.	Pressure	1500 - 2400 psia
2.	Inlet Temperature	401 - 569 °F
3.	Mass Velocity	1.5 - 3.5 x 10^6 lb/hr-ft^2

The results of the spike test series indicated that the spike effect on DNB is so small that it lies within the repeatability of DNB measurements. The spike geometry modeled in the above rod bundle experiment was also more severe than that presently ascribed to fuel densification effects, and hence, the absence of a spike effect indicated that a special spike factor in DNB need not be incorporated into the BVPS-2 reactor design.

Effects of Pellet Eccentricity and Clad Ovality on DNB

Individual fuel pellets can be eccentrically located in the clad at BOL. The clad may also assume an oval shape at some later time in life. Both of these cases will produce azimuthal variations of the pellet clad gap. However, these local heat flux peaks will have limited axial lengths at any azimuthal angle.

For the eccentric case the local heat flux peak at a given azimuthal angle will have a maximum length

Insert D p. 4.4-4 to 4.4-5 (cont.)

equal to several pellet lengths. This is due to the randomness of the angle of contact of the pellets in the rod at BOL. The randomness has been verified by observation of radiographs of Beznau Unit 1 fuel rods and is due in part to the variation in pellet diameter.

For the clad ovality case, the local heat flux peak also has a maximum length equal to several pellets at a given azimuthal angle. This is due to the randomness of the azimuthal location of the cracked pellet fragments in the axial direction.

The recent spike DNB tests (Hill, Motley, and Cadek 1973) described previously indicate that for 360° circumferential heat flux spikes at 20% magnitude and 6" long, a special spike factor on DNB need not be incorporated into Westinghouse reactor designs which incorporate the Westinghouse type mixing vane grids. Since the 6 inch length is equivalent to 10 pellet lengths, no reduction in DNBR due to pellet eccentricity or clad ovality is applied in DNB evaluations. Similarly, the heat flux engineering hot channel factor, F(E,Q) of 1.03 which allowed for variations in manufacturing tolerances and was used to determine the local maximum linear heat generation rate at a point, the "hot spot", is no longer considered in DNB evaluations. This subfactor was determined by statistically combining the tolerances for the fuel pellet diameter, density, enrichment, eccentricity and the fuel rod diameter. F(E,Q) continues to be applied in determining the peak power and in fuel pellet temperature evaluations.

The effect of manufacturing tolerances which affect the integrated values along a channel, i. e., enthalpy rise engineering hot channel subfactor corresponding to pellet diameter, density and enrichment, and fuel rod diameter, pitch and bowing, are still considered in all DNB evaluations as described in Section 4.4.2.2.4.1.

~~Figure 4.4-1 shows the 17 by 17 data obtained in this test program. The predicted heat flux include a 0.88 multiplier which is part of the 17 by 17 modified spacer factor. However, as noted previously (Section 4.4.2.1), a multiplier of 0.865 has been conservatively applied for all DNB analyses.~~ Delete

~~The test results indicated that a reactor core using this geometry may operate with a minimum DNBR of 1.28 and satisfy the design criterion. However, as stated in Section 4.4.1.1, a minimum DNBR of 1.30 is conservatively used for BVPS-2.~~

4.4.2.2.2 Definition of Departure from Nucleate Boiling Ratio

The DNB heat flux ratio (DNBR) as applied to this design when all flow cell walls are heated is:

$$DNBR = \frac{q''_{DNB,\ N}\ \cancel{\frac{F'_s}{F}}}{q''_{loc}} \qquad (4.4\text{-}1)$$

where $q''_{DNB,N}$ is the heat flux predicted by the applicable DNB correlation; for the correlation

$$q''_{DNB,N} = \frac{q''_{DNB,\ EU}}{F} \qquad (4.4\text{-}2)$$

and $q''_{DNB,\ EU}$ is the uniform DNB heat flux as predicted by the W-3 DNB correlation (Tong 1967) when all flow cell walls are heated.

F is the flux shape factor to account for non-uniform axial heat flux distributions (Tong 1967) with the "C" term modified by Tong (1972).

~~F'_s is the modified spacer factor described by Motley (et al 1975a) using an axial grid spacing coefficient, $K_s = 0.046$ and a thermal diffusion coefficient (TDC) of 0.038, based on the 26-inch grid spacing data (Motley and Cadek 1972). Since the actual grid spacing is approximately 20 inches, these values are conservative since the DNB performance was found to improve and TDC to increase as axial grid spacing is decreased by Motley and Cadek (1972) and Cadek (et al 1975).~~

q''_{loc} is the actual local heat flux.

The DNBR as applied to this design when a cold wall is present is:

$$DNBR = \frac{q''_{DNB,N,CW}}{q''_{loc}} \qquad (4.4-3)$$

where:

$$q''_{DNB,N,CW} = \frac{q''_{DNB,EU,Dh} \times CWF}{F} \qquad (4.4-4)$$

where:

$q''_{DNB,EU,Dh}$ is the uniform DNB heat flux as predicted by the W-3 cold wall DNB correlation (Tong 1972) when not all flow cell walls are heated (thimble cold wall cell).

~~F_s is the same as those used for typical cell.~~

Insert E. CWF is the cold wall factor.

4.4.2.2.3 Mixing Technology

The rate of heat exchange by mixing between flow channels is proportional to the difference in the local mean fluid enthalpy of the respective channels the local fluid density and flow velocity. The proportionality is expressed by the dimensionless TDC which is defined as:

$$TDC = \frac{w'}{\rho V a} \qquad (4.4-5)$$

where:

w' = flow exchange rate per unit length ($lb_m/ft\text{-}sec$)
ρ = fluid density (lb_m/ft^3)
V = fluid velocity (ft/sec)
a = lateral flow area between channels per unit length (ft^2/ft)

The application of the TDC in the THINC analysis for determining the overall mixing effect or heat exchange rate is presented by Chelemer (et al ~~1970~~ 1969).

Insert E p. 4.4-6

$$CWF\ (Tong\ 1972) = 1.0 - Ru\ [13.76 - 1.372e^{1.78x} - 4.732\left(\frac{G}{10^6}\right)^{-0.0535} - 0.0619\left(\frac{P}{1000}\right)^{0.14} - 8.509Dh^{0.107}] \quad (4.4\text{-}4a)$$

and $Ru = 1 - De/Dh$

For the WRB-1 correlation,

$$q''_{DNB,\,N} = \frac{q''\ WRB\text{-}1}{F}$$

where F is the same flux shape factor that is used with the W-3 correlation.

Various mixing tests have been performed at Columbia University by Cadek (et al 1975). These series of tests, using the "R" mixing vane grid design on 13-, 26-, and 32-inch grid spacing, were conducted in pressurized water loops at Reynolds numbers similar to that of a pressurized water reactor (PWR) core under the following single- and two-phase (subcooled boiling) flow conditions:

Pressure	1,500 to 2,400 (psia)
Inlet temperature	332 to 642 (^{o}F)
Mass velocity	1.0 to 3.5 x 10^{6} ($lb_m/hr\text{-}ft^2$)
Reynolds number	1.34 to 7.45 x 10^{5}
Bulk outlet quality	-52.1 to 13.5 (percent)

The thermal diffusion coefficient is determined by comparing the THINC Code predictions with the measured subchannel exit temperatures. Data for 26-inch axial grid spacing are presented on Figure 4.4-8 where TDC is plotted versus the Reynolds number. Thermal diffusion coefficient is found to be independent of Reynolds number, mass velocity, pressure, and quality over the ranges tested. The two-phase data (local, subcooled boiling) fell within the scatter of the single phase data. The effect of two-phase flow on the value of TDC has been demonstrated by Cadek (et al 1975), Rowe and Angle (1967, 1969), and Gonzalez-Santalo and Griffith (1972). In the subcooled boiling region, the values of TDC were indistinguishable from the single-phase values. In the quality region, Rowe and Angle (1967, 1969) show that in the case with rod spacing similar to that in PWR core geometry, the value of TDC increased with quality to a point and then decreased, but never below the single-phase value. Gonzalez-Santalo and Griffith (1972) showed that the mixing TDC increased as the void fraction increased.

The data from these tests on the "R" grid showed that a design TDC value of 0.038 (for 26-inch grid spacing) can be used in determining the effect of coolant mixing in the THINC analysis.

A mixing test program similar to the one described previously was conducted at Columbia University for the current 17 by 17 geometry and mixing vane grids on 26-inch spacing (Motley et al 1975b). The mean value of TDC obtained from these tests was 0.051 ~~0.059~~, and all data were well above the current design value of 0.038.

Since the actual reactor grid spacing is approximately 20 inches, additional margin is available for this design, as the value of TDC increases as grid spacing decreases (Cadek et al 1975).

4.4.2.2.4 Hot Channel Factors

The total hot channel factors for heat flux and enthalpy rise are defined as the maximum-to-core average ratios of these quantities.

The heat flux hot channel factor considers the local maximum linear heat generation rate at a point (the hot spot), and the enthalpy rise hot channel factor involves the maximum integrated linear heat generation rate along a channel (the hot channel).

Each of the total hot channel factors is composed of a nuclear hot channel factor (Section 4.4.4.3) describing the fission power distribution and an engineering hot channel factor, which allows for variations in flow conditions and fabrication tolerances. The engineering hot channel factors are made up of subfactors which account for the influence of the variations of fuel pellet diameter, density, enrichment, and eccentricity; inlet flow distribution; flow redistribution; and flow mixing.

The heat flux engineering hot channel factor (F^E_Q) is used to evaluate the maximum linear heat generation rate in the core. This subfactor is determined by statistically combining the fabrication variations for fuel pellet diameter, density, and enrichment, and has a value of 1.03 at the 95 percent probability level with 95 percent confidence. ~~Hill (et al 1973) emphasize that no DNB penalty needs to be taken for the short relatively low intensity heat flux spikes caused by variations in the preceding parameters, as well as fuel pellet eccentricity and fuel rod diameter variation.~~

Insert F

Insert G

4.4.2.2.4.1 Enthalpy Rise Engineering Hot Channel Factor, $F_{AH}{}^E$

The effect of variations in flow conditions and fabrication tolerances on the hot channel enthalpy rise is directly considered in the THINC core thermal subchannel analysis (Section 4.4.4.5.1) under any reactor operating condition. The items included in the consideration of the enthalpy rise engineering hot channel factor are discussed as follows:

Pellet Diameter, Density, and Enrichment and Fuel Rod Diameter, Pitch and Bowing

Design values employed in the THINC analysis related to the above fabrication variations are based on applicable limiting tolerances such that these design values are met for 95 percent of the limiting channels at a 95 percent confidence level. Measured manufacturing data on Westinghouse 17 by 17 fuel show the tolerances used in this evaluation are conservative. In addition, each fuel assembly is inspected to assure that the channel spacing design criteria are met. The effect of variations in pellet diameter, enrichment, and density is employed in the THINC analysis as a direct multiplier on the hot channel enthalpy rise. The fuel rod diameter, pitch, and bowing variation (including inpile effects) is considered in the preparation of the THINC input values, such as axial flow area, equivalent hydraulic diameter, and lateral cross-flow area for the hot channel. This effect (pitch reduction) is used as part of the margin to offset rod bow penalties (Section 4.4.2.2.5).

Insert F p. 4.4-8

eccentricity and the fuel rod diameter,

Insert G p. 4.4-8

Thus, it is expected that a statistical sampling of the fuel assemblies of the reference plant will yield a value no larger than 1.03.

Inlet Flow Maldistribution

The consideration of inlet flow maldistribution in core thermal performances is discussed in Section 4.4.4.2.2. A design basis of 5 percent reduction in reactor coolant flow to the hot assembly is used in the THINC-IV analysis.

Flow Redistribution

The flow redistribution accounts for the reduction in flow in the hot channel resulting from the high flow resistance in the channel due to the local or bulk boiling. The effect of the non-uniform power distribution is inherently considered in the THINC analysis for every operating condition which is evaluated.

Flow Mixing

The subchannel mixing model incorporated in the THINC Code and used in reactor design is based on experimental data (Cadek 1975) discussed in Sections 4.4.2.2.3 and 4.4.4.5.1. The mixing vanes incorporated in the spacer grid design induce additional flow mixing between the various flow channels in a fuel assembly as well as between adjacent assemblies. This mixing reduces the enthalpy rise in the hot channel resulting from local power peaking or unfavorable mechanical tolerances.

4.4.2.2.5 Effects of Rod Bow on DNBR

The phenomenon of fuel rod bowing, as described in Skaritka (1979), must be accounted for in the DNBR safety analysis of Condition I and Condition II events for each plant application. Applicable generic credits for margin resulting from retained conservatism in the evaluation of DNBR and/or margin obtained from measured plant operating parameters (such as $F^N_{\Delta H}$ or core flow), which are less limiting than those required by the plant safety analysis, can be used to offset the effect of rod bow.

The safety analysis for BVPS-2 maintained sufficient margin ~~of 9.1 percent (design limit DNBR of 1.30 vs. 1.28, grid spacing (K_S) of 0.046 vs. 0.059, thermal diffusion coefficient of 0.038 vs. 0.059, DNB multiplier of 0.863 vs. 0.88, and pitch reduction)~~ as discussed in Section 4.4.1.1, to accommodate full and low flow DNBR penalties identified in Westinghouse (1981) and USNRC (1986) (<1.3 percent for the worst case which occurs at a burnup of 24,000 MWD/MTU).

The maximum rod bow penalties accounted for in the design safety analysis are based on an assembly average burnup of 24,000 MWD/MTU. At burnups greater than 24,000 MWD/MTU, credit is taken for the effect of $F^N_{\Delta H}$ burndown due to the decrease in fissionable isotopes and the buildup of fission product inventory, and no additional rod bow penalty is required (USNRC 1986).

4.4.2.3 ~~Linear Heat Generation Rate~~

Insert I

~~The core average and maximum linear heat generation rates are given in Table 4.4-1. The method of determining the maximum linear heat generation rate is given in Section 4.3.2.2.~~

4.4.2.4 Void Fraction Distribution

The calculated core average and the hot subchannel maximum and average void fractions are presented in Table 4.4-2 for operation at full power with ~~design~~ hot channel factors. The void fraction distribution in the core at various radial and axial locations is presented by Hochreiter and Chelemer (1973). The void models used in the THINC-IV Code are described in Section 4.4.2.7.3. ~~Normalized core flow and enthalpy rise distributions are shown on Figures 4.4-3 through 4.4-5.~~

Insert H →

4.4.2.5 Core Coolant Flow Distribution

Assembly average coolant mass velocity and enthalpy at various radial and axial core locations are given. Typical coolant enthalpy rise and flow distributions for the 4 feet elevation (1/3 of core height) are shown on Figure 4.4-~~24~~ for the 8 feet elevation (2/3 of core height) on Figure 4.4-~~25~~, and at the core exit on Figure 4.4-~~26~~. These distributions are for the full power conditions as given in Table 4.4-1. ~~and for the radial power density distribution shown on Figure 4.3-7.~~

The THINC Code analysis for this case utilized a uniform core inlet enthalpy and inlet flow distribution. No orificing is employed in the reactor design.

4.4.2.6 Core Pressure Drops and Hydraulic Loads

4.4.2.6.1 Core Pressure Drops

The analytical model and experimental data used to calculate the pressure drops shown in Table 4.4-1 are described in Section 4.4.2.7. ~~The core pressure drop includes the eight grid fuel assembly, lower core plate, and upper core plate pressure drops.~~ The full power operation pressure drop values shown in Table 4.4-1 are the unrecoverable pressure drops across the vessel, including the inlet and outlet nozzles, and across the core. These pressure drops are based on the best estimate flow for actual plant operating conditions as described in Section 5.1.1. Section 5.1.1 also defines and describes the thermal design flow (minimum flow) which is the basis for reactor core thermal performance and the mechanical design flow (maximum flow) which is used in the mechanical design of the reactor vessel internals and fuel assemblies. Since the best estimate flow is that flow which is most likely to exist in an operating plant, the calculated core pressure drops in Table 4.4-1 ~~are based on this best estimate~~ will be greater than pressure drops previously quoted using the thermal design flow.

Insert H p. 4.4-10

Since void formation due to subcooled boiling is an important supporting cause of interassembly flow redistribution, a sensitivity study was performed with THINC-IV using the void model by Hochreiter and Chelemer (1973).

The results of this study showed that because of the realistic crossflow model used in THINC-IV, the minimum DNBR in the hot channel is relatively insensitive to variations in this model. The range of variations considered in this sensitivity study covered the maximum uncertainty range of the data used to develop each part of the void fraction correlation.

Insert I p. 4.4-10

4.4.2.3 Flux Tilt Considerations

Significant quadrant power tilts are not anticipated during normal operation since this phenomenon is caused by some asymmetric perturbation. A dropped or misaligned RCCA could cause changes in hot-channel factors; however, these events are analyzed separately in Chapter 15. This discussion will be confined to flux tilts caused by X-Y xenon transients, inlet temperature mismatches, enrichment variations within tolerances and so forth.

The design value of the enthalpy rise hot-channel factor $F(N,\Delta H)$ which includes an 8% uncertainty (as discussed in Section 4.3.2.2.7), is assumed to be sufficiently conservative that flux tilts up to and including the alarm point (see the Technical Specifications) will not result in values of $F(N,\Delta H)$ greater than that assumed. The design value of F(Q) does not include a specific allowance for quadrant flux tilts.

Insert J p. 4.4-10a

The pressure drops quoted in Table 4.4-1 are based on seven grids and conservatively estimated grid pressure loss coefficients. Phase 1 of the D-loop tests (Nakazato, DeMario 1974) resulted in a measured core pressure drop of a magnitude sufficiently lower than the predicted pressure drop that the pressure drops quoted in Table 4.4-1 will be conservative even with the addition of an eighth grid. Further verification of the 17x17 core pressure drop and corresponding uncertainties have been obtained from Phase 2 of the D-loop tests.

Insert 5

Uncertainties associated with the core pressure drop values are discussed in Section 4.4.2.9.2.

4.4.2.6.2 Hydraulic Loads

The fuel assembly holddown springs (Figure 4.2-2) are designed to keep the fuel assemblies in contact with the lower core plate under all ANS Condition I and II events with the exception of the turbine overspeed transient associated with a loss of external load. The holddown springs are designed to tolerate the possibility of an over deflection associated with fuel assembly liftoff for this case and provide contact between the fuel assembly and the lower core plate following this transient. More adverse flow conditions occur during a LOCA. These conditions are presented in Section 15.6.5.

Hydraulic loads at normal operating conditions are calculated considering the mechanical design flow which is described in Section 5.1 and accounting for the minimum core bypass flow based on manufacturing tolerances. Core hydraulic loads at cold plant start-up conditions are based on the cold mechanical design flow, but are adjusted to account for the coolant density difference. Conservative core hydraulic loads for a pump overspeed transient, which could possibly create flow rate 20 percent greater than the mechanical design flow, are evaluated to be ~~approximately~~ greater than twice the fuel assembly weight.

Core hydraulic loads were measured during the prototype assembly tests described in Section 1.5. Further discussion is presented by DeMario (1974).

phase water. These assumptions apply to the core and vessel pressure drop calculations for the purpose of establishing the reactor coolant loops flow rate. Two-phase considerations are neglected in the vessel pressure drop evaluation because the core average void is negligible (Table 4.4-2). Two-phase flow considerations in the core thermal subchannel analyses are considered and the models are discussed in Section 4.4.4.2.3. Core and vessel pressure losses are calculated by equations of the form:

$$\Delta P_L = \left(K + F \frac{L}{D_e}\right) \frac{\rho V^2}{2 g_c (144)} \qquad (4.4\text{-}8)$$

where:

ΔP_L = unrecoverable pressure drop (lb_f/in^2)
ρ = fluid density (lb_m/ft^3)
L = length (ft)
D_e = equivalent diameter (ft)
V = fluid velocity (ft/sec)
g_c = 32.174 (lb_m-ft/lb_f-sec^2)
K = form loss coefficient (dimensionless)
F = friction loss coefficient (dimensionless)

Fluid density is assumed to be constant at the appropriate value for each component in the core and vessel. Because of the complex core and vessel flow geometry, precise analytical values for the form and friction loss coefficients are not available. Therefore, experimental values for these coefficients are obtained from geometrically similar models.

Values are quoted in Table 4.4-1 for unrecoverable pressure loss across the reactor vessel, including the inlet and outlet nozzles, and across the core. The results of full scale tests of core components and fuel assemblies were utilized in developing the core pressure loss characteristics. The pressure drop for the vessel was obtained by combining the core loss with correlation of 1/7th scale model hydraulic test data on a number of vessels (Hetsroni 1964, 1965) and form loss relationships (Idel'chik 1960). Moody's (1944) curves were used to obtain the single phase friction factors.

Insert K →

Tests of the reactor coolant loop flow rates will be made (Section 4.4.5.1) prior to initial criticality to verify that the flow rates used in the design, which were determined in part from the pressure losses calculated by the method described here, are conservative.

Insert K p. 4.4-12

Core pressure drops will be confirmed when the results of the Hydraulic Verification Tests become available. These hydraulic verification tests include hydraulic head losses and effects of velocity changes as well as unrecoverable pressure losses. The effects of velocity changes are small since the static pressure taps are located at elevations of approximately equal flow areas (and therefore approximately equal velocities). When wall static pressure taps are used near ambient fluid conditions, it can be shown analytically that the elevation head losses do not contribute to the measured core pressure drops. Therefore, data from the hydraulic verification tests can be directly applied to confirm the pressure drop values quoted in Table 4.4-1 which are based on unrecoverable pressure losses only.

Insert L p. 4.4-13

the safety analysis limit DNBR

Insert M p. 4.4-13

for DNBRs greater than or equal to the safety analysis DNBR limit

4.4.2.7.3 Void Fraction Correlation

There are three separate void regions considered in flow boiling in a PWR as illustrated on figure 4.4-~~5~~8. They are the wall void region (no bubble detachment), the subcooled boiling region (bubble detachment) and the bulk boiling region.

In the wall void region, the point where local boiling begins is determined when the clad temperature reaches the amount of superheat predicted from Thom's (et al 1955-1966) correlation (Section 4.4.2.7.1). The void fraction in this region is calculated using Maurer's (1960) relationship. The bubble detachment point, where the superheated bubbles break away from the wall, is determined by using Griffith's (et al 1958) relationship.

The void fraction in the subcooled boiling region (that is, after the detachment point) is calculated from Bowring's (1962) correlation. This correlation predicts the void fraction from the detachment point to the bulk boiling region.

The void fraction in the bulk boiling region is predicted by using homogeneous flow theory and assuming no slip. The void fraction in this region is therefore a function only of the thermodynamic quality.

4.4.2.8 Thermal Effects of Operational Transients

Departure from nucleate boiling core safety limits are generated as a function of reactor coolant temperature, pressure, core power, and axial power imbalance. Steady state operation within these safety limits ensures that the minimum DNBR is not less than ~~1.30~~.* Insert L.
Figure 15.0.3-1 shows the ~~DNBR equals 1.30~~* limit lines and the Insert M.
resulting overtemperature ΔT trip lines (which become part of the Technical Specifications) plotted as ΔT versus T_{avg} for various pressures. This system provides adequate protection against anticipated operational transients that are slow with respect to fluid transport delays in the RCS. In addition, for fast transients, for example, uncontrolled rod bank withdrawal at power incident, (Section 15.4.2) specific protection functions are provided as described in Section 7.2 and the use of these protection functions is described in Chapter 15. The thermal response of the fuel rod is discussed in Section 4.4.4.~~8~~

4.4.2.9 Uncertainties in Estimates

4.4.2.9.1 Uncertainties in Fuel and Clad Temperatures

As discussed in Section 4.4.2.11, the fuel temperature is a function of crud, oxide, clad gap, and pellet conductances. Uncertainties in the fuel temperature calculation are essentially of two types: 1) fabrication uncertainties such as variations in the pellet and clad dimensions and the pellet density; and 2) model uncertainties such as variations in the pellet conductivity and the gap

4.4.2.9.4 Uncertainty in Departure from Nucleate Boiling Correlation

The uncertainty in the DNB correlation (Section 4.4.2.2) can be written as a statement on the probability of not being in DNB based on the statistics of the DNB data. This is discussed in Section 4.4.2.2.2.

4.4.2.9.5 Uncertainties in Departure from Nucleate Boiling Ratio Calculations

The uncertainties in the DNBRs calculated by THINC analysis (Section 4.4.4.5.1) due to uncertainties in the nuclear peaking factors are accounted for by applying conservatively high values of the nuclear peaking factors and including measurement error allowances. In addition, conservative values for the engineering hot channel factors are used as discussed in Section 4.4.2.2.4. ~~The results of a sensitivity study (Hochreiter and Chelemer 1973) with THINC-IV show that the minimum DNBR in the hot channel is relatively insensitive to variations in the core-wide radial power distribution (for the same value of $F^N_{\Delta H}$).~~

The ability of the THINC-IV code to accurately predict flow and enthalpy distributions in rod bundles is discussed in Section 4.4.4.5.1 and presented by Hochreiter (et al 1973). Studies have been performed by Hochreiter and Chelemer (1973) to determine the sensitivity of the minimum DNBR in the hot channel to the void fraction correlation (Section 4.4.2.7.3); the inlet velocity and exit pressure distributions assumed as boundary conditions for the analysis; and the grid pressure loss coefficients. The results of these studies show that the minimum DNBR in the hot channel is relatively insensitive to variations in these parameters. The range of variations considered in these studies covered the range of possible variations in these parameters.

the corewide radial power distribution (for constant $F(N,\Delta H)$)

4.4.2.9.6 Uncertainties in Flow Rates

The uncertainties associated with reactor coolant loop flow rates are discussed in Section 5.1. A thermal design flow is defined for use in core thermal performance evaluations which ~~accounts for both prediction and measurement uncertainties.~~ In addition, another 6.5 ~~4.5~~ percent of the thermal design flow is assumed to be ineffective for core heat removal capability because it bypasses the core through the various available vessel flow paths described in Section 4.4.4.2.1.

is less than the Best Estimate Loop Flow (by approximately 5%)

4.4.2.9.7 Uncertainties in Hydraulic Loads

As discussed in Section 4.4.2.6.2, hydraulic loads on the fuel assembly are evaluated for a pump overspeed transient which creates flow rates 20 percent greater than the mechanical design flow. As stated in Section 5.1, the mechanical design flow is greater than the

best estimate or most likely flow rate values for the actual plant operating condition (by approximately 4.0%).

4.4.2.9.8 Uncertainty in Mixing Coefficient

The value of the mixing coefficient used in THINC analyses for this application is 0.038. The mean value of TDC obtained in the "R" grid mixing tests described in Section 4.4.2.2.1 was 0.042 (for 26-inch grid spacing). The value 0.038 is one standard deviation below the mean value; and approximately 90 percent of the data gives values of TDC greater than 0.038 (Cadek et al 1975).

The results of the mixing tests done on 17 by 17 geometry, as discussed in Section 4.4.2.2.3, had a mean value of TDC of 0.059 and standard deviation equal to 0.007. Hence the current design value of TDC is almost three standard deviations below the mean for 26-inch grid spacing.

4.4.2.10 Flux Tilt Considerations

Significant quadrant power tilts are not anticipated during normal operation since this phenomenon is caused by some asymmetric pertubation. A dropped or misaligned rod cluster control assembly could cause changes in hot channel factors; however, these events are analyzed separately in Chapter 15.

Other possible causes for quadrant power tilts include X-Y xenon transients, inlet temperature mismatches, enrichment variations within tolerances, and so forth.

In addition to the preceding unanticipated quadrant power tilts, other readily explainable asymmetries may be observed during calibration of the excore detector quadrant power tilt alarm. During operation, incore maps are taken at least once per month and, periodically, additional maps are obtained for calibration purposes. Each of these maps is reviewed for deviations from the expected power distributions. Asymmetry in the core, from quadrant to quadrant, is frequently a consequence of the design when assembly and/or component shuffling and rotation requirements do not allow exact symmetry preservation. In each case, the acceptability of an observed asymmetry, planned or otherwise depends solely on meeting the required accident analyses assumptions.

In practice, once acceptability has been established by review of the incore maps, the quadrant power tilt alarms and related instrumentation are adjusted to indicate zero quadrant power tilt ratio as the final step in the calibration process. This action ensures that the instrumentation is correctly calibrated to alarm in the event an unexplained or unanticipated change occurs in the quadrant to quadrant relationships between calibration intervals. Proper functioning of the quadrant power tilt alarm is important because no allowances are made in the design for increased hot

channel factors due to unexpected flux tilts since all likely causes are prevented by design or procedures, or are specifically analyzed. Finally, in the event that unexplained flux tilts do occur, the Technical Specifications provide appropriate corrective actions to ensure continued safe operation of the reactor.

4.4.2.11 Fuel and Cladding Temperatures (Excluding Dens. & Conv.)

Consistent with the thermal-hydraulic design bases described in Section 4.4.1, the following discussion pertains mainly to fuel pellet temperature evaluation. A discussion of fuel clad integrity is presented in Section 4.2.3.1.

The thermal-hydraulic design assures that the maximum fuel temperature is below the melting point of UO_2 (Section 4.4.1.2). To preclude center melting and as a basis for overpower protection system set points, a calculated centerline fuel temperature of 4,700°F has been selected as the overpower limit. This provides sufficient margin for uncertainties in the thermal evaluations as described in Section 4.4.2.9.1. The temperature distribution within the fuel pellet is primarily a function of the local power density and the UO_2 thermal conductivity. However, the computation of radial fuel rod temperature distributions combines crud, oxide, clad gap, and pellet conductances. The factors which influence these conductances, such as gap size (or contact pressure), internal gas pressure, gas composition, pellet density, and radial power distribution within the pellet, etc. have been combined into a semi-empirical thermal model (Section 4.2.3.3) with the model modifications for time dependent fuel densification given by Hellman (1975). This thermal model enables the determination of these factors and their net effects on temperature profiles. The temperature predictions have been compared to inpile fuel temperature measurements (Kjaerheim and Rolstad 1967; Kjaerheim 1969; Cohen et al 1960; Clough and Sayers 1964; Stora et al 1964; Devold 1968; and Balfour et al 1966) and melt radius data (Nelson et al 1964 and Duncan 1962) with good results.

According to Hellman (1975), fuel rod thermal evaluations (fuel centerline, average and surface temperatures) are determined throughout the fuel rod lifetime with consideration of time dependent densification. To determine the maximum fuel temperatures, various burnup rods, including the highest burnup rod are analyzed over the rod linear power range of interest.

INSERT N →

The principal factors which are employed in the determination of the fuel temperature are discussed below.

4.4.2.11.1 UO_2 Thermal Conductivity

The thermal conductivity of uranium dioxide was evaluated from data reported by Howard and Gulvin (1960); Lucks and Deem (1961); Daniel (et al 1962); Feith (1962); Vogt (et al 1964); Nishijima (et al

Insert N p. 4.4-17

Effect of Fuel Densification on Fuel Rod Temperatures

Fuel densification results in fuel pellet shrinkage. This affects the fuel temperatures in the following ways:

1. Pellet radial shrinkage increased the pellet diametral gap which results in increased thermal resistance of the gap, and thus, higher fuel temperatures (see Section 4.2.3.3).

2. Pellet axial shrinkage may produce pellet to pellet gaps which results in local power spikes, described in Section 4.3.2.2.5 and thus, higher total heat flux hot channel factor, F(Q), and local fuel temperature.

3. [illegible] shrinkage will result in a fuel stack height reduction and an increased [illegible] generation rate (kW/ft) for a constant core power level. Using the [illegible] noted in Section 5.3 of Hellman 1973, the increase in linear power for [illegible] fications listed in Table 4.3-1 is 0.2%.

[illegible] an 1973, fuel rod thermal evaluations (fuel centerline, average and [illegible] ves) are determined throughout the fuel rod lifetime with consi[illegible] dependent densification. Maximum fuel average and surface temperatures, shown in Figure 4.4-9 as a function of the LHGR, are peak values attained during the fuel lifetime. Figure 4.4-10 presents the peak value of fuel centerline temperature versus linear power density which is attained during the fuel lifetime.

The maximum pellet temperatures at the hot spot during full power steady state and at the maximum overpower trip point are shown in Table 4.4-1.

Insert O p.4.4-20

Figure 4.4-12 shows the axial variations of average clad temperature for the average power rod both at beginning and end-of-life.

1965); Ainscough and Wheeler (1968); Godfrey (et al 1964); Stora (et al 1964); Bush (1965); Asamoto (et al 1968); Kruger (1965); and Gyllander (1971).

At higher temperatures, thermal conductivity is best obtained by utilizing the integral conductivity to melt, which can be determined with more certainty. From an examination of the data, it has been concluded that the best estimate for the value of $\int_{2,800°C} K dt$ is 93 W/cm. This conclusion is based on the integral values reported by Duncan (1962); Gyllander (1971); Lyons (et al 1966); Coplin (1968); Bain (1962); and Stora (1970).

The design curve for the thermal conductivity is shown on Figure 4.4-7. The section of the curve at temperatures between 0°C and 1,300°C is in excellent agreement with the recommendation of the International Atomic Energy Agency (1966) panel. The section of the curve above 1,300°C is derived for an integral value of 93 W/cm (Duncan 1962, Gyllander 1971, and Stora 1970).

Thermal conductivity of UO_2 at 95 percent theoretical density can be represented best by the following equation:

$$K = \frac{1}{11.8 + 0.0238T} + 8.775 \times 10^{-13} T^3 \qquad (4.4\text{-}9)$$

where:

K = W/cm-°C
T = °C

4.4.2.11.2 Radial Power Distribution in UO_2 Fuel Rods

An accurate description of the fuel rod radial power distribution as a function of burnup is needed for determining the power level for incipient fuel melting and other important performance parameters such as pellet thermal expansion, fuel swelling, and fission gas release rates.

Radial power distributions in UO_2 fuel rods are determined with the neutron transport theory code, LASER. The LASER Code has been validated by comparing the code predictions on radial burnup and isotopic distributions with measured radial microdrill data (Poncelet 1965 and Nodvick 1970). A radial power depression factor f, is determined using radial power distributions predicted by LASER. The factor f enters into the determination of the pellet centerline temperature, T_c, relative to the pellet surface temperature, T_s, through the expression:

roughness (Dean 1962). This information together with the pellet and clad inner surface roughness for Westinghouse fuel leads to the following correlation:

$$h = 0.6P + \frac{K_{gas}}{\delta_r} \qquad (4.4\text{-}12)$$

where:

P = contact pressure (psi)

4.4.2.11.4 Surface Heat Transfer Coefficients

The fuel rod surface heat transfer coefficients during subcooled forced convection and nucleate boiling are presented in Section 4.4.2.7.1.

4.4.2.11.5 Fuel Clad Temperatures

The outer surface of the fuel rod at the hot spot operates at a temperature of approximately 660°F for steady state operation at rated power throughout core life due to the presence of nucleate boiling. Initially (beginning-of-life), this temperature is that of the clad metal outer surface.

During operation over the life of the core, the buildup of oxides and crud on the fuel rod surface causes the clad surface temperature to increase. Allowance is made in the fuel center melt evaluation for this temperature rise. Since the thermal-hydraulic design basis limits DNB, adequate heat transfer is provided between the fuel clad and the reactor coolant so that the core thermal output is not limited by considerations of clad temperature. ← Insert O

4.4.2.11.6 Treatment of Peaking Factors

The total heat flux hot channel factor, F_Q, is defined as the ratio of the maximum to average core heat flux. The design value for F_Q as presented in Table 4.3-2 and discussed in Section 4.3.2.2.6 is 2.32 for normal operation. This results in a peak linear power of 12.1 kW/ft at full power conditions.

As described in Section 4.3.2.2.6, the peak linear power resulting from overpower transients/operator errors (assuming maximum overpower of 118 percent) is 18.0 kW/ft. The centerline temperature kW/ft must be below the UO_2 melt temperature over the lifetime of the rod, including allowances for uncertainties. The fuel temperature design basis is discussed in Section 4.4.1.2 and results in a maximum allowable calculated centerline temperature of 4,700°F. The peak

4. Flow introduced between the baffle and the barrel for the purpose of cooling these components and which is not considered available for core cooling.

5. Flow in the gaps between the fuel assemblies on the core periphery and the adjacent baffle wall.

These flow paths are evaluated to confirm that the design value of the core bypass flow is met. The design value of core bypass flow for BVPS-2 is equal to ~~4.5~~ or less than 6.5 percent of the total vessel flow.

Of the total allowance, 2.0 percent is associated with the core and the remainder is associated with the internals (items 2 through 5). Calculations have been performed using drawing tolerance in the worst direction and accounting for uncertainties in pressure losses. Based on these calculations, the core bypass is no greater than the preceding design values quoted.

Flow model test results for the flow path through the reactor are discussed in Section 4.4.2.7.2.

4.4.4.2.2 Inlet Flow Distributions

Data from several 1/7th scale hydraulic reactor model tests (Hetsroni 1964 and 1965, and Carter 1972) have been utilized in arriving at the core inlet flow maldistribution criteria to be used in the THINC analyses Section 4.4.4.5.1). THINC-I analyses made, using this data have indicated that a conservative design basis is to consider 5 percent reduction in the flow to the hot assembly (Shefcheck 1972). The same design basis of 5 percent reduction to the hot assembly inlet is used in THINC-IV analyses.

The experimental error estimated in the inlet velocity distribution has been considered as outlined by Hochreiter and Chelemer (1973) where the sensitivity of changes in inlet velocity distributions to hot channel thermal performance is shown to be small. Hochreiter and Chelemer (1973) studies made with the improved THINC model (THINC-IV) show that it is adequate to use the 5 percent reduction in inlet flow to the hot assembly for a reactor coolant loop out of service based on the experimental data presented by Hetsroni (1964 and 1965).

The effect of the total flow rate on the inlet velocity distribution was studied in the experiments by Hetsroni (1964). As was expected, on the basis of the theoretical analysis, no significant variation could be found in inlet velocity distribution with reduced flow rate.

4.4.4.2.3 Empirical Friction Factor Correlations

Two empirical friction factor correlations are used in the THINC-IV Code (Section 4.4.4.5.1).

4.4.4.3.1 Nuclear Enthalpy Rise Hot Channel Factor, $F^N_{\Delta H}$

Given the local linear power density q' (kW/ft) at a point x, y, z in a core with N fuel rods and height H,

$$F^N_{\Delta H} = \frac{\text{hot rod power}}{\text{average rod power}} = \frac{\text{Max} \int_0^H q'(x_0, y_0, z)\,dz}{\frac{1}{N}\sum_{\substack{\text{all}\\ \text{rods}}} \int_0^H q'(x,y,z)\,dz} \qquad (4.4\text{-}14)$$

The way in which $F^N_{\Delta H}$ is used in the DNB calculation is important. The location of minimum DNBR depends on the axial profile and the value of DNBR depends on the enthalpy rise to that point. Basically, the maximum value of the rod integral is used to identify the most likely rod for minimum DNBR. An axial power profile is obtained which when normalized to the design value of $F^N_{\Delta H}$ recreates the axial heat flux along the limiting rod. The surrounding rods are assumed to have the same axial profile with rod average powers which are typical distributions found in hot assemblies. In this manner, worst case axial profiles can be combined with worst case radial distributions for reference DNB calculations.

It should be noted again that $F^N_{\Delta H}$ is an integral and is used as such in DNB calculations. Local heat fluxes are obtained by using hot channel and adjacent channel explicit power shapes which take into account variations in horizontal power shapes throughout the core. The sensitivity of the THINC-IV analysis to radial power shapes is discussed by Hochreiter and Chelemer (1973).

For operation at ~~a fraction P of~~ full power, the design $F^N_{\Delta H}$ used is ~~given by:~~ 1.62 this analysis basis conservatively bounds the $F_{\Delta H}$ limits as presented in the technical specifications.

$$F^N_{\Delta H} \leq \frac{1.62}{1.55}\left[1 + 0.3\,(1-P)\right] \qquad (4.4\text{-}15)$$

For operation at a fraction P of full power relaxation of $F_{\Delta H}$ is allowed.
The permitted relaxation of $F^N_{\Delta H}$ is included in the DNB protection setpoints and allows radial power shape changes with rod insertion to the insertion limits (McFarlane 1975), thus allowing greater flexibility in the nuclear design.

4.4.4.3.2 Axial Heat Flux Distributions

As discussed in Section 4.3.2.2, the axial heat flux distribution can vary as a result of rod motion, power change, or due to a spatial

xenon transient which may occur in the axial direction. Consequently, it is necessary to measure the axial power imbalance by means of the excore nuclear detectors (Section 4.3.2.2.7) and protect the core from excessive axial power imbalance. ~~The reference axial shape used in establishing core DNB limits (that is, overtemperature ΔT protection system setpoints) is a chopped cosine with a peak to average value of 1.55. The reactor trip system provides automatic reduction of the trip setpoints on excessive axial power imbalance. To determine the magnitude of the setpoint reduction, the reference shape is supplemented by other axial shapes skewed to the bottom and top of the core.~~ Insert 5

~~The course of those accidents in which DNB is a concern is analyzed in Chapter 15 assuming that the protection setpoints have been set on the basis of these shapes. In many cases the axial power distribution in the hot channel changes throughout the course of the accident due to rod motion, reactor coolant temperature, and power level changes.~~

~~The initial conditions for the accidents for which DNB protection is required are assumed to be those permissible within the constant axial offset control strategy for the load maneuvers described by Morita (et al 1974). In the case of the loss of flow accident, the hot channel heat flux profile is very similar to the power density profile in normal operation preceding the accident. It is therefore possible to illustrate the calculated minimum DNBR for conditions representative of the loss of flow accident as a function of the flux difference initially in the core. All power shapes were evaluated with a full power radial peaking factor ($F^N_{\Delta H}$) of 1.56. The radial contribution to the hot rod power shape is conservative both for the initial condition and for the condition at the time of minimum DNBR during the loss of flow transient. Based on the analysis, a design shape is chosen which results in a calculated minimum DNBR that bounds all the normal operation shapes.~~ delete

4.4.4.4 Core Thermal Response

A general summary of the steady state thermal-hydraulic design parameters including thermal output, flow rates, etc, is provided in Table 4.4-1 for all reactor coolant loops in operation.

As stated in Section 4.4.1, the design bases of the application are to prevent DNB and to prevent fuel melting for ANS Condition I and II events. The protective systems described in Chapter 7 (Instrumentation and Control) are designed to meet these bases. The response of the core to ANS Condition II transients is given in Chapter 15.

Insert P p. 4.4-26

The Reactor Trip System provides automatic reduction of the trip setpoint in the Overtemperature ΔT channels on excessive axial power imbalance; that is, when an extremely large axial offset corresponds to an axial shape which could lead to a DNBR which is less than that calculated for the reference DNB design axial shape.

The reference DNB design axial shape used in this amendment is a chopped cosine shape with a peak average value of 1.55. The use of a 1.55 cosine instead of the 1.48 cosine results in increased operating flexibility.

There are fewer axial power shapes which give DNBRs less than the DNBR for a 1.55 cosine than there are shapes which give DNBRs less than the DNBR for a 1.48 cosine. Thus, greater axial power imbalances can be allowed when the reference DNB design axial shape is a 1.55 cosine.

4.4.4.5 Analytical Techniques

4.4.4.5.1 Core Analysis

The objective of reactor core thermal design is to determine the maximum heat removal capability in all flow subchannels and show that the core safety limits, as presented in the Technical Specifications, are not exceeded while compounding engineering and nuclear effects. The thermal design takes into account local variations in dimensions, power generation, flow redistribution, and mixing. THINC-IV is a realistic three dimensional matrix model which has been developed to account for hydraulic and nuclear effects on the enthalpy rise in the core (Hochreiter and Chelemer 1973 and Hochreiter et al 1973). The behavior of the hot assembly is determined by superimposing the power distribution among the assemblies upon the inlet flow distribution while allowing for flow mixing and flow distribution between assemblies. The average flow and enthalpy in the hottest assembly is obtained from the core-wide, assembly-by-assembly analysis. The local variations in power, fuel rod and pellet fabrication, and mixing within the hottest assembly are then superimposed on the average conditions of the hottest assembly in order to determine the conditions in the hot channel.

4.4.4.5.2 Steady State Analysis

The THINC-IV computer program, as approved by the U.S. Nuclear Regulatory Commission (USNRC 1978), is used to determine reactor coolant density, mass velocity, enthalpy, vapor void, static pressure, and DNBR distributions along parallel flow channels within a reactor core under all expected operating conditions. The THINC-IV Code is further described by Hochreiter and Chelemer (1973) and Hochreiter (et al 1973), including models and correlations used. In addition, a discussion on experimental verification of THINC-IV is given by Hochreiter (et al 1973).

← Insert C

~~The effect of crud on the flow and enthalpy distribution in the core is accounted for directly in the THINC-IV evaluations by assuming a crud thickness several times that which would be expected to occur. This results in a slightly conservative evaluation of the minimum DNBR. Operating experience of Westinghouse designed reactors has indicated that a flow resistance allowance for possible crud deposits is not required. There has been no detectable long-term flow reduction reported to any plant. Inspection of the inside surfaces of steam generator tubes removed from operating plants has confirmed that there is no significant surface deposition that would affect system flow. Althought not all of the coolant piping surfaces have been inspected, the small piping friction contribution to the total system resistance and the lack of significant deposition on piping near steam generator nozzles support the conclusion that an allowance for piping deposition is not necessary. Estimates of uncertainties are discussed in Section 4.4.2.9.~~

Insert Q p. 4.4-27

The momentum and energy exchange between elements in the array are described by the equations for the conservation of energy and mass, the axial momentum equation and two lateral momentum equations which couple each element with its neighbors. The momentum equations used in THINC-IV are similar to the Euler equations (Valentine 1959) excepting that frictional loss terms have been incorporated which represent the combined effects of frictional and form drag due to the presence of grids and fuel assembly nozzles in the core. The crossflow resistance model used in the later momentum equations was developed from experimental data for flow normal to tube banks (Idel' chik 1960 and Kay, London 1955). The energy equation for each element also contains additional terms which represent the energy gain or loss due to the crossflow between elements.

The unique feature in THINC-IV is that lateral momentum equations, which include both inertial and crossflow resistance terms, have been incorporated into the calculational scheme. This differentiates THINC-IV from other thermal-hydraulic programs in which only the lateral resistance term is modeled. Another important consideration in THINC-IV is that the entire velocity field is solved, en masse, by a field equation while in other codes such as THINC-I (Chelemer, Weisman and Tong 1969) and COBRA (Rowe 1971) the solutions are obtained by stepwise integration throughout the array.

The resulting formulation of the conservation equations are more rigorous for THINC-IV; therefore, the solution is more accurate. In addition, the solution method is complex and some simplifying techniques must be employed. Since the reactor flow is chiefly in the axial direction, the core flow field is primarily one-dimensional and it is reasonable to assume that the lateral velocities and the parameter gradients are larger in the axial direction than the lateral direction. Therefore, a perturbation technique can be used to represent the axial and lateral parameters in the conservation equations. The lateral velocity components are regarded as perturbed quantities which are smaller than the unperturbed and perturbed component with the unperturbed component equaling the core average value at a given elevation and the perturbed value is the difference between the local value and the unperturbed component. Since the magnitudes of the unperturbed and perturbed parameters are significantly different, they can be solved separately. The unperturbed equations are one-dimensional and can be solved with the resulting solutions becoming the coefficients of the perturbed equations. An iterative method is then used to solve the system of perturbed equations which couples all the elements in the array.

Three THINC-IV computer runs constitute one design run; a corewide analysis, a hot assembly analysis, and a hot subchannel analysis. While the calculational method is identical for each run, the elements which are modeled by THINC-IV change from run-to-run. In the corewide analysis, the computational elements represent a quarter of the hot assembly. For the last computation, a quarter of the hot assembly is analyzed and each individual subchannel is represented as a computational element.

The first computation is a corewide, assembly-by-assembly analysis which used an inlet velocity distribution modeled from experimental reactor models (Hetsroni 1964, 1965) (Carter 1972) (see Section 4.4.4.2.2). In the corewide analysis the core is considered to be made up of a number of contiguous fuel assembly divided axially into increments of equal length. The system of perturbed and unperturbed equations are temperature and void fraction in each assembly. The system of equations is solved using the specified inlet velocity distribution and a known exit pressure condition

at the top of the core. This computation determines the interassembly energy and flow exchange at each elevation for the hot assembly. THINC-IV stores this information, then uses it for the subsequent hot assembly analysis.

In the second computation, each computational element represents one-fourth of the hot assembly. The inlet flow and the amount of momentum and energy interchange at each elevation is knows from the previous corewide calculation. The same solution technique is used to solve for the local parameters in the hot one-quarter assembly.

While the second computation provides an overall analysis of the thermal and hydraulic behavior of the hot quarter assembly, it does not consider the individual channels in the hot assembly. The third computation further divides the hot assembly into channels consisting of individual fuel rods to form flow channels. The local variations in power, fuel rod and pellet fabrication, fuel rod spacing and mixing (engineering hot channel factors) within the hottest assembly are imposed on the average conditions of the hottest fuel assembly in order to determine the conditions in the hot channel. The engineering hot channel factors are described in Section 4.4.2.2.4.

Insert R →

4.4.4.5.3 Experimental Verification

Extensive additional experimental verification is presented by Hochreiter (et al 1973).

The THINC-IV analysis is based on a knowledge and understanding of the heat transfer and hydrodynamic behavior of the reactor coolant flow and the mechanical characteristics of the fuel elements. The use of the THINC-IV analysis provides a realistic evaluation of the core performance and is used in thermal analyses as described previously.

4.4.4.5.4 Transient Analysis

The THINC-IV thermal-hydraulic computer code does not have a transient capability. Since the third section of the THINC-I program (Chelemer et al 1979) does have this capability, this code (THINC-III) continues to be used for transient DNB analysis.

The conservative equations needed for the transient analysis are included in THINC-III by adding the necessary accumulation terms to the conservative equations used in the steady state (THINC-I) analysis. The input description must now include one or more of the following time dependent arrays:

1. Inlet flow variation,
2. Heat flux distribution, and/or
3. Inlet pressure history.

At the beginning of the transient, the calculation procedure is carried out as in the steady state analysis. The THINC-III Code is first run in the steady state mode to ensure conservatism with respect to THINC-IV and in order to provide the steady state initial conditions at the start of the transient. The time is incremented by an amount determined either by the user or by the program itself. At each new time step, the calculations are carried out with the addition of the accumulation terms which are evaluated using the information from the previous time step. This procedure is continued until a preset maximum time is reached.

At preselected intervals, a complete description of the reactor coolant parameter distributions within the array as well as DNBR are printed out. In this manner the variation of any parameter with time can be readily determined.

At various times during the transient, steady state THINC-IV is applied to show that the application of the transient version of THINC-I is conservative.

The THINC-III Code does not have the capability for evaluating fuel rod thermal response. This is treated by the methods described in Section 15.0.11.

Insert S →

Insert R p. 4.4-28

An experimental verification (Hochreiter, Chelemer and Chu 1973) of the THINC-IV analysis for corewide, assembly-to-assembly enthalpy rises as well as enthalpy rise in a non-uniformly heated rod bundle has been obtained. In these experimental tests, the system pressure, inlet temperature, mass flow rate and heat fluxes were typical of the Beaver Valley core design.

During the operation of a reactor, various incore monitoring systems obtain measured data indicating the core performance. Assembly power distributions and assembly mixed mean temperature are measured and can be converted into the proper three-dimensional power input needed for the THINC programs. This data can then be used to verify the Westinghouse Thermal-Hydraulic design codes.

One standard startup test is the natural circulation test in which the core is held at a very low power (2%) and the pumps are turned off. The core will then be cooled by the natural circulation currents created by the power differences in the core. During natural circulations, a thermal siphoning effect occurs resulting in the hotter assemblies gaining flow, thereby, creating significant interassembly crossflow. As described in the preceding section the most important feature of THINC-IV is the method by which cross flow is evaluated. Thus, tests with significant cross flow are of more value in the code verification.

Interassembly crossflow is caused by radial variations in pressure. Radial pressure gradients are in turn caused by variations in the axial pressure drops in different assemblies. Under normal operating conditions (subcooled forced convection) the axial pressure drop is due mainly to friction losses. Since all assemblies have the same geometry, all assemblies have nearly the same axial pressure drops and crossflow velocities are small. However, under natural circulation conditions (low flow) the axial pressure drop is due primarily to the difference in elevation head (or coolant density) between assemblies (axial velocity is low and therefore axial friction losses are small). This phenomenon can result in relatively large radial pressure gradients and therefore higher crossflow velocities than at normal reactor operating conditions.

The incore instrumentation was used to obtain the assembly-by-assembly core power distribution during natural circulation test. Assembly exit temperatures during the natural circulation tests on a 157 assembly, three-loop plant were predicted using THINC-IV. The predicted data points were plotted as assembly temperature rise versus assembly power and a least square fitting program was used to generate an equation which best fit the data. The result is the straight line presented in Figure 4.4-13. The measured assembly exit temperatures are reasonably uniform, as indicated in this figure, and are predicted closely by the THINC-IV code. This agreement verifies the lateral momentum equations and the crossflow resistance model used in THINC-IV. The larger crossflow resistance used in THINC-I reduces the flow redistribution so the THINC-IV gives better agreement with the experimental data.

Data has also been obtained for Westinghouse plants operating from 67 percent to 101 percent of full power. A representative cross section of the data obtain from a two-loop and a three-loop reactor were analyzed to verify the THINC-IV calculational method. The THINC-IV predictions were compared with the experimental data as shown in Figured 4.4-14 and 4.4-15. The predicted assembly exit temperatures were compared with the measured exit temperatures for each data run. The standard deviation of the measured and predicted assembly exit temperatures were calculated and compared for both THINC-IV and THINC-I and are given in Table 4.4-3. As the standard deviations indicate, THINC-IV generally fits the data somewhat more accurately than THINC-I. For the core

inlet temperatures and power of the data examined, the coolant flow is essentially single phase. Thus one would expect little interassembly crossflow and small differences between THINC-IV and THINC-I predictions as seen in the tables. Both codes are conservative and predict exit temperatures higher than measured values for the high powered assemblies.

An experimental verification of the THINC-IV subchannel calculation method has been obtained from exit temperature measurements in a non-uniformly heated rod bundle (Weisman, Wenzel, Tang, Fitzsimmons, Thorne, Batch 1968). The inner nine heater rods were operated at approximately 20 percent more power than the outer rods to create a typical PWR intra-assembly power distribution. The rod bundle was divided into 36 subchannels and the temperatures rise was calculated by THINC-IV using the measured flow and power for each experimental test.

Figure 4.4-16 shows, the typical run, a comparison of the measured and predicted temperature rises as a function of the power density in the channel. The measurements represent an average of two to four measurements taken in various quadrants of the bundle. It is seen that the THINC-IV results predict the temperature gradient across the bundle very well. In Figure 4.4-17, the measured and predicted temperature rise are compared for a series of runs at different pressures, flow, and power levels.

Again, the measured points represent the average of the measurements taken in the various quadrants. It is seen that the THINC-IV predictions provide a good representation of the data.

Insert S p. 4.4-28

4.4.4.5.5 Fuel Temperatures

As discussed in 4.4.2.2, the fuel rod behavior is evaluated utilizing a semi-empirical thermal model which considers in addition to the thermal aspects such items as clad creep, fuel swelling, fission gas release, release of absorbed gases, cladding corrosion and elastic deflection, and helium solubility.

A detailed description of the thermal model can be found in supplemental information from Salvatori (1972, 1973) to the AEC with the modifications for time dependent densification given in Hellman 1973.

4.4.4.5.6 Hydrodynamic Instability

The analytical methods used to access hydraulic instability are discussed in Section 4.4.3.5.

4.4.4.6 Hydrodynamic and Flow Power Coupled Instability

→ Insert 7"

~~Boiling flows may be susceptible to thermchydrodynamic instabilities~~ (Boure et al 1973). These instabilities are undesirable in reactors since they may cause a change in thermohydraulic conditions that may lead to a reduction in the ~~DNB~~ heat flux relative to that observed during a steady flow condition or to undesired forced vibrations of core components. ~~Therefore, a thermohydraulic design criterion was developed which states that modes of operation under ANS Condition I and II events shall not lead to thermohydrodynamic instabilities.~~

Insert T p. 4.4-28a

4.4.4.6 Hydrodynamic and Flow Power Coupled Instability

In steady state, two-phase, heated flow, a potential for flow instability in parallel closed channels exists. Although such a potential may not exist in the Westinghouse open lattice array core, it has been evaluated on a conservative basis. The instability may be a flow excursion from one state to another, or it may be a self-sustained oscillation about one state (Boure, Bergles, and Tong 1971). Either type is undesirable in a nuclear reactor. First, sustained flow oscillations may cause undesirable forced mechanical vibration of components. Second, flow oscillation may cause system control problems by varying the moderator coefficient. Third, it has been found (Ruddick 1953)(Lowdermilk, Lanso and Siegel 1958) that during flow oscillations the critical heat flux necessary for DNB may be considerably lower than in steady flow.

When the flow channels of a reactor core having common inlet and outlet plenums operate hydraulically in parallel, all have the same pressure drop. An instability in one or more of these channels where boiling occurs does not significantly change the overall pressure drop because the flow is redistributed to a large number of other stable channels, and the condition of constant imposed pressure drop is satisfied. This type of oscillation is thermohydrodynamic and can best be understood by realizing that a boiling channel constitutes a time-varying, spatial distributed parameter system. In a two-phase flow the hydrodynamic coupling with a potential for positive feedback may lead to sustained oscillations having sizable amplitudes. Thus, a temporary reduction in the inlet flow rate to a boiling channel will increase the rate of evaporation, thereby raising the average void fraction. This disturbance affects the elevation, acceleration, and frictional pressure drop as well as the heat transfer behavior. For certain conditions of channel geometry, thermal properties of the heated wall, flow rate, inlet enthalpy, heat flux, etc., resonance may occur and sustained oscillations then result.

The flow instability of a group of parallel flow channels having common plenums at the inlet and exit has been investigated analytically. Westinghouse has developed the HYDNA (Tong, et al. 1961) digital computer program for predicting the hydrodynamic stability of parallel closed channels. To verify the capability of HYDNA to predict flow instability, the program was used to analyze the experimental results reported in Quandt 1961. The results of this comparison are presented in Table 4.4-4 and a typical result is plotted in Figure 4.4-18.

Using the HYDNA program, a generic closed channel analysis was done utilizing core coolant conditions typical of a Westinghouse four-loop reactor rated at 3250 MWt. The results, presented in Figure 4.4-19, predict inception or thermohydrodynamic instability at a power level in excess of 185 percent of rated power. Additional analyses made with the program indicates that:

1. 17x17 fuel assembly cores show no significant differences from the 15x15 cores with respect to thermoinstabilities.

2. The power and flow conditions corresponding to operation with one main reactor coolant loop out of service show the margin of inception of thermohydrodynamic instability for this mode of operation is greater than the margin for operation with all reactor coolant loops in service.

A distinguishing feature of Westinghouse PWRs such as Beaver Valley is that the many parallel, heated flow channels in the reactor core are of the open type. That is, there is very little resistance

to lateral flow leaving the flow channels of high power density. There is also energy transfer from channels of high power density to lower power density channels.

This coupling with cooler channels has led to the opinion that an open channel configuration is more stable than the above closed channel analysis under the same boundary conditions. Because of the difficulty of a concise analysis of instability in open channel flow, and the absence of experimental data, Westinghouse conducted an experimental program (Rosenthal 1968, 1972) to verify that the open type flow channel does yield a stability benefit. The test section consisted of three parallel channels with heat input to two of these channels (Figure 4.4-20). The two heated channels were coupled by valves at six axial elevations. Upon detection of flow instability in the hot channel, the coupling valves were opened and both channels became stable, as illustrated in Figure 4.4-21. Holding all test parameters constant, the reclosing of these valves alone caused a flow in the hot channel to become unstable again. This behavior was observed on all runs performed and is presented as evidence:

1. That open channels are more stable than closed channels.

2. Evaluations of the hydrodynamic stability of Westinghouse PWRs with PWRs with HYDNA are conservative.

4.4.4.7 Temperature Transient Effects Analysis

Waterlogging damage of a fuel rod could occur as a consequence of a power increase on a rod after water has entered the fuel rod through a clad defect. Water entry will continue until the fuel rod internal pressure is equal to the reactor coolant pressure. A subsequent power increase raises the temperature and, hence, could raise the pressure of the water contained within the fuel rod. The increase in hydrostatic pressure within the fuel rod then drives a portion of the water from the fuel rod through the water entry defect. Clad distortion and/or rupture can occur if the fuel rod internal pressure increase is excessive due to insufficient venting of water to the reactor coolant. This occurs when there is both a rapid increase in the temperature of the water within the fuel rod and a small defect, Zircaloy clad fuel rods which have failed due to water logging (Stephen 1970) (Western NY Nuclear Research Center 1971) indicate that very rapid power transients are required for fuel failure. Normal operational transients are limited to about 40 cal/gm-min peak rod while the Spert tests (Stephen 1970) indicate that 120 to 150 cal/gm is required to rupture the clad even with very short transients (5.5 msec. period). Release of the internal fuel rod pressure is expected to have a minimal effect on the reactor coolant system (Stephen 1970) and is not expected to result in failure of additional fuel rod (Stephen 1970). Ejection of fuel pellet fragments into the coolant stream is not expected (Stephen 1979) (Western N.Y. Nuclear Research Center 1971). A clad breech due to waterlogging is thus expected to be similar to any fuel rod failure mechanism which exposes fuel pellets to the reactor coolant stream. Waterlogging has not been identified as the mechanism for clad distortion or perforation of any Westinghouse Zircaloy-4 clad fuel rods.

An excessively high fuel rod internal gas pressure could cause clad failure. One of the fuel rod design bases (Section 4.2.1.) is that the fuel rod internal gas pressure does not exceed the nominal coolant pressure even at the overpower condition. During operational transients, fuel rod clad rupture due to high internal gas pressure is precluded by meeting the above design basis.

4.4.4.4.8 Potentially Damaging Temperature Effects During Transients

The fuel rod experiences many operational transients (intentional maneuvers) during its residence

in the core. A number of thermal effects must be considered when analyzing the fuel rod performance.

The clad can be in contact with the fuel pellet at some time in the fuel lifetime. Clad-pellet interaction occurs if the fuel pellet temperature is increased after the clad is in contact with the pellet. Clad-pellet interaction is discussed in Section 4.2.1.3.1.

Increasing the fuel temperature results in an increased fuel rod internal pressure. One of the fuel rod design bases is that the fuel rod internal pressures do not exceed the nominal coolant pressure even at the overpower condition (Section 4.2.1.1.1.).

The potential effects of operation with waterlogged fuel are discussed in Section 4.4.4.7 which concluded that waterlogging is not a concern during operational transients.

Clad flattening, as noted in Section 4.2.1.3.1, has been observed in some operating power reactors. Thermal expansion (axial) of the fuel rod stack against a flattened section of clad could cause failure of the clad. This is no longer a concern because clad flattening is precluded during the fuel residence in the core (see section 4.2.1.3.1).

There could be a differential thermal expansion between the fuel rods and the guide thimbles during a transient. Excessive bowing of the fuel rods could occur if the grid assemblies did not allow axial movement of the fuel rods relative to the grids. Thermal expansion of the fuel rods is considered in the grid design so that axial loads imposed on the fuel rods during a thermal transient will not result in excessively bowed fuel rods (see Section 4.2.1.2.2).

4.4.4.9 Energy Release During Fuel Element Burnout

As discussed, the core is protected from going through DNB over the full range of possible operating conditions. In the extremely unlikely event that DNB should occur, the clad temperature will rise due to the steam blanketing at the rod surface and the consequent degradation in heat transfer. During this time there is a potential for a chemical reaction between the cladding and the coolant. However, because of the relatively good film boiling heat transfer following DNB, the energy release resulting from this reaction is insignificant compared to the power produced by the fuel.

DNB With Physical Burnout

Westinghouse (Weisman, Wenzel, and Tong 1968) has conducted DNB tests in 25-rod bundle where physical burnout occurred with one rod. After this occurrence, the 25 rod test section was used for several days to obtain more DNB data from the other rods in the bundle. The burnout and deformation of the rod did not affect the performance of neighboring rods in the test section during the burnout or the validity of the subsequent DNB data points as predicted by the W-3 correlation. No occurrences of flow instability or other abnormal operation was observed.

DNB With Return to Nucleate Boiling

Additional DNB tests have been conducted by Westinghouse (Tong, et al. 1967) in 19 and 21 rod bundles. In these tests, DNB without physical burnout was experienced more that once on single rods in the bundles for short periods of time. Each time, a reduction in power of approximately 10 percent was sufficient to reestablish nucleate boiling on the surface of the rod. During these and subsequent tests, no adverse effects were observed on this rod or any other rod in the bundle as a

consequence of operating in DNB.

4.4.4.10 Energy Release or Rupture of Waterlogged Fuel Elements

A full discussion of waterlogging including energy release is contained in Section 4.4.4.7. It is noted that the resulting energy release is not ~~excepted~~ expected to affect neighboring fuel rods.

Two specific types of flow instabilities are considered for Westinghouse PWR operation. These are the Ledinegg, or flow excursion type of static instability, and the density wave type of dynamic instability.

A Ledinegg instability involves a sudden change in flow rate from one steady state to another. This instability occurs (Cadek et al 1975) when the slope of the RCS pressure drop-flow rate curve $\left(\frac{\partial \Delta P}{\partial G}\right)_{internal}$ becomes algebraically smaller than the loop supply (pump head) pressure drop-flow rate curve $\left(\frac{\partial \Delta P}{\partial G}\right)_{external}$. The criterion for stability is thus $\left(\frac{\partial \Delta P}{\partial G}\right)_{internal} \geq \left(\frac{\partial \Delta P}{\partial G}\right)_{external}$. The Westinghouse RCP head curve has a negative slope $\left(\frac{\partial \Delta P}{\partial G}\right)_{external} < 0$ whereas the RCS pressure drop flow curve has a positive slope $\left(\frac{\partial \Delta P}{\partial G}\right)_{internal} > 0$ over the ANS Condition I and ANS Condition II operational ranges. Thus, the Ledinegg instability will not occur.

The mechanism of density wave oscillations in a heated channel has been described by Lahey and Moody (1977). Briefly, an inlet flow fluctuation produces an enthalpy perturbation. This perturbs the length and the pressure drop of the single phase region and causes quality or void perturbations in the two phase regions which travel up the channel with the flow. The quality and length perturbations in the two-phase region create two-phase pressure drop perturbations. However, since the total pressure drop across the core is maintained by the characteristics of the fluid system external to the core, then the two-phase pressure drop perturbation feeds back to the single phase region. These resulting perturbations can be either attenuated or self-sustained.

A simple method has been developed by Saha (et al 1976) for parallel closed channel systems to evaluate whether a given condition is stable with respect to the density wave type of dynamic instability. This method has been used to assess the stability of typical Westinghouse reactor designs (Virgil C. Summer FSAR; Braidwood-1 FSAR; and South Texas Project-1 FSAR) including Virgil C. Summer, under ANS Condition I and II operations. The results indicate that a large margin to density wave instability exists. for example, increases on the order of 200 percent of rated reactor power would be required for the predicted inception of this type of instability.

The application of the method by Saha (et al 1976) to Westinghouse reactor designs is conservative due to the parallel open channel

feature of Westinghouse PWR cores. For such cores, there is little resistance to lateral flow leaving the flow channels of high power density. There is also energy transfer from channels of high power density to lower power density channels. This coupling with cooler channels has led to the opinion that an open channel configuration is more stable than the above closed channel analysis under the same boundary conditions. Flow stability tests (Kakac et al 1974) have been conducted where the closed channel systems were shown to be less stable than when the same channels were cross connected at several locations. The cross connections were such that the resistance from channel to channel cross flow and enthalpy perturbations would be greater than that which would exist in a PWR core which has a relatively low resistance to cross flow.

Flow instabilities which have been observed have occurred almost exclusively in closed channel systems operating at low pressures relative to the Westinghouse PWR operating pressures. Kao (et al 1973) analyzed parallel closed channel stability experiments simulating a reactor core flow. These experiments were conducted at pressures up to 2,200 psia. The results showed that for flow and power levels typical of power reactor conditions, no flow oscillations could be induced above 1,200 psia.

Additional evidence that flow instabilities do not adversely affect thermal margin is provided by the data from the rod bundle DNB tests. Many Westinghouse rod bundles have been tested over wide ranges of operating conditions with no evidence of permature DNB or of inconsistent data which might be indicative of flow instabilities in the rod bundle.

In summary, it is concluded that thermohydrodynamic instabilities will not occur under ANS Condition I and II modes of operation for Westinghouse PWR designs.

A large power margin, greater than doubling rated power, exists to predicted inception of such instabilities. Analysis has been performed which shows that minor plant to plant differences in Westinghouse reactor designs such as fuel assembly arrays, core power to flow ratios, fuel assembly length, etc will not result in gross deterioration of the power margins.

4.4.4.11 Fuel Rod Behavior Effects from Coolant Flow Blockage

Reactor coolant flow blockages can occur within the reactor coolant channels of a fuel assembly or external to the reactor core. The effects of the blockage within the assembly on fuel rod behavior is more pronounced than external blockages of the same magnitude. In both cases the flow blockages cause local reductions in reactor coolant flow. The amount of local flow reduction, where it occurs, and how far along the flow stream the reduction persists are considerations which will influence the fuel rod behavior. The effects of reactor coolant flow blockages in terms of maintaining

rated core performance are determined both by analytical and experimental methods. The experimental data are usually used to a[illegible]ment analytical tools such as computer programs similar to the THINC-IV program. Inspection of the DNB correlation identified in Section 4.4.2.2 and discussed by Tong (1967) shows that the predicted DNBR is dependent upon the local values of quality and mass velocity.

The THINC-IV Code is capable of predicting the effects of local flow blockages on DNBR within the fuel assembly on a subchannel basis, regardless of where the flow blockage occurs. Hochreiter (et al 1973) discuss that for a fuel assembly similar to the Westinghouse design, THINC-IV accurately predicts the flow distribution within the fuel assembly when the inlet nozzle is completely blocked. Full recovery of the flow was found to occur about 30 inches downstream of the blockage. With the reactor operating at the nominal full power conditions specified in Table 4.4-1, the effects of an increase in enthalpy and decrease in mass velocity in the lower portion of the fuel assembly would not result in the reactor reaching a minimum DNBR ~~of 1.20~~, *below the safety limit value.*

From a review of the open literature, it is concluded that flow blockage in "open lattice cores" similar to the Westinghouse cores cause flow perturbations which are local to the blockage. For instance, Ohtsubo and Uruwashi (1972) show that the mean bundle velocity is approached asymptotically about 4 inches downstream from a flow blockage in a single flow cell. Similar results were also found for 2 and 3 cells completely blocked. Basmer (et al 1972) tested an open lattice fuel assembly in which 41 percent of the subchannels were completely blocked in the center of the test bundle between spacer grids. Their results show the stagnant zone behind the flow blockage essentially disappears after 1.65 L/De or about 5 inches for their test bundle. They also found that leakage flow through the blockage tended to shorten the stagnant zone or, in essence, the complete recovery length. Thus, local flow blockages within a fuel assembly have little effect on subchannel enthalpy rise. The reduction in local mass velocity is then the main parameter which affects the DNBR. If the standard plants were operating at full power and nominal steady state conditions as specified in Table 4.4-1, a reduction in local mass velocity greater than ~~35~~ *70* percent would be required to reduce the DNBR ~~from 1.83~~ to *the safety limit* ~~1.30~~. The above mass velocity effect on the DNB correlation was based on the assumption of a fully developed flow along the full channel length. In reality a local flow blockage is expected to promote turbulence and thus would likely not effect DNBR at all.

Reactor coolant flow blockages induce local crossflows as well as promote turbulence. Fuel rod vibration could occur, caused by this crossflow component, through vortex shedding or turbulent mechanisms. If the crossflow velocity exceeds the limit established for fluid elastic stability, large amplitude whirling results. The limits for a controlled vibration mechanism are established from studies of vortex shedding and turbulent pressure fluctuations. The crossflow

Fuel rod behavior is changed under the influence of a sufficiently high crossflow component.

velocity required to exceed fluid elastic stability limits is dependent on the axial location of the blockage and the characterization of the crossflow (jet flow or not). These limits are greater than those for vibratory fuel rod wear. Crossflow velocity above the established limits can lead to mechanical wear of the fuel rods at the grid support locations. Fuel rod wear due to flow induced vibration is considered in the fuel rod fretting evaluation (Section 4.2).

4.4.5 Testing and Verification

4.4.5.1 Tests Prior to Initial Criticality

A reactor coolant flow test is performed following fuel loading, but prior to initial criticality. Reactor coolant loop pressure drop data are obtained in this test. This data allows determination of the reactor coolant flow rates at reactor operating conditions. This test verifies that proper reactor coolant flow rates have been used in the core thermal and hydraulic analysis. Chapter 14 describes the initial test programs.

4.4.5.2 Initial Power and Plant Operation

Core power distribution measurements are made at several core power levels (Chapter 14). These tests are used to ensure that conservative peaking factors are used in the core thermal and hydraulic analysis.

Additional demonstration of the overall conservatism of the THINC analysis was obtained by comparing THINC predictions to incore thermocouple measurements (Burke et al 1976). These measurements were performed on the Zion reactor. No further in-reactor testing is planned.

4.4.5.3 Component and Fuel Inspections

Inspections performed on the manufactured fuel are described in Section 4.2.4. Fabrication measurements critical to thermal and hydraulic analysis are obtained to verify that the engineering hot channel factors in the design analyses (Section 4.4.2.2.4) are met.

4.4.6 Instrumentation Requirements

4.4.6.1 Incore Instrumentation

Instrumentation is located in the core so that moveable neutron detectors and fixed thermocouples provide radial, axial, and azimuthal core characteristics for all core quadrants.

The incore instrumentation system is comprised of thermocouples, positioned to measure fuel assembly coolant outlet temperatures at

preselected position, and fission chamber detectors positioned in guide thimbles which run the length of selected fuel assemblies to measure the neutron flux distribution. Figure 4.4-8 shows the number and location of instrumented assemblies in the core.

The core-exit thermocouples provide a backup to the flux monitoring instrumentation for monitoring power distribution. The routine, systematic, collection of thermocouple readings by the operator provides a data base. From this data base, abnormally high or abnormally low readings, quadrant temperature tilts, or systematic departures from a prior reference map can be deduced. these two complementary systems are more useful when taken together than either system alone would be.

The moveable incore neutron detector system would be used for more detailed mapping if the thermocouple system were to indicate an abnormality. The incore instrumentation system is further discussed in Section 7.7.1.9.

The incore instrumentation is provided to obtain data from which fission power density distribution in the core, reactor coolant enthalpy distribution in the core, and fuel burnup distribution may be determined.

4.4.6.2 Overtemperature and Overpower ΔT Instrumentation

The overtemperature ΔT trip protects the core against low DNBR. The overpower ΔT trip protects against excessive power (fuel rod rating protection).

As discussed in Section 7.2.1.1.2, factors included in establishing the overtemperature ΔT and overpower ΔT trip setpoints include the reactor coolant temperature in each reactor coolant loop and the axial distribution of core power through the use of the two section excore neutron detectors.

4.4.6.3 Instrumentation to Limit Maximum Power Output

The output of the three ranges (source, intermediate, and power) of detectors, with the electronics of the nuclear instruments, are used to limit the maximum power output of the reactor within their respective ranges.

There are eight radial locations containing a total of eight neutron flux detectors installed around the reactor in the neutron shield tank, two proportional counters for the source range installed on opposite "flat" portions of the core containing the primary start up sources at an elevation approximately one quarter of the core height. Two compensated ionization chambers for the intermediate range, located in the same instrument wells and detector assemblies as the source range detectors, are positioned at an elevation corresponding to 1/2 of the core height. Four dual section uncompensated ionization chamber assemblies for the power range are

installed vertically at the four corners of the core and are located equidistant from the reactor vessel at all points and, to minimize neutron flux pattern distortions, within 1 foot of the reactor vessel. Each power range detector provides two signals corresponding to the neutron flux in the upper and lower sections of a core quadrant. Three ranges of detectors are used as inputs to monitor neutron flux from a completely shutdown condition to 120 percent of full power, with the capability of recording overpower excursions up to 200 percent of full power.

Insert U → The output of the power range channels is used for:

1. The rod speed control function,

2. Alerting the operator to an excessive power unbalance between the quadrants, and

3. Protecting the core against rod ejection accidents ~~against the consequences of reactivity and power distribution anomalies discussed in Section 15.4.~~ Insert V →

~~The remaining two instrument wells contain the detectors for the post-accident neutron flux monitoring system discussed in Section 4.4.6.6.~~

4.4.6.4 Instrumentation for Detection of Inadequate Core Cooling

Instrumentation for indication of inadequate core cooling conditions has been provided for BVPS-2. The installed instrumentation includes core exit thermocouples, core subcooling margin and reactor vessel level monitoring. BVPS-2 has submitted a response to TMI Action Item II.F.2 of NUREG-0737, "Instrumentation for Detection of Inadequate Core Cooling," which describes in detail the characteristics of the installed instrumentation. This system description can be found in response to SER Open Issue No. 3, transmitted by DLC via letter 2NRC-6-037.

Insert W →

4.4.6.5 Loose Parts and Monitoring System

The loose parts monitoring system (LPMS) monitors for the presence of loose metallic parts within the reactor coolant system (RCS). The system consists of ten active instrumentation channels which monitor at five strategic locations on the exterior surface of the RCS boundary. Each channel contains a piezoelectric accelerometer (sensor) and a signal preamplifier located within the reactor

Insert U p. 4.4-34

The difference in neutron flux between the upper and lower sections of the power range detectors are used to limit the Overtemperature ΔT and Overpower ΔT trip setpoints and to provide the operator with an indication of the core power axial offset. In addition,

Insert V p. 4.4-34

4. Protect the core against adverse power distributions resulting from dropped rods.

Details of the neutron detectors and nuclear instrumentation design and the control and trip logic are given in Chapter 7. The limitations on neutron detector operation and trip setpoints are given in the Technical Specifications.

Insert W p. 4.4-34

4.4.6.4.1 Reactor Vessel Level Instrumentation

The Reactor Vessel Level Instrumentation System (RVLIS) uses differential pressure measuring devices to measure the vessel fluid level or relative void content of the primary coolant. The fluid level or void information is displayed in the main control room for use by the operator to:

- Assist in detecting the presence of a gas bubble or void in the reactor vessel,
- Assist in detecting the approach of inadequate core cooling, and
- Indicate the formation of a void in the RCS.

The RVLIS is described in more detail in Section 7.8.3.

containment buildings. Signal conditioning, diagnostic, and alarm equipment is installed in the data acquisition cabinet located in the main control building. The LPMS system is nonsafety-related. Conformance with Regulatory Guide 1.133 is discussed in Section 1.8.

Two sensors each are fastened mechanically to the RCS boundary at each of the following potential loose part collection regions:

1. Reactor pressure vessel - upper head region

2. Reactor pressure vessel - lower head region

3. Each steam generator - reactor coolant inlet region

The output signal from each sensor is amplified by the preamplifier. The amplified signal is processed through individual detector modules which provide noise and spurious signal rejection and alarm initiation. This signal is blocked during rod motion with the aid of the Control Rod Drive Inhibitor Box to prevent spurious alarm signals.

Alarm signal are sent from the detector modules to the master alarm module. The master alarm module provides output signals for audible and visual alarms at the LPMS data acquisition cabinet, a main control panel annunciator alarm, and automatic starting of the four channel tape recorders. The signal for the alarming channel and the three channels in proximity to the alarming channel are recorded. The LPMS also provides audio monitoring for any channel, allowing comparision to any previously recorded signals.

The on-line sensitivity of the LPMS is such that the system will detect a loose part that weighs from 0.25 lb to 30 lb and that impacts with a kinetic energy of 0.5 ft-lb on the inside surface of the RCS pressure boundary within 3 feet of the sensor.

The piezoelectric sensors and hardline cables inside the containment are designed for LOCA or steamline break temperatures, pressures, and humidity. The preamplifier and other cables are designed for a maximum temperature of 135°F and the same pressure and humidity as the sensors. All of the equipment inside the containment is designed to remain operational for the radiation exposures anticipated during their lifetime.

The LPMS will be tested and calibrated prior to plant start-up. A description of the testing is found in Section 14.2.12. In addition, capabilities exist for periodic on-line channel checks and functional tests for off-line calibration at refueling outages.

After initial plant start-up, the LPMS will be calibrated every 18 months and a spectrum analysis conducted monthly. A channel test will be performed at least once per 24 hours to ensure operability.

4.4.6.6 Post-Accident Neutron Flux Monitoring System

The post-accident neutron flux monitoring is an excore design containing two fission chambers housed within the neutron shield tank. This system is environmentally qualified for post-accident use and provides redundant neutron indication over the range of 10^0 to 10^5 counts per second and 10^{-4} to 200 percent power.

The post-accident flux monitoring system supplies outputs to the following:

1. Plant safety monitoring system (PSMS) (Section 7.7.2.10) per Regulatory Guide 1.97

2. Alternate shutdown panel (ASP) (Section 7.4.1.3) per BTP CMEB 9.5-1.

3. Recording device.

4.4.7 References for Section 4.4

- Ainscough, J. B.; and Wheeler, M. J. 1968. Thermal Diffusivity and Thermal Conductivity of Sintered Uranium Dioxide. Proceedings of the Seventh Conference of Thermal Conductivity, p 467, National Bureau of Standards, Washington, D.C.

- Asamoto, R. R.; Anselin, F. L.; and Conti, A. E. 1968. The Effect of Density on the Thermal Conductivity of Uranium Dioxide. GEAP-5493.

- Bain, A. S. 1962. The Heat Rating Required to Produce Center Melting In Various UO_2 Fuels. ASTM Special Technical Publication, No. 306, pp 30-46, Philadelphia, PA.

- Balfour, M. G.; Christensen, J. A.; and Ferrari, H. M. 1966. In-Pile Measurement of UO_2 Thermal Conductivity. WCAP-2923.

- Basmer, P.; Kirsh, D.; and Schultheiss, G. F. 1972. Investigation of the Flow Pattern in the Recirculation Zone Downstream of Local Coolant Blockages in Pin Bundles. Atomwirtschaft, 17, No. 8, p 416-417.

- Boure, J. A.; Bergles, A. E.; and Tong, L. S. 1973. Review of Two-Phase Flow Instability. Nuclear Engineering Design 25, p 165-192.

- Bowring, R. W. 1962. Physical Model, Based on Bubble Detachment, and Calculation of Steam Voidage in the Subcooled Region of a Heated Channel. HPR-10.

- Burke, T. M.; Meyer, C. E.; and Shefcheck, J. 1976. Analysis of Data from the Zion (Unit 1) THINC Verification Test. WCAP-8454.

• Bush, A. J. 1965. Apparatus of Measuring Thermal Conductivity to 2500°C. Westinghouse Research Laboratories Report 64-1P6-401-43, (Proprietary).

Braidwood UFSAR, USNRC Docket No. 50-456.

• Cadek, F. F.; Motley, F. E.; and Dominicis, D. P. 1975. Effect of Axial Spacing on Interchannel Thermal Mixing with the R Mixing Vane Grid. WCAP-7941-P-A (Proprietary) and WCAP-7959-A.

• Cadek, F. F. 1975. Interchannel Thermal Mixing with Mixing Vane Grids. WCAP-7667-A (Proprietary) and WCAP-7755-A.

• Carter, F. D. 1972. Inlet Orificing of Open PWR Cores. WCAP-9004 (Proprietary) and WCAP-7836.

• Chelemer, H.; Weisman, J.; and Tong, L. S. ~~1970.~~ 1969. Subchannel Thermal Analysis of Rod Bundle Cores. WCAP-7015, Revision 1.

• Christensen, J. A.; Allio, R. J.; and Biancheria, A. 1965. Melting Point of Irradiated UO_2. WCAP-6065.

• Clough, D. J. and Sayers, J. B. 1964. The Measurement of the Thermal Conductivity of UO_2 Under Irradiation in the Temperature Range 150°-1600°C. AERE-R-4690, UKAEA Research Group, Harwell.

• Cohen, I.; Lustman, B.; and Eichenberg, D. 1960. Measurement of the Thermal Conductivity of Metal-Clad Uranium Oxide Rods during Irradiation. WAPD-228.

Coplin, D. H. et al 1968. The Thermal Conductivity of UO_2 by Direct In-Reactor Measurements. GEAP-5100-6.

Daniel, J. L.; Matolich, Jr. J.; and Deem, H. W. 1962. Thermal Conductivity of UO_2. HW-69945.

Dean, R. A. 1962. Thermal Contact Conductance Between UO_2 and Zircaloy-2. CVNA-127.

Nakazato, S.;
DeMario, E. E. 1974. Hydraulic Flow Test of the 17 x 17 Fuel Assembly. WCAP-8278 (Proprietary) and WCAP-8279.

Devold, I. 1968. A Study of the Temperature Distribution in UO_2 Reactor Fuel Elements, AE-318, Aktiebolaget Atomenergi, Stockholm, Sweden.

Dittus, F. W. and Boelter, L. M. K. 1930. Heat Transfer in Automobile Radiators of the Tubular Type. California University Publication in England, 2, No. 13, 443461.

Duncan, R. N. 1962. Rabbit Capsule Irradiation of UO_2. CVTR Project, DVNA-142.

Feith, A. D. 1962. Thermal Conductivity of UO_2 by a Radial Heat Flow Method. TID-21568.

Godfrey, T. G.; Fulkerson, W.; Killied, T. G.; Moore, J. P.; and McElroy, D. L. 1964. Thermal Conductivity of Uranium Dioxide and Armco Iron by an Improved Radial Heat Flow Technique. ORNL-3556.

Gonzalez-Santalo, J. M. and Griffith, P. (1972). Two-phase Glow Mixing in Rod Bundle Subchannels. ASME Paper 72-WA/NE-19.

Griffith, P.; Clark, J. A.; and Rohsenow, W. M. (1958). Void Volumes in Subcooled Boiling Systems. ASME Paper No. 58-HT-19.

Gyllander, J. A. 1971. In-Pile Determination of the Thermal Conductivity UO_2 in the Range 500-2500°C. AE-411.

Hellman, J. M. (Ed) ~~1975~~ 1973. Fuel Densification Experimental Results and Model for Reactor Application. WCAP-8218-P-A (Proprietary) and WCAP-8219-A.

Hetsroni, G. 1964. Hydraulic Tests of the San Onofre Reactor Model. WCAP-3269-8.

Hetsroni, G. 1965. Studies of the Connecticut-Yankee Hydraulic Model. NYO-3250-2.

Hill, K. J.; Motley, F. E.; and Cadek, F. F. 1973. Effect of Local Heat Flux Spikes on DNB in Non-Uniform Heated Rod Bundles. WCAP-8174 (Proprietary) and WCAP-8202.

Hill, K. W.; Motley, F. E.; Cadek, F. F.; and Wenzel, A. H. 1975. Effect of 17 x 17 Fuel Assembly Geometry on DNB. WCAP-8296-P-A (Proprietary) and WCAP-8297-A

• Hochreiter, L. E. and Chelemer, H. 1973. Application of the THINC IV Program to PWR Design. WCAP-8054 (Proprietary) and WCAP-8195.

• Hochreiter, L. E.; Chelemer, H.; and Chu, P. T. 1973. THINC-IV: An Improved Program for Thermal and Hydraulic Analysis of Rod Bundle Cores. WCAP-7956.

• Howard, V. C. and Gulvin, T. G. 1960. Thermal Conductivity Determinations of Uranium Dioxide by a Radial Flow Method. UKAEA IG-Report 51.

• Idel'chik, I. E. 1960. Handbook of Hydraulic Resistance, AEC-TR-6630.

• International Atomic Energy Agency 1966. Thermal Conductivity of Uranium Dioxide. Report of the Panel held in Vienna, April, 1965. IAEA Technical Reports Series, No. 59, Vienna, The Agency.

Kakac, S.; Veziroglu, T. N.; Akyuzlu, K.; and Berkol, O. 1974. Sustained and Transient Boiling Flow Instabilities in a Cross-Connected Four-Parallel-Channel Upflow System. Proceedings of 5th International Heat Transfer Conference, Tokyo, Japan.

Kao, H. S.; Morgan, C. D.; and Parker, W. B. 1973. Prediction of Flow Oscillation in Reactor Core Channel. Trans. ANS, Vol. 16, pp 212-213.

• Kjaerheim, G. and Rolstad, E. 1967. In Pile Determination of UO Thermal Conductivity, Density Effects and Gap Conductance. HPR-80.

• Kjaerheim, G. 1969. In-Pile Measurements of Center Flue Temperatures and Thermal Conductivity Determination of Oxide Fuels. Paper IFA-175 presented at the European Atomic Energy Society Symposium on Performance Experience of Water-Cooled Power Reactor Fuel, Stockholm, Sweden.

• Kruger, O. L. 1968. Heat Transfer Properties of Uranium and Plutonium Dioxide. Paper 11-N-68F presented at the Fall meeting of Nuclear Division of the American Ceramic Society, Pittsburgh, PA.

Lahey, R. T. and Moody, F. J. 1977. The Thermal Hydraulics of a Boiling Water Reactor. American Nuclear Society.

• Lucks, C. F. and Deem, H. W. 1961. Thermal Conductivity and Electrical Conductivity of UO. In Progress Reports Relating to Civilian Applications, BMI-1448 (Rev.) for June, 1960; BMI-1489 (Rev.) for December, 1960, and BMI-1518 (Rev.) for May, 1961.

- Lyons, M. F. et al. 1966. UO_2 Power and Pellet Thermal Conductivity During Irradiation. GEAP-5100-1.

- Maurer, G. W. 1960. A Method of Predicting Steady State Boiling Vapor Fractions in Reactor Coolant Channels. WAPD-BT-19, pp 58-70.

- McFarlane, A. F. 1975. Power Peaking Factors. WCAP-7912-P-A (Proprietary) and WCAP-7912-A.

- Moody, L. F. 1944. Friction Factors for Pipe Flow. Transaction of the American Society of Mechanical Engineers, 66, 671-684.

Morita, T. et al. 1974. Power Distribution Control and Load Following Procedures, WCAP-8385 (Proprietary) and WCAP-8403.

Motley, F. E. and Cadek, F. F. 1972. Application of Modified Spacer Factor to L Grid Typical and Cold Wall Cell DNB. WCAP-7988 (Proprietary) and WCAP-8030-A.

Motley, F. E.; Wenzel, A. H.; and Cadek, F. F. 1975a. Critical Heat Flux Testing of 17 x 17 Fuel Assembly Geometry with 22-Inch Grid Spacing. WCAP-8536 (Proprietary) and WCAP-8537.

- Motley, F. E.; Wenzel, A. H.; and Cadek, F. F. 1975b. The Effect of 17 x 17 Fuel Assembly Geometry on Interchannel Thermal Mixing. WCAP-8298-P-A (Proprietary) and WCAP-8299-A.

Motley, F. E. and Cadek, F. F. 1975c. DNB Test Results for New Mixing Vane Grids. WCAP-7695-P-A (Proprietary) and WCAP-7958-A.

- Nelson, R. C.; Coplin, D. H.; Lyons, M. F.; and Weidenbaum, B. 1964. Fission Gas Release from UO_2 Fuel Rods with Gross Central Melting. GEAP-4572.

- Nishijima, T.; Dawada, T.; and Ishihata, A. 1965. Thermal Conductivity of Sintered UO_2 and Al_2O_3 at High Temperatures. Journal of the American Ceramic Society. 48, 31 34.

- Nodvick, R. J. 1970. Saxton Core II Fuel Performance Evaluation, Part II, and Evaluation of Mass Spectrometric and Radiochemical Materials Analyses of Irradiated Saxton Plutonium Fuel. WCAP-3385-56.

- Novendstern, E. H. and Sandberg, R. O. 1966. Single-Phase Local Boiling & Bulk Boiling Pressure Drop Correlations. WCAP-2850-L (Proprietary) and WCAP-7916.

- Ohtsubo, A. and Uruwashi, S. 1972. Stagnant Fluid Due to Local Flow Blockage. Journal Nuclear Science Technology, 9, No. 7, p 433-434.

- Owens, Jr. W. L. 1961. Two-Phase Pressure Gradient. In: International Developments in Heat Transfer, Part II, pp 363-368, ASME New York, N.Y.

- Ponsel, G. 1965. Burnup Physics of Heterogeneous Reactor Lattices. WCAP-6069.

- Rowe, D. S. and Angle, C. W. 1967. Crossflow Mixing Between Parallel Flow Channels During Boiling, Part II Measurements of Flow and Enthalpy in Two Parallel Channels. BNWL-371, Part 2.

- Rowe, D. S. and Angle, C. W. 1969. Crossflow Mixing Between Parallel Flow Channels During Boiling, Part III Effect of Spacers on Mixing Between Two Channels. BNWL-371, Part 3.

Saha, P.; Ishii, M.; and Zuber, N. 1976. An Experimental Investigation of the Thermally Induced Flow Oscillations in Two-Phase Systems. Journal of Heat Transfer, pp 616-662.

- Shefcheck, J. 1972. Applications of the THINC Program to PWR Design, WCAP-7359-L (Proprietary) and WCAP-7838.

- Skaritka, J. (Ed.) 1979. Fuel Rod Bow Evaluation. WCAP-8691, Revision 1 (Proprietary) and WCAP-8692, Revision 1 (Non-proprietary).

South Texas Project-1 UFSAR, USNRC Docket No. 50-498.

- Stora, J. P.; Debernardy, Desigoyer, B.; Delmas, R.; Deschamps, P.; Ringot, C.; and Lavaud, B. 1964. Thermal Conductivity of Sintered Uranium Oxide under In-Pile Conditions, EURAEC-1095.

- Stora, J. P. 1970. In-Reactor Measurements of the Integrated Thermal Conductivity of UO_2 - Effect of Porosity. Trans. ANS, 13, pp 137-138.

- Thom, J. R. S.; Walker, W. M.; Fallon, T. A.; and Reising, G. F. S. 1965-66. Boiling in Sub-cooled Water During Flow up Heated Tubes or Annuli, Proceedings of the Institute for Mechanical Engineers, 180, Pt. C, 226-46.

- Tong, L. S. 1967. Prediction of Departure from Nucleate Boiling for an Axially Non-Uniform Heat Flux Distribution. Journal Nuclear Energy, 21, pp 241-248.

- Tong, L. S. 1972. Boiling Crisis and Critical Heat Flux. USAEC Critical Review Series, TID-25887.

Virgil C. Summer UFSAR, USNRC Docket No. 50-395.

- Vogt, J.; Grandell, L.; and Runfors, U. 1964. Determination of the Thermal Conductivity of Unirradiated Uranium Dioxide. AB Atomenergi Report RMB-527, 1964, Quoted by IAEA Technical Report Series No. 59, Thermal Conductivity of Uranium Dioxide.

• Weisman, J. 1959. Heat Transfer to Water Flowing Parallel to Tube Bundles, Nuclear Science Engineers, 6, 78-79.

USNRC 1978. Personal communication between C. Eicheldiner, Westinghouse and J. F. Stoltz, USNRC. Subject: Staff Evaluations of WCAP-7956, WCAP-8054 (Proprietary) WCAP-8567, and WCAP-8762, Letter dated April 19, 1978.

• Westinghouse 1981. Letter, E.P. Rahe, Jr. (Westinghouse) to J.R. Miller (USNRC), NS-EPR-2515, dated October 9, 1981, entitled: Partial Response to Request Number 1 for Additional Information on WCAP-8691, Revision 1, and letter, E.P. Rahe, Jr. (Westinghouse) to J.R. Miller (USNRC), NS-EPR-2572, dated March 16, 1982, entitled: Remaining Response to Request Number 1 for Additional Information on WCAP-8691, Revision 1.

• USNRC 1986. letter, C.H. Berlinger (USNRC) to E.P. Rahe, Jr. (Westinghouse), dated June 18, 1986, entitled: Request for Reduction in Fuel Assembly Burnup Limit for Calculation of Maximum Rod Bow Penalty.

Add additional References

ADDITIONAL REFERENCES TO SECTION 4.4

D. H. Risher, Jr., "An evaluation of the Rod Ejection Accident in Westinghouse Pressurized Water Reactors Using Spatial Kinetics Methods," WCAP-7588, Revision 1, Westinghouse Electric Corporation (December, 1971).

D. H. Coplin, et al., "The Thermal Conductivity of UO_2 by Direct In-reactor Measurement," GEAP-5100-6, General Electric Corporation (March, 1968).

A. M. Ross and R. L. Stoute, "Heat Transfer Coefficient Between UO_2 and Zircaloy-2," AECL-1552, Atomic Energy of Canada, Ltd. (June, 1962).

L. S. Tong, Boiling Heat Transfer and Two-Phase Flow, John Wiley & Sons, New York (1965).

L. S. Tong, "Critical Heat Fluxes on Rod Bundles," in "Two-Phase Flow and Heat Transfer in Rod Bundles," 31-41, American Society of Mechanical Engineers, New York (1969).

F. E. Motley, K. W. Hill, F. F. Cadek, J. Shefcheck, "New Westinghouse Correlation WRB-1 for Predicting Critical Heat Flux in Rod Bundles with Mixing Vane Grids," WCAP-8762-P-A, Westinghouse Electric Corporation (July 1984).

S. Ray, "MINI Revised Thermal Design Procedure (MINI RTDP)," WCAP-12178-P, Westinghouse Electric Corporation (March 1989).

H. R. Valentine, "Applied Hydrodynamics," Buttersworth Publishers, London, (1959).

W. M. Kays and A. L. London, "Compact Heat Exchangers," National Press, Palo Alto, (1955).

D. S. Rowe, "COBRA-III, A Digital Computer Program for Steady State and Transient Therma Hydraulic Analysis of Rod Bundle Nuclear Fuel Elements," BNWL-B-82, Battell Pacific Northwest Laboratory (1971).

J. Weisman, A. J. Wenzel, L. S. Tong, D. Fitzsimmons, W. Thorne, and J. Batch, "Experimental Determination of the Departure for Nucleate Boiling in Large Rod Bundles at High Pressures," Chemical Engineering Program Symposium Ser. 64, No. 82, 114-125 (1968).

M. Ruddick, "An Experimental Investigation of the Heat Transfer at High Rates Between A Tube and Water with Conditions at or Near Boiling," PhD. Thesis, University of London, (1953).

W. H. Lowdermilk, C. D. Lanso and B. L. Siegel, "Investigation of Boiling Burnout and Flow Stability for Water Flowing in Tubes," NACA-TN-4382, National Aeronautics and Space Administration (September, 1958).

L. S. Tong, et al., "HYDNA - Digital Computer Program for Hydrodynamic Transients in A Pressure Tube Reactor or a Closed Channel Core," CVNA-77, Westinghouse Electric Corporation (1961).

E. R. Quandt, "Analysis and Measurement of Flow Oscillation," Chemical Engineering Program Symposium Ser. 57, No. 32, 111-126 (1961).

R. L. Rosenthal, "An Experimental Investigation of the Effect of Open Channel Flow on Thermal-Hydrodynamic Flow Instability," WCAP-7240, (October, 1968), Westinghouse Electric Corporation (Proprietary), and WCAP-7966, Westinghouse Electric Corporation (December, 1972).

L. A. Stephen, "The Effects of Cladding Material and Heat Treatment on the Response of Waterlogged UO_2 Fuel Rods to Power Bursts," IN-ITR-111, Aeoject Nuclear, Idaho National Engineering Laboratory (January, 1970).

Western New York Nuclear Research Center Correspondence with the AEC on (February 11 and August 27, 1971), Docket 50-57.

L. S. Tong, et al., "Critical Heat Flux (DNB) in Square and Triangular Array Rod Bundles," presented at the Japan Society of Mechanical Engineers Semi-International Symposium held at Tokyo, Japan, 25-34 (September 4-8, 1967).

Supplemental information on fuel design transmitted from R. Salvatori, Westinghouse NES, to D. Knuth, AEC, as attachments to letters NS-SL-518 (12/22/71), NS-SL-521 (12/19/72), NS-SL-524 (12/29/72) and NS-SL-543 (1/12/73), (Westinghouse Proprietary), and supplemental information on fuel design transmitted from R. Salvatori, Westinghouse NES, to D. Knuth, AEC, as attachments to letters NS-SL-527 (1/2/73) and NS-SL-544 (1/12/73).

A. J. Friedland, and S. Ray, "Revised Thermal Design Procedure," WCAP-11397 (Proprietary), (February 1987) and Letter, A. C. Thadani (USNRC) to W. J. Johnson (Westinghouse), "Acceptance for Referencing of Licensing Topical Report WCAP-11397, Revised Thermal Design Procedure," (January 1989).

Letter from A. C. Thadani (USNRC) to W. J. Jonnson (Westinghouse), "Acceptance for Referencing of Licensing Topical Report WCAP-9226-P/9227-NP, Reactor Core Response to Excessive Secondary Steam Releases," (January 31, 1989).

D. B. Owen, "Factors for One-Sided Tolerance Limits and for Variable Sampling Plant," SCR-607, (March 1963).

TABLE 4.4-1

THERMAL AND HYDRAULIC COMPARISON

Design Parameters	BVPS-2	V. C. Summer
Reactor core heat output (MWt)	2,652	2,775
Reactor core heat output (10^6 Btu/hr)	9,051	9,471
Heat generated in fuel (%)	97.4	97.4
System pressure, nominal (psia)	2,250	2,250
System pressure, minimum steady state (psia)	2,220	2,220
Minimum DNBR at nominal design conditions		
Typical flow channel	~~2.26~~ 2.43	1.98
Thimble (cold wall) flow channel	~~1.85~~ 2.30	1.68
Minimum DNBR for design transients	>1.30	>1.30
DNB correlation	~~WRB-1~~ ~~"R" (W-3 with modified spacer factor)~~	"R" (W-3 with modified spacer factor)
Coolant Flow		
Total thermal flow rate (10^6 lbm/hr)	100.8	109.6
Effective flow rate for heat transfer (10^6 lbm/hr)	~~94.25~~ ~~96.3~~	102.6
Effective flow area for heat transfer (ft^2)	41.5 (STD) 41.6 (VSH)	41.6
Average velocity along fuel rods (ft/sec)	~~13.3~~ ~~14.4~~	15.6
Average mass velocity (10^6 lbm/hr-ft^2)	2.~~17~~ (STD) 2.~~32~~ (VSH)	2.47
Coolant Temperatures		
Nominal inlet (°F)	542.5	556.0
Average rise in vessel (°F)	67.~~5~~ 4	62.8
Average rise in core (°F)	~~70.3~~ 71.6	66.6

TABLE 4.4-1 (Cont)

Design Parameters	BVPS-2	V. C. Summer
Average in core (°F)	~~579.4~~ 580.2	591.2
Average in vessel (°F)	576.2	589.0
Heat Transfer		
Active heat transfer, surface area (ft^2)	48,600	48,600
Average heat flux (Btu/hr-ft^2)	181,405	189,800
Maximum heat flux for normal operation (Btu/hr-ft^2)	~~435,400~~ ~~430,900~~*	440,400
Average linear power (kW/ft)	5.20	5.44
Peak linear power for normal operation (kW/ft)	12.1*	12.6
Peak linear power resulting from overpower transients/operator errors, assuming a maximum overpower of 118% (kW/ft)**	18.0	18.0
Peak linear power which would result in centerline melt (kW/ft)***	>18.0	>18.0
Power density (kW per liter of core)****	38.4	38.4
Specific power (kW per kg. uranium)****	38.4	38.4
Fuel Central Temperature		
Peak at linear power for prevention of centerline melt (°F)	4,700	4,700
Pressure drop*****		
Across core (psi)	~~20.7 ± 4.1~~ ~~21.4 ± 2.1~~	23.2 ± 2.3
Across vessel, including nozzle (psi)	~~40.1 ± 6.0~~ ~~36.9 ± 3.7~~	40.7 ± 4.1

NOTES:

*This limit is associated with the value of F_Q = 2.~~32~~ 40.

**See Section 4.3.2.2.6.

***See Section 4.4.2.11.6.

****Based on cold dimensions and 95 percent of theoretical density fuel.

*****Based on best estimate reactor coolant flow rate as discussed in Section 5.1.

TABLE 4.4-2

VOID FRACTIONS AT NOMINAL REACTOR CONDITIONS
WITH DESIGN HOT CHANNEL FACTORS

	Average (%)	Maximum (%)
Core	0.33 ~~0.28~~	-
Hot Subchannel	~~3.5~~ 4.0	~~14.0~~ 4

TABLE AND FIGURE INSERTION INSTRUCTIONS

INSERT TABLES 4.4-3 AND 4.4-4 (SEE ATTACHED).

REPLACE FIGURE 4.4-1 WITH NEW FIGURE 4.4-1.

CHANGE OLD FIGURE 4.4-2 TO NEW FIGURE 4.4-3. INSERT NEW FIGURES 4.4-1A AND 4.4-2 (SEE ATTACHED).

REPLACE OLD FIGURES 4.4-3, 4.4-4, AND 4.4-5 WITH NEW FIGURES (INCREASED F(ΔH)) AND RENUMBER THE FIGURES 4.4-4, 4.4-5 AND 4.4-6.

CHANGE OLD FIGURE 4.4-6 TO NEW FIGURE 4.4-8. DELETE OLD FIGURE 4.4-8.

CHANGE OLD FIGURE 4.4-7 TO NEW FIGURE 4.4-11, INSERT NEW FIGURES 4.4-9 AND 4.4-10 (SEE ATTACHED).

CHANGE OLD FIGURE 4.4-9 TO NEW FIGURE 4.4-22, INSERT NEW FIGURES 4.4-12 4.4-13, 4.4-14, 4.4-15, 4.4-16, 4.4-17, 4.4-18, 4.4-19, 4.4-20 AND 4.4-21.

TABLE 4.4-3

COMPARISON OF THINC-IV AND THINC-I PREDICTIONS WITH DATA FROM REPRESENTATIVE WESTINGHOUSE TWO AND THREE LOOP REACTORS

Reactor	Power (MWt)	% Full Power	Measured Inlet Temp (°F)	σrms(F) THINC-I	σ(F) THINC-IV	Improvement (F) for THINC-IV over THINC-I
Ginna	847	65.1	543.7	1.97	1.83	0.14
	854	65.7	544.9	1.56	1.46	0.10
	857	65.9	543.9	1.97	1.82	0.15
	947	72.9	543.8	1.92	1.74	0.18
	961	74.0	543.7	1.97	1.79	0.18
	1,091	83.9	542.5	1.73	1.54	0.19
	1,268	97.5	542.0	2.35	2.11	0.24
	1,284	98.8	540.2	2.69	2.47	0.22
	1,284	98.9	541.0	2.42	2.17	0.25
	1,287	99.0	544.4	2.26	1.97	0.29
	1,294	99.5	540.8	2.20	1.91	0.29
	1,295	99.6	542.0	2.10	1.83	0.27
Robinson	1,427.0	65.1	548.0	1.85	1.88	0.03
	1,422.6	64.9	549.4	1.39	1.39	0.00
	1,579.0	88.0	550.0	2.35	2.34	0.01
	2,207.3	100.7	534.0	2.41	2.41	0.00
	2,213.9	101.0	533.8	2.52	2.44	0.08

TABLE 4.4-4

COMPARISON OF HYDNA WITH EXPERIMENTAL DATA

Value at Last Stable Condition[1]				Exit Enthalpy		HYDNA Exit Quality	Power at Which Oscillations Occurred		Frequency of Oscillations	
Pressure (psia)	Inlet Subcooling (°F)	Mass Flow Rate (10^6 lb/hr^2)	Heat Flux (10^6 Btu/hr ft^2)	Experimental (Btu/lb)	HYDNA (Btu/lb)	(%)	Experimental (%)	HYDNA (%)	Experimental (cps)	HYDNA (cps)
600	36	0.658	0.365	680	687	29.4	102	110	2.0	2.5
600	36	0.853	0.514	701	711	32.8	102	104	2.9	3.0
800	55	0.495	0.270	698	697	27.2	102	110	1.2	1.6
800	55	0.530	0.307	712	713	29.5	102	104	1.3	1.6
1,600	145	0.590	0.478	823	817	35.8	102	110	--	1.1

[1] i.e., 100 percent power

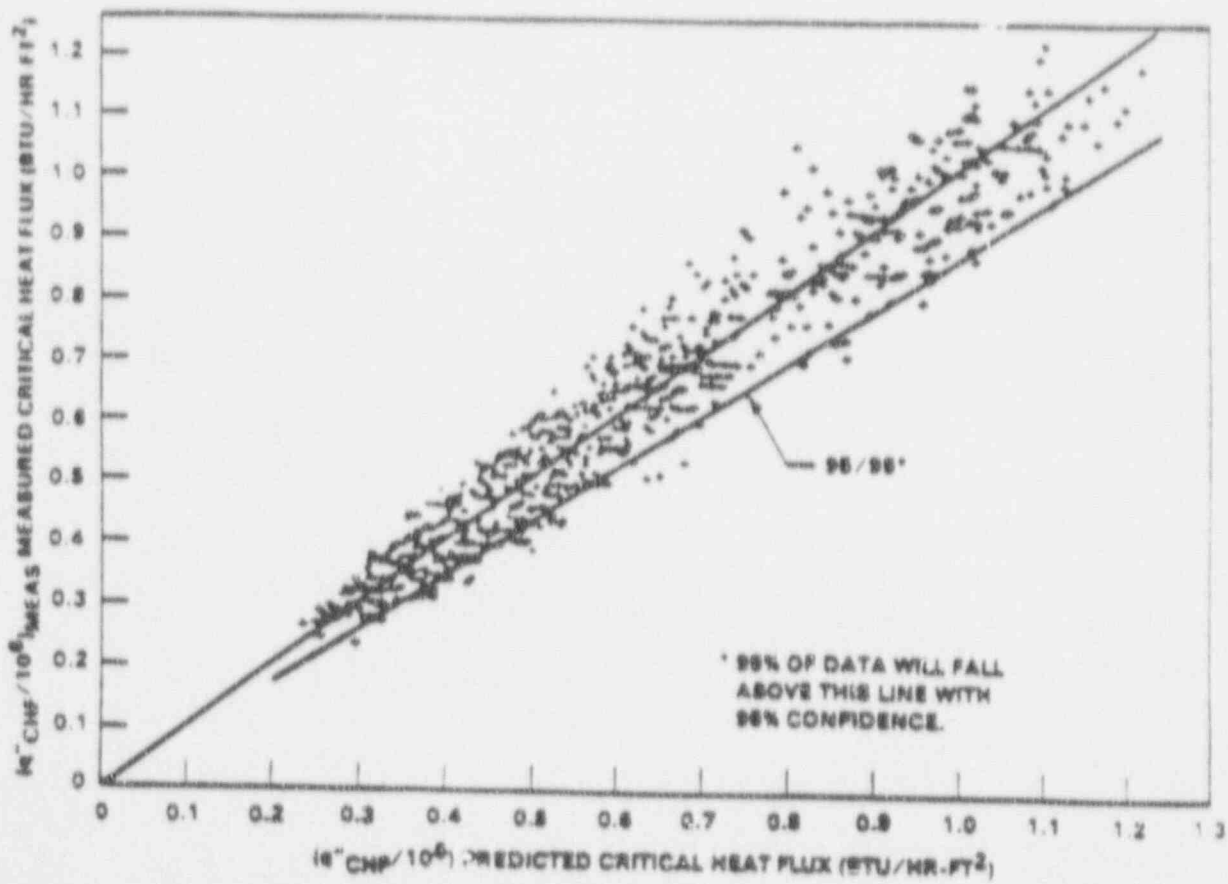

4.4-1

FIGURE ~~8.3-6~~
MEASURED VERSUS PREDICTED CRITICAL HEAT FLUX - WRB-1 CORRELATION

BEAVER VALLEY POWER STATION UNIT NO. ~~1~~ 2
UPDATED FINAL SAFETY ANALYSIS REPORT

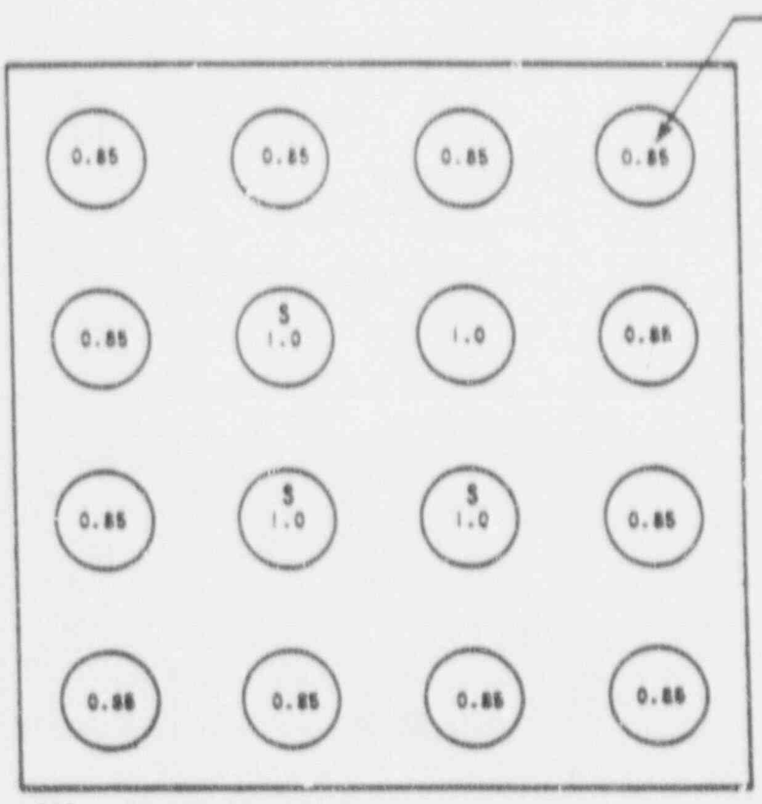

"S" - SPIKED ROD LOCATIONS

FIGURE 4.4-1A
TEST SECTION CROSS-SECTION FOR DNB SPIKE TEST
BEAVER VALLEY POWER STATION UNIT NO. 2
UPDATED FINAL SAFETY ANALYSIS REPORT

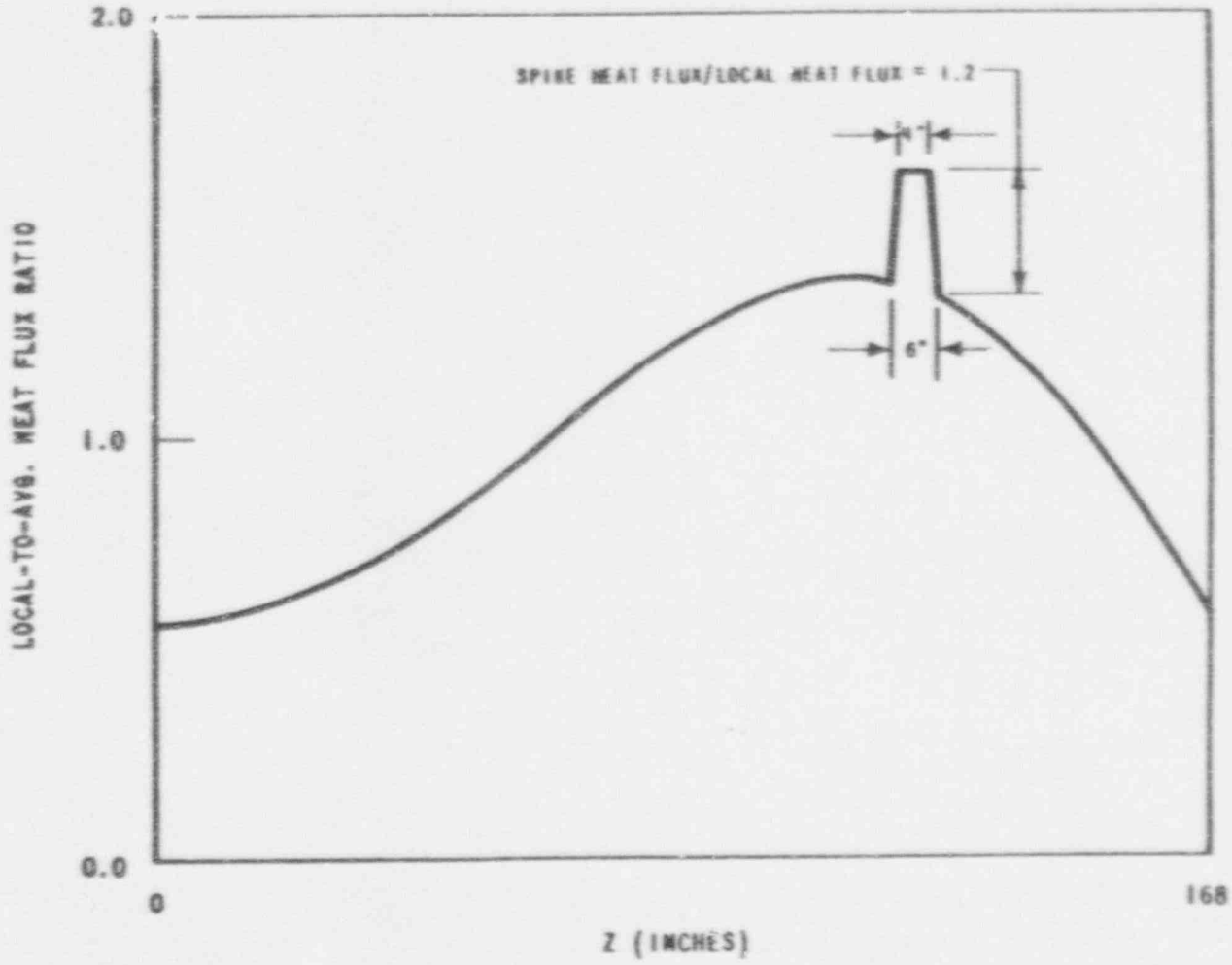

FIGURE 4.4-2
AXIAL HEAT FLUX PROFILE WITH 20% SPIKE FOR 168 INCH RODS
BEAVER VALLEY POWER STATION UNIT NO. 2
UPDATED FINAL SAFETY ANALYSIS REPORT

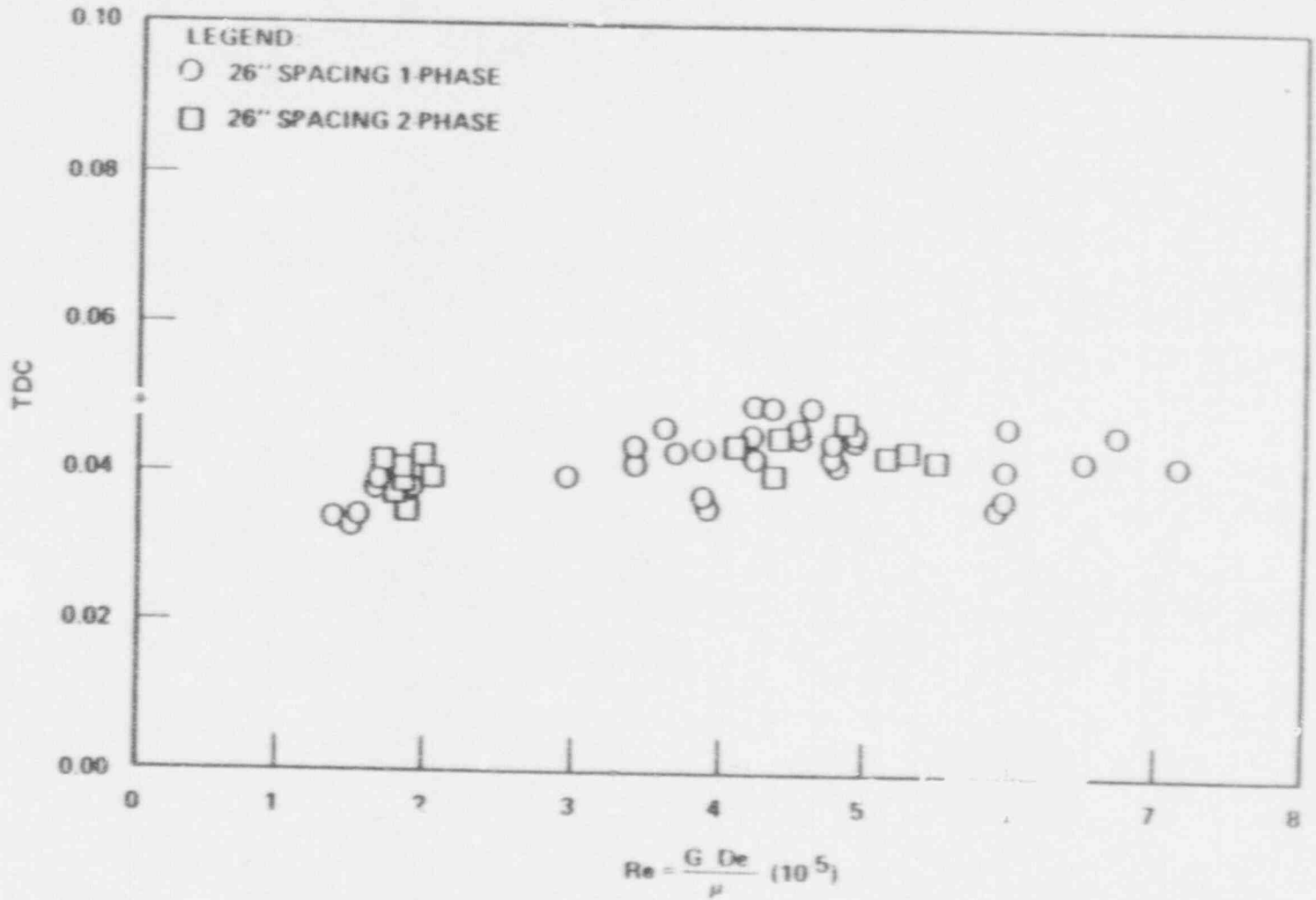

FIGURE 4.4-3
TDC VS. REYNOLDS NUMBER FOR 26 INCH GRID SPACING
BEAVER VALLEY POWER STATION - UNIT 2
FINAL SAFETY ANALYSIS REPORT

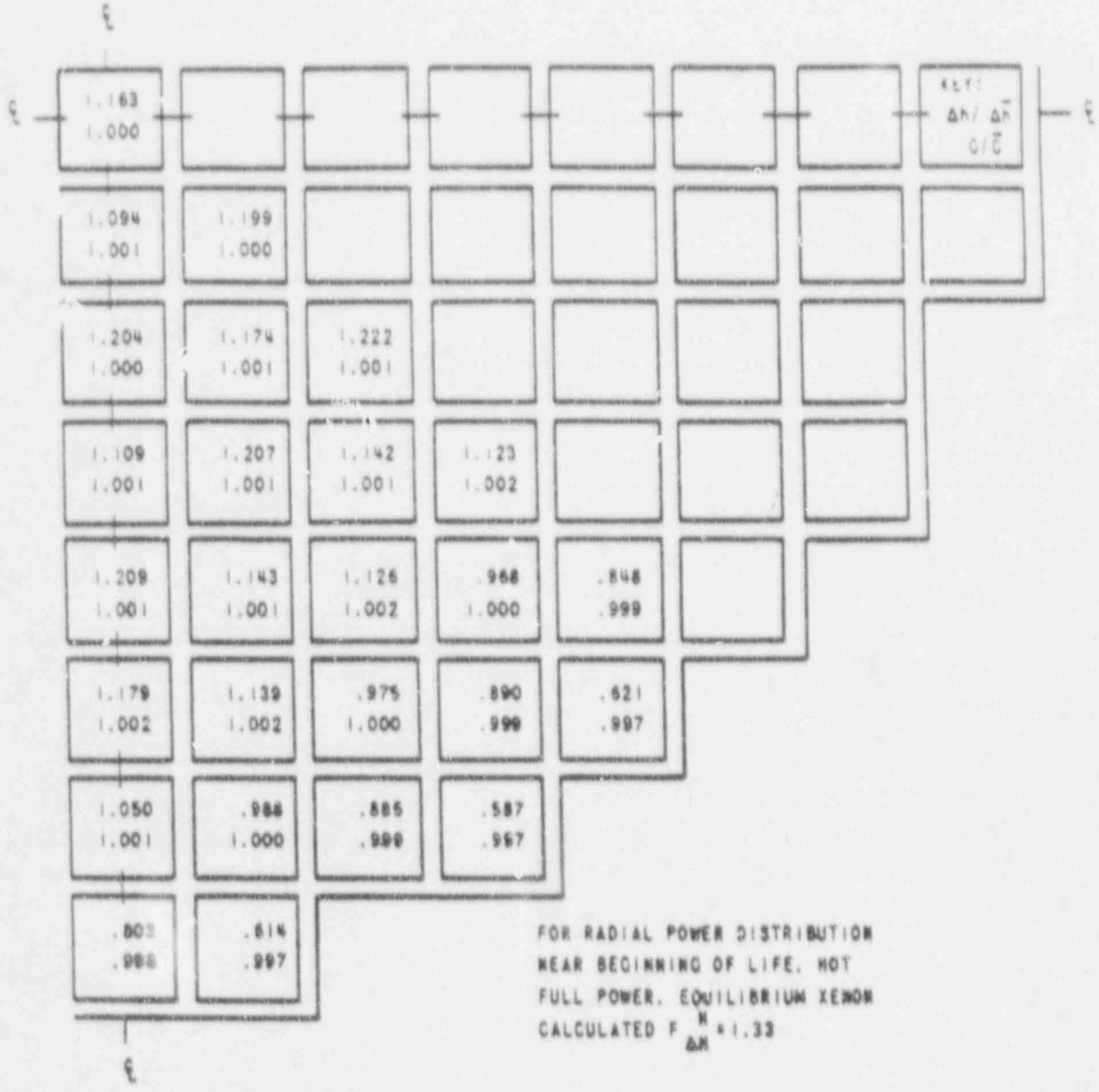

FOR RADIAL POWER DISTRIBUTION NEAR BEGINNING OF LIFE. HOT FULL POWER. EQUILIBRIUM XENON CALCULATED $F^{N}_{\Delta H} = 1.33$

FIGURE 4.4-4
NORMALIZED RADIAL FLOW AND ENTHALPY DISTRIBUTION AT 4 FT ELEVATION
BEAVER VALLEY POWER STATION UNIT NO. 2
UPDATED FINAL SAFETY ANALYSIS REPORT

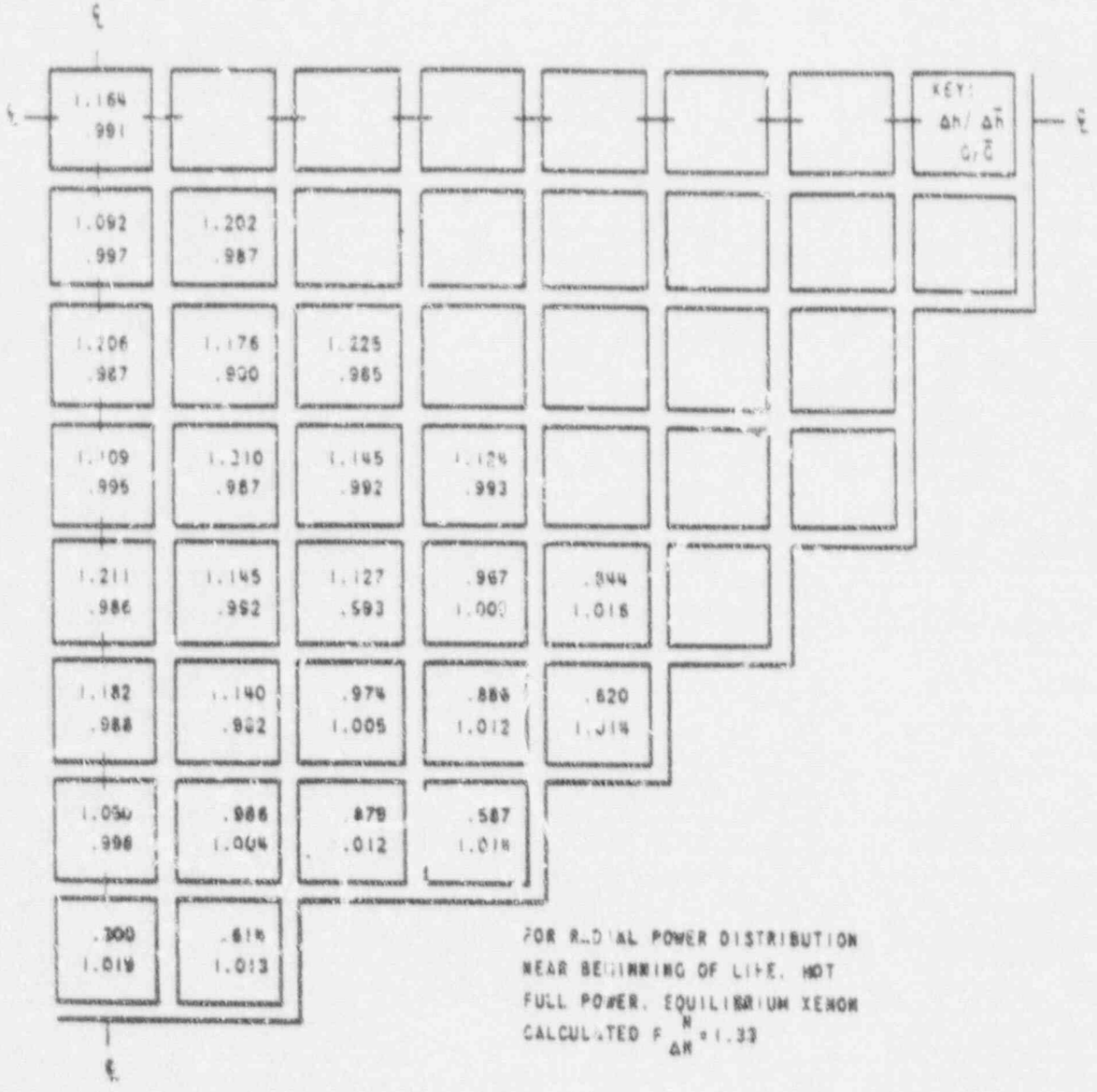

FOR RADIAL POWER DISTRIBUTION NEAR BEGINNING OF LIFE, HOT FULL POWER, EQUILIBRIUM XENON CALCULATED $F^{N}_{\Delta H} = 1.33$

FIGURE 4.4-5
NORMALIZED RADIAL FLOW AND ENTHALPY DISTRIBUTION AT 8 FT ELEVATION
BEAVER VALLEY POWER STATION UNIT NO. 2
UPDATED FINAL SAFETY ANALYSIS REPORT

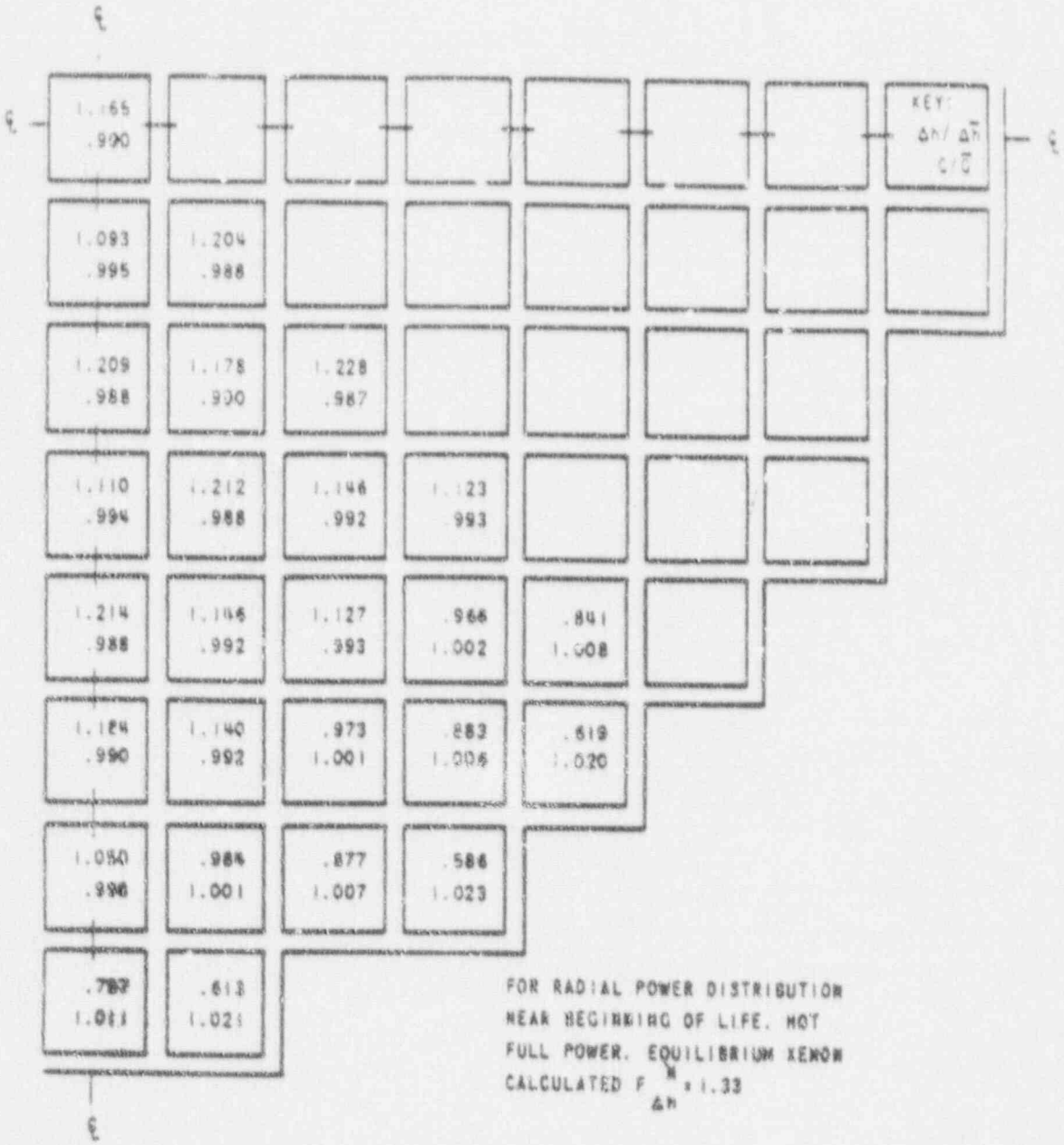

FOR RADIAL POWER DISTRIBUTION NEAR BEGINNING OF LIFE, HOT FULL POWER, EQUILIBRIUM XENON CALCULATED $F^{N}_{\Delta H} = 1.33$

FIGURE 4.4-6
NORMALIZED RADIAL FLOW AND ENTHALPY DISTRIBUTION AT 12 FT ELEVATION - CORE EXIT

FIGURE 4.4-7
Radial Power Density Distribution

DELETE THIS PAGE

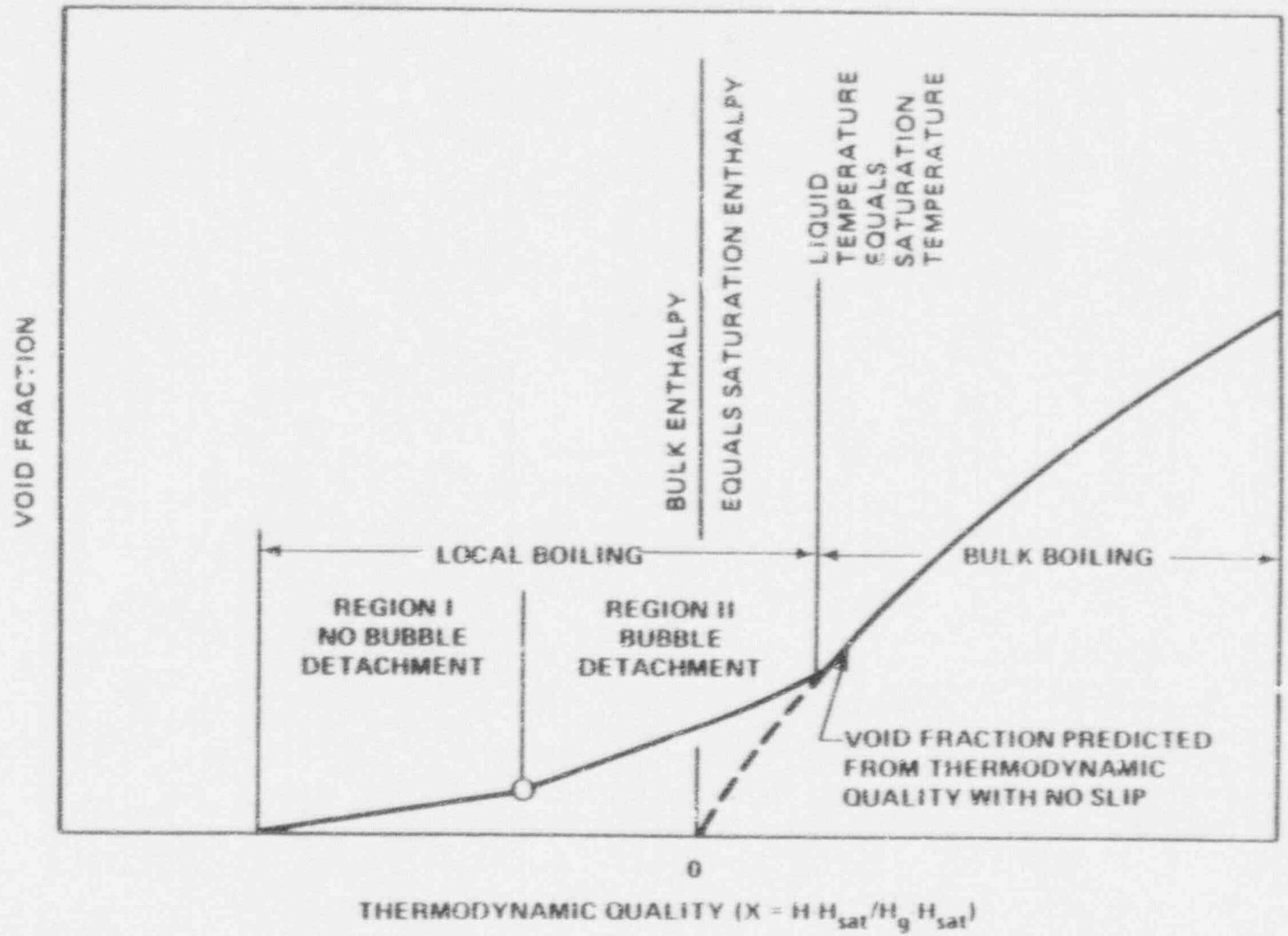

FIGURE 4 4-8
VOID FRACTION VS.
THERMODYNAMIC QUALITY
BEAVER VALLEY POWER STATION - UNIT 2
FINAL SAFETY ANALYSIS REPORT

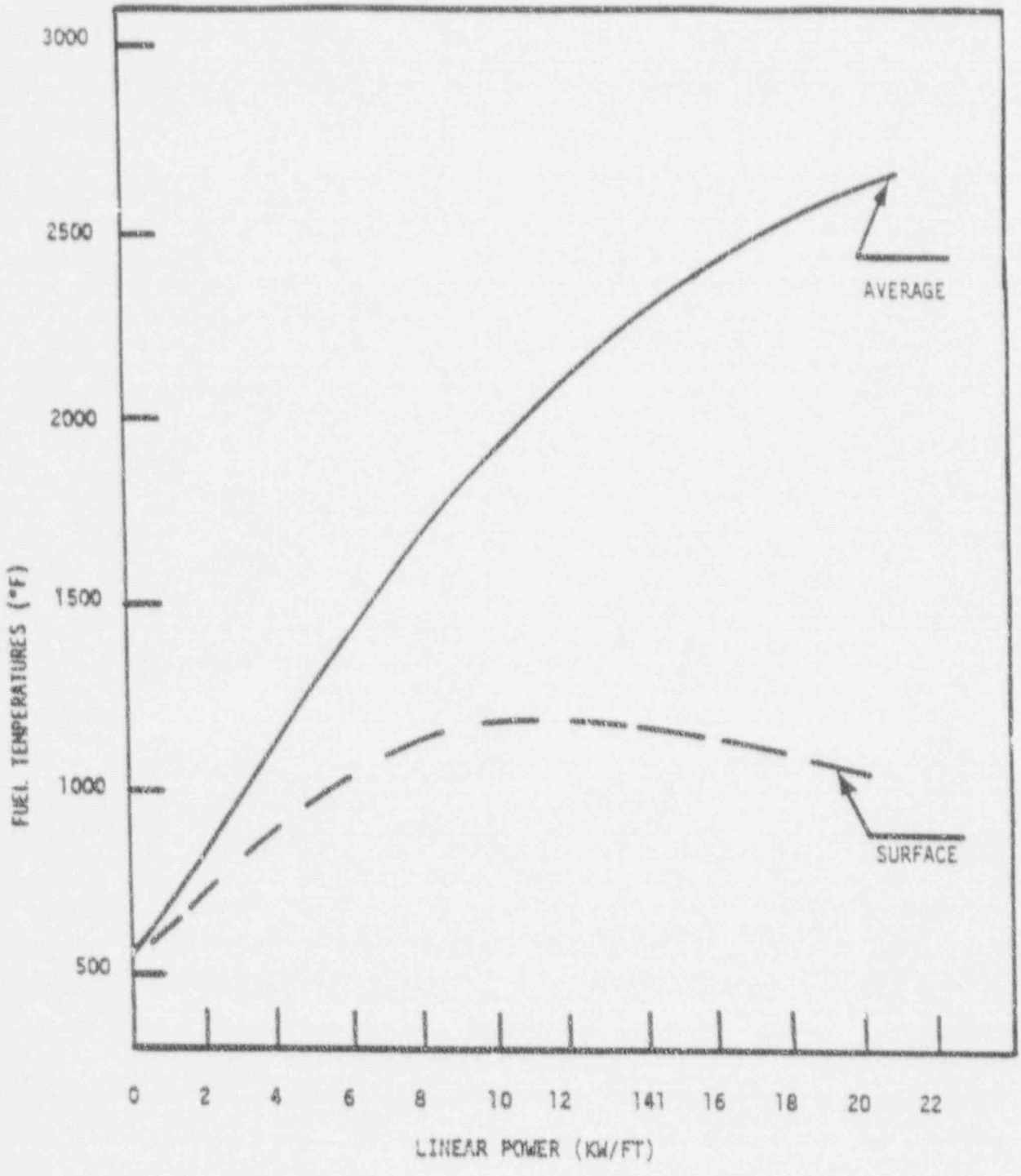

FIGURE 4.4-9
PEAK FUEL AVERAGE AND SURFACE TEMPERATURES DURING FUEL ROD LIFETIME VS LINEAR POWER
BEAVER VALLEY POWER STATION UNIT NO. 2
UPDATED FINAL SAFETY ANALYSIS REPORT

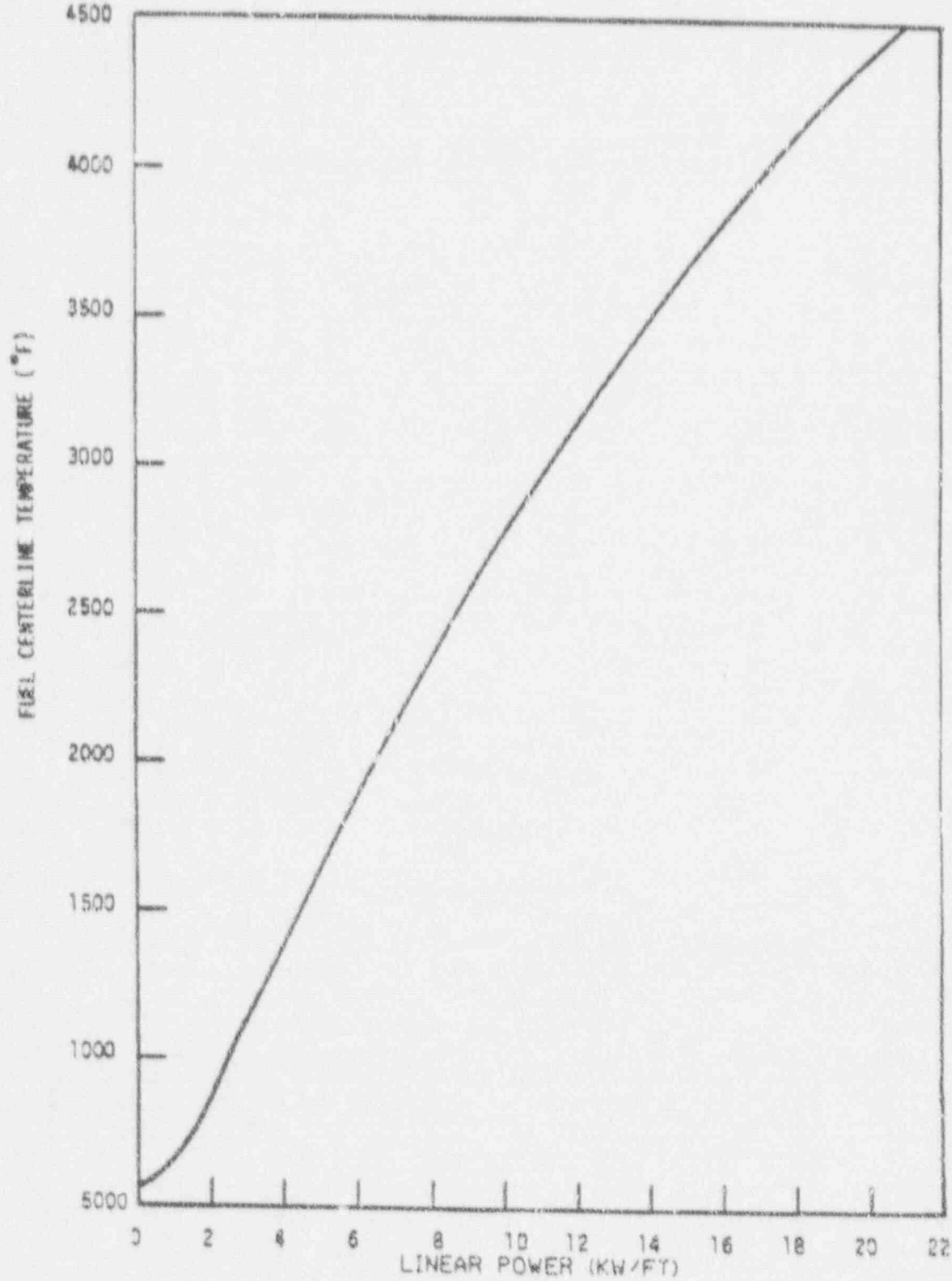

FIGURE 4.4-10
PEAK FUEL CENTERLINE TEMPERATURE DURING FUEL ROD LIFETIME VS LINEAR POWER
BEAVER VALLEY POWER STATION 2
UPDATED FINAL SAFETY ANALYSIS REPORT

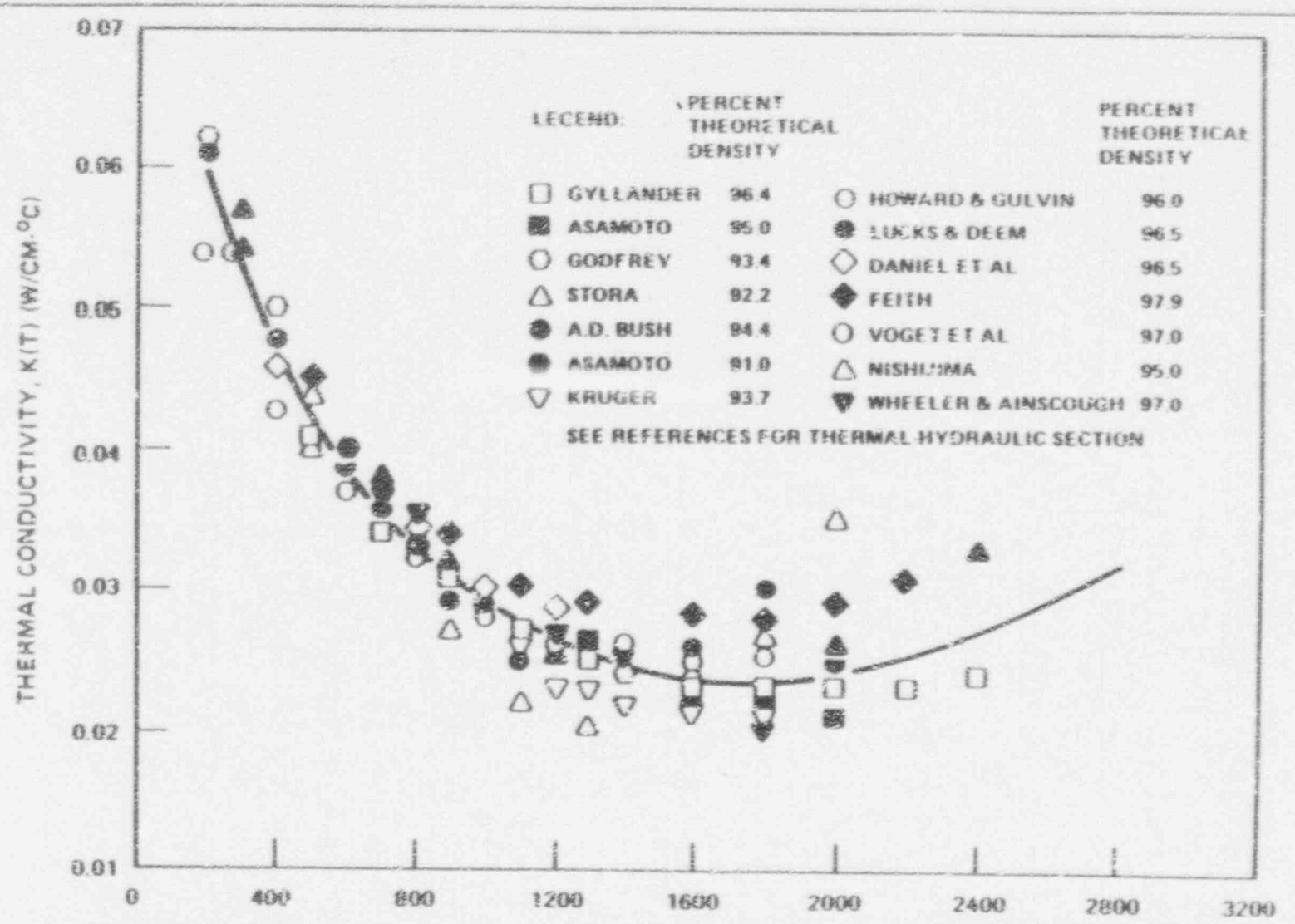

FIGURE 4.4-11
THERMAL CONDUCTIVITY OF UO_2 (DATA CORRECTED TO 95% THEORETICAL DENSITY)
BEAVER VALLEY POWER STATION - UNIT 2
FINAL SAFETY ANALYSIS REPORT

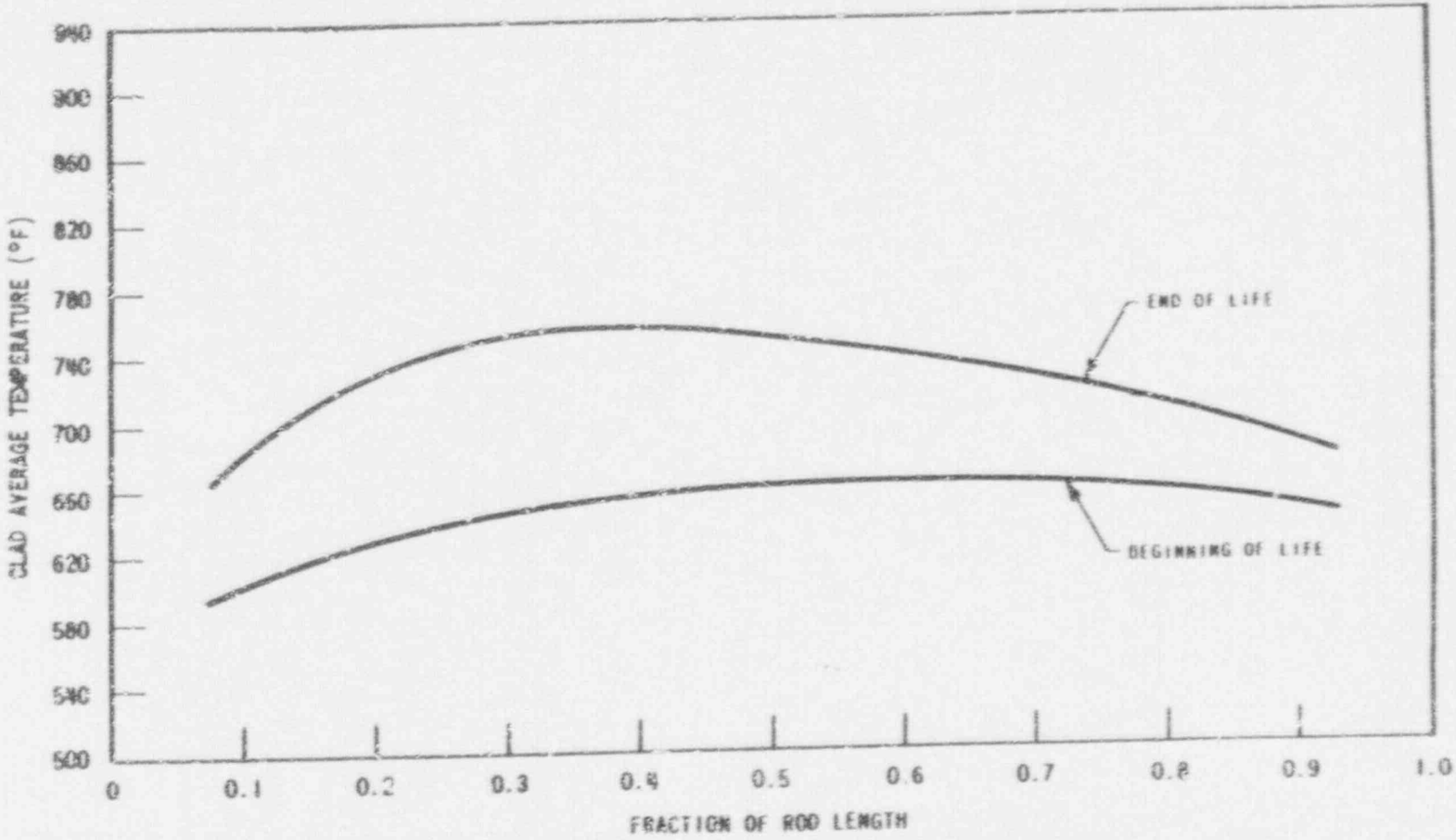

FIGURE 4.4-12
AXIAL VARIATION OF AVERAGE CLAD TEMPERATURE FOR ROD OPERATING AT 5.43 KW/FT
BEAVER VALLEY POWER STATION UNIT NO. 2
UPDATED FINAL SAFETY ANALYSIS REPORT

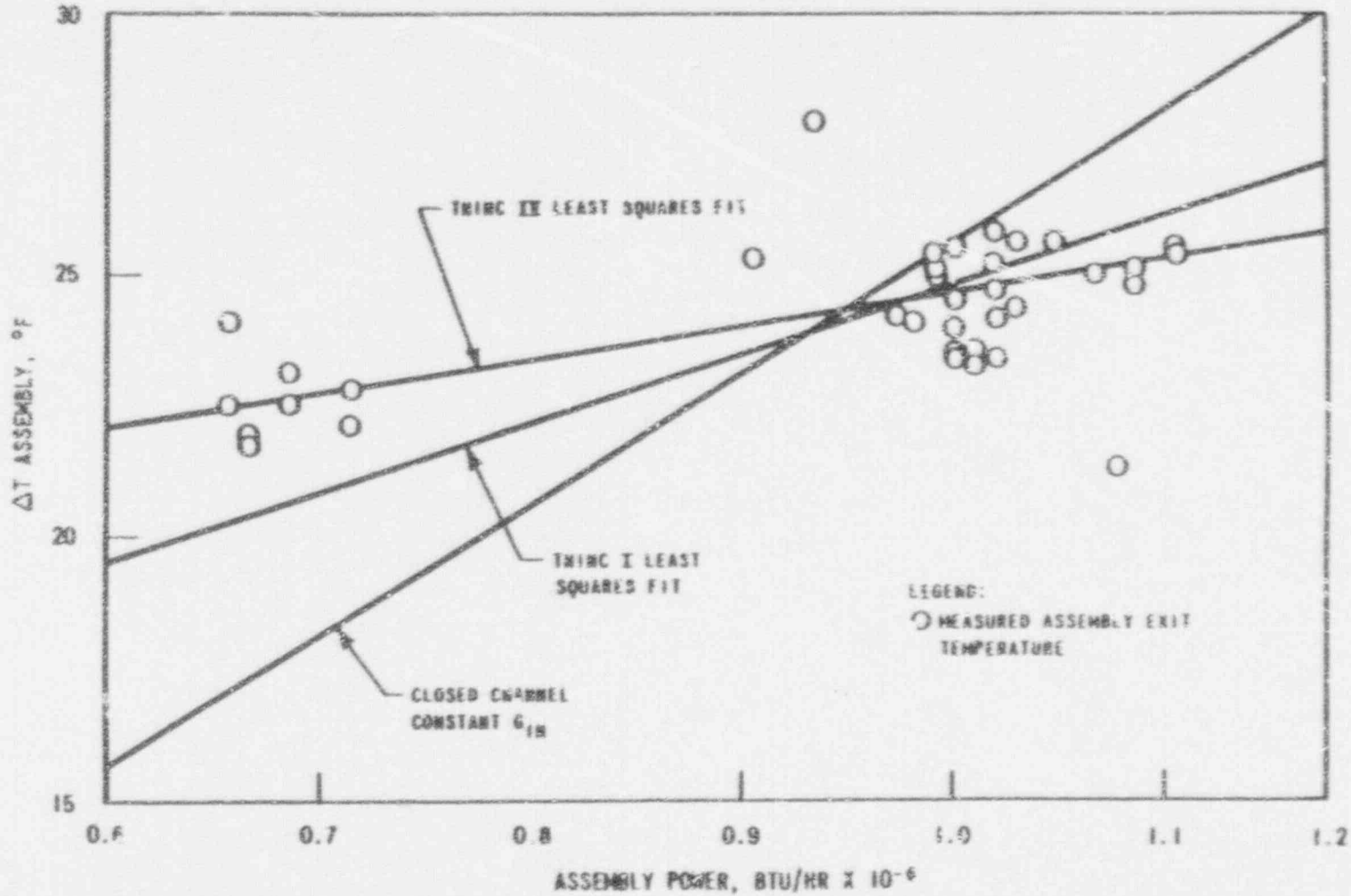

FIGURE 4.4-13
POWER NATURAL CIRCULATION TEST
BEAVER VALLEY POWER STATION UNIT NO. 2
UPDATED FINAL SAFETY ANALYSIS REPORT

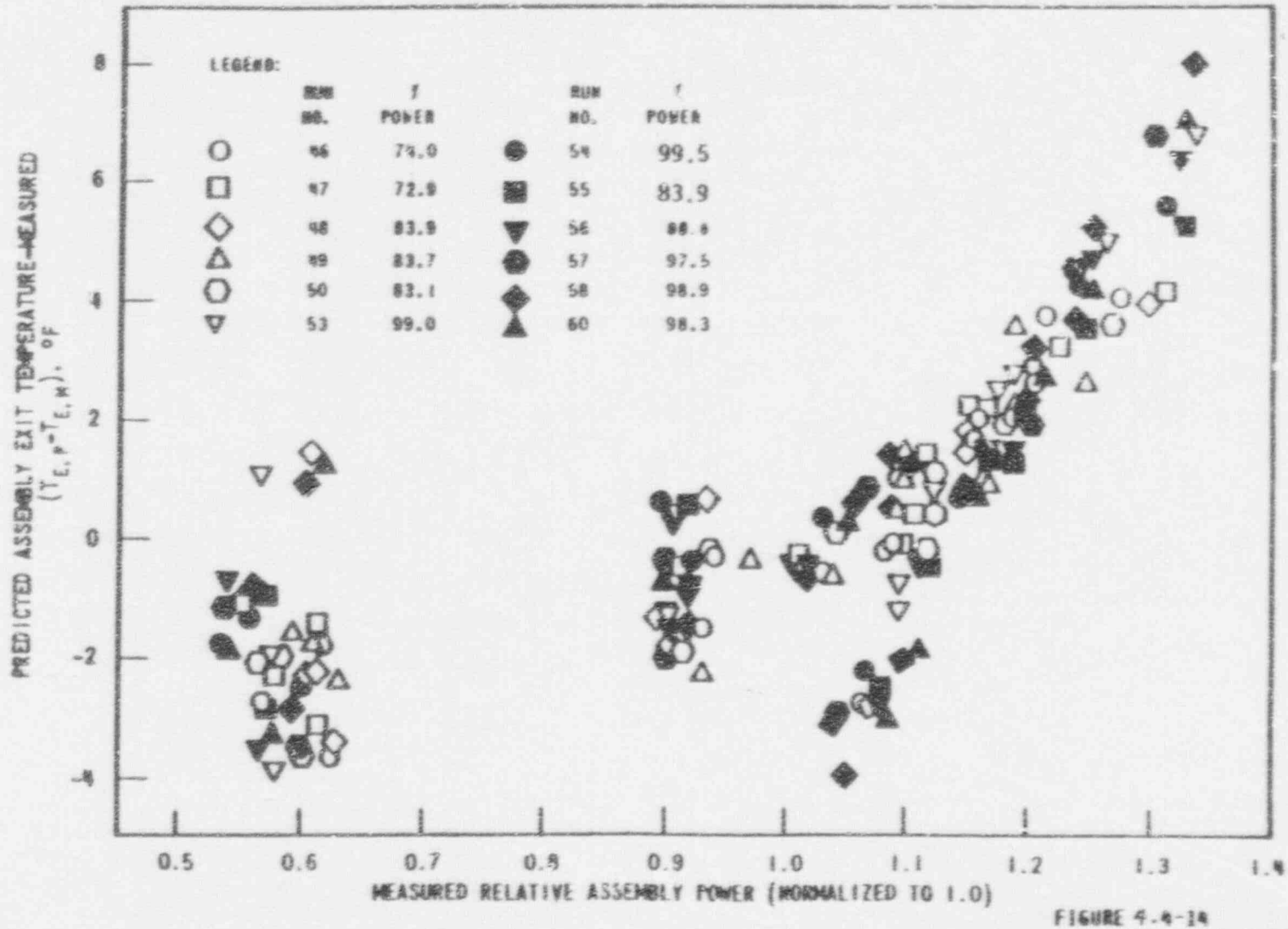

FIGURE 4.4-14
COMPARISON OF A REPRESENTATIVE 4 TWO-LOOP REACTOR INCORE THERMOCOUPLE MEASUREMENTS WITH THINC-IV PREDICTIONS
BEAVER VALLEY POWER STATION UNIT NO. 2
UPDATED FINAL SAFETY ANALYSIS REPORT

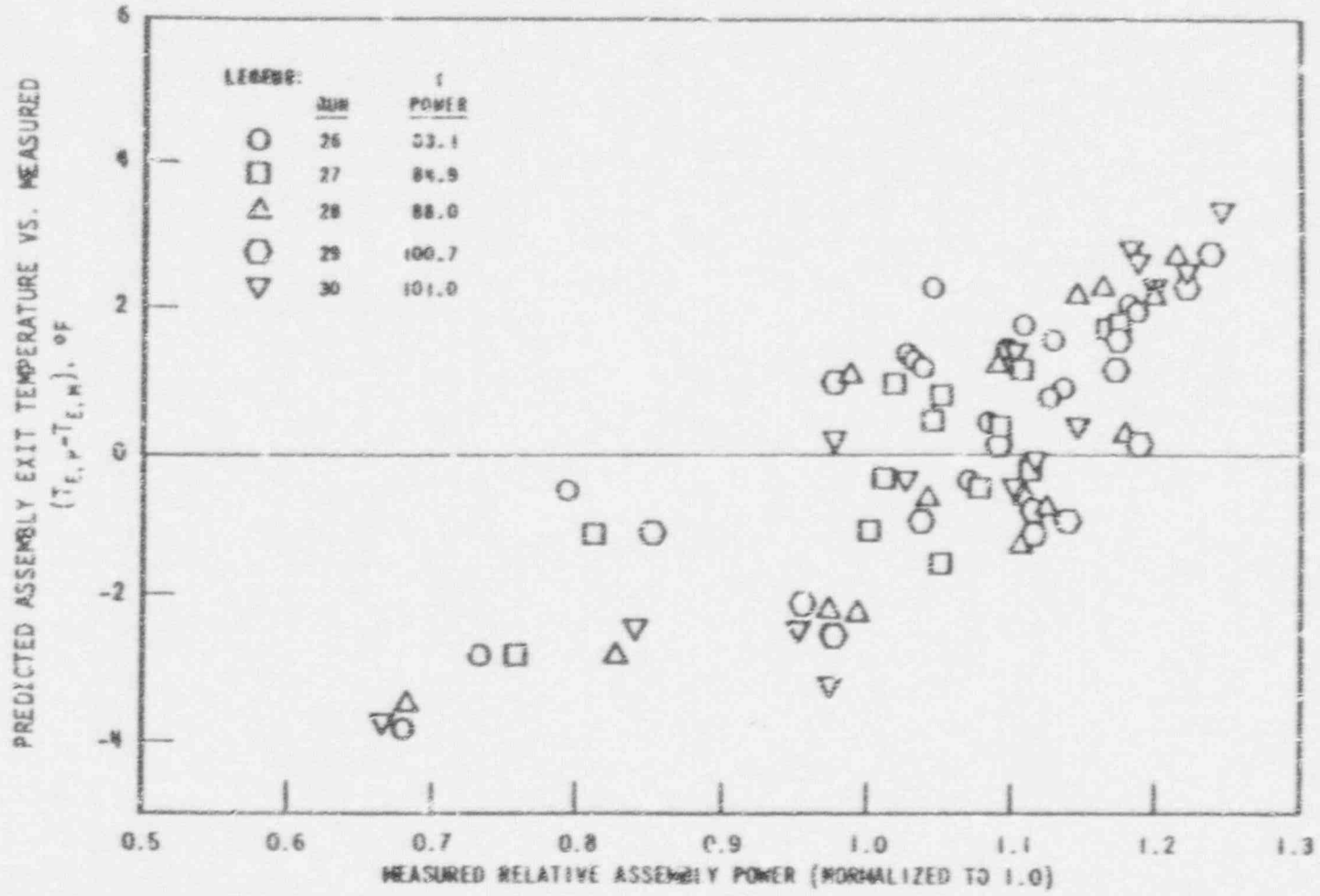

FIGURE 4.4-15
COMPARISON OF A REPRESENTATIVE W TWO-LOOP REACTOR INCORE THERMOCOUPLE MEASUREMENTS WITH THINC-IV PREDICTIONS
BEAVER VALLEY POWER STATION UNIT NO. 2
UPDATED FINAL SAFETY ANALYSIS REPORT

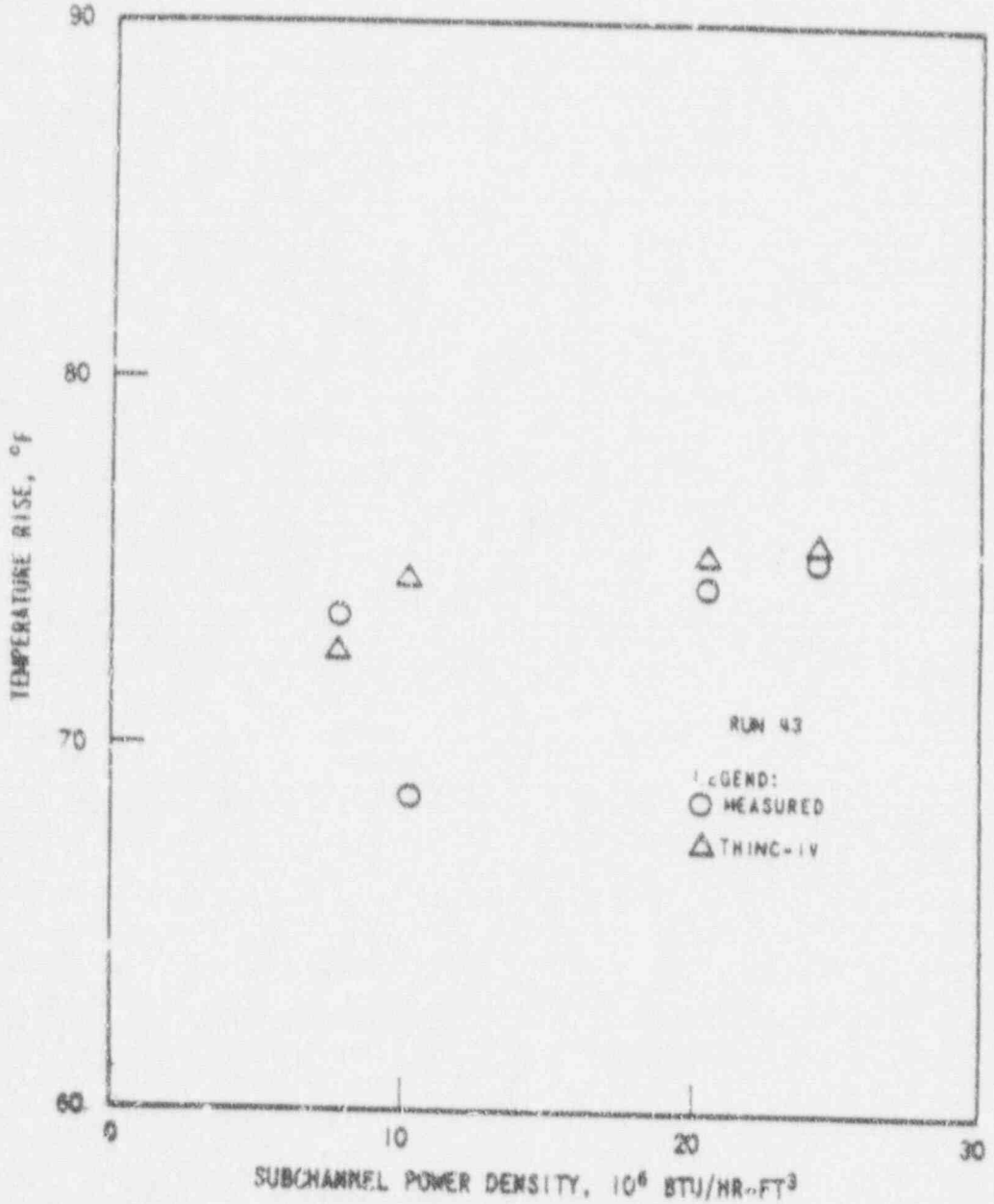

FIGURE 4.4-16
HANFORD SUBCHANNEL TEMPERATURE DATA
COMPARISON WITH THINC-IV
BEAVER VALLEY POWER STATION UNIT NO. 2
UPDATED FINAL SAFETY ANALYSIS REPORT

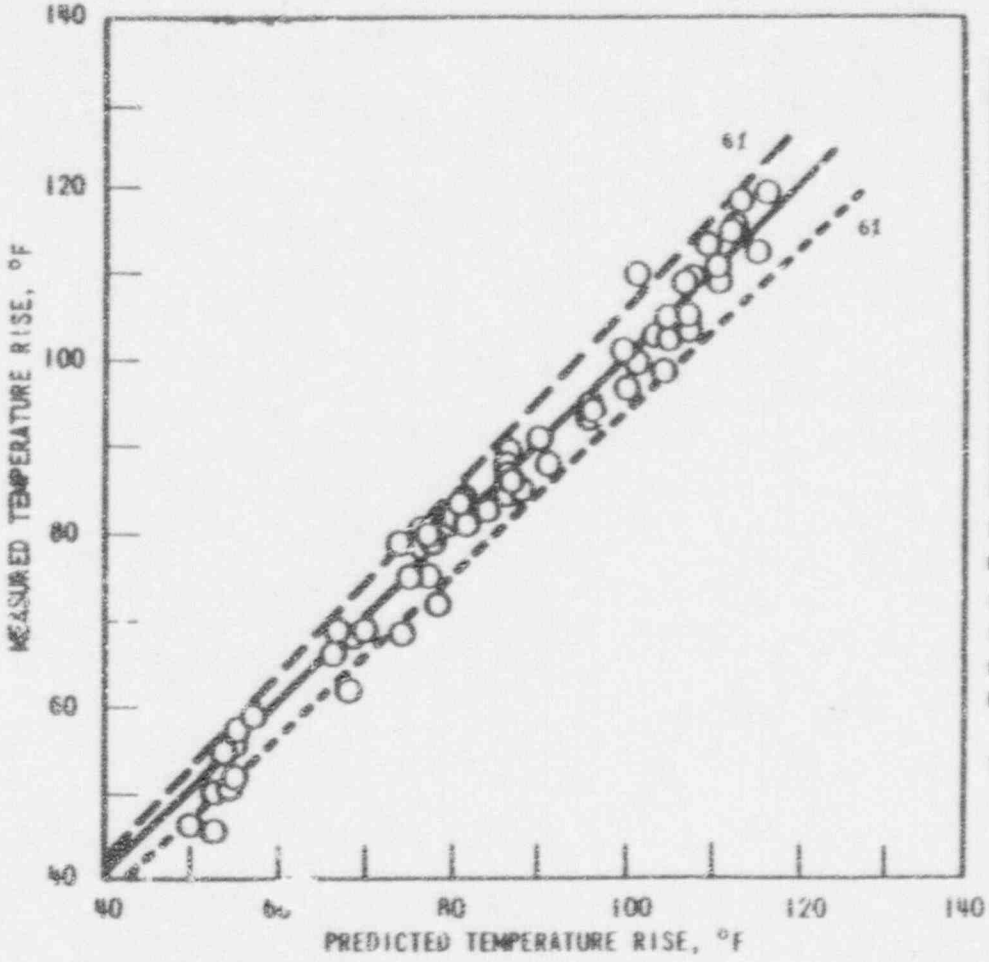

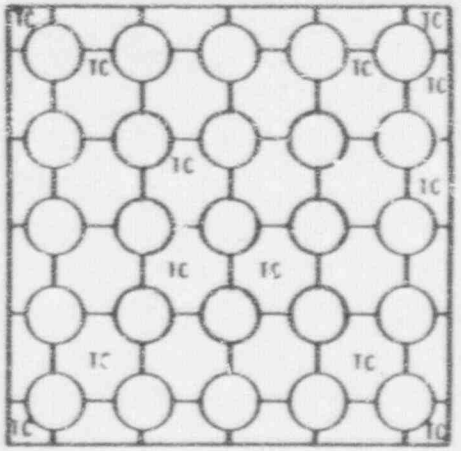

PRESSURE	2014 PSIA
MASS FLOW	$0.5\text{-}2.2\times10^{6}$ LB/$_{m}$FT^{2}-HR
ROD DIAMETER	0.422 INCHES
ROD PITCH	0.555 INCHES
HEATED LENGTH	84 INCHES
HEAT FLUX DISTRIBUTION	
INNER ROD: OUTER ROD	1.204: 1.0

TC - THERMOCOUPLE LOCATION

FIGURE 4.4-17
HANFORD SUBCRITICAL TEMPERATURE DATA
COMPARISON WITH THINC-IV
BEAVER VALLEY POWER STATION UNIT NO. 2
UPDATED FINAL SAFETY ANALYSIS REPORT

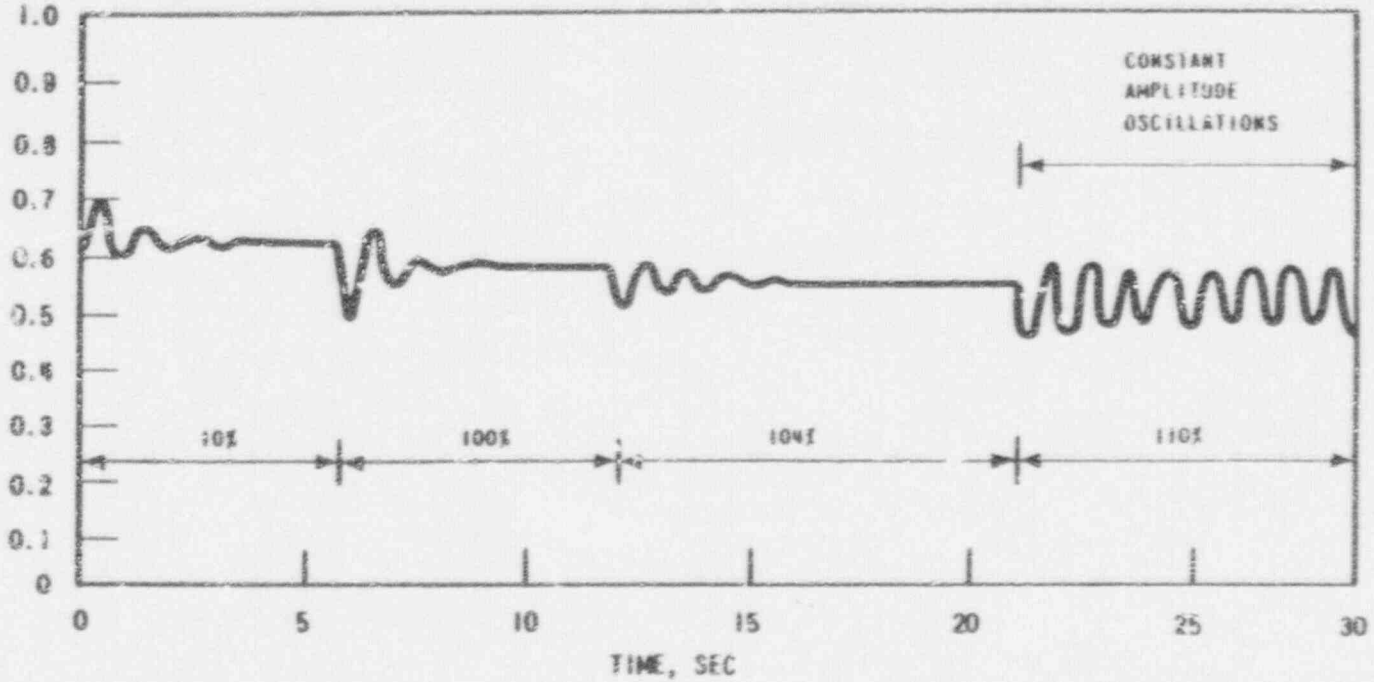

FIGURE 4.4-18
HYDNA RESULTS INDICATING POWER LEVEL
AT WHICH FLOW OSCILLATIONS OCCUR
BEAVER VALLEY POWER STATION UNIT NO. 2
UPDATED FINAL SAFETY ANALYSIS REPORT

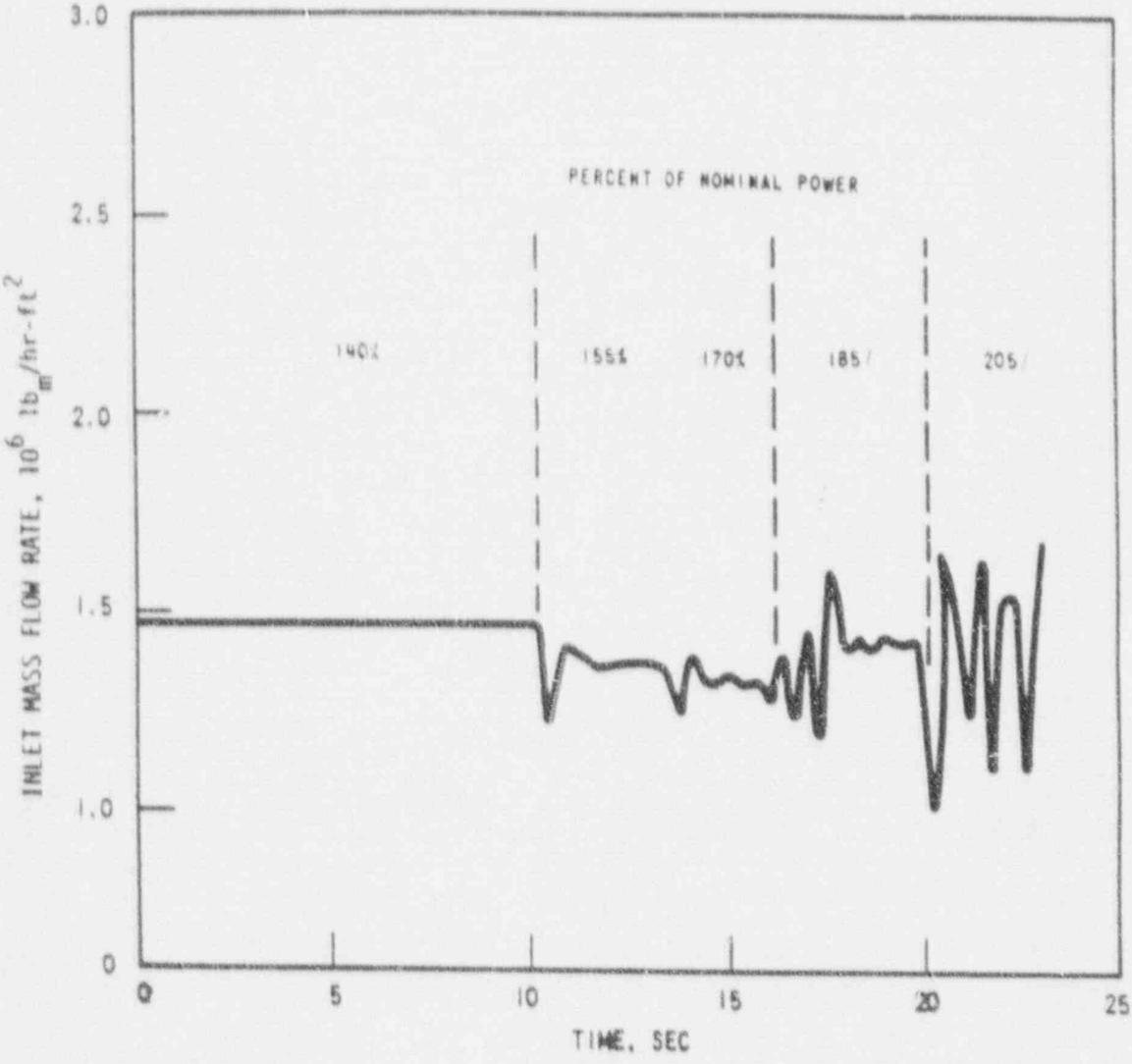

FIGURE 4.4-19
HYDRODYNAMIC FLOW INSTABILITY STUDY,
NORMAL POWER = 3250 MW
BEAVER VALLEY POWER STATION UNIT NO. 2
UPDATED FINAL SAFETY ANALYSIS REPORT

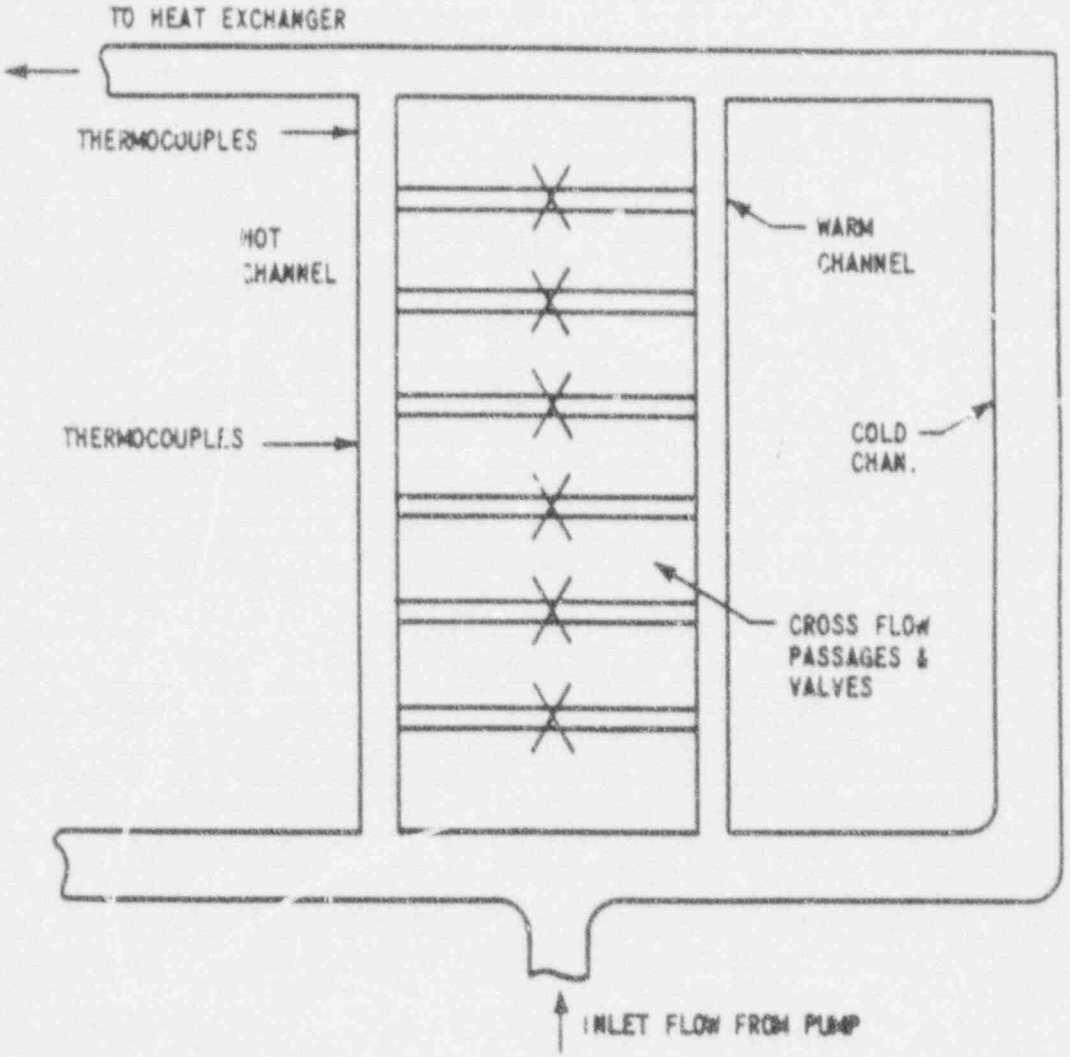

FIGURE 4.4-20
PARALLEL CHANNEL TEST STATION
BEAVER VALLEY POWER STATION UNIT NO. 2
UPDATED FINAL SAFETY ANALYSIS REPORT

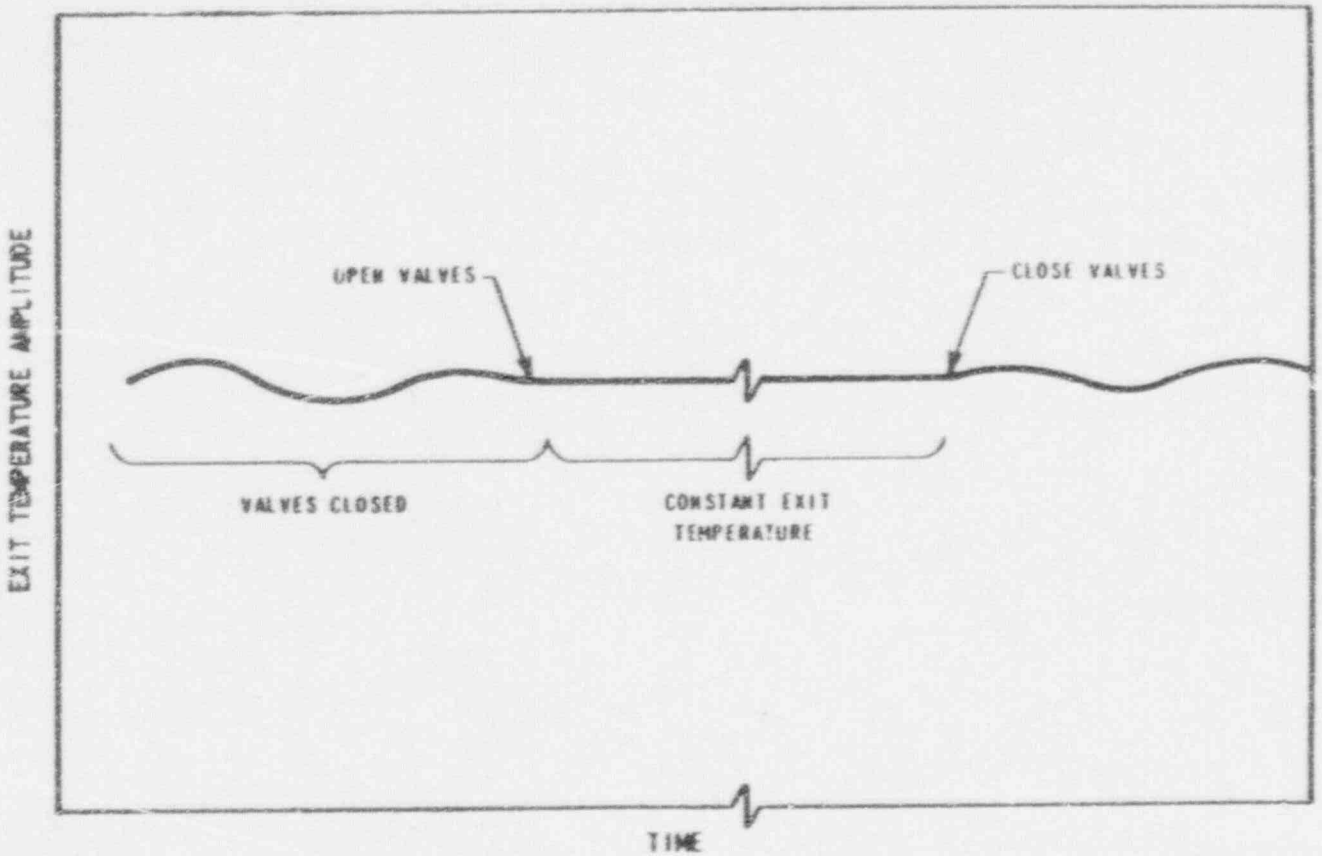

FIGURE 4.4-21
EXPERIMENTAL FLOW STABILITY DATA
BEAVER VALLEY POWER STATION UNIT NO. 2
UPDATED FINAL SAFETY ANALYSIS REPORT

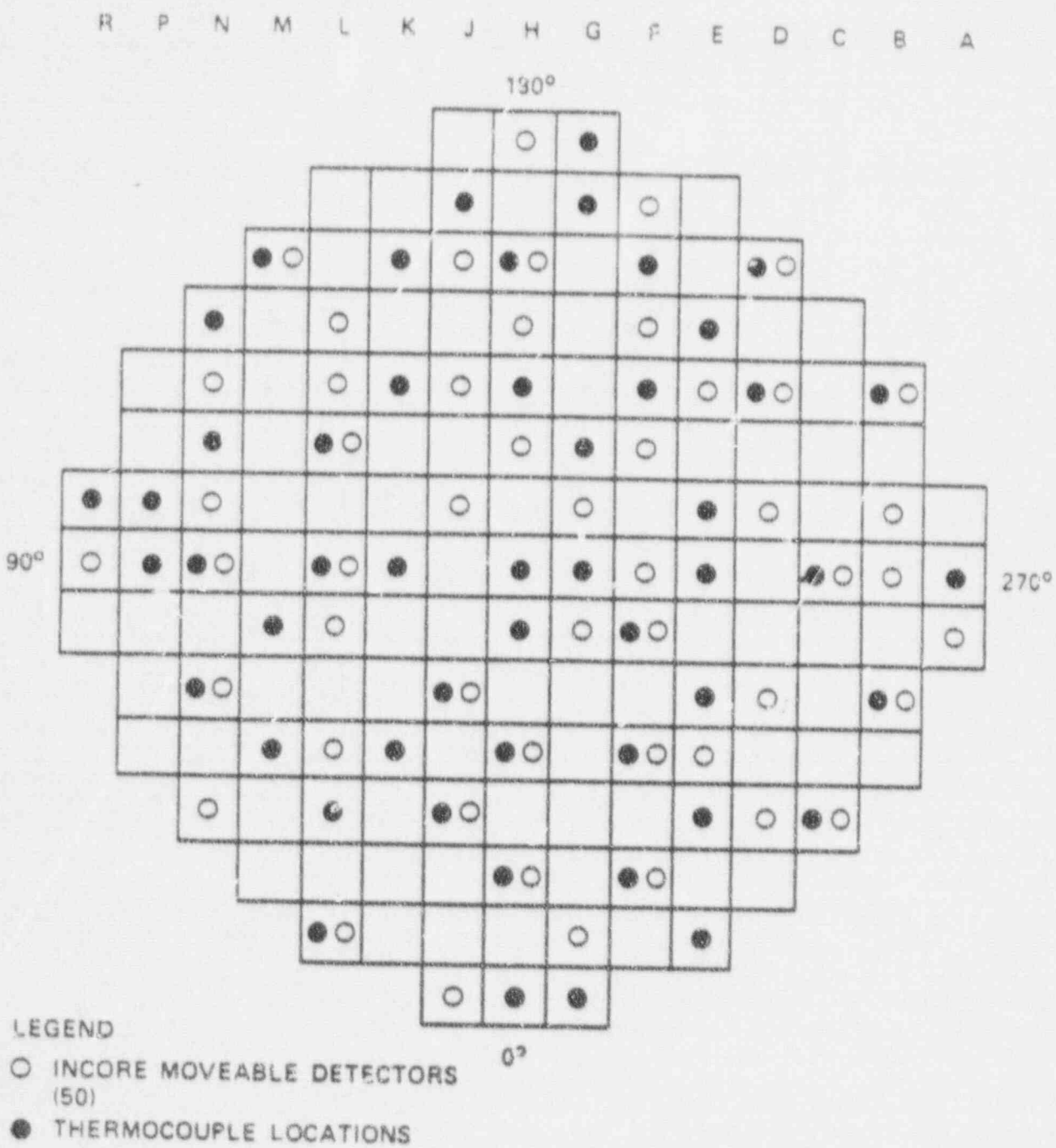

FIGURE 4.4-22
DISTRIBUTION OF INCORE INSTRUMENTATION
BEAVER VALLEY POWER STATION-UNIT 2
FINAL SAFETY ANALYSIS REPORT

FSAR Chapter 15 Markup

Section 15.3

corresponding to Permissive 8, low flow in any two loops will actuate a reactor trip. Above Permissive 7, two or more RCP circuit breakers opening will actuate a reactor trip which serves as a backup to the low flow trip.

15.3.1.2 Analysis of Effects and Consequences

Method of Analysis

~~Two cases have been analyzed:~~
The loss of one reactor coolant pump with three loops in operation has been analyzed.
~~1. Loss of pump with three loops in operation.~~

~~2. Loss of pump with two loops in operation.~~

This transient is analyzed by three digital computer codes: 1) the LOFTRAN (Burnett et al 1972) Code is used to calculate the loop and core flow during the transient, the time of reactor trip based on the calculated flows, the nuclear power transient, and the primary system pressure and temperature transients; 2) the FACTRAN (Hunin 1972) Code is then used to calculate the heat flux transient based on the nuclear power and flow from LOFTRAN; and 3) the THINC Code (Section 4.4) is used to calculate th departure from nucleate boiling ratio (DNBR) during the transient based on the heat flux determined by the FACTRAN and flow from LOFTRAN. The DNBR transients presented represent the minimum of the typical or thimble cell.

Initial Conditions

Initial operating conditions assumed are the most adverse with respect to the margin to DNB (that is, maximum steady-state power level, minimum steady-state pressure, and maximum steady-state coolant average temperature). Section 15.0.3 provides an explanation of initial conditions. ~~With two or three loops operating, the maximum power level (including errors) allowed for that mode of operation is assumed.~~

Reactivity Coefficients

The most negative Doppler-only power coefficient is used (Figure 15.0-2). This is equivalent to a total integrated Doppler reactivity from 0 to 100 percent power of 0.016$\Delta\rho$.

The least negative moderator temperature coefficient (Figure 15.0-3) is assumed since this results in the maximum core power during the initial part of the transient when the minimum DNBR is reached.

Flow Coastdown

The flow coastdown analysis is based on a momentum balance around each reactor coolant loop and across the reactor core. This momentum balance is combined with the continuity equation, a pump momentum

balance, and the pump characteristics and is based on high estimates of system pressure losses.

Plant systems and equipment which are necessary to mitigate the effects of the accident are discussed in Section 15.0.8 and listed in Table 15.0-6. No single active failure in any of these systems or equipment will adversely affect the consequences of the accident.

Results

Figures 15.3-1 through 15.3-4 show the transient response for the loss-of-reactor coolant pump with three loops initially in operation. Figure 15.3-4 shows the DNBR to be always greater than the limit value.

~~Figures 15.3-5 through 15.3-8 show the transient response for the loss-of-reactor coolant pump with two loops initially in operation. The minimum DNBR is greater than the limit value, as shown on Figure 15.3-8.~~

~~For both cases analyzed,~~ Since DNB ~~does not~~ is not expected to occur, the ability of the reactor coolant to remove heat from the fuel is not significantly reduced. Thus, the average fuel and clad temperatures do not increase significantly above their respective initial values.

The calculated sequence of events for the ~~two~~ case associated with analyzed is shown in Table 15.3-1. The affected RCP will continue to coast down, and the core flow will reach a new equilibrium value ~~corresponding to~~ the two ~~number of~~ pumps still in operation. Following reactor trip, the plant will come to a stabilized condition at hot standby with one or more RCPs in operation. Normal operating procedures may then be followed. The operating procedures would call for operator action to control RCS boron concentration and pressurizer level using the chemical and volume control system (CVCS), and to maintain steam generator level through control of the main or auxiliary feedwater system (AFWS). Any action required of the operator to maintain the plant in a stabilized condition will be in a time frame in excess of ten minutes following reactor trip.

15.3.1.3 Radiological Consequences

A partial loss of reactor coolant flow from full load would esult in a reactor and turbine trip. Assuming, in addition, that the condenser is not available, atmospheric steam dump may be required.

There are only minimal radiological consequences associated with this event. Fuel damage as a result of this transient is not postulated. The radiological consequences resulting from atmospheric steam dump are less severe than those of the loss of nonemergency ac power to station auxiliaries described in Section 15.2.6.

grid frequency distrubances and the resulting nuclear steam supply system protection requirements which are generally applicable.

The reactor trip on low reactor coolant loop flow is provided to protect against loss of flow conditions which affect only one reactor coolant loop. This function is generated by two out of three flow signals per reactor coolant loop. Above Permissive 8, low flow in any loop will actuate a reactor trip. Between approximately 10 percent power (Permissive 7) and the power level corresponding to Permissive 8, low flow in any two loops will actuate a reactor trip. If the maximum grid frequency decay rate is low enough, this trip function will protect the core from underfrequency events. This effect is fully described by Baldwin (et al 1975).

Insert A →

15.3.2.2 Analysis of Effects and Consequences

~~Two cases have been analyzed:~~
The complete loss of flow transient has been analyzed for a

1. Loss of three pumps with three loops in operation.

~~2. Loss of two pumps with two loops in operation.~~

These transients are analyzed by three digital computer codes. First, the LOFTRAN (Burnett 1972) Code is used to calculate the loop and core flow during the transient, the time of reactor trip based on the calculated flows, the nuclear power transient, and the primary system pressure and temperature transients. The FACTRAN (Hunin 1972) Code is then used to calculate the heat flux transient based on the nuclear power and flow from LOFTRAN. Finally, the THINC Code (Section 4.4) is used to calculate the DNBR during the transient based on the heat flux from FACTRAN and flow from LOFTRAN run. The DNBR transients presented represent the minimum of the typical or thimble cell.

The method of analysis and assumptions made regarding initial operating conditions and reactivity coefficients are identical to those discussed in Section 15.3.1, except that following the loss of power supply to all pumps at power, a reactor trip is actuated by either RCP power supply undervoltage or underfrequency.

Results

Figures 15.3-9 through 15.3-12 show the transient response for the loss of power to all RCPs with three loops in operation. The reactor is assumed to be tripped on an undervoltage signal. Figure 15.3-12 shows the DNBR to be always greater than the limit value.

~~Figures 15.3-13 through 15.3-16 show the transient response for the loss of power to all RCPs with two loops in operation. The reactor is again assumed to be tripped on an undervoltage signal. The minimum DNBR is greater than the limit value, as shown on Figure 15.3-16.~~

15.3.2 Complete Loss of Forced Reactor Coolant Flow
Insert for Zirc Grids

Insert A

Normal power for the reactor coolant pumps is supplied through busses from a transformer connected to the generator. Each pump is on a separate bus. When the generator trip occurs, the busses are automatically transferred to a transformer supplied from external power lines, and the pumps will continue to supply coolant flow to the core. Following any turbine trip, where there are no electrical faults which require tripping the generator from the network, the generator remains connected to the network for approximately 30 seconds. The reactor coolant pumps remain connected to the generator thus ensuring full flow for 30 seconds after the reactor trip before any transfer is made.

~~For both cases analyzed,~~ Since DNB ~~does not~~ is not expected to occur, the ability of the primary coolant to remove heat from the fuel rod is not greatly reduced. Thus, the average fuel and cladding temperatures do not increase significantly above their respective initial values. The calculated sequence of events for the ~~two~~ cases analyzed are shown in Table 15.3-1. The RCPs will continue to coast down, and natural circulation flow will eventually be established, as demonstrated in Section 15.2.6. With the reactor tripped, a stable plant condition will be attained. Normal plant shutdown may then proceed. The operating procedures would call for operator action to control RCS boron concentration and pressurizer level using the CVCS and to maintain steam generator level through control of the main feedwater system or AFWS.

15.3.2.3 Radiological Consequences

A complete loss-of-reactor coolant flow from full load results in a reactor and turbine trip. Assuming, in addition, that the condenser is not available, atmospheric steam dump would be required. The quantity of steam released would be less than that of the main steam line break described in Section 15.1.5.

There are only minimal radiological consequences associated with this event. Since fuel damage is not postulated, the radiological consequences resulting from this event are less severe than those of the MSLB analyzed in Section 15.1.5.3.

15.3.2.4 Conclusions

The analysis performed has demonstrated that for the complete loss of forced reactor coolant flow, the DNBR does not decrease below the limit value at any time during the transient. Thus, the DNB design-basis as described in Section 4.4 is met. The radiological consequences are not limiting.

15.3.3 Reactor Coolant Pump Shaft Seizure (Locked Rotor)

15.3.3.1 Identification of Causes and Accident Description

The accident postulated is an instantaneous seizure of a RCP rotor (Section 5.4). Flow through the affected reactor coolant loop is rapidly reduced, leading to an initiation of a reactor trip on a low flow signal.

Following initiation of the reactor trip, heat stored in the fuel rods continues to be transferred to the coolant causing the coolant to expand. At the same time, heat transfer to the shell side of the steam generators is reduced, first because the reduced flow results in a decreased tube side film coefficient and then because the reactor coolant in the tubes cools down while the shell side temperature increases (turbine steam flow is reduced to zero upon plant trip). The rapid expansion of the coolant in the reactor core,

combined with reduced heat transfer in the steam generators causes an insurge into the pressurizer and a pressure increase throughout the RCS. The insurge into the pressurizer compresses the steam volume, actuates the automatic spray system, opens the power-operated relief valves (PORVs), and opens the pressurizer safety valves in that sequence. The PORVs are designed for reliable operation and would be expected to function properly during the accident. However, for conservatism, their pressure reducing effect as well as the pressure reducing effect of the spray is not included in the analysis.

This event is classified as an ANS Condition IV incident (a limiting fault) as defined in Section 15.0.1.

15.3.3.2 Analysis of Effects and Consequences

Method of Analysis

Two digital computer codes are used to analyze this transient. The LOFTRAN Code (Burnett 1984) is used to calculate the resulting loop and core flow transients following the pump seizure, the time of reactor trip based on the loop flow transients, the nuclear power following reactor trip, and to determine the peak pressure. The thermal behavior of the fuel located at the core hot spot is investigated using the FACTRAN Code, (Hunin 1972) which uses the core flow and nuclear power calculated by LOFTRAN. The FACTRAN Code includes a film boiling heat transfer coefficient.

Two ~~Three~~ cases are analyzed:

1. Three loops operating, one locked rotor

~~2. Two loops operating, one locked rotor~~

2. Three loops operating, one locked rotor, loss of power to the other reactor coolant pumps

At the beginning of the postulated locked rotor accident (that is, at the time the shaft in one of the RCPs is assumed to seize), the plant is assumed to be in operation under the most adverse steady-state operating conditions (that is, maximum steady-state power level, maximum steady-state pressure, and maximum steady-state coolant average temperature). Plant characteristics and initial conditions are further discussed in Section 15.0.3. ~~With two loops operating, the maximum power level (including errors) allowed in that mode of operation is assumed.~~

For the peak pressure evaluation, the initial pressure is conservatively estimated as 30 psi above nominal pressure (2,250 psig) to allow for errors in the pressurizer pressure measurement and control channels. This is done to obtain the highest possible rise in the coolant pressure during the transient. To obtain the maximum pressure in the primary side, conservatively high

loop pressure drops are added to the calculated pressurizer pressure. The pressure responses shown on Figure 15.3-18 ~~and 15.3-22~~ are the responses at the point in the RCS having the maximum pressure.

Evaluation of the Pressure Transient

After pump seizure, the neutron flux is rapidly reduced by control rod insertion. Rod motion is assumed to begin one second after the flow in the affected loop reaches 87 percent of nominal flow. No credit is taken for the pressure reducing effect of the pressurizer relief valves, pressurizer spray, steam dump, or controlled feedwater flow after plant trip. Insert A

Although these operations are expected to occur and would result in a low peak pressure, an additional degree of conservatism is provided by ignoring their effect. The pressurizer safety valves are full open at 2,575 psia and their capacity for steam relief is as described in Section 5.4.

Evaluation of DNB in the Core During the Accident

For this accident, DNB is assumed to occur in the core, and therefore, an evaluation of the consequences with respect to fuel rod thermal transients is performed. Results obtained from analysis of this "hot spot" condition represent the upper limit with respect to cladding temperature and zirconium water reaction.

In the evaluation, the rod power at the hot spot is assumed to be 2.544 times the average rod power level (that is, F_Q at the initial core power = 2.544). Insert B.

Film Boiling Coefficient

The film boiling coefficient is calculated in the FACTRAN Code using the Bishop-Sandberg-Tong film boiling correlation. The fluid properties are evaluated at film temperature (average between wall and bulk temperatures). The program calculates the film coefficient at every time step based upon the actual heat transfer conditions at the time. The neutron flux, system pressure, bulk density, and mass flow rate as a function of time are used as program input.

For this analysis, the initial values of the pressure and the bulk density are used throughout the transient since they are the most conservative with respect to cladding temperature response. For conservatism, DNB was assumed to start at the beginning of the accident.

Fuel Clad Gap Coefficient

The magnitude and time dependence of the heat transfer coefficient between fuel and clad (gap coefficient) has a pronounced influence on the thermal results. The larger the value of the gap coefficient,

15.3.3 Reactor Coolant Pump Shaft Seizure (Locked Rotor)

Insert for Zirc Grids

Insert A

The time delay of 1.0 second used in connection with the low flow reactor trip is a very conservative allowance for the total time delay between the time the flow reaches 87 percent of the nominal and the time the rods begin moving into the core. This total includes individual delays associated with the following: Flow sensors/transmitters, solid state protection system input relays, solid state protection system, voltage drop on reactor trip breaker undervoltage and control rod gripper release.

Insert B

The number of rods in DNB was conservatively calculated as 18% of the total rods in the core.

the more heat is transferred between pellet and cladding. Based on investigations on the effect of the gap coefficient upon maximum cladding temperature during the transient, the gap coefficient was assumed to increase from a steady-state value consistent with initial

the

fuel temperature to 10^4 Btu/hr·ft²-°F at the initiation of the transient. Thus, the large amount of energy stored in the fuel because of the small initial value is released to the cladding at the initiation of the transient.

Zirconium Steam Reaction

The zirconium-steam reaction can become significant above 1,800°F (cladding temperature). The Baker-Just parabolic rate equation shown as follows is used to define the rate of the zirconium-steam reaction.

$$\frac{d(w^2)}{dt} = 33.3 \times 10^6 \exp\left[\frac{(-45,500)}{1.986\ T}\right] \qquad (15.3\text{-}1)$$

where:

w = amount reacted (mg/cm²)

t = time (sec)

T = temperature (°K)

The reaction heat is 1,510 cal/gm.

The effect of zirconium-steam reaction is included in the calculation of the "hot spot" cladding temperature transient.

Plant systems and equipment which are available to mitigate the effects of the accident are discussed in Section 15.0.8 and listed in Table 15.0-6. No single active failure in any of these systems or equipment will adversely affect the consequences of the accident.

Results

1. Locked Rotor with Three Loops Operating

The transient results for this case are shown on Figures 15.3-17 through 15.3-20. The results of these calculations are summarized in Table 15.3-2a. The peak RCS pressure reached during the transient is less than that which would cause stresses to exceed the faulted condition stress limits. Also, the peak cladding surface temperature is considerably less than 2,700°F. It should be noted that the cladding temperature was conservatively calculated assuming that DNB occurs at the initiation of the transient.

~~2. Locked Rotor with Two Loops Operating~~

~~The transient results for this case are shown on Figure 15.3-21 through 15.3-24. The results of these calculations are also summarized in Table 15.3-2. The peak RCS pressure is slightly higher than for the previous case, but is still less than that which would cause stresses to exceed the faulted condition stress limits. The cladding temperature transient is still well below the 2,700°F limit.~~

2. Locked Rotor with Three Loops Operating, Loss of Power to the Remaining Pumps

The transient results for this case are shown on Figures 15.3-17 through 15.3-20. The results of these calculations are summarized in Table 15.3-2b. The peak RCS pressure reached during the transient is less than that which would cause stresses to exceed the faulted condition stress limits. Also, the peak cladding surface temperature is considerably less than 2,700°F. Both the peak RCS pressure and the peak cladding surface temperature for this case are similar to the 3-loop transient with power available as discussed on the previous page.

The calculated sequence of events for the ~~three~~ two cases analyzed is shown in Table 15.3-1. Figure 15.3-17 ~~and 15.3-21~~ show that the core flow reaches a new equilibrium value by 10 seconds. With the reactor tripped, a stable plant condition will eventually be attained. Normal plant shutdown may then proceed.

Following reactor trip, Beaver Valley Power Station - Unit 2 (BVPS-2) will approach a stabilized condition at hot standby; normal plant operating procedures may then be followed to maintain a hot condition or to cool the plant to cold shutdown. The operating procedures would call for operator action to control RCS boron concentration and pressurizer level using the CVCS, and to maintain steam generator level through control of the main feedwater system or AFWS. Any action required of the operator to maintain BVPS-2 in a stabilized condition will be in a time frame in excess of ten minutes following reactor trip.

15.3.3.3 Radiological Consequences

The radiological consequences of a postulated locked rotor accident are analyzed with the primary and secondary coolant concentrations assumed to be at Technical Specification limits. The primary to secondary system leakage rate is at the Technical Specification value of 1 gpm. No gap activity is assumed to be released into the primary coolant since there is no fuel failure postulated. The primary conlant and secondary side iodine and noble gas concentrations are presented in Table 15.0-8.

TABLE 15.3-1

TIME SEQUENCE OF EVENTS FOR INCIDENTS WHICH RESULT
IN A DECREASE IN REACTOR COOLANT SYSTEM FLOW
(WITH OFFSITE POWER)

Accident	Event	Time (sec)
Partial Loss of Forced Reactor Coolant Flow		
Three loops operating, one pump coasting down	Coastdown begins	0.
	Low flow reactor trip	1.4
	Rods begin to drop	2.4
	Minimum DNBR occurs	3.6
~~Two loops operating, one pump coasting down~~	~~Coastdown begins~~	~~0.~~
	~~Low flow reactor trip~~	~~2.53~~
	~~Rods begin to drop~~	~~3.53~~
	~~Minimum DNBR occurs~~	~~4.6~~

Accident	Event	Three Loop Operation	Two Loop Operation
Complete Loss of Forced Reactor Coolant Flow	All operating pumps lose power and begin coasting down	0	0
	Reactor coolant pump undervoltage trip point reached	0 ~~1.0~~	1.0
	Rods begin to drop	1.5	1.5
	Minimum DNBR occurs	3.4	3.0
Reactor coolant pump shaft seizure (locked rotor) (with offsite power)	Rotor on one pump locks	0	0
	Low flow trip point reached	0.06	0.20
	Rods begin to drop	1.06	1.20
	Maximum RCS pressure occurs	2.8	3.5
	Maximum cladding temperature occurs	3.6	3.8

TABLE 15.3-1 (Cont)

Accident	Event	Time (sec) Three Loop Operation
Reactor coolant pump shaft seizure (locked rotor) (without offsite power)	Rotor on one pump locks	0
	Low flow trip point reached	0.06
	Rods begin to drop	1.06
	Reactor coolant pumps lose power, coastdown begins	1.05
	Maximum RCS pressure occurs	3.2
	Maximum cladding temperature occurs	3.9

TABLE 15.3-2

SUMMARY OF RESULTS FOR LOCKED ROTOR TRANSIENTS

	3 Loops Operating ~~Initially~~ (with offsite Power)	2 Loops Operating ~~Initially~~ (without offsite Power)
Maximum reactor coolant system pressure (psia)	~~2,600~~ 2,597	2,641
Maximum cladding temperature (°F) core hot spot	~~1,897~~ 1,795	~~1,779~~ 1,870
$Zr-H_2O$ reaction at core hot spot (percent by weight)	~~0.39~~ 0.269	~~0.33~~ 0.415

TABLE 15.3-2a

SUMMARY OF RESULTS FOR LOCKED ROTOR TRANSIENTS
(WITH OFFSITE POWER)

	3 Loops Operating Initially	2 Loops Operating Initially
Maximum reactor coolant system pressure (psia)	2,608	2,647
Maximum cladding temperature (°F) core hot spot	1,897	1,773
Zr-H_2O reaction at core hot spot (percent by weight)	0.39	0.33

Delete this Page

TABLE 15.3-2b

SUMMARY OF RESULTS FOR LOCKED ROTOR TRANSIENTS
(WITHOUT OFFSITE POWER)

	3 Loops Operating Initially
Maximum reactor coolant system pressure (psia)	2,638
Maximum cladding temperature (°F) core hot spot	1,872
Zr-H_2O reaction at core hot spot (percent by weight)	0.40

Delete this Page

Replace Figures with following page

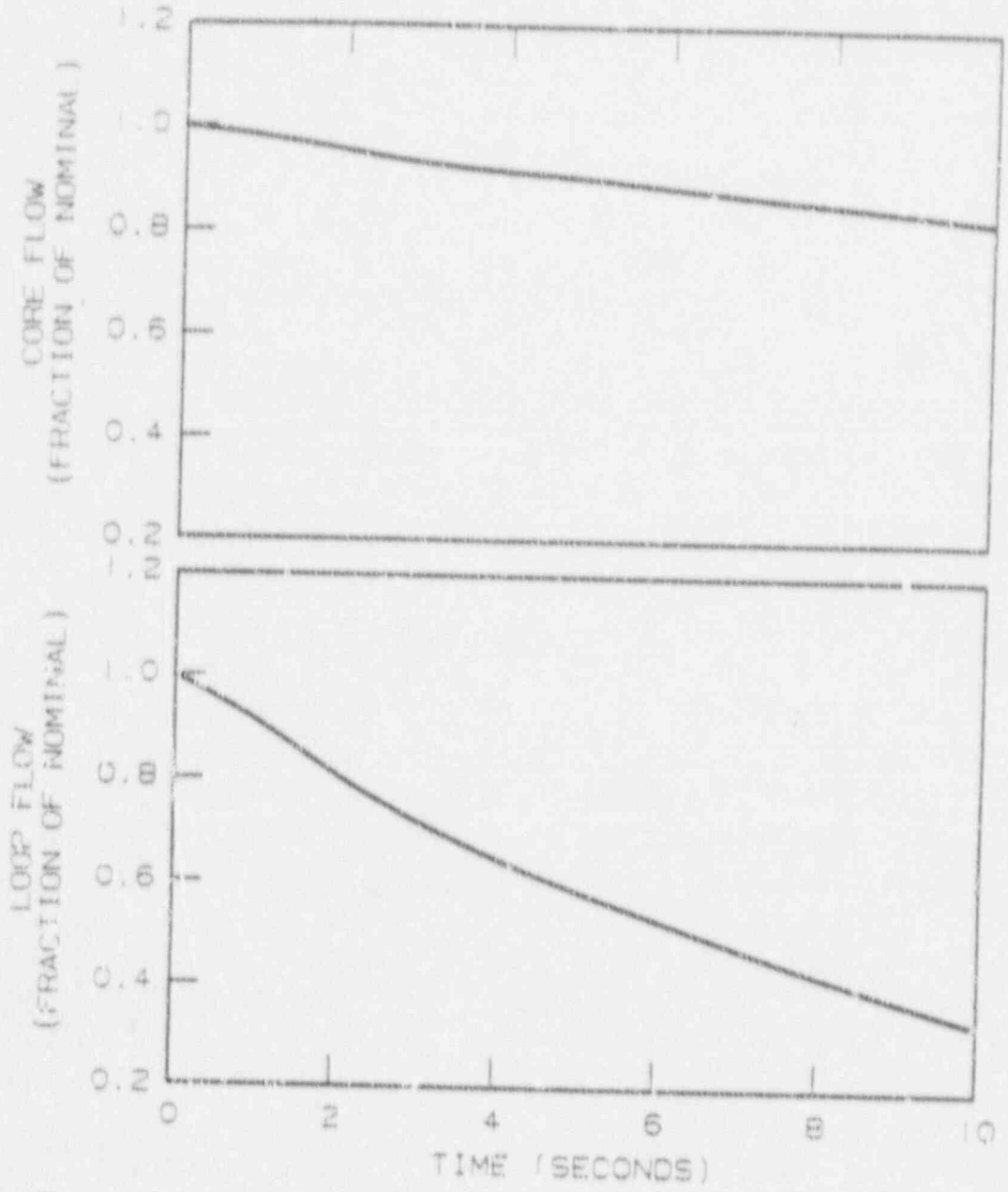

FIGURE 15.3-1
FLOW TRANSIENTS FOR
PARTIAL LOSS OF FLOW,
THREE LOOPS IN OPERATION,
ONE PUMP COASTING DOWN
BEAVER VALLEY POWER STATION-UNIT 2
FINAL SAFETY ANALYSIS REPORT

002-D 18621.15

Figure 15.3-1
Flow Transients for Partial Loss of Flow
Three Loops in Operation,
One Pump Coasting Down

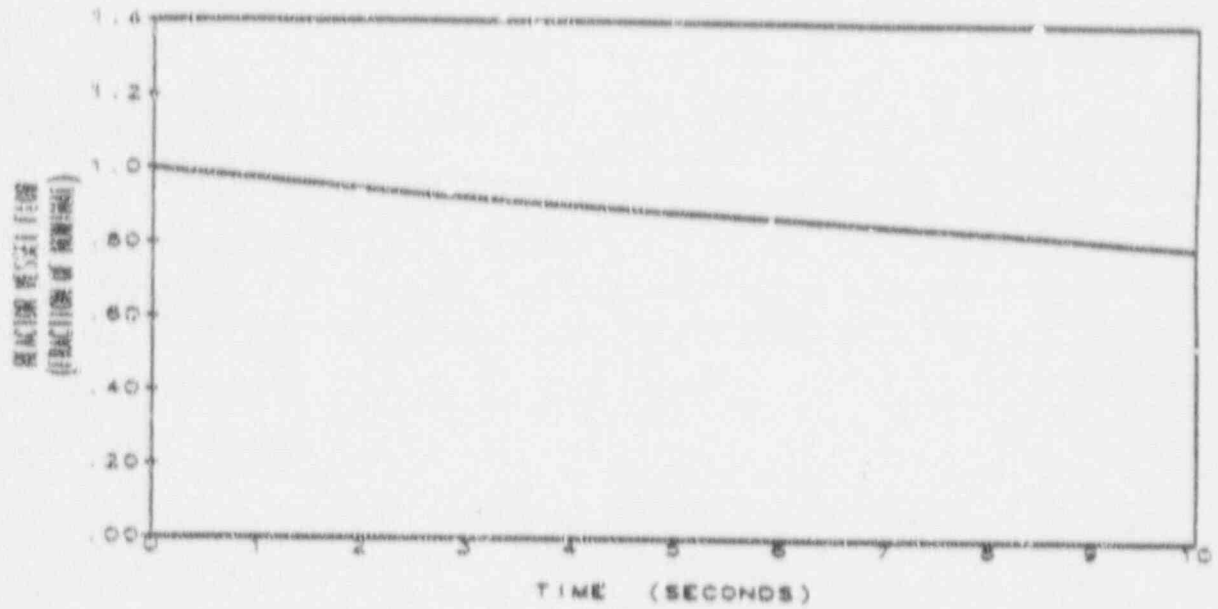

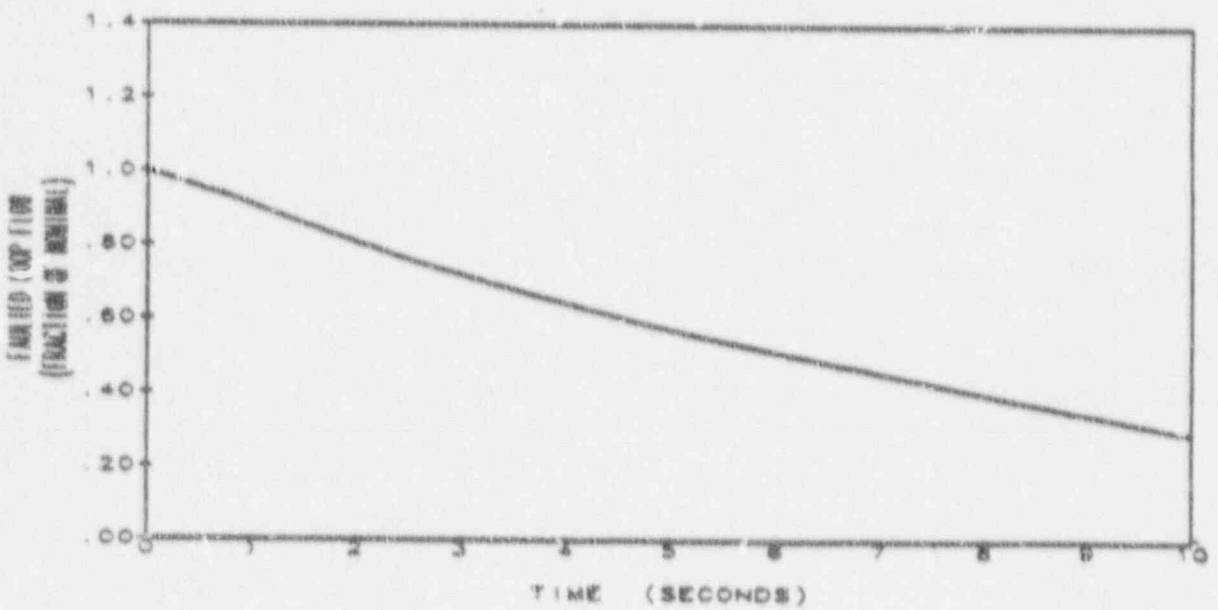

Replace Figure with following page

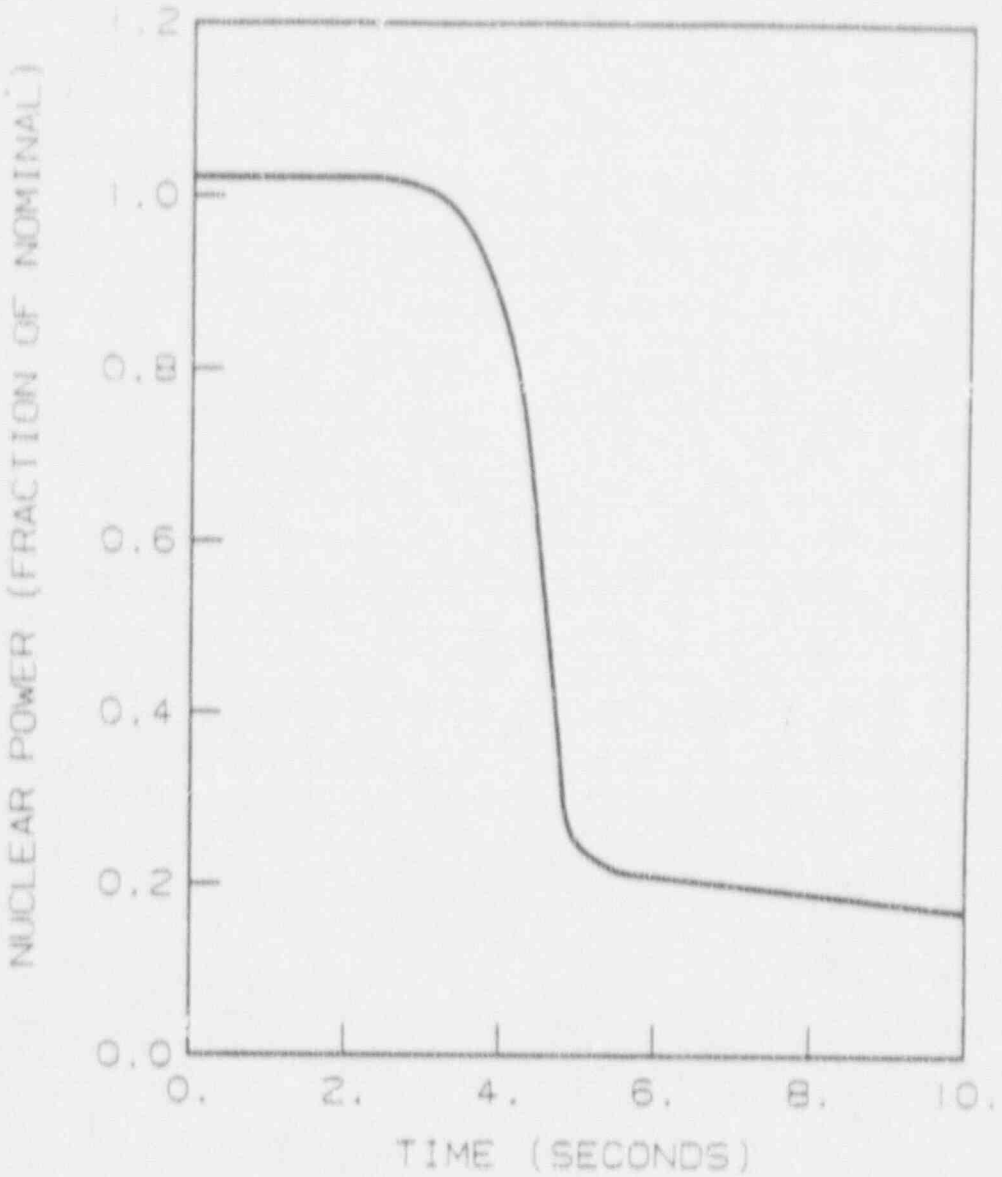

FIGURE 15.3-2
NUCLEAR POWER TRANSIENT FOR
PARTIAL LOSS OF FLOW,
THREE LOOPS IN OPERATION,
ONE PUMP COASTING DOWN
BEAVER VALLEY POWER STATION-UNIT 2
FINAL SAFETY ANALYSIS REPORT

001 0-18621 2

Figure 15.3-2

Nuclear Power and RCS Pressure for
Partial Loss of Flow
Three Loops of Operation,
One Pump Coasting Down

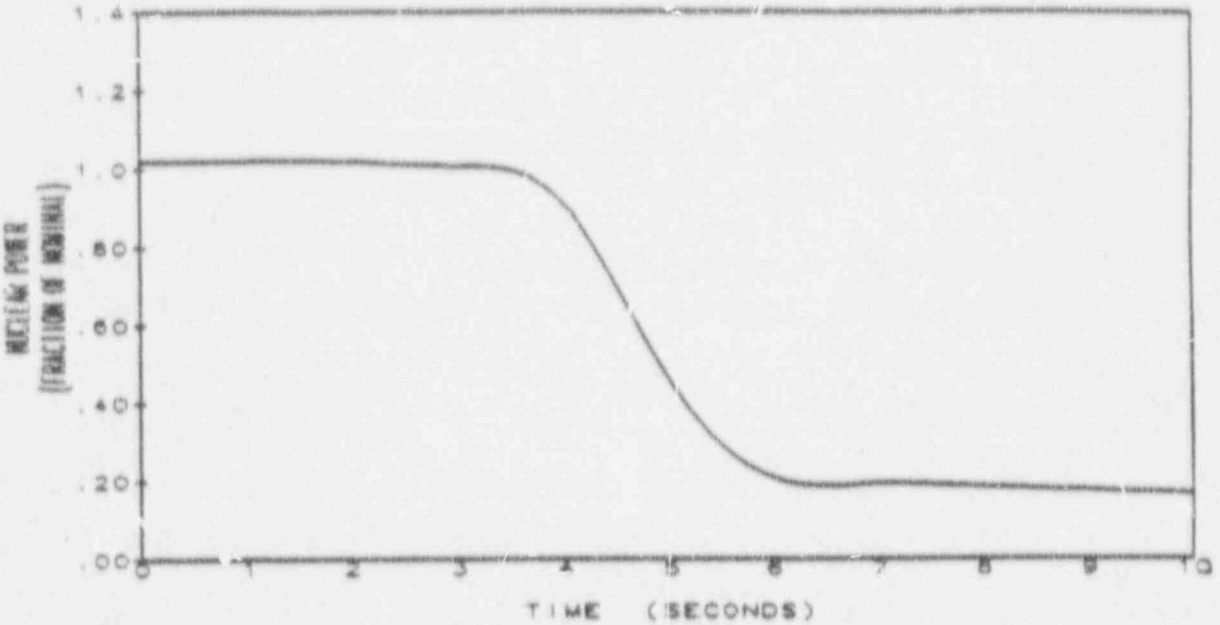

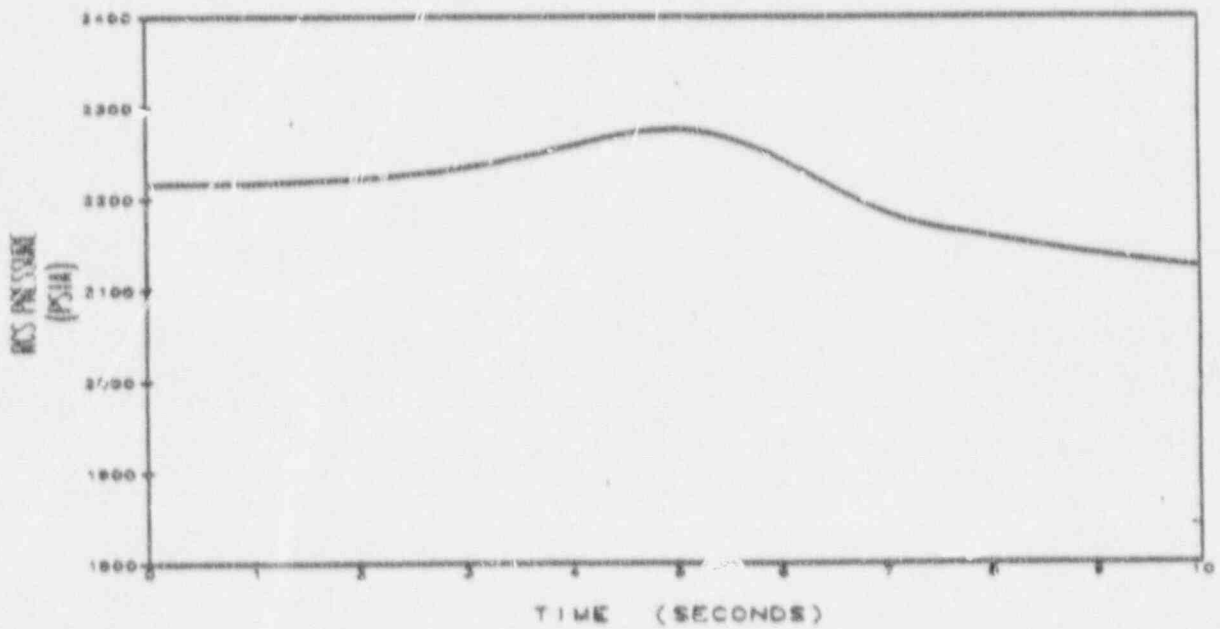

Replace Figures with following Page

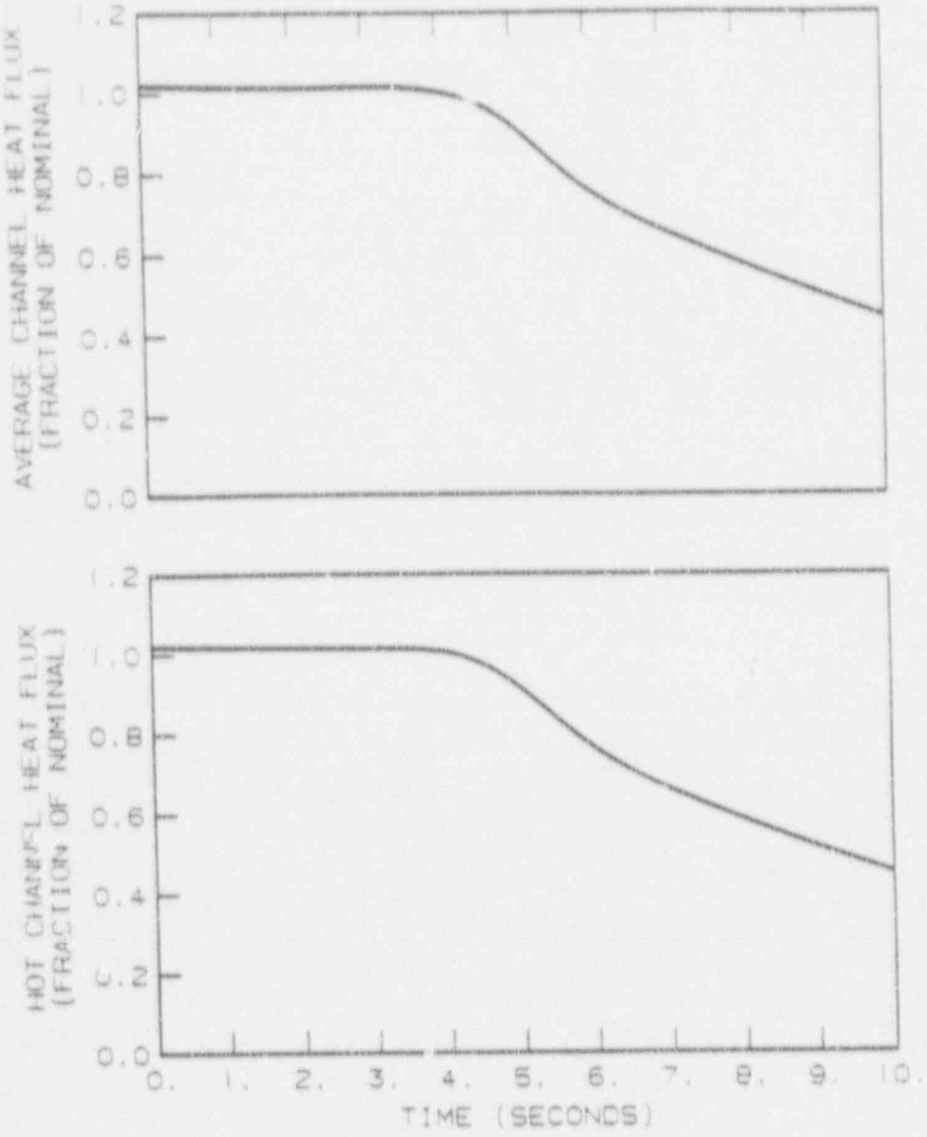

FIGURE 15.3-3
AVERAGE AND HOT CHANNEL
HEAT FLUX TRANSIENT
FOR PARTIAL LOSS OF FLOW,
THREE LOOPS IN OPERATION,
ONE PUMP COASTING DOWN
BEAVER VALLEY POWER STATION-UNIT 2
FINAL SAFETY ANALYSIS REPORT

Figure 15.3-3

Average and Hot Channel Heat Flux Transient
for Partial Loss of Flow
Three Loops in Operation,
One Pump Coasting Down

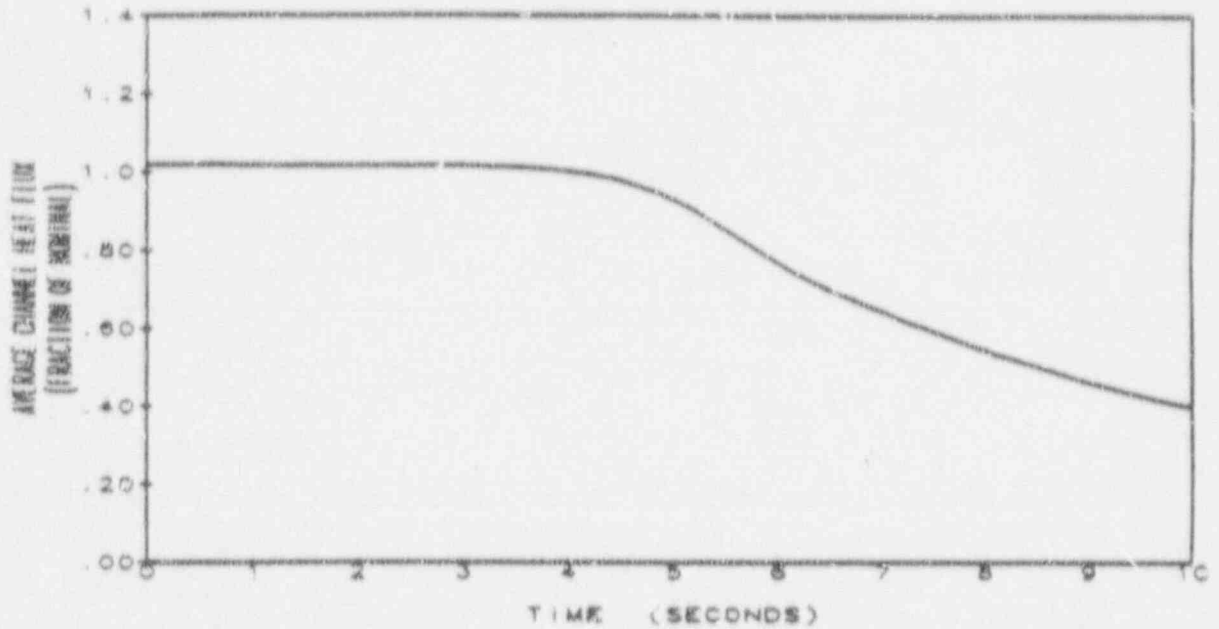

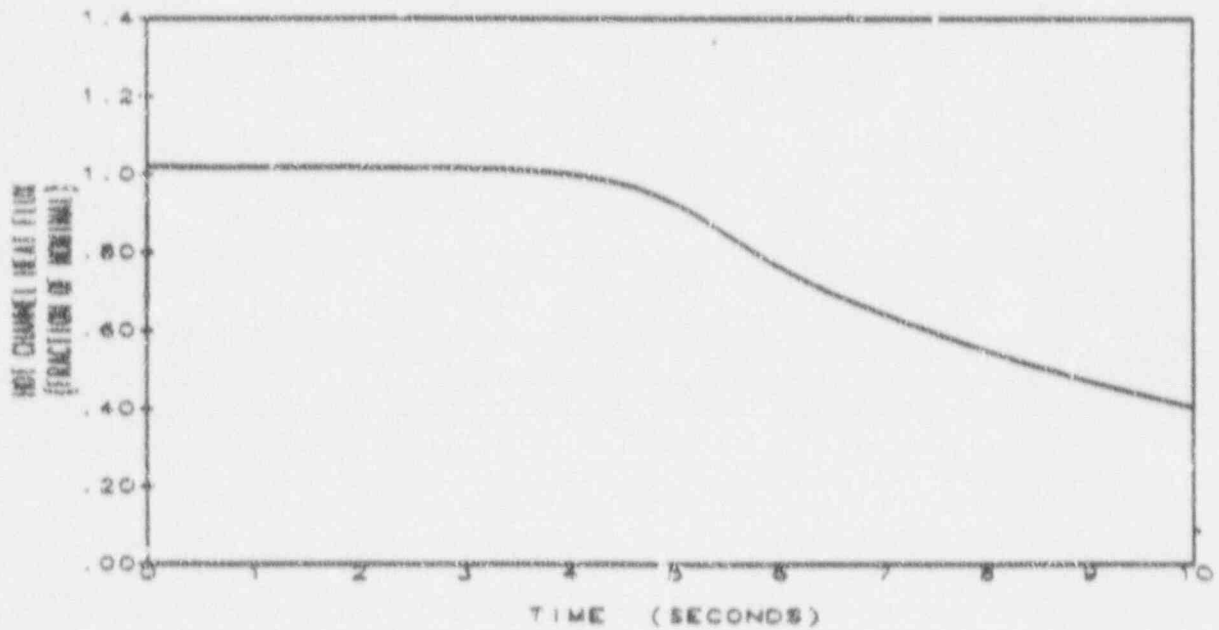

Replace Figure with following Page

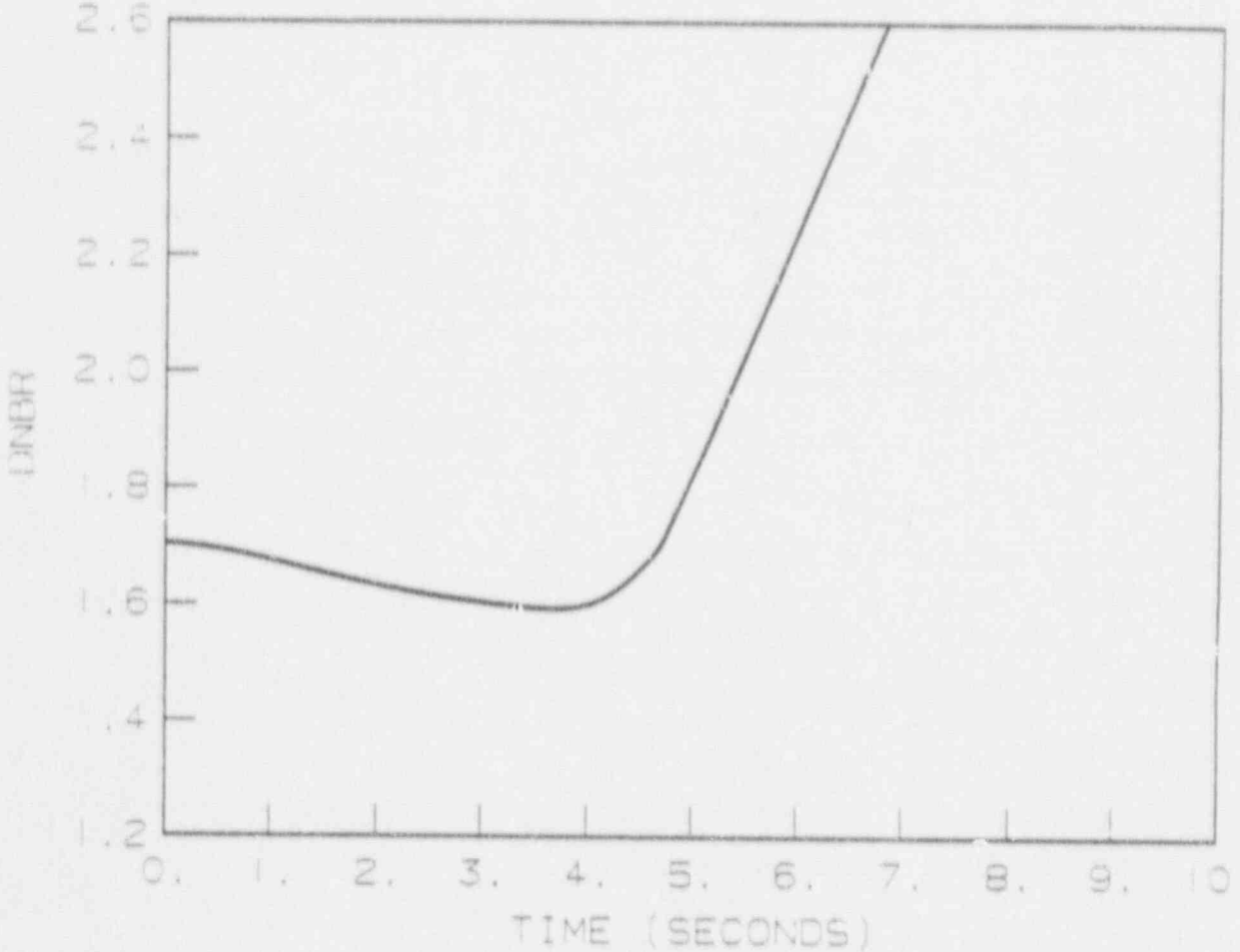

FIGURE 15.3-4
DNBR VS TIME FOR
PARTIAL LOSS OF FLOW,
THREE LOOPS IN OPERATION,
ONE PUMP COASTING DOWN
BEAVER VALLEY POWER STATION-UNIT 2
FINAL SAFETY ANALYSIS REPORT

001 D 18621 4

Figure 15.3-4

DNBR versus Time for Partial Loss of Flow
Three Loops in Operation,
One Pump Coasting Down

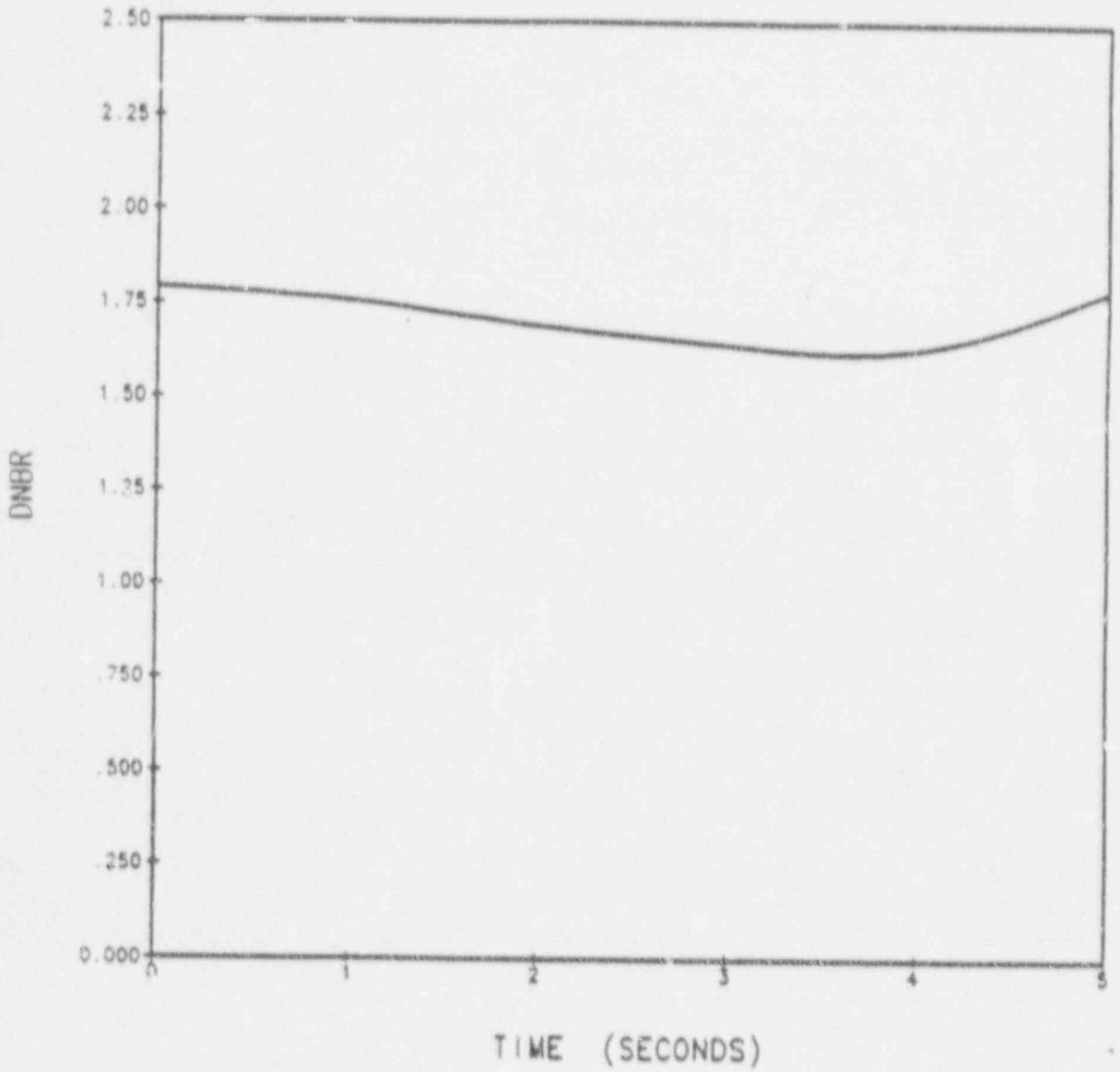

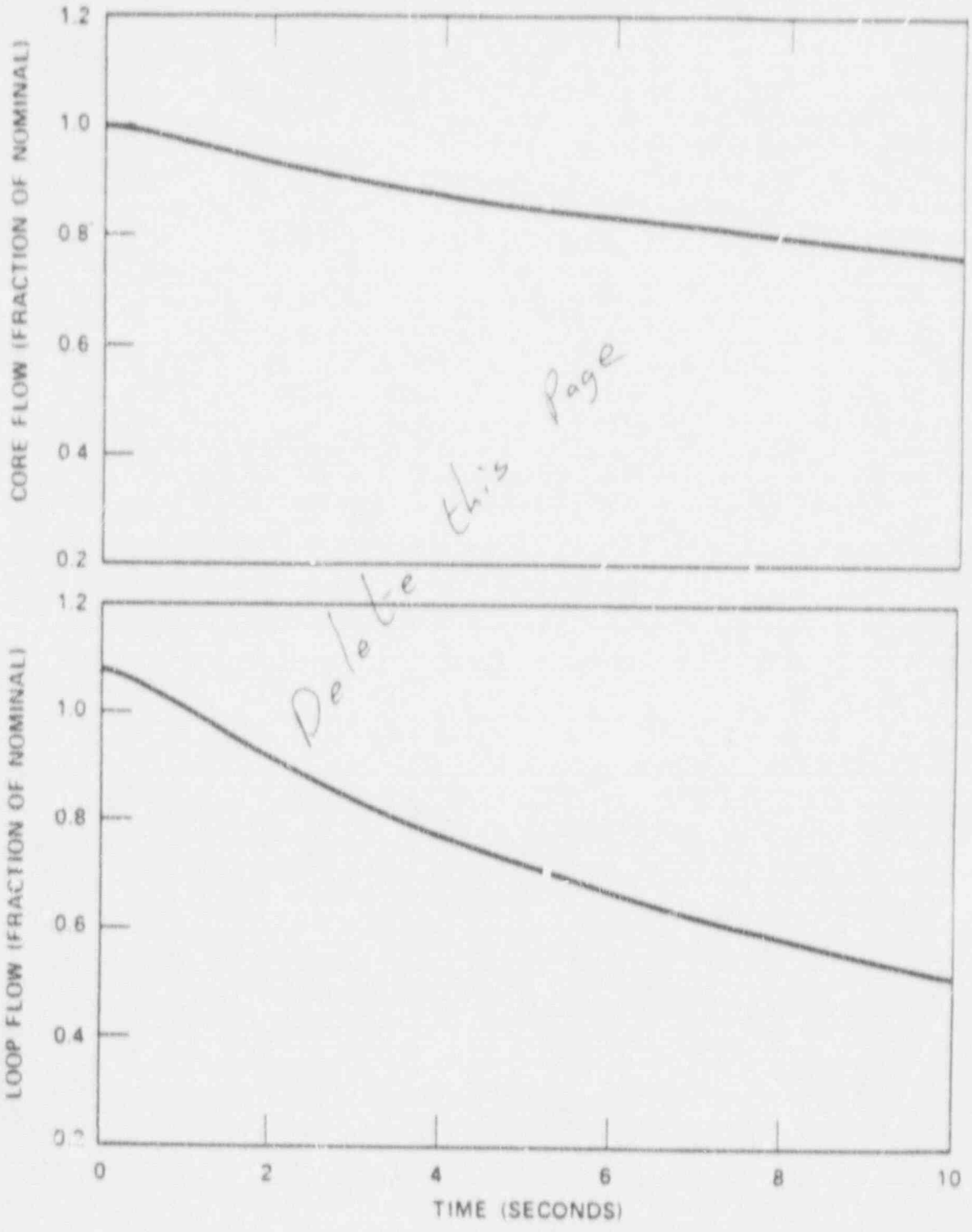

Delete this Page

FIGURE 15.3-5
FLOW TRANSIENT FOR
PARTIAL LOSS OF FLOW,
TWO LOOPS IN OPERATION,
ONE PUMP COASTING DOWN
BEAVER VALLEY POWER STATION-UNIT 2
FINAL SAFETY ANALYSIS REPORT

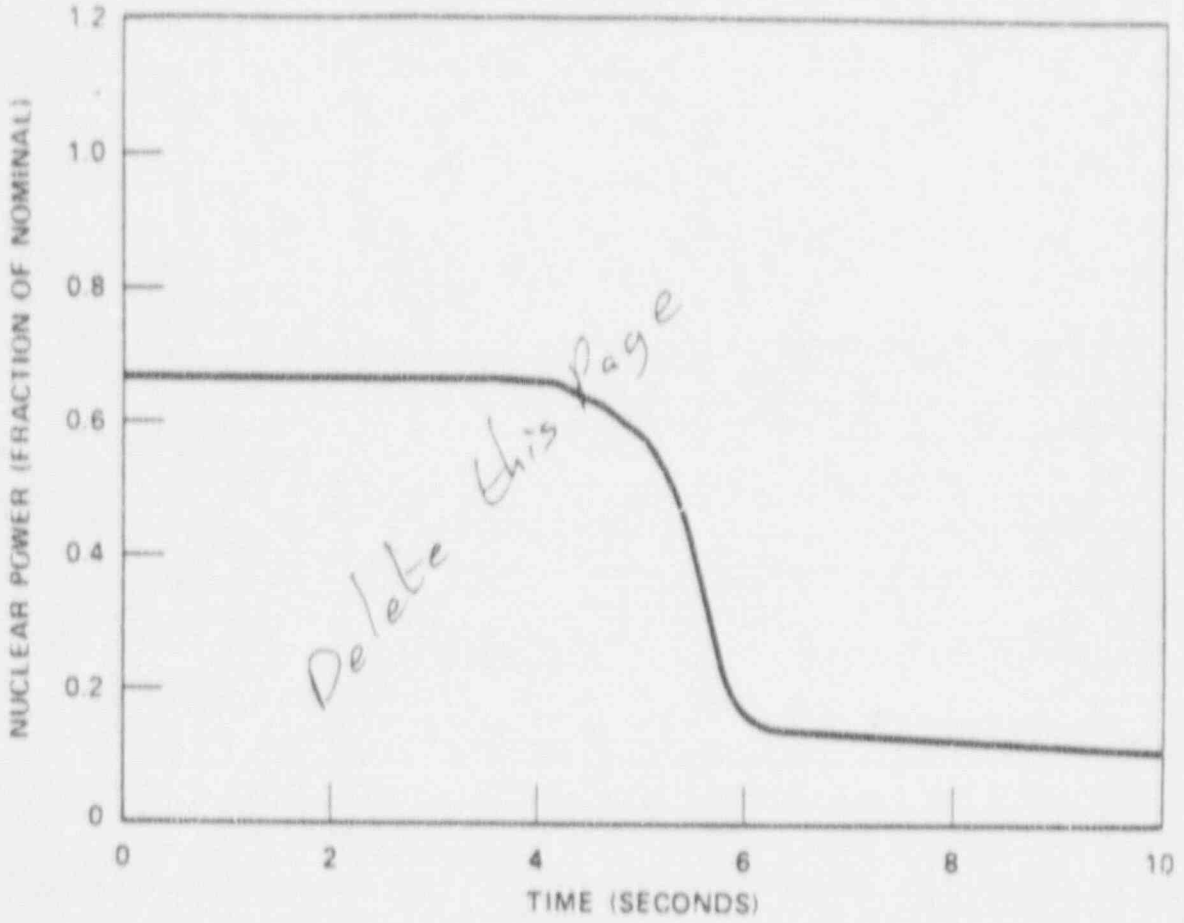

FIGURE 15.3-6
NUCLEAR POWER TRANSIENT
FOR PARTIAL LOSS OF FLOW,
TWO LOOPS IN OPERATION,
ONE PUMP COASTING DOWN
BEAVER VALLEY POWER STATION-UNIT 2
FINAL SAFETY ANALYSIS REPORT

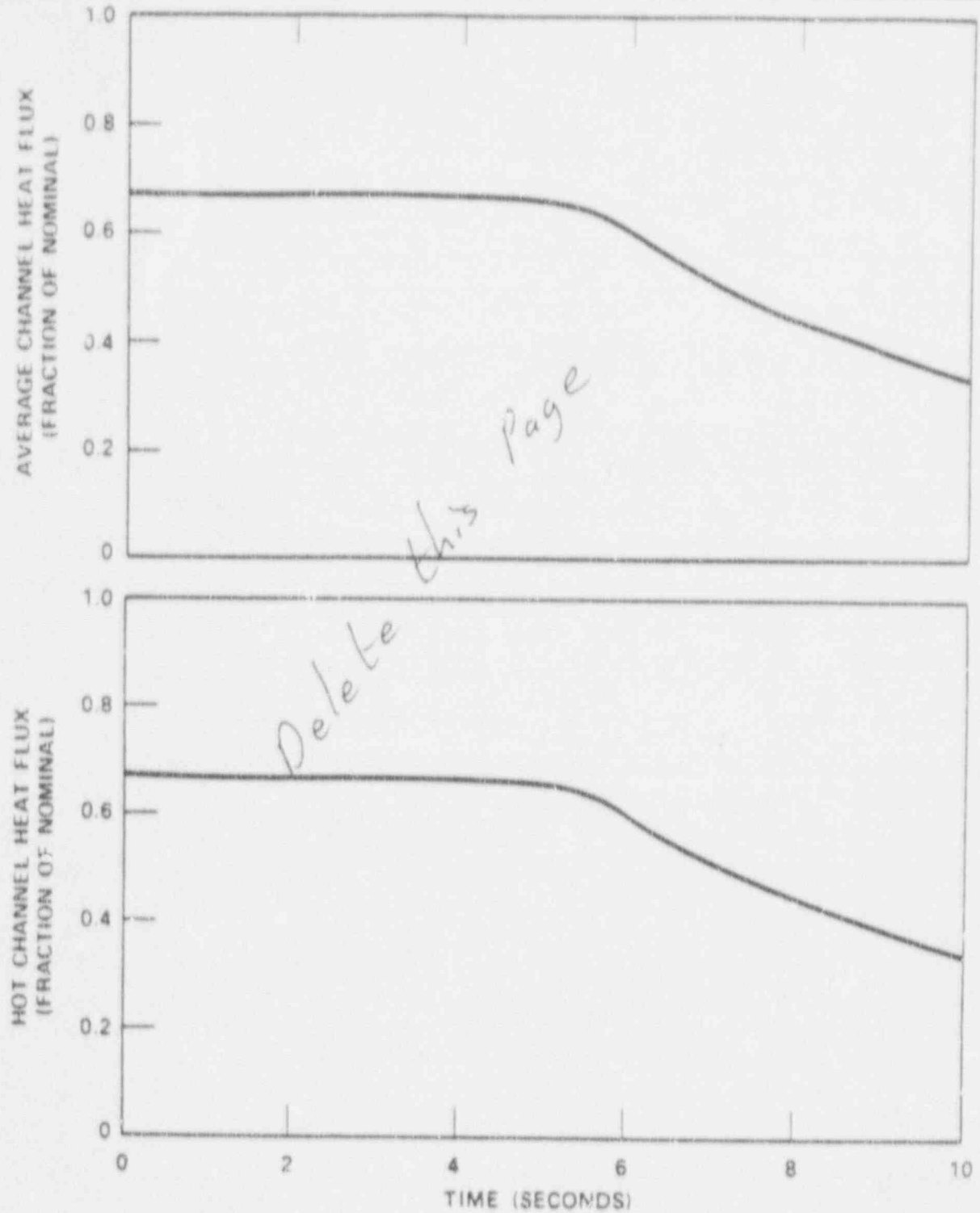

Delete this page

FIGURE 15.3-7
AVERAGE AND HOT CHANNEL
HEAT FLUX TRANSIENTS
FOR PARTIAL LOSS OF FLOW,
TWO LOOPS IN OPERATION,
ONE PUMP COASTING DOWN
BEAVER VALLEY POWER STATION-UNIT 2
FINAL SAFETY ANALYSIS REPORT

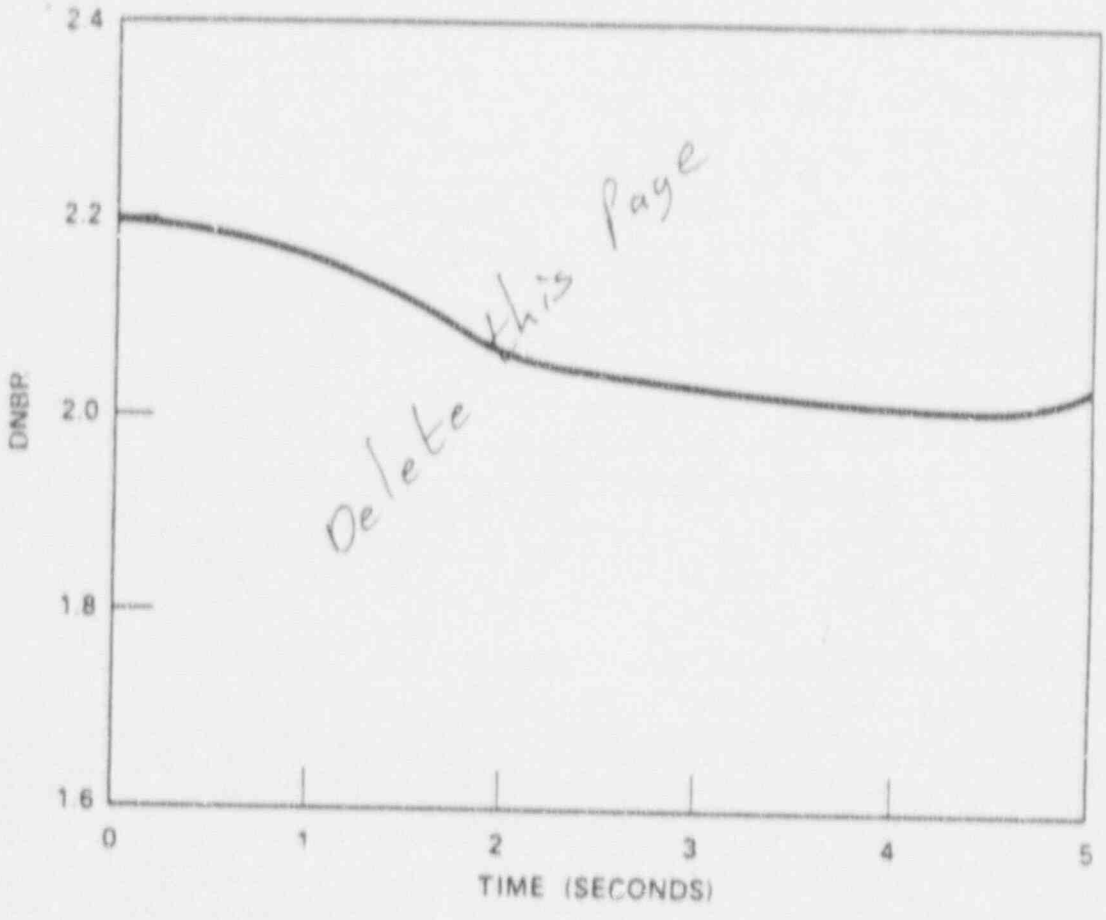

FIGURE 15.3-8
DNBR VS. TIME FOR PARTIAL LOSS OF FLOW, TWO LOOPS IN OPERATION, ONE PUMP COASTING DOWN
BEAVER VALLEY POWER STATION-UNIT 2
FINAL SAFETY ANALYSIS REPORT

Replace Figure with following Page

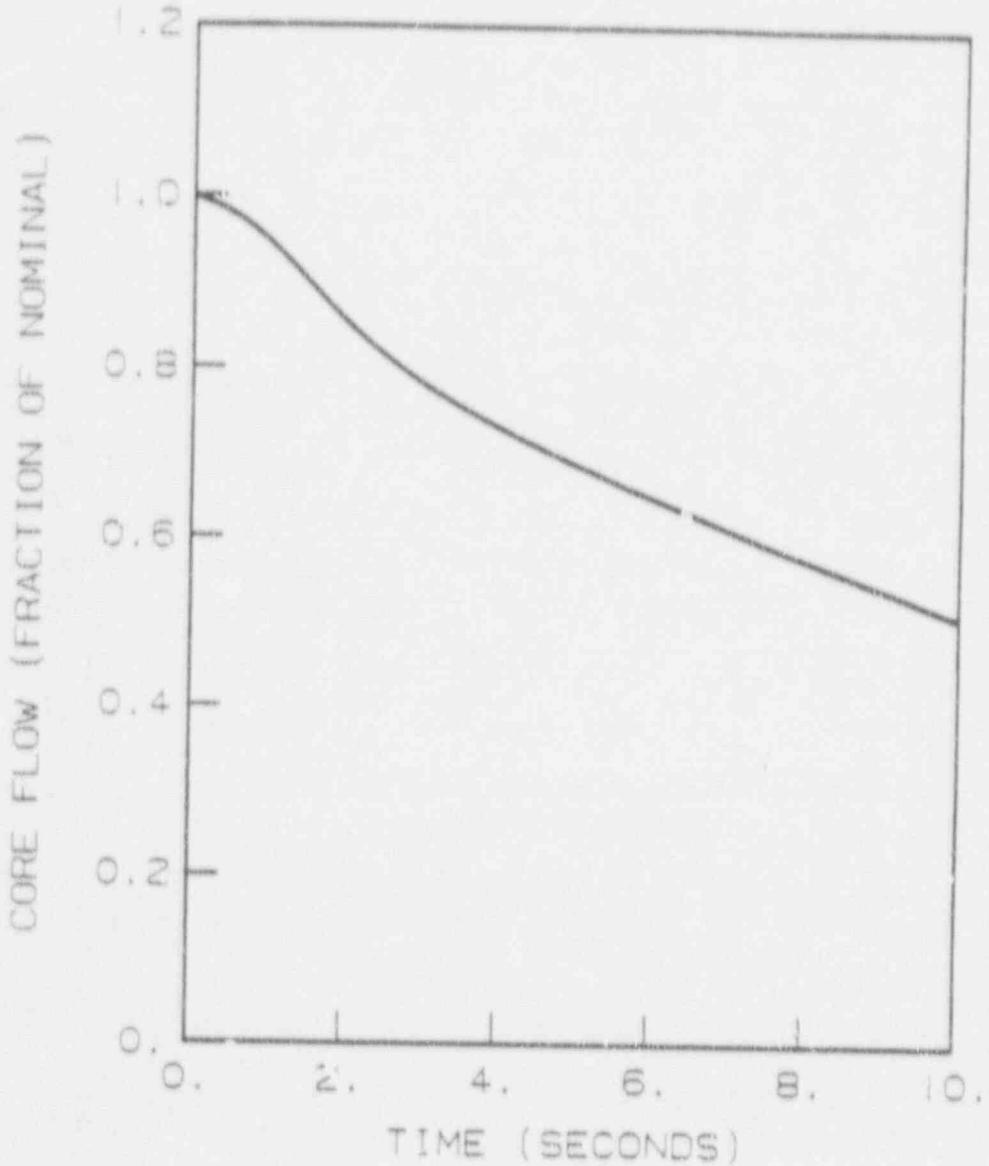

FIGURE 15.3-9
CORE FLOW COASTDOWN VS. TIME FOR THREE LOOPS IN OPERATION, THREE PUMPS COASTING DOWN, COMPLETE LOSS OF FLOW
BEAVER VALLEY POWER STATION-UNIT 2
FINAL SAFETY ANALYSIS REPORT

001-D-18621.5

Figure 15.3-9

Core Flow Coastdown versus Time for Three Loops In Operation,
Three Pumps Coasting Down,
Complete Loss of Flow

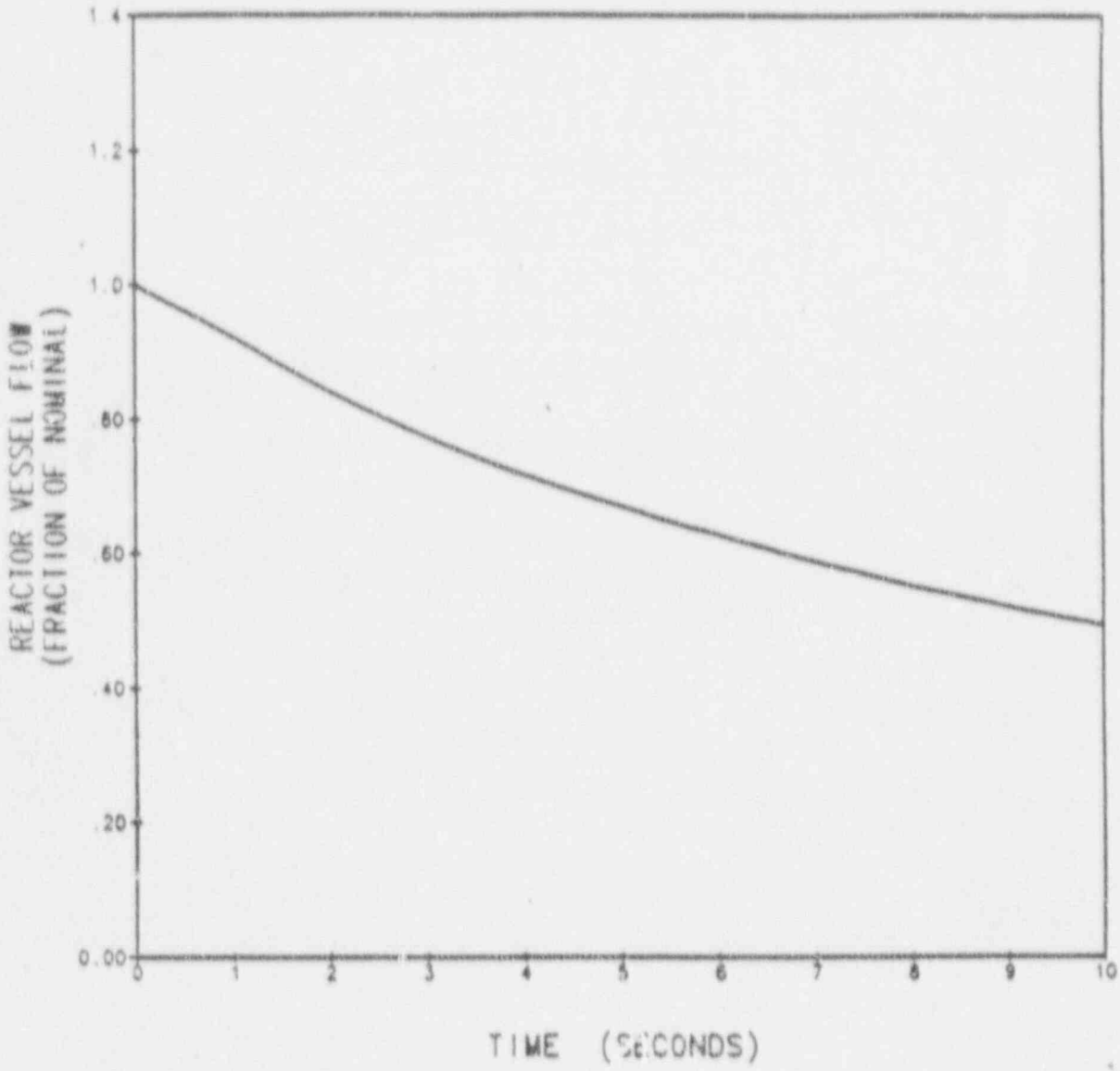

Replace Figures with following Page

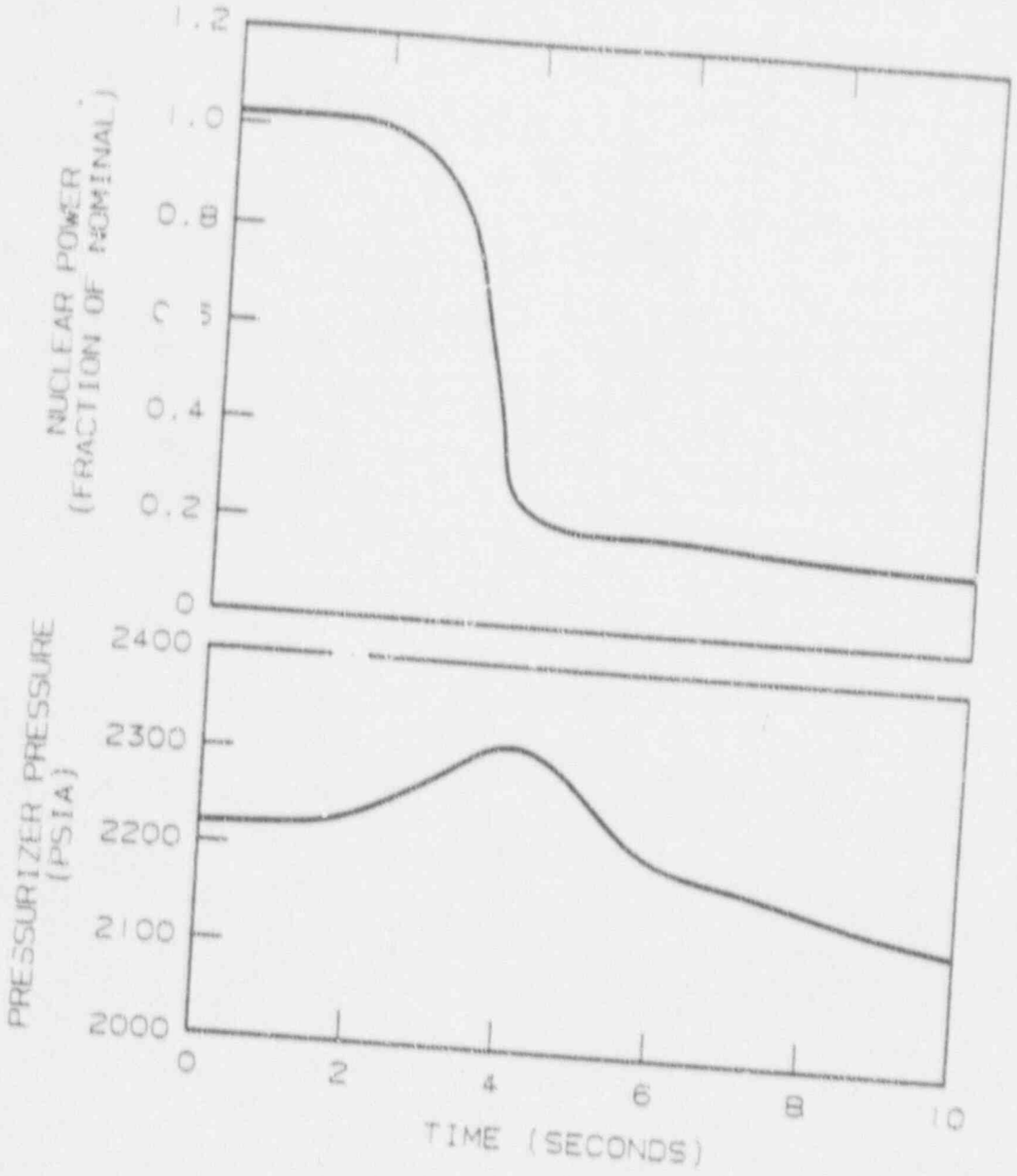

FIGURE 15.3-10
NUCLEAR POWER TRANSIENT AND
PRESSURIZER PRESSURE TRANSIENT
FOR THREE LOOPS IN OPERATION,
THREE LOOPS COASTING DOWN,
COMPLETE LOSS OF FLOW
BEAVER VALLEY POWER STATION-UNIT 2
FINAL SAFETY ANALYSIS REPORT

002-0-18621.14

Figure 15.3-10

Nuclear Power Transient and Pressurizer Pressure Transient
For Three Loops in Operation,
Three Loops Coasting Down,
Complete Loss of Flow

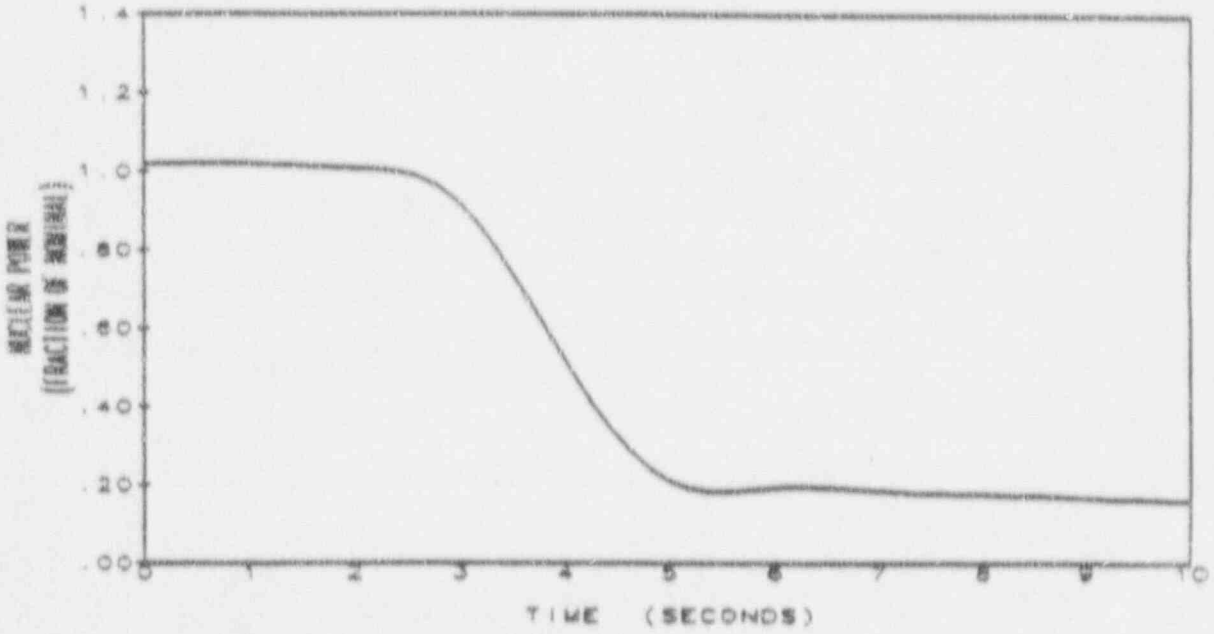

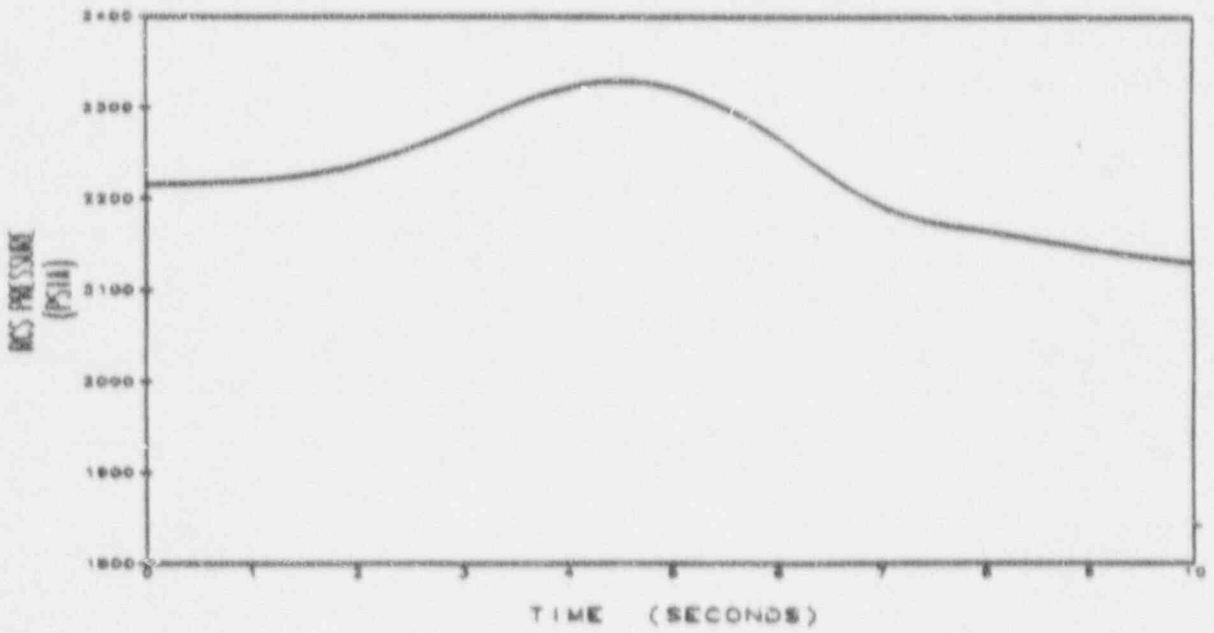

Replace Figures with following Page

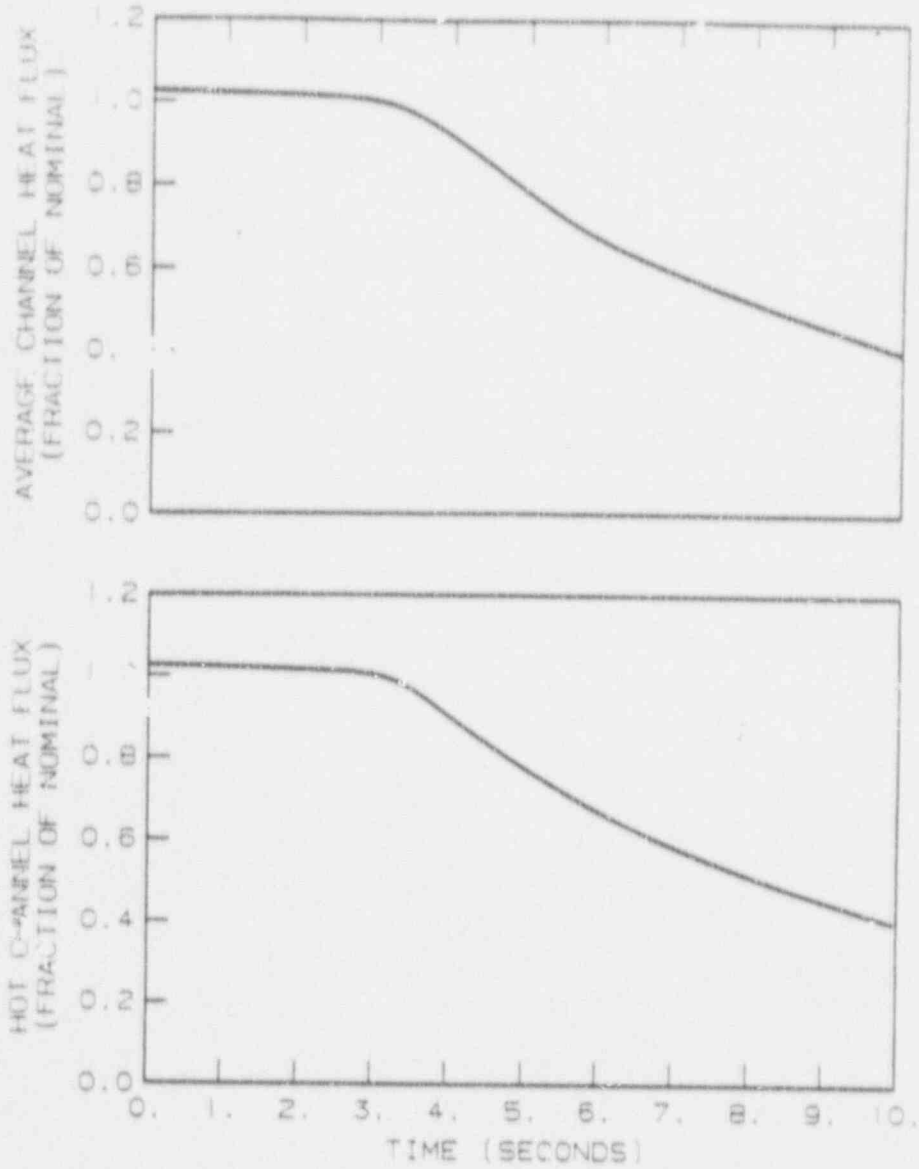

FIGURE 15.3-11
AVERAGE AND HOT CHANNEL HEAT FLUX TRANSIENTS FOR THREE LOOPS IN OPERATION, THREE PUMPS COASTING DOWN, COMPLETE LOSS OF FLOW
BEAVER VALLEY POWER STATION-UNIT 2
FINAL SAFETY ANALYSIS REPORT

001:D:18621.7

Figure 15.3-11

Average and Hot Channel Heat Flux Transients
for Three Loops in Operation,
Three Pumps Coasting Down,
Complete Loss of Flow

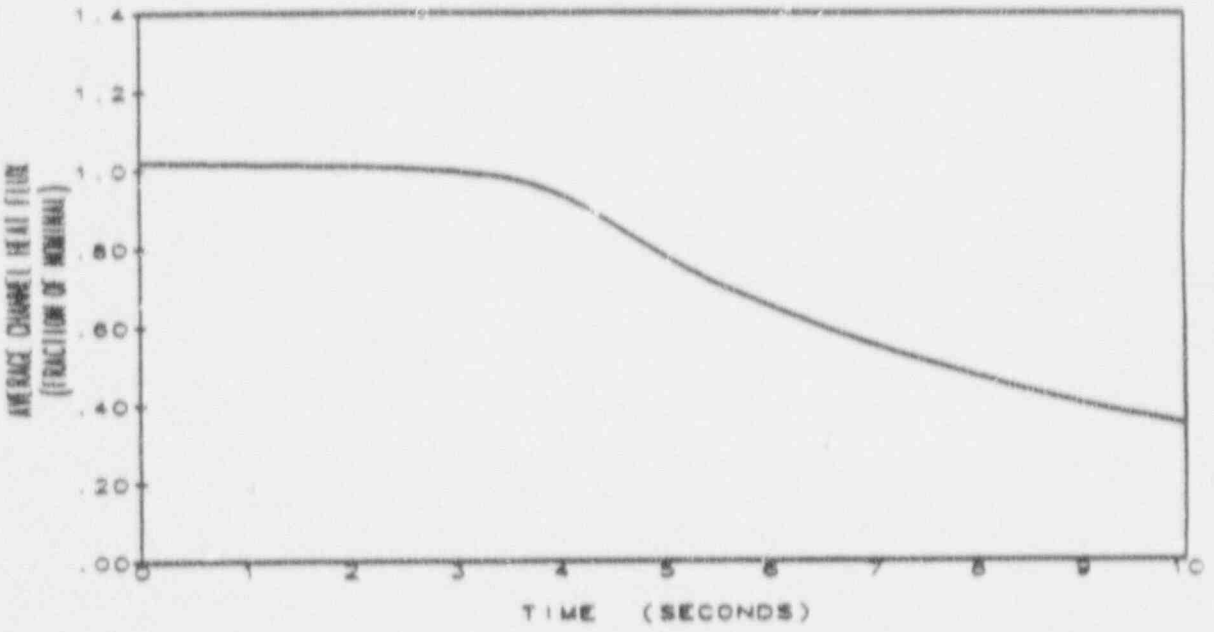

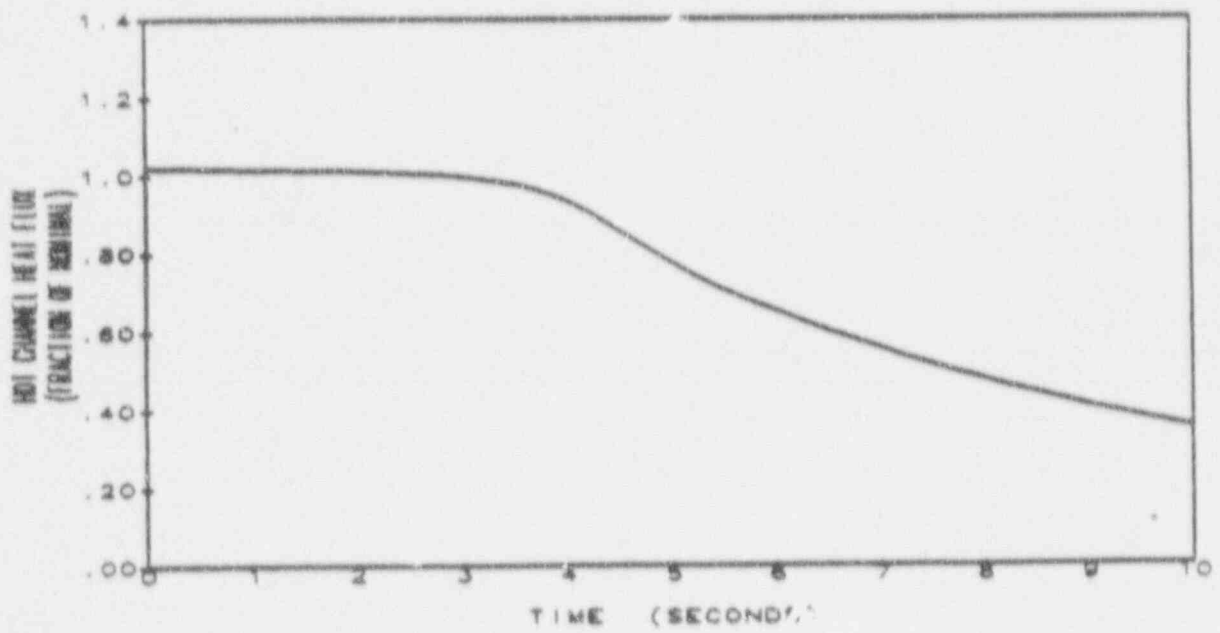

Replace Figure with following Page

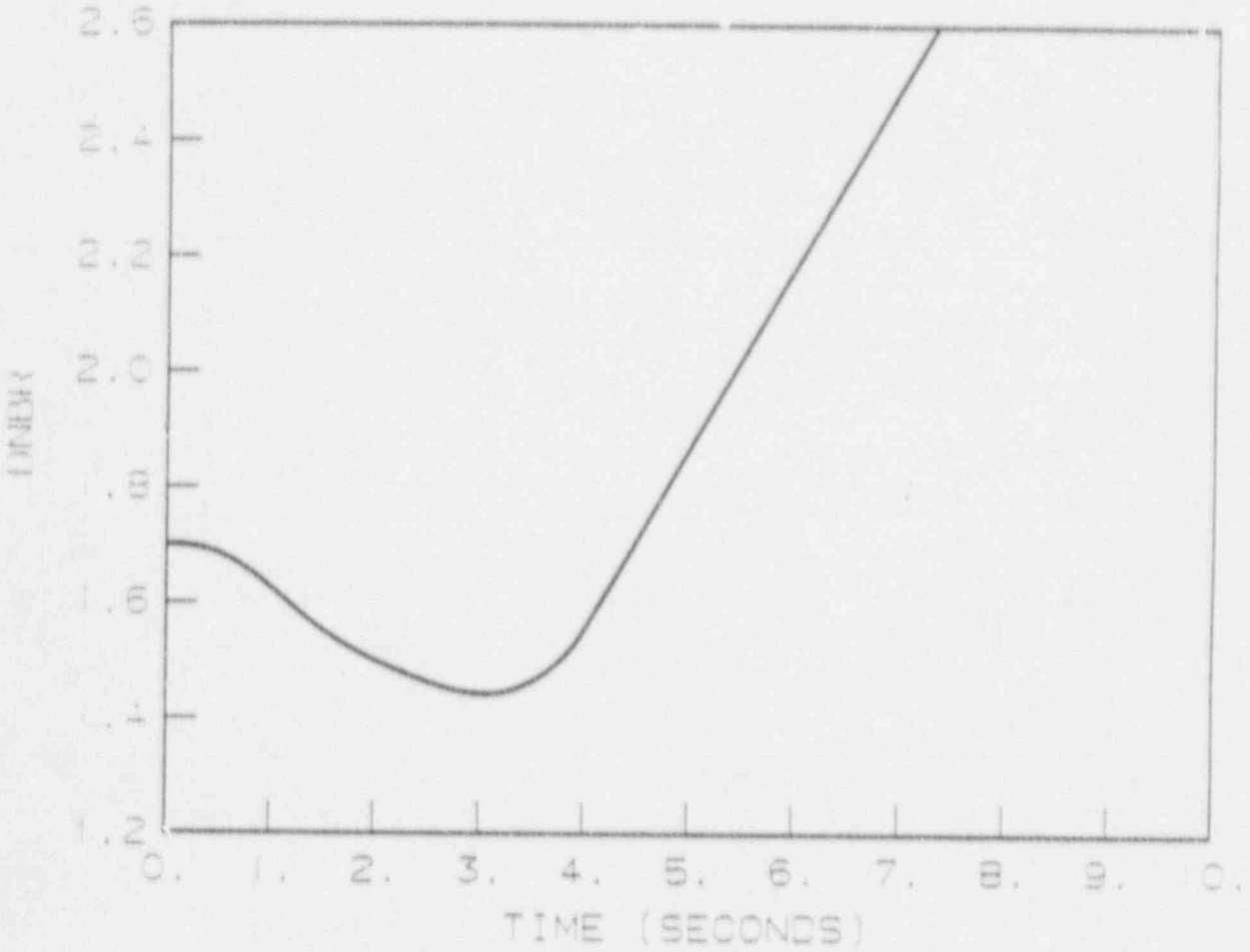

FIGURE 15.3-12
DNBR VS. TIME FOR THREE LOOPS IN OPERATION, THREE PUMPS COASTING DOWN, COMPLETE LOSS OF FLOW
BEAVER VALLEY POWER STATION-UNIT 2
FINAL SAFETY ANALYSIS REPORT

001 D-18621.8

Figure 15.3-12

DNBR vs Time for Three Loops in Operation,
Three Pumps Coasting Down,
Complete Loss of Flow

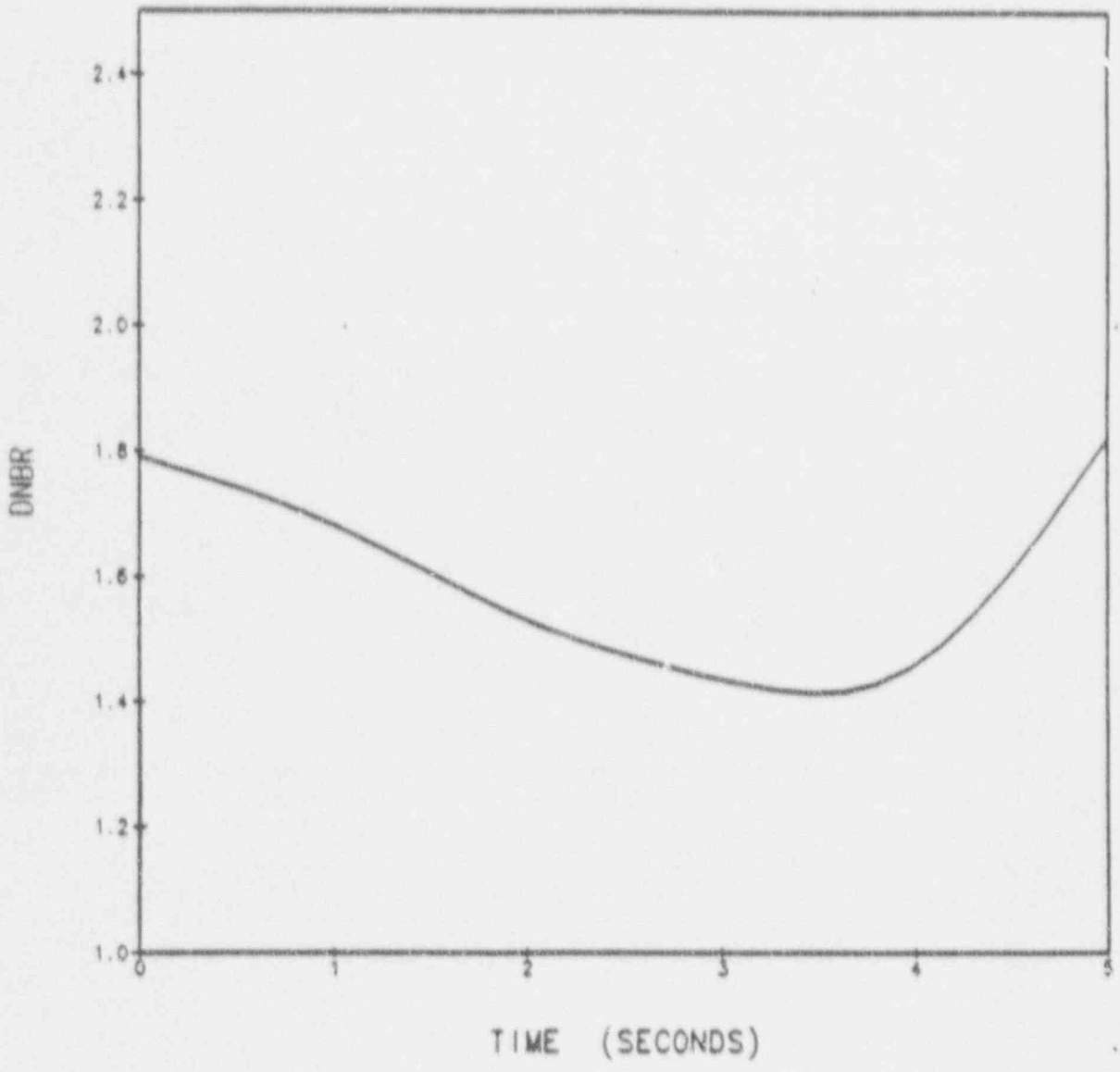

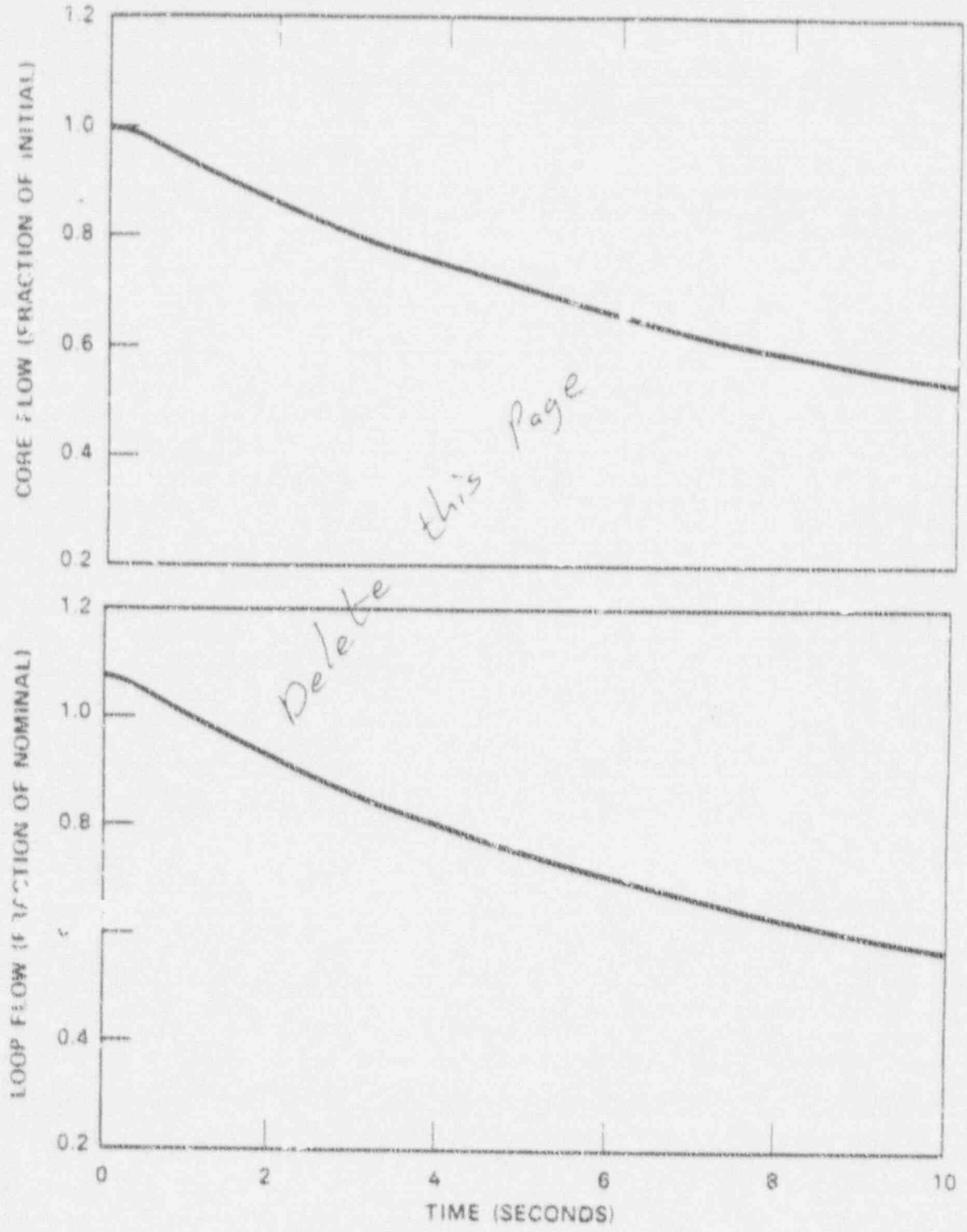

Delete this page

FIGURE 15.3-13
FLOW TRANSIENTS FOR
TWO LOOPS IN OPERATION,
TWO PUMPS COASTING DOWN,
COMPLETE LOSS OF FLOW
BEAVER VALLEY POWER STATION-UNIT 2
FINAL SAFETY ANALYSIS REPORT

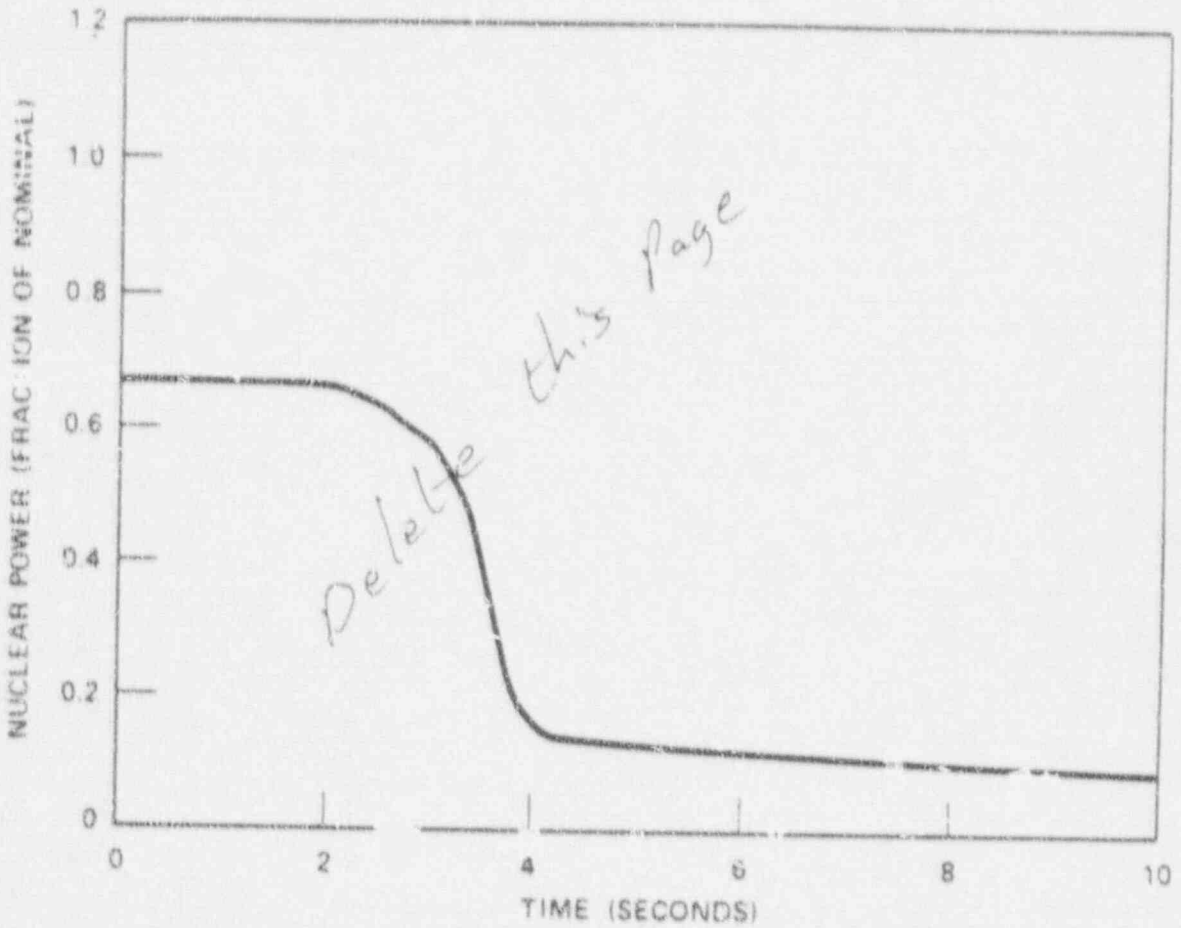

FIGURE 15.3-14
NUCLEAR POWER TRANSIENT
FOR TWO LOOPS IN OPERATION,
TWO PUMPS COASTING DOWN,
COMPLETE LOSS OF FLOW
BEAVER VALLEY POWER STATION-UNIT 2
FINAL SAFETY ANALYSIS REPORT

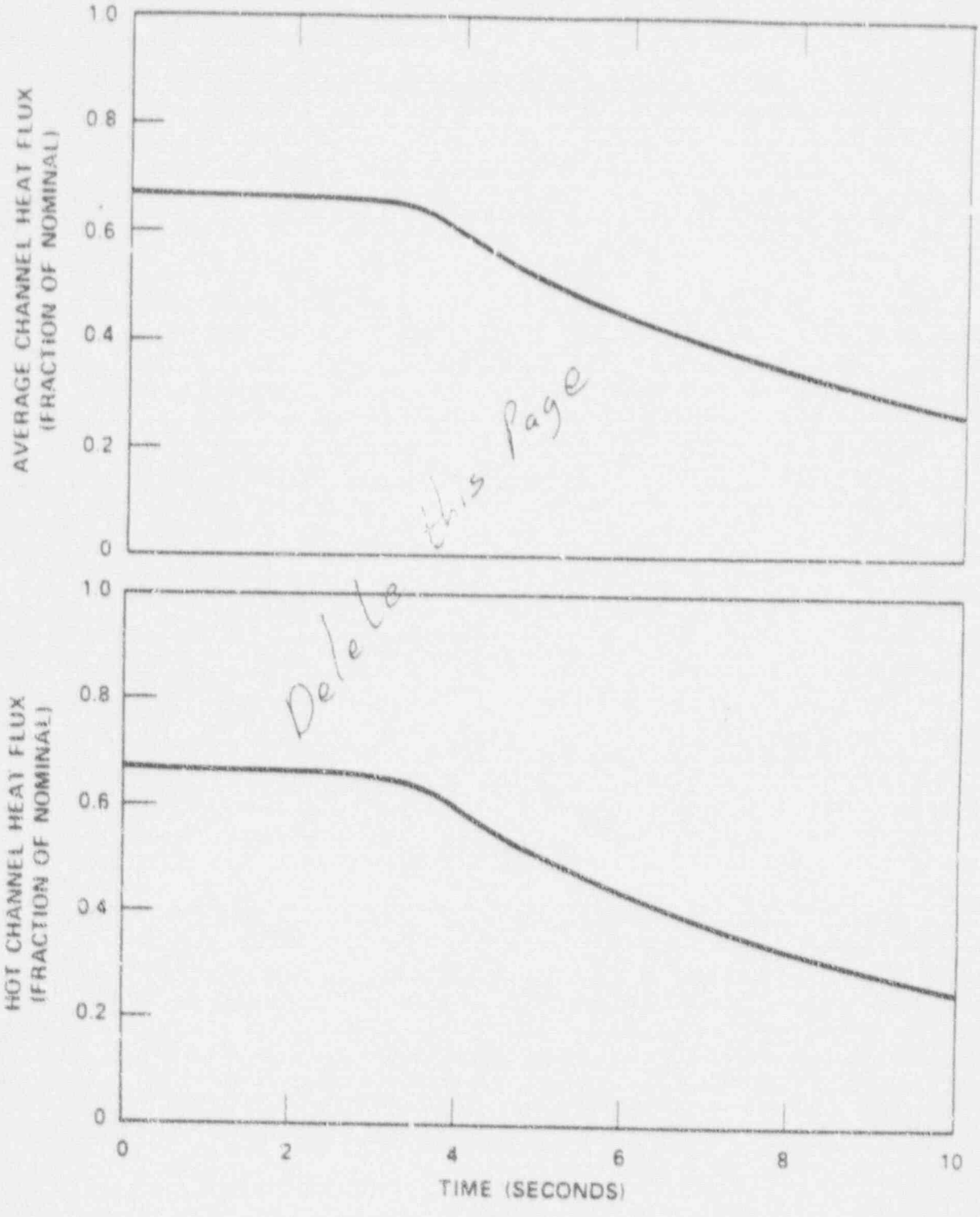

Delete this page

FIGURE 15.3-15
AVERAGE AND HOT CHANNEL
HEAT FLUX TRANSIENTS
FOR TWO LOOPS IN OPERATION,
TWO PUMPS COASTING DOWN
BEAVER VALLEY POWER STATION-UNIT 2
FINAL SAFETY ANALYSIS REPORT

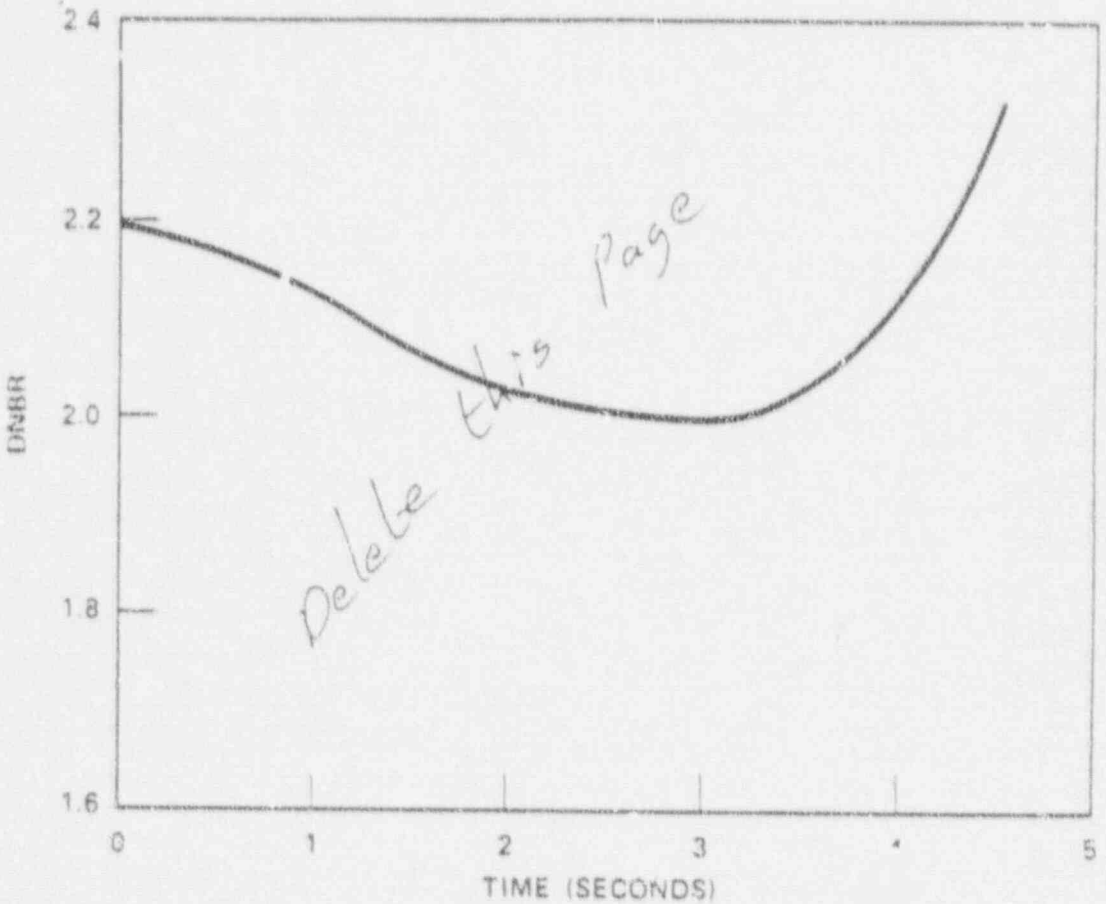

FIGURE 15.3-16
DNBR VS. TIME FOR TWO LOOPS IN OPERATION, TWO PUMPS COASTING DOWN, COMPLETE LOSS OF FLOW
BEAVER VALLEY POWER STATION - UNIT 2
FINAL SAFETY ANALYSIS REPORT

Replace Figures with following Page

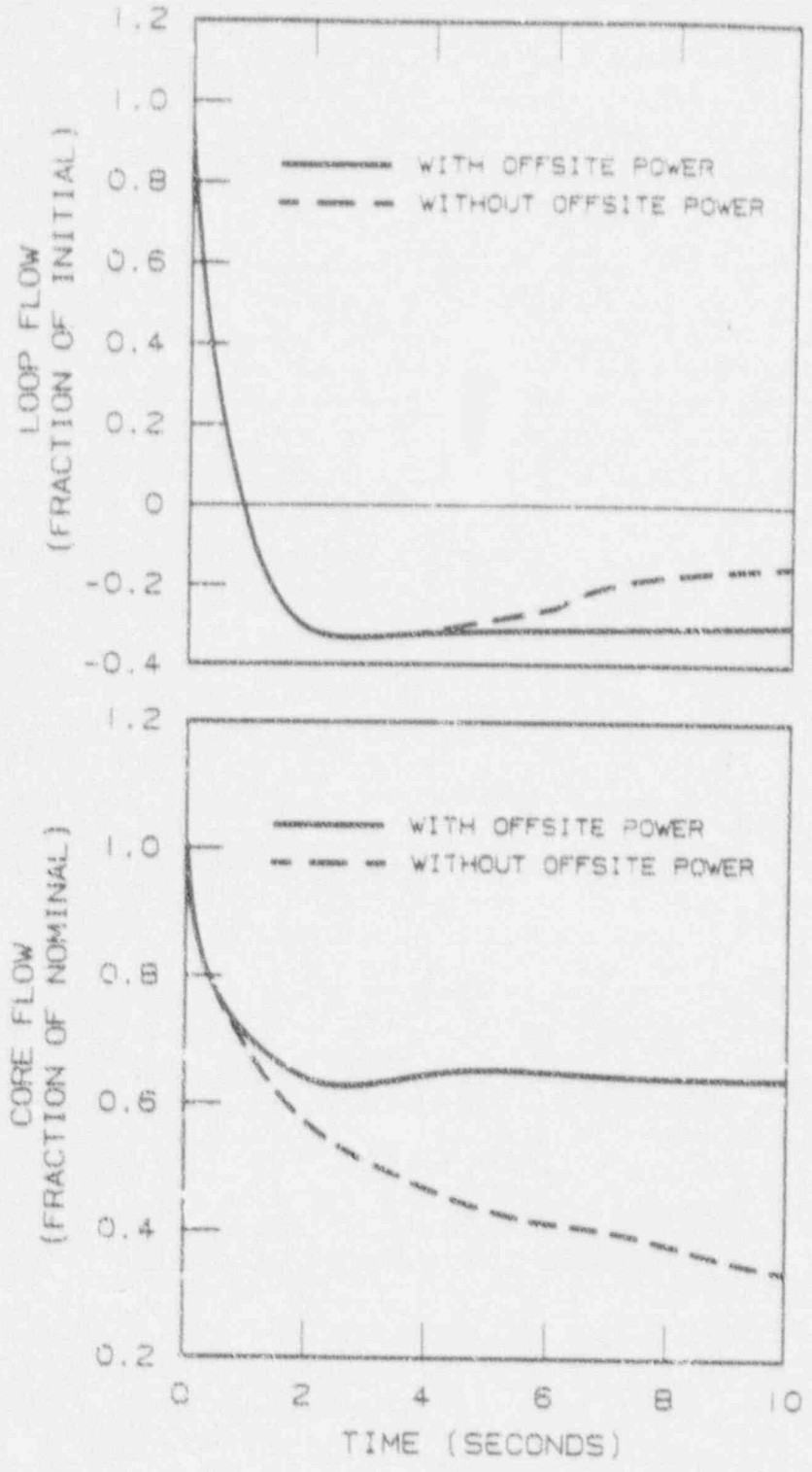

FIGURE 15.3-17
FLOW TRANSIENTS FOR THREE LOOPS IN OPERATION, ONE LOCKED ROTOR
BEAVER VALLEY POWER STATION-UNIT 2
FINAL SAFETY ANALYSIS REPORT

004-0-19190-1

Figure 15.3-17

Flow Transients for Three Loops in Operation,
One Locked Rotor

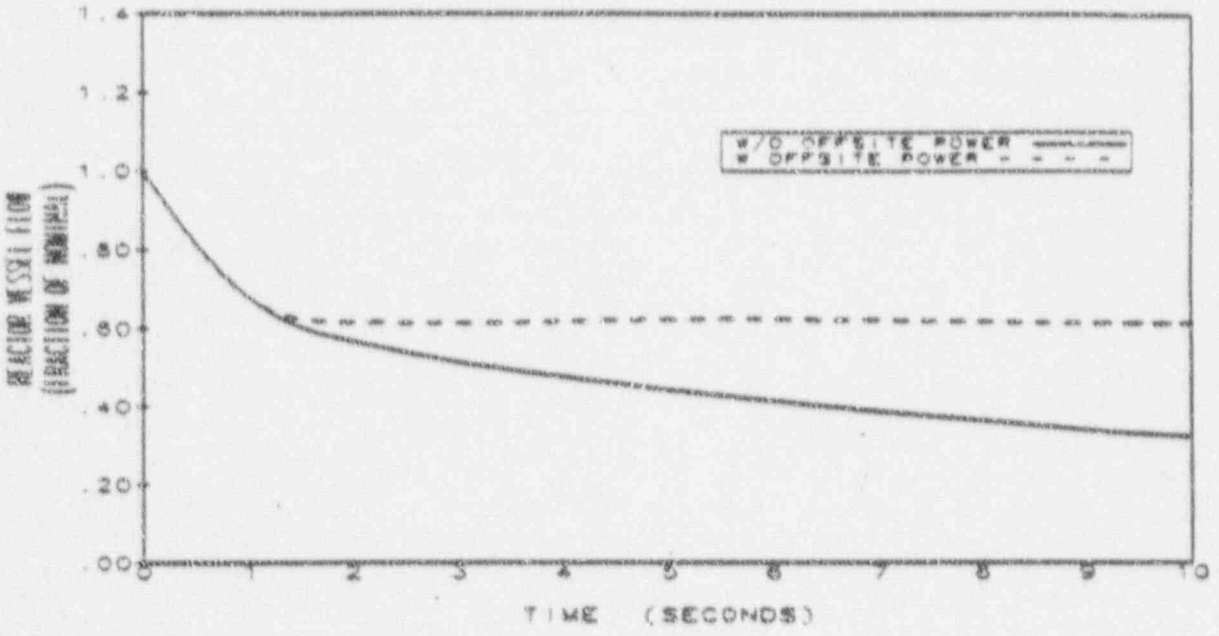

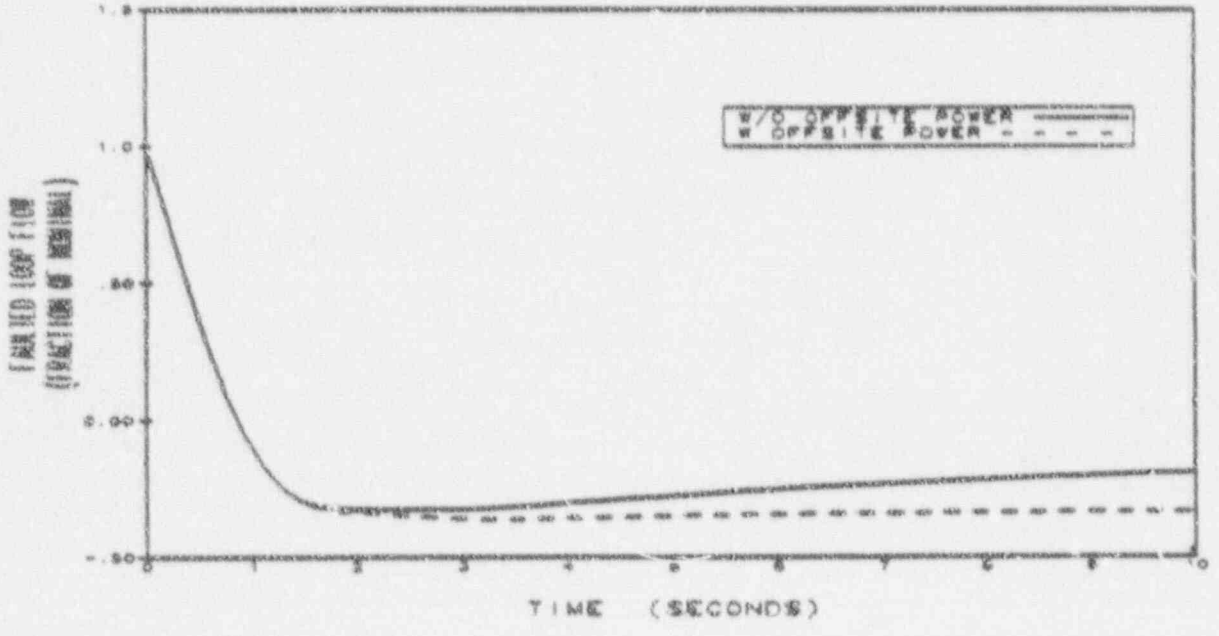

Replace Figure with Following Page

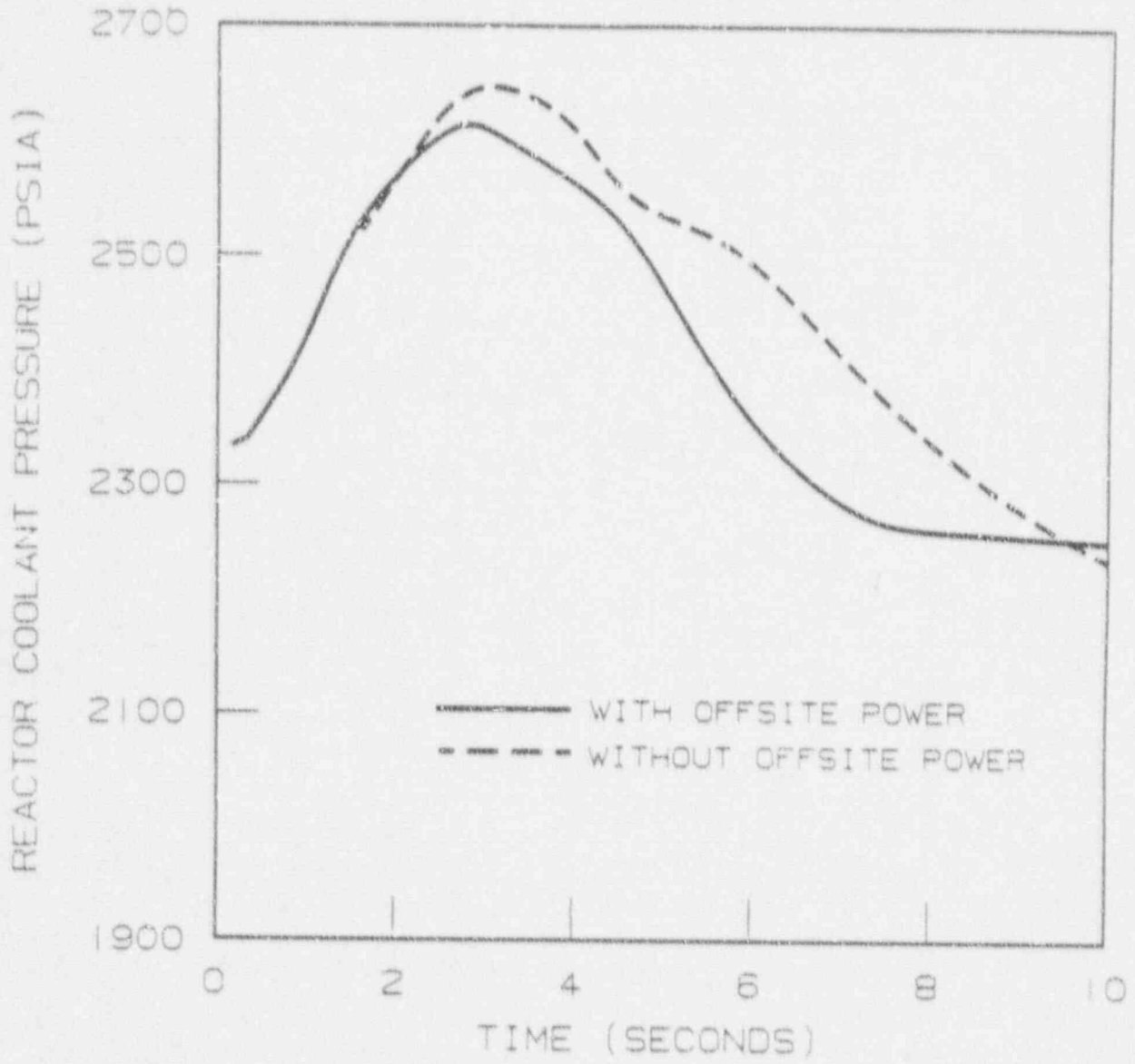

FIGURE 15.3-18
REACTOR COOLANT SYSTEM PRESSURE TRANSIENT FOR THREE LOOPS IN OPERATION, ONE LOCKED ROTOR
BEAVER VALLEY POWER STATION-UNIT 2
FINAL SAFETY ANALYSIS REPORT

004-0-19190-2

Figure 15.3-18

Reactor Coolant System Pressure Transient
for Three Loops in Operation
One Locked Rotor

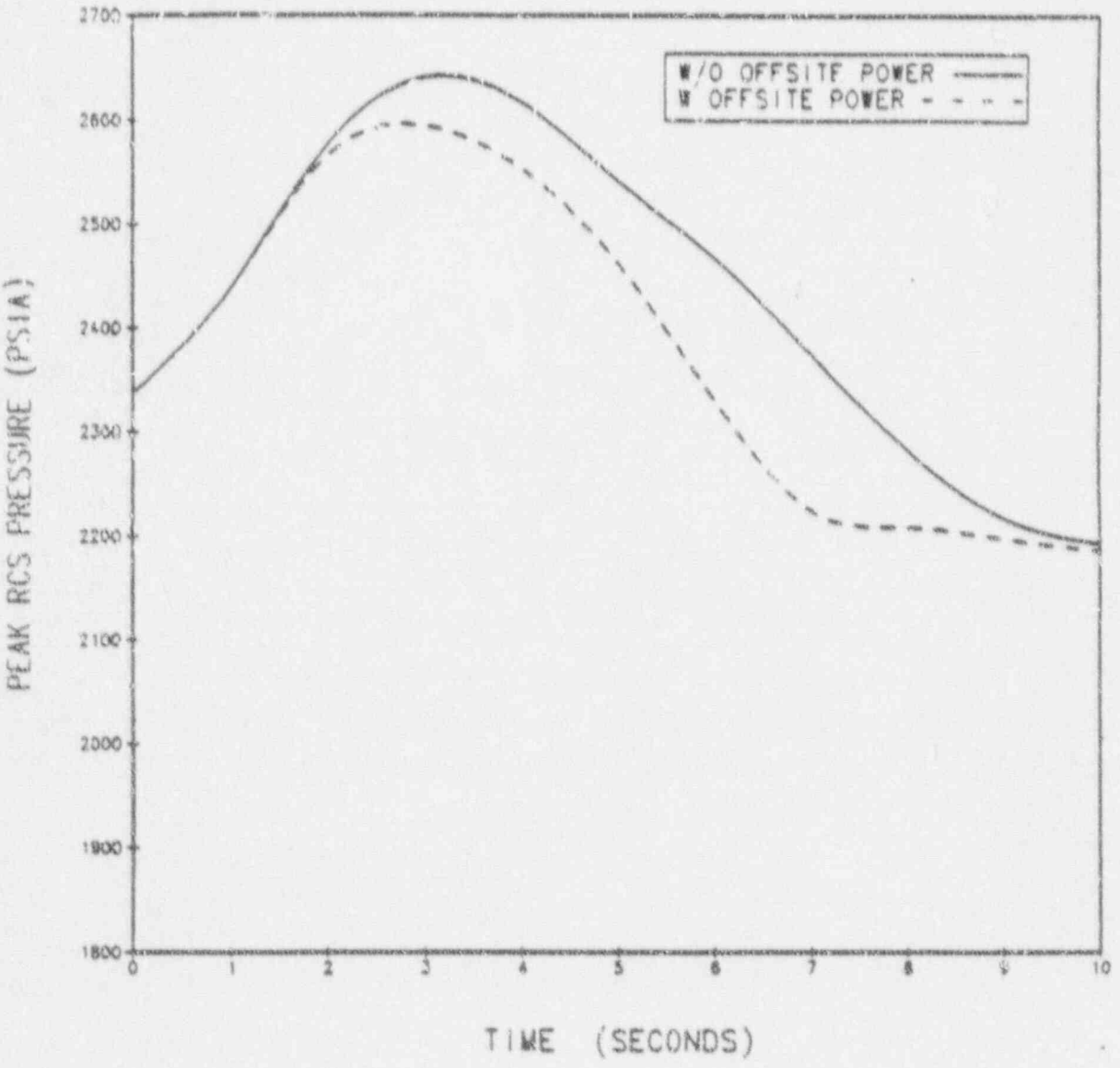

Replace Figures with following Page

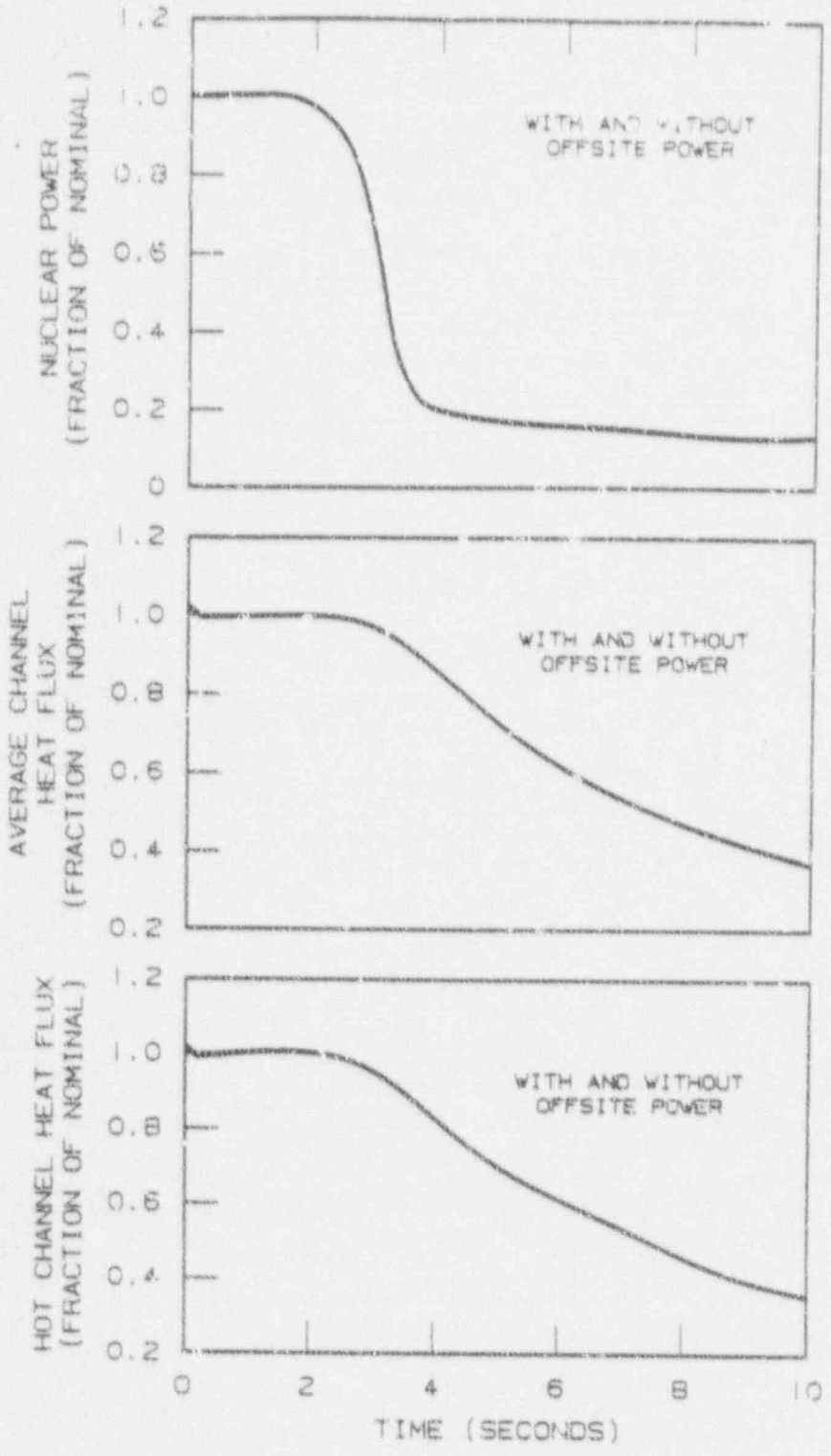

FIGURE 15.3-19
NUCLEAR POWER TRANSIENT, AVERAGE AND HOT CHANNEL HEAT FLUX TRANSIENTS FOR THREE LOOPS IN OPERATION, ONE LOCKED ROTOR

BEAVER VALLEY POWER STATION-UNIT 2
FINAL SAFETY ANALYSIS REPORT

Figure 15.3-19

Nuclear Power Transient, Average and Hot Channel Heat Flux Transients for Three Loops in Operation, One Locked Rotor

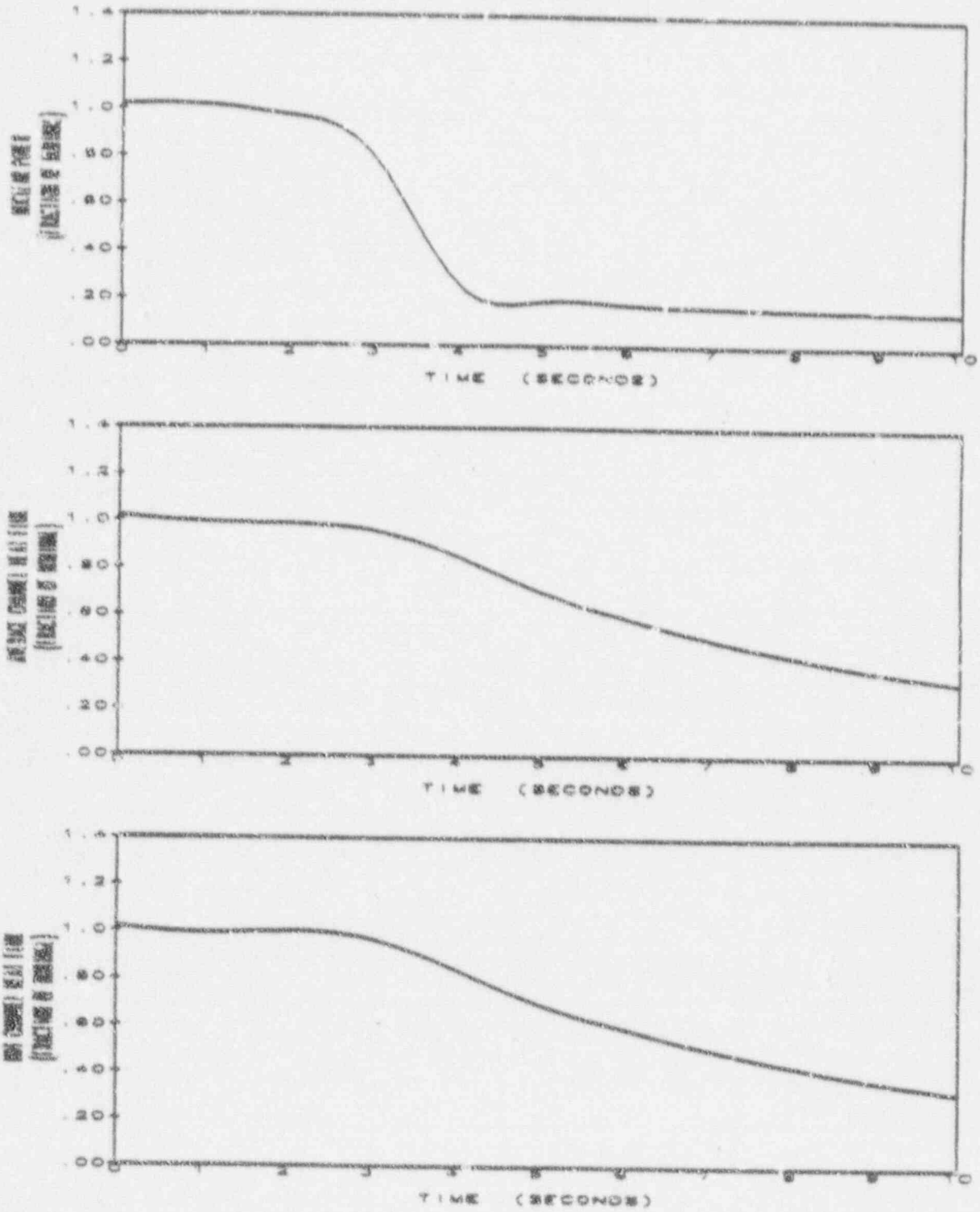

Replace Figures with following Page

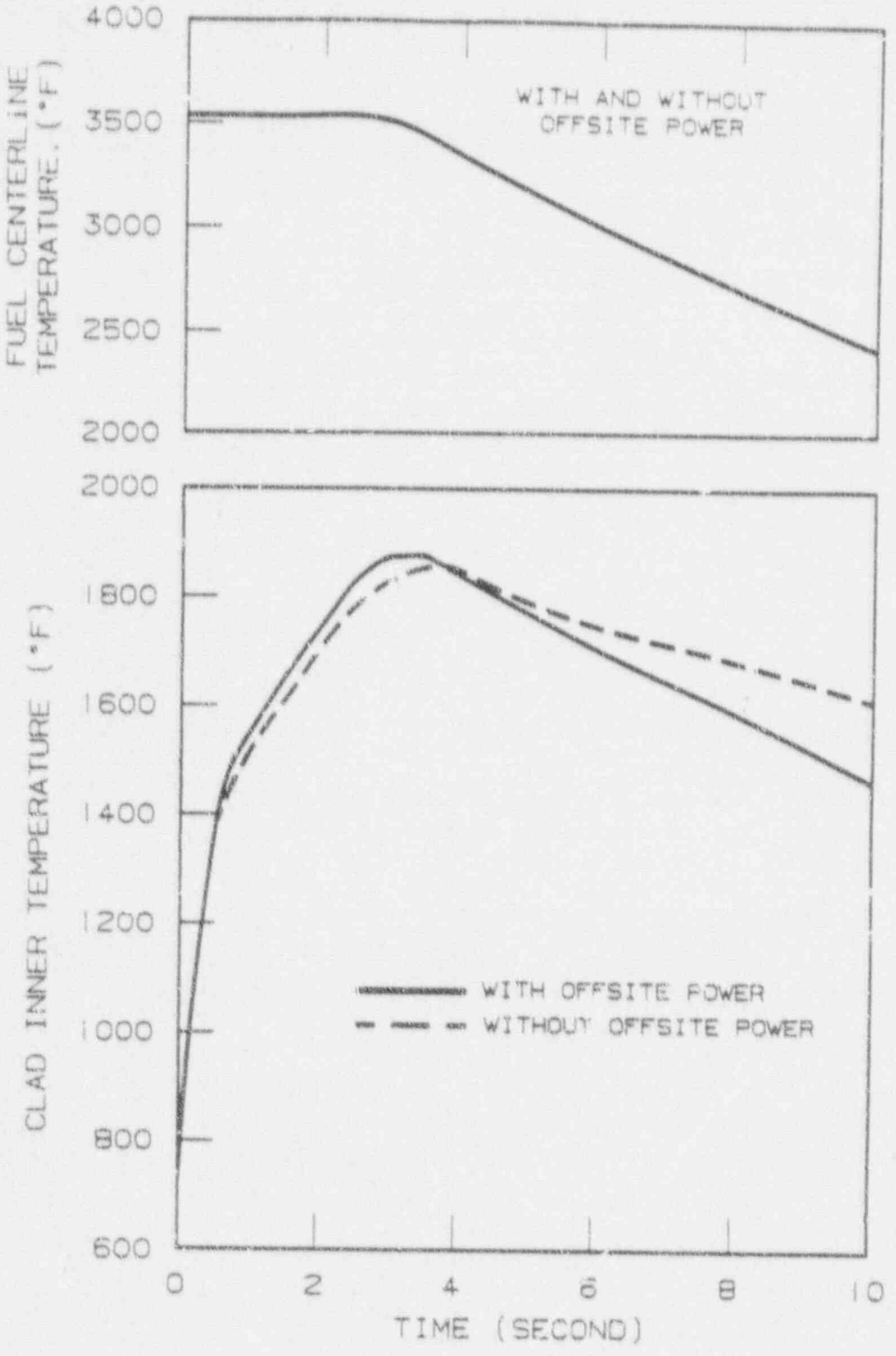

FIGURE 15.3-20
MAXIMUM CLAD AND FUEL CENTERLINE TEMPERATURES AT HOT SPOT FOR THREE LOOPS IN OPERATION, ONE LOCKED ROTOR

Figure 15.3-20

Maximum Clad and Fuel Centerline Temperatures at Hot Spot for Three Loops in Operation One Locked Rotor

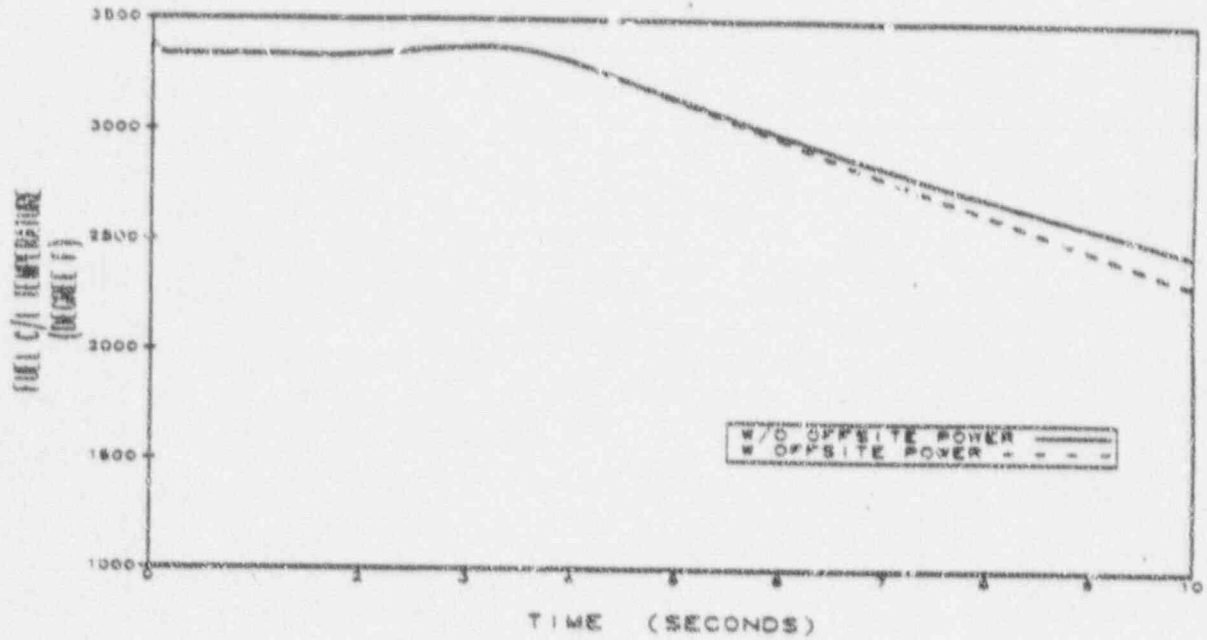

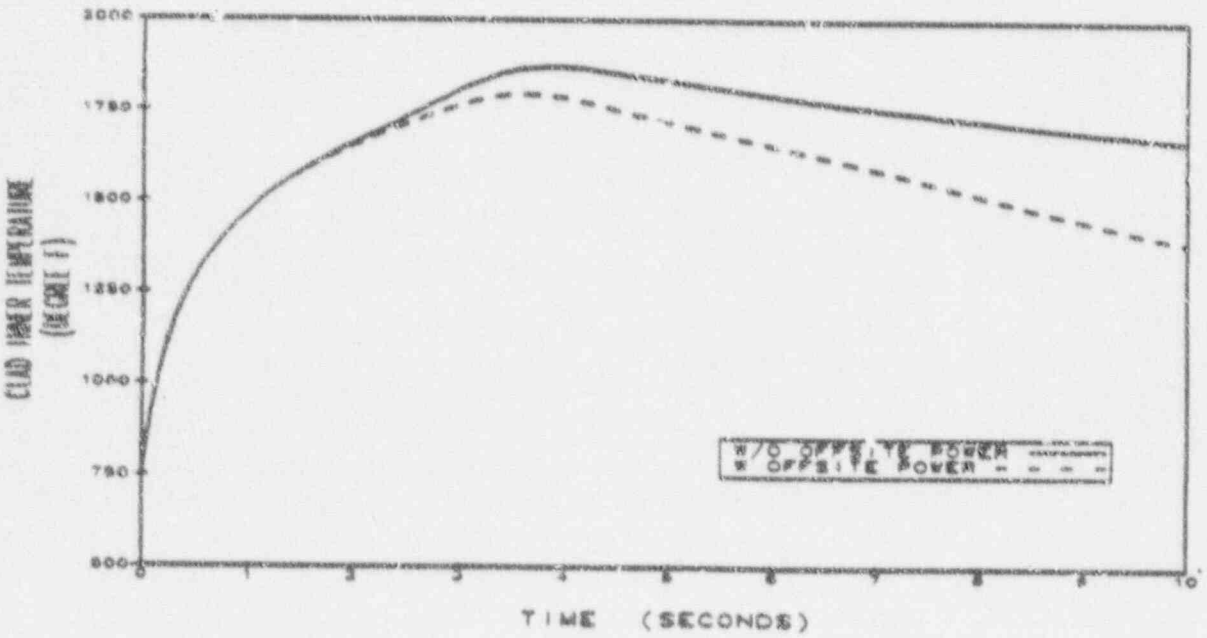

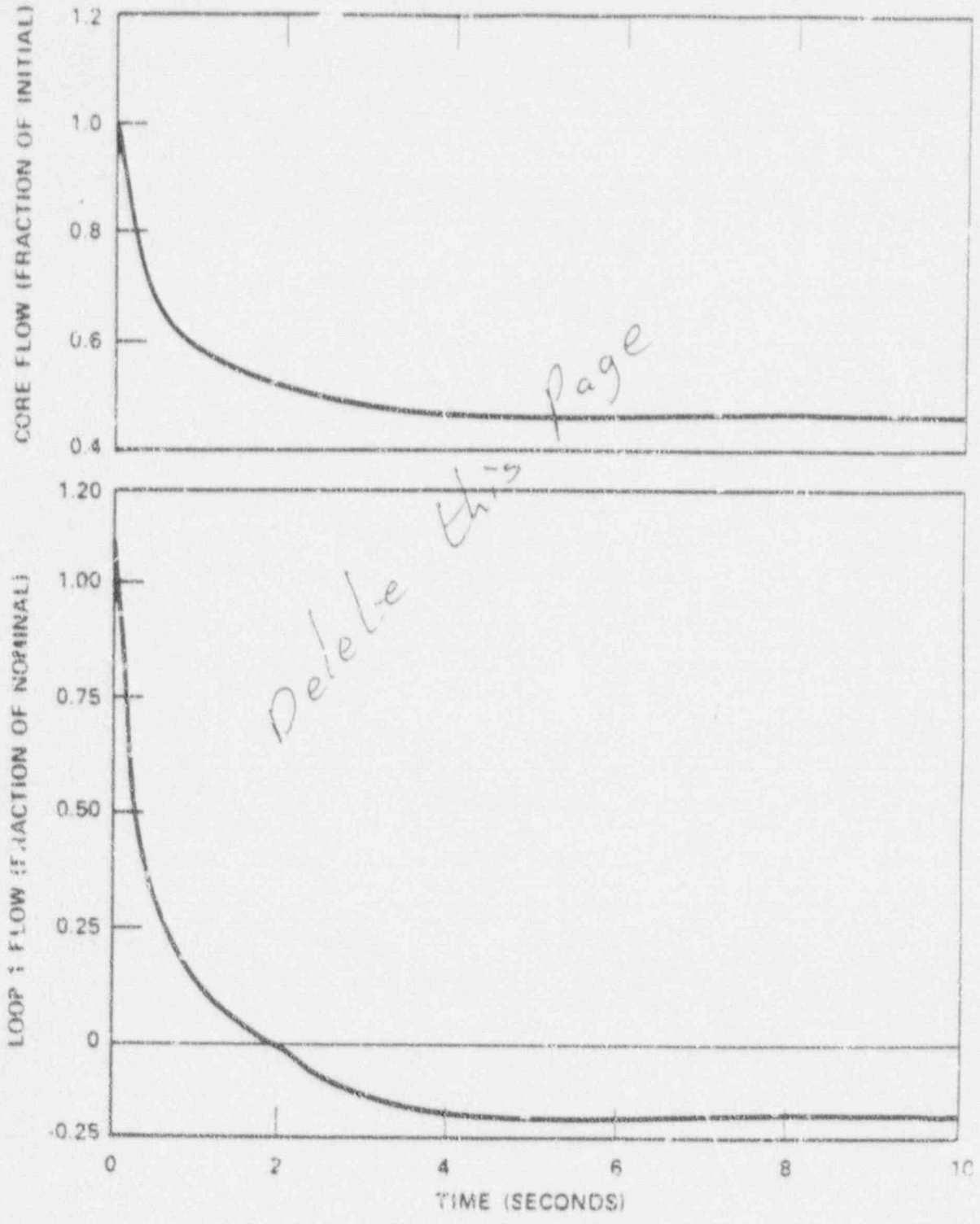

Delete this page

FIGURE 15.3-21
FLOW TRANSIENTS FOR
TWO LOOPS IN OPERATION,
ONE LOCKED ROTOR
BEAVER VALLEY POWER STATION-UNIT 2
FINAL SAFETY ANALYSIS REPORT

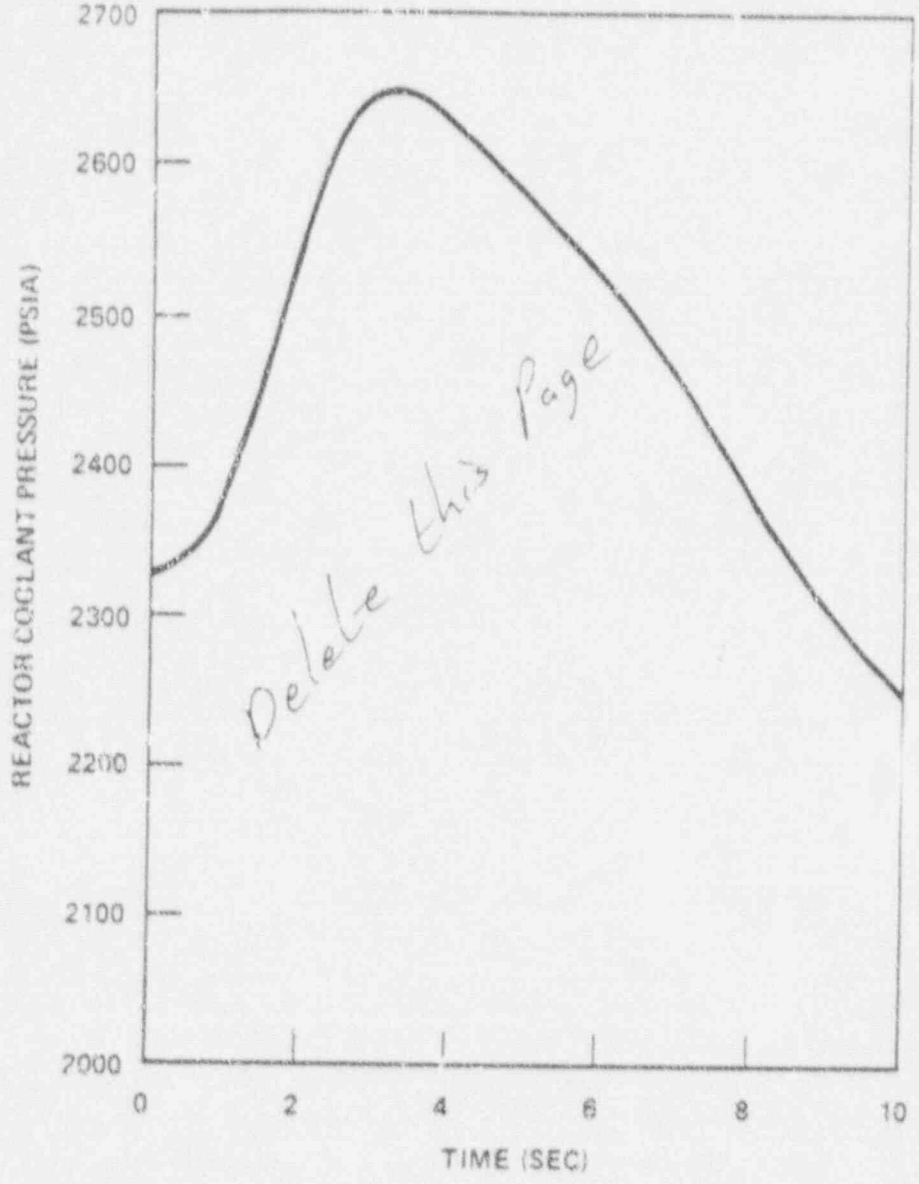

FIGURE 15.3-22
REACTOR COOLANT SYSTEM PRESSURE TRANSIENT FOR TWO LOOPS IN OPERATION, ONE LOCKED ROTOR
BEAVER VALLEY POWER STATION-UNIT 2
FINAL SAFETY ANALYSIS REPORT

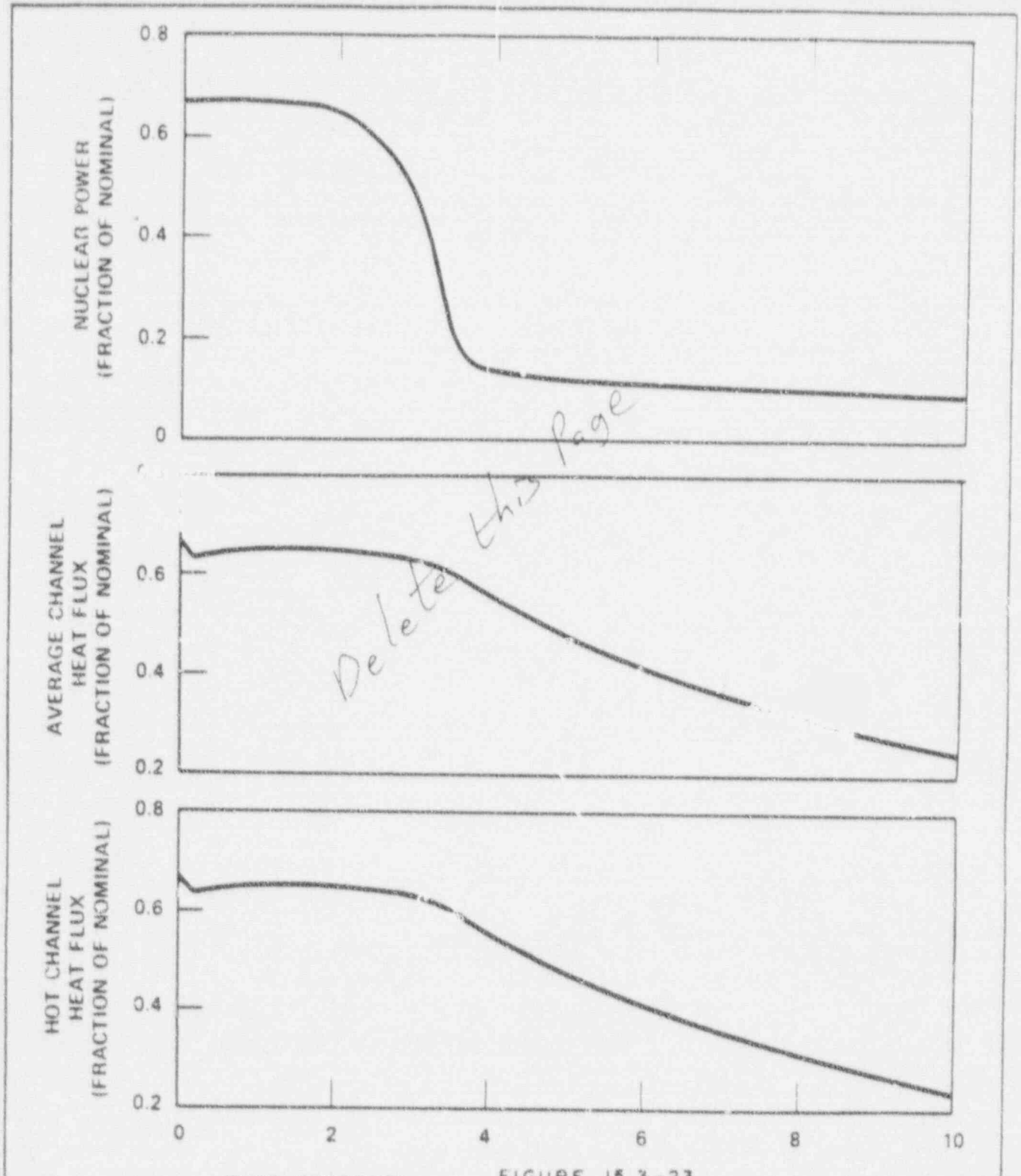

FIGURE 15.3-23
NUCLEAR POWER TRANSIENT, AVERAGE AND HOT CHANNEL HEAT FLUX TRANSIENTS FOR TWO LOOPS IN OPERATION, ONE LOCKED ROTOR
BEAVER VALLEY POWER STATION-UNIT 2
FINAL SAFETY ANALYSIS REPORT

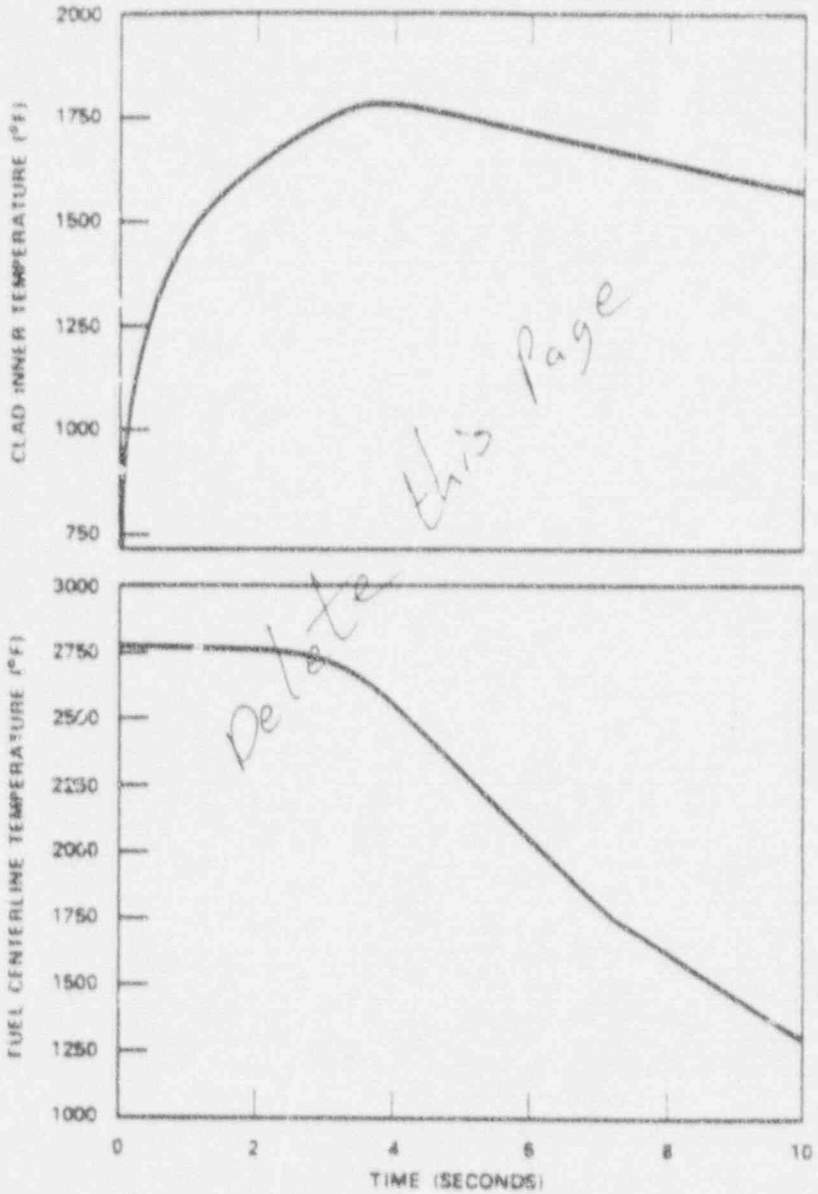

FIGURE 15.3-24

MAXIMUM CLAD INNER & FUEL CENTERLINE TEMPERATURES AT HOT SPOT FOR TWO LOOPS IN OPERATION, ONE LOCKED ROTOR

BEAVER VALLEY POWER STATION-UNIT 2
FINAL SAFETY ANALYSIS REPORT

Section 15.4

15.4.8.1.2 Limiting Criteria

This event is classified as an ANS Condition IV incident (Section 15.0.1). Due to the extremely low probability of an RCCA ejection accident, some fuel damage could be considered an acceptable consequence.

Comprehensive studies of the threshold of fuel failure, and of the threshold of significant conversion of the fuel thermal energy to mechanical energy, have been carried out as part of the SPERT project by the Idaho Nuclear Corporation (Taxelius 1970). Extensive tests of UO_2 zirconium-clad fuel rods representative of pressurized water reactor type cores have demonstrated failure thresholds in the range of 240 to 257 cal/gm. However, other rods of a slightly different design have exhibited failures as low as 225 cal/gm. These results differ significantly from the TREAT (Liimataninen and Testa 1966) results, which indicated a failure threshold of 280 cal/gm. Limited results have indicated that this threshold decreases by about 10 percent with fuel burnup. The clad failure mechanism appears to be melting for zero burnup rods and brittle fracture for irradiated rods. Also important is the conversion ratio of thermal to mechanical energy. This ratio becomes marginally detectable above 300 cal/gm for unirradiated rods and 200 cal/gm for irradiated rods; catastrophic failure, (large fuel dispersal, large pressure rise) even for irradiated rods, did not occur below 300 cal/gm.

In view of the preceeding experimental results, criteria are applied to ensure that there is little or no possibility of fuel dispersal in the coolant, gross lattice distortion, or severe shock waves. These criteria are:

1. Average fuel pellet enthalpy at the hot spot below ~~225~~ 200 cal/gm for unirradiated fuel.
2. Average clad temperature at the hot spot below the temperature at which cladding embrittlement may be expected (2,700°F).
3. Peak reactor coolant pressure less than that which could cause stresses to exceed the faulted condition stress limits, and
4. Fuel melting will be limited to less than 10 percent of the fuel volume at the hot spot even if the average fuel pellet enthalpy is below the limits of criterion 1 listed previously.

Delayed Neutron Fraction, βeff

Calculations of the effective delayed neutron fraction (βeff) typically yield values no less than 0.70 percent at beginning-of-life and 0.50 percent at end-of-life for the first cycle. The accident is sensitive to β_{eff} if the ejected rod worth is equal to or greater than β_{eff} as in zero power transients. In order to allow for future cycles, pessimistic estimates of β_{eff} of 0.55 percent at beginning of cycle and 0.4~~4~~7 percent at end of cycle were used in the analysis.

Trip Reactivity Insertion

The trip reactivity insertion assumed is given in Table 15.4-2 and includes the effect of one stuck RCCA adjacent to the ejected rod. These values are reduced by the ejected rod reactivity. The shutdown reactivity was simulated by dropping a rod of the required worth into the core. The start of rod motion occurred 0.5 second after the high neutron flux trip point was reached. This delay is assumed to consist of 0.2 second for the instrument channel to produce a signal, 0.15 second for the trip breaker to open, and 0.15 second for the coil to release the rods. A curve of trip rod insertion versus time was used which assumed that insertion to the dashpot does not occur until 2.7 ~~3.3~~ seconds after the start of fall. The choice of such a conservative insertion rate means that there is over one second after the trip point is reached before significant shutdown reactivity is inserted into the core. This conservatism is important for hot full power accidents.

The minimum design shutdown margin available for this plant at hot zero power (HZP) may be reached only at end-of-life in the equilibrium cycle. This value includes an allowance for the worst stuck rod, an adverse xenon distribution, conservative Doppler and moderator defects, and an allowance for calculational uncertainties. Physics calculations for this plant have shown that the effect of two stuck RCCAs (one of which is the worst ejected rod) is to reduce the shutdown margin by about an additional 1.0 ~~0.895~~ percent Δk/k. Therefore, following a reactor trip resulting from an RCCA ejection accident, the reactor will be subcritical when the core returns to HZP.

Depressurization calculations have been performed for a typical four-loop plant assuming the maximum possible size break (2.75-inch diameter) located in the reactor pressure vessel head. The results show a rapid pressure drop and a decrease in system water mass due to the break. The emergency core cooling system (ECCS) is actuated on low pressurizer pressure or level within one minute after the break. The RCS pressure continues to drop and reaches saturation (approximately 1,200 psi depending on the system temperature) in about eight minutes. Due to the large thermal inertia of primary and secondary system, there has been no significant decrease in the RCS temperature below no-load by this time, and the depressurization itself has caused an increase in shutdown margin by about